

**Analytical characterization and formulation development of a trivalent
subunit rotavirus vaccine for the developing world**

By

© 2019

Sanjeev Agarwal

M.S. Pharmaceutical Chemistry, 2016, The University of Kansas, Lawrence, KS

B.Pharm. (Honors), 2013, Birla Institute of Technology & Science, Pilani, India

Submitted to the graduate degree program in Pharmaceutical Chemistry and the Graduate
Faculty of the University of Kansas in partial fulfillment of the requirements for the degree of
Doctor of Philosophy.

Chairperson: David B. Volkin, Ph.D

William D. Picking, Ph.D

Teruna J. Siahaan, Ph.D

Thomas J. Tolbert, Ph.D

Prajnaparamita Dhar, Ph.D

Date Defended: June 18, 2019

The Dissertation Committee for Sanjeev Agarwal certifies that this is the approved version of the following dissertation:

Analytical characterization and formulation development of a trivalent subunit rotavirus vaccine for the developing world

Chairperson: David B. Volkin, Ph.D

Date Approved: June 18, 2019

Abstract

Although live attenuated, orally delivered rotavirus (RV) vaccines are available globally to provide protection against enteric RV disease, efficacy is substantially lower in low to middle income settings leading to interest in the development of alternate RV vaccines. Moreover, the high cost and limited supply of current RV vaccines are prohibitive to their successful introduction in the developing countries where the need for RV vaccines is most. One promising new RV vaccine candidate is a trivalent non-replicating rotavirus vaccine (NRRV), comprised of three recombinant fusion proteins (truncated rotavirus VP8 subunit proteins fused to the P2 CD4⁺ T cell epitope from tetanus toxoid). The three NRRV antigens are referred to as P2-VP8-P[4], P2-VP8-P[6], and P2-VP8-P[8]. A monovalent P2-VP8-P[8] adsorbed to Alhydrogel adjuvant was found to be safe and immunogenic in the early phase clinical trials in infants and toddlers in South Africa. Consequently, the trivalent vaccine consisting of all three P2-VP8-P[x] antigens adsorbed to Alhydrogel is currently being evaluated in Phase I/II clinical trials in South Africa.

Successful development and eventual commercialization of this recombinant subunit RV vaccine candidate will not only depend on clinical safety and efficacy results, but also the ability to produce the NRRV vaccine at low cost and abundant supply for use in the developing world. This dissertation work contributes towards developing analytical tools and formulation strategies (for both bulk drug substance and adjuvanted final drug product) to support the pharmaceutical development of this subunit RV vaccine candidate. A stable formulation should maintain the structural integrity, physicochemical stability, and ultimately the safety and efficacy of this vaccine throughout its shelf-life.

First, a wide variety of analytical techniques were employed to compare the physicochemical properties of the three NRRV recombinant fusion proteins. Various environmental stresses were used to evaluate antigen stability and elucidate their degradation pathways. The P2-VP8-P[4] and P2-VP8-P[6] antigens displayed similar conformational stability profiles while P2-VP8-P[8] was more stable. Forced degradation studies with each NRRV antigen revealed Met¹ was most susceptible to oxidation, the single Cys residue (at position 172 in P[8] and 173 in P[4] and P[6]) formed inter-molecular disulfide bonds (P2-VP8-P[6] was most susceptible), and Asn⁷ showed the highest increased levels of deamidation. These results are visualized in a structural model of the NRRV antigens. Although the potential impact of physicochemical structural alterations on immunogenicity is unknown at this time, the stability-indicating analytical tools developed and the structural knowledge gained in this work will be useful to (1) set critical manufacturing process parameters to ensure consistency, (2) monitor key structural attributes during comparability assessments, and (3) develop stable formulations for the bulk drug substance and adjuvanted final drug product.

Second, we focused on the aggregation propensity of the three NRRV antigens and developed stable formulations for long-term storage of frozen liquid bulks of each antigen in a common formulation buffer. The P2-VP8-P[8] antigen was most susceptible to shaking and freeze-thaw-induced aggregation. Each NRRV antigen formed aggregates with structurally altered protein (with exposed apolar regions and inter-molecular β -sheet) and dimers containing a non-native disulfide bond. From excipient screening studies with P2-VP8-P[8], sugars/polyols (e.g., sucrose, trehalose, mannitol, sorbitol) and various detergents (e.g., Pluronic F-68, polysorbate 20 and 80, PEG-3350) were identified as stabilizers against aggregation. By combining promising

excipients, candidate bulk formulations were optimized to not only minimize agitation-induced aggregation, but also particle formation due to freeze-thaw stress.

Third, we explored the use of an aluminum adjuvant and two preservatives to develop an adjuvanted multi-dose formulation with goal to further reduce the NRRV vaccine cost. The compatibility and stability of monovalent P2-VP8-P[8] antigen with Alhydrogel, with and without the vaccine preservative thimerosal, was examined using a wide variety of physicochemical and immunochemical methods. Antigen structural integrity was intact upon Alhydrogel binding as measured by ELISA, fluorescence spectroscopy, differential scanning calorimetry (DSC) and SDS-PAGE combined with LC-MS peptide mapping. An immediate destabilizing effect of thimerosal was observed upon heating by DSC. Over three months of storage, the aluminum adsorbed P2-VP8-P[8] antigen was stable at 4°C, while instability was observed at 25°C and 37°C which was greatly accelerated by thimerosal addition. Compatibility of aluminum-adsorbed P2-VP8-P[8] antigen with an alternative preservative (2-phenoxyethanol) was also evaluated and similar incompatibility was observed. Due to limited availability of P2-VP8-P[4] and P2-VP8-P[6] antigens, key assays from P2-VP8-P[8] studies were performed with these monovalent aluminum-adsorbed antigens. Varying levels of preservative incompatibility were observed depending on the antigen, temperature, and analytical method. In summary, these results demonstrate good overall stability of the monovalent aluminum-adsorbed NRRV antigens at 4°C for three months in the absence of preservative. However, additional formulation development efforts are required to produce a stable multi-dose formulation of the NRRV vaccine.

Dedicated to:

My parents

Om Prakash and Lalita Agarwal

my brother and sisters

Rajeev, Savita, and Sarita Agarwal

and my beloved wife

Khushboo Kapadia

Acknowledgements

This dissertation work would not have been accomplished without the support and guidance of several individuals. I would like to start by thanking my research advisor and mentor, Dr. David Volkin, for giving me the opportunity to work in his laboratories. I entered his lab with a very little understanding of the field but had the curiosity to identify and solve problems. I am thankful to David for assigning a vaccine development project to me which has helped in not only shaping me as a pharmaceutical scientist but has also prepared me for the real-world challenges. He always believed in my abilities, supported my ideas and research initiatives which has helped me in striving for the best and in boosting my confidence. He always stressed on the importance of delivering good scientific presentations and effective communication of the research findings. I have learned a great deal about scientific writing, work organization, and time management from him and will always look up to him as a source of knowledge and guidance.

I would like to thank Dr. Sangeeta Joshi (Director and co-founder, VAFC) for her scientific insights and guidance through-out my dissertation work. She has been instrumental in encouraging my research activities in the lab and providing essential mentorship at every stage. I would like to thank her for providing me with opportunities to present our findings to our collaborators during teleconferences and scientific meetings. I would also like to sincerely thank Dr. William Picking, Dr. Teruna Siahaan, Dr. Thomas Tolbert, and Dr. Prajnaparamita Dhar for agreeing to serve on my dissertation committee. I appreciate their time and efforts in reviewing my progress and I immensely value their scientific insights and critical analysis of my work.

I would like to extend my special thanks to Dr. John Hickey and Dr. Neha Sahni (former member) for their contributions to this work and for training me on various techniques over the

years. I would like to acknowledge Dr. Jain Xiong, and Dr. Ron Toth (former member) for their valuable contributions to various projects. Many thanks to the current (Dr. Kawaljit Kaur, Dr. Vineet Gupta, Nishant Sawant, Kaushal Jerajani, Dr. David Holland III) and past members of my lab who have helped, encouraged and supported me in this long journey. I would also like to thank our collaborators at PATH (Dr. Robert Sitrin, Dr. Stanley Cryz, and Dr. George Robertson) for the numerous scientific discussions and their critical review of my manuscripts.

I thankfully acknowledge the funding from Bill & Melinda Gates Foundation and PATH which supported this project. I would also like to recognize the financial support in the form of tuition from Gretta Jean & Gerry D Goetsch fellowship. I am grateful that I had a chance to pursue my PhD at the Pharmaceutical Chemistry Department. I have learnt a lot from the esteemed faculty and the rigorous curriculum of the department. I am also thankful to my colleagues in the department for their friendship and encouragement.

This accomplishment would be incomplete without the mention of my former advisor, Dr. Yatin Gokarn. He introduced me to the world of biologics and protein formulations. He always encouraged me to aim for the best. His guidance and tutelage have played an instrumental role in shaping my career, both professional and personal. He will always be my role model and a source of inspiration. I also want to express my heartfelt gratitude to Dr. Maneesh Nerurkar; I still remember the telephone conversation from 6 years ago which laid the foundation of my career. A special thanks to my former mentor, Dr. Divya Chandra, for her scientific insight, discussion and critique during my internship at Merck. She has been a constant source of help and wisdom during my job search and has played a key role in navigating me in the right direction.

All achievements have their own share of ups and downs and my journey has been no different. I survived the tough times and savored the good moments in the company of friends I made along the way. A special mention to Steve and Janice Sizemore for being very kind friends.

They are the first people I met in Lawrence and our friendship has continued to grow stronger with time and I look up to them as guardians. Although I live thousands of miles away from my family, their unwavering support and belief has always motivated me. I would like to thank both my sets of parents, Om Prakash & Lalita Agarwal, and Bhupendra & Kalpana Kapadia, for believing in me and for always praying for my success. I also acknowledge the sacrifices and hardships my siblings went through while growing up to ensure that I received the best education which has shaped my life for the better. This would sound clichéd but I truly dedicate this success to my loving wife, Khushboo Kapadia. She has been an equal part of this endeavor and I cannot thank her enough for her unconditional love and sacrifices. She always made sure that I am enjoying life and have a reason to smile. Finally, I would like to thank god for giving me the strength, patience and courage to survive through these years and achieve this feat.

Table of Contents

Abstract.....	iii
Acknowledgements	vii
List of Tables	xiv
List of Figures.....	xv
List of Supplementary Tables	xvii
List of Supplementary Figures	xviii
Chapter 1: Introduction	1
1.0 Motivation and Overview.....	2
1.1 Rotavirus	3
1.1.1 Structure and strain classification.....	3
1.1.2 Burden and epidemiology.....	4
1.1.3 Transmission and replication.....	4
1.1.4 Symptoms and immunity.....	5
1.1.5 Treatment options	6
1.1.6 Rotavirus Vaccines	6
1.1.7 Trivalent non-replicating rotavirus (NRRV) vaccine candidate.....	12
1.2 Analytical tools to characterize and develop subunit vaccines	16
1.2.1 Potency assays	16
1.2.2 Physicochemical Assays.....	21
1.3 Formulation development of subunit vaccine candidates for developing countries	26
1.3.1 Vaccine bulk antigen (DS) manufacturing	27
1.3.2 Interface between DS and DP formulation development to improve efficiency.....	28
1.3.3 Vaccine drug product (DP) formulation.....	30
1.4 Tables	34
1.5 Figures.....	39
Chapter 2: Recombinant subunit rotavirus trivalent vaccine candidate: physicochemical comparisons and stability evaluations of three protein antigens.....	46
2.0 Introduction	47
2.1 Materials and Methods	49

2.1.1 Intact Protein Mass Spectroscopy.....	50
2.1.2 LC-MS Peptide Mapping.....	51
2.1.3 Fourier-Transform Infrared (FTIR) Spectroscopy	51
2.1.4 Far-UV Circular Dichroism (CD) Spectroscopy	52
2.1.5 Intrinsic Tryptophan Fluorescence Spectroscopy and Static Light Scattering (SLS) ..	53
2.1.6 SDS-PAGE	53
2.1.7 Size Exclusion Chromatography (SEC)	54
2.1.8 Sedimentation Velocity Analytical Ultracentrifugation (SV-AUC)	55
2.1.9 Reversed-Phase Ultra High Performance Liquid Chromatography (RP-UHPLC)	55
2.1.10 Hydrophobic Interaction Chromatography (HIC)	56
2.1.11 Differential Scanning Calorimetry (DSC).....	57
2.1.12 Extrinsic ANS Fluorescence Spectroscopy	57
2.1.13 OD ₃₅₀ (turbidity) analysis	58
2.1.14 Physical stability profile comparisons using data visualization tools	58
2.1.15 Chemical stability profile comparisons at elevated temperature and solution pH and in presence of H ₂ O ₂	59
2.1.16 Modeling of NRRV antigen structure	59
2.2 Results	60
2.2.1 Physicochemical characterization and comparisons of the three NRRV antigens.....	60
2.2.2 Physical stability profiles and comparisons of the three NRRV antigens as a function of temperature and pH	62
2.2.3 Chemical stability profiles and comparisons of the three NRRV antigens	65
2.2.4 Structural modeling and comparisons of the three NRRV antigens.....	68
2.3 Discussion	68
2.4 Figures.....	74
2.5 Supplemental Figures.....	83
Chapter 3: Developing stable frozen liquid bulk formulations to minimize aggregation and particle formation of the three NRRV antigens	92
3.0 Introduction	93
3.1 Materials and Methods	95
3.1.1 Colloidal Stability Studies Using Agitation Stress.....	96
3.1.2 Visual Appearance and Turbidity	97
3.1.3 UV-Visible spectroscopy.....	97

3.1.4 Micro-Flow Imaging (MFI).....	97
3.1.5 Resonance Mass Measurement (RMM)	98
3.1.6 Sedimentation Velocity Analytical Ultracentrifugation (SV-AUC)	98
3.1.7 Size Exclusion Chromatography (SEC)	98
3.1.8 Fourier Transform Infrared Spectroscopy (FTIR).....	98
3.1.9 Fourier Transform Infrared Microscopy.....	99
3.1.10 Extrinsic (ANS) Fluorescence Spectroscopy	99
3.1.11 SDS-PAGE	100
3.1.12 Ammonium Sulfate (AS) Precipitation Assay.....	100
3.1.13 Excipient Screening for NRRV Antigens under Agitation, Thermal and Freeze-thaw Stresses	101
3.2 Results	103
3.2.1 Colloidal stability assessments and characterization of aggregates and particles	103
3.2.2 Screening stabilizing excipients to minimize shaking and thermal induced aggregation of NRRV antigens	106
3.2.3 Optimizing lead stabilizers to further minimize shaking and thermal induced aggregation of NRRV antigens.....	108
3.2.4 Optimizing buffering agent and solution pH to minimize shaking and thermal induced aggregation of NRRV antigens.....	109
3.2.5 Evaluation of candidate formulations for frozen liquid bulk drug substance of three NRRV antigens.....	111
3.3 Discussion	112
3.4 Tables	119
3.5 Figures	120
3.6 Supplementary Tables	128
3.7 Supplementary Figures.....	129
Chapter 4: Effect of aluminum adjuvant and preservatives on structural integrity and physicochemical stability profiles of the three NRRV antigens.....	133
4.0 Introduction	134
4.1 Materials and Methods	136
4.1.1 Measuring Zeta Potential.....	137
4.1.2 Antigen-Adjuvant Binding Study.....	137
4.1.3 Langmuir Binding Isotherms.....	138
4.1.4 Steady State Intrinsic Tryptophan Fluorescence	139

4.1.5 Differential Scanning Calorimetry (DSC).....	139
4.1.6 Time-resolved Intrinsic Tryptophan Fluorescence.....	139
4.1.7 SDS-PAGE Analysis + LC-MS Peptide Mapping, of desorbed protein	140
4.1.8 Inhibition ELISA	142
4.1.9 Accelerated/Real Time Storage Stability Study	143
4.2 Results	144
4.2.1 P[8] Antigen-Alhydrogel Adjuvant Interactions	144
4.2.2 P[8] Antigen-Alhydrogel Adjuvant-Thimerosal Interactions.....	145
4.2.3 Storage stability of monovalent P[8]-Alhydrogel drug product.....	146
4.2.4 P[4] and P[6] Antigen-Alhydrogel-Thimerosal interactions	149
4.2.5 Comparison of Thimerosal vs. 2-Phenoxyethanol on P[8]-AH storage stability.....	150
4.3 Discussion	151
4.4 Tables	158
4.5 Figures.....	159
4.6 Supplementary Tables.....	168
4.7 Supplementary Figures.....	169
Chapter 5	180
Chapter summaries and future directions.....	180
5.0 Overview	181
5.1 Chapter 2	182
5.2 Chapter 3	184
5.3 Chapter 4	185
Bibliography	189

List of Tables

Chapter 1

Table 1.1. Comparison of currently available RV vaccines.....	34
Table 1.2. Potential factors for the reduced efficacy of orally administered, live attenuated viral RV vaccines in developing countries.....	35
Table 1.3. RV vaccines currently in development with alternate routes of administration and vaccine types.....	36
Table 1.4. Summary of analytical tools available to characterize recombinant protein subunit vaccines and to apply to their formulation development.....	37
Table 1.5. Comparison of expression systems used for production of vaccine bulk antigens.....	38

Chapter 2

No Tables

Chapter 3

Table 3.1. Composition and osmolality values of 8 candidate frozen liquid formulations.....	119
--	-----

Chapter 4

Table 4.1. Summary of NRRV antigen (P[8], P[6], and P[4]) and aluminum adjuvant (Alhydrogel, AH) binding parameters in different formulations.....	158
---	-----

Chapter 5

No Tables

List of Figures

Chapter 1

Figure 1.1. Schematic representation of a rotavirus virion highlighting the structural proteins..	39
Figure 1.2. Distribution of medically important RV strains from 2007 - 2012.	40
Figure 1.3. Change in RV associated mortality rate from 1990 to 2016.	41
Figure 1.4. Potential factors for reduced efficacy of commercially available, orally delivered, live attenuated viral RV vaccines in developing countries	42
Figure 1.5. Societal and public health benefits of combination vaccines.....	43
Figure 1.6. Composition and nomenclature of the three recombinant fusion protein antigens that comprise the NRRV candidate vaccine	44
Figure 1.7. Analytical tools and their strengths vs. weaknesses in terms of assay properties vs. relevance to vaccine clinical performance	45

Chapter 2

Figure 2.1. Primary structure analysis of the three NRRV antigens.....	74
Figure 2.2. Higher order structure (HOS) analysis	75
Figure 2.3. Size, aggregation, and heterogeneity analysis	76
Figure 2.4. Higher-order structure (HOS) stability and aggregation propensity	77
Figure 2.5. Biophysical stability profile from radar chart analysis.....	78
Figure 2.6. Forced degradation (Asn deamidation) studies	79
Figure 2.7. Forced degradation (non-native disulfide formation) studies.....	80
Figure 2.8. Forced oxidation studies as a function of hydrogen peroxide concentration.	81
Figure 2.9. Structural modeling of the three NRRV protein antigens.	82

Chapter 3

Figure 3.1. Colloidal stability assessment and comparison of the three NRRV antigens.....	120
Figure 3.2. Morphology and structural analysis of protein within aggregates/particles.....	121
Figure 3.3. Excipient screening against agitation stress of P[8]	122
Figure 3.4. Excipient screening against thermal stress of P[8].....	123
Figure 3.5. Effect of excipient concentrations and combinations on thermal and shaking induced aggregation propensity of P[8].....	124
Figure 3.6. Effect of different buffer types and pH conditions on thermal and shaking induced aggregation propensity of P[8].....	125
Figure 3.7. Comparison of candidate bulk formulations versus current formulation	126
Figure 3.8. Effects of PS-80 concentration during freeze-thaw and shaking stresses on physical stability.....	127

Chapter 4

Figure 4.1. Surface charge and percent P[8] antigen binding to Alhydrogel (AH) in different buffers.	159
Figure 4.2. P[8] antigen interactions with the aluminum adjuvant Alhydrogel.....	160
Figure 4.3. Effect of thimerosal on the conformational stability of Alhydrogel-bound P[8] antigen.....	161
Figure 4.4. ELISA antibody binding for AH-bound P[8] antigen during storage	162
Figure 4.5. Physical stability profiles of AH-bound P[8] antigen during storage	163
Figure 4.6. Non-native disulfide formation at Cys172 and deamidation at Asn7 of the AH-bound P[8] antigen.....	164
Figure 4.7. Effect of adjuvant (Alhydrogel, AH) and preservative (thimerosal) on physicochemical stability of P[4] antigen.....	165
Figure 4.8. Effect of adjuvant (Alhydrogel, AH) and preservative (thimerosal) on physicochemical stability of P[6] antigen.....	166
Figure 4.9. Destabilizing effect of in-use concentrations of thimerosal (0.01% w/v) vs. 2-phenoxyethanol (1.0 %).....	167

Chapter 5

No Figures

List of Supplementary Tables

Chapter 1

No Supplementary Tables

Chapter 2

No Supplementary Tables

Chapter 3

Supplementary Table S3.1. Comparison of aggregate and particle formation in different size ranges for the three NRRV antigens. 128

Chapter 4

Supplementary Table S4.1. Summary of onset temperature, melting temperature and apparent enthalpy of unfolding from conformational stability analysis by DSC. 168

Chapter 5

No Supplementary Tables

List of Supplementary Figures

Chapter 1

No Supplementary Figures

Chapter 2

Supplemental Figure S2.1. Primary structure analysis of the NRRV antigens.....	83
Supplemental Figure S2.2. Biophysical stability profile and data for radar chart analysis.....	84
Supplemental Figure S2.3. Forced degradation (Asn deamidation) studies	85
Supplemental Figure S2.4. Forced degradation (non-native disulfide formation) studies with P[4].....	86
Supplemental Figure S2.5. Forced degradation (non-native disulfide formation) studies with P[8].....	87
Supplemental Figure S2.6. Forced oxidation studies of P[4] antigen	88
Supplemental Figure S2.7. Forced oxidation studies of P[6] antigen	89
Supplemental Figure S2.8. Forced oxidation studies of P[8] antigen	90
Supplemental Figure S2.9. Forced oxidation studies of the three NRRV antigens	91

Chapter 3

Supplementary Figure S3.1. Morphology, higher order structure and chemical composition of aggregates/particles formed for P[4] and P[6] antigens.....	129
Supplementary Figure S3.2. Total sub-visible particles and OD ₃₅₀ value of P[4] and P[6] solutions after shake stressed for 6 h	130
Supplementary Figure S3.3. Effects of down-selected buffer types and pH conditions on shaking induced and thermal induced aggregation propensity of P[4] and P[6]	131
Supplementary Figure S3.4. Sub-visible particle distribution analysis of P[4] and P[6] antigens after 0, 1, and 5 FT cycles.....	132

Chapter 4

Supplementary Figure S4.1. Schematic description of the vaccine sample preparation workflow in ten formulations with and without 0.01% w/v thimerosal for 12 week storage stability study.....	169
Supplementary Figure S4.2. Tertiary structure integrity and stability analyses of NRRV antigens bound to aluminum adjuvant Alhydrogel compared to in solution controls	170
Supplementary Figure S4.3. SDS-PAGE analysis of P[8] antigen under non-reducing and reducing conditions after forced desorption	173
Supplementary Figure S4.4. Oxidation propensity of Met ⁹⁹ of the P[8] antigen bound to Alhydrogel.	174
Supplementary Figure S4.5. Conformational stability and antibody binding of monovalent P[4] and P[6] antigens bound to Alhydrogel	175

Supplementary Figure S4.6. SDS-PAGE analysis of P[4] antigen under non-reducing and reducing conditions after forced desorption	176
Supplementary Figure S4.7. SDS-PAGE analysis of P[6] antigen under non-reducing and reducing conditions after forced desorption	177
Supplementary Figure S4.8. Non-native disulfide formation at Cys ¹⁷² and deamidation at Asn ⁷ of the monovalent P[4] and P[6] antigens bound to Alhydrogel	178
Supplementary Figure S4.9. Deamidation analysis of Asn ⁹⁰ of the P[6] antigen bound to Alhydrogel	179

Chapter 5

No Supplementary Figures

Chapter 1

Introduction

1.0 Motivation and Overview

Rotavirus (RV) is a major cause of childhood morbidity and mortality by causing a diarrheal disease. Prior to the RV vaccine introduction in 2006, it was projected that every child will get this infection before reaching 5 years of age. This would have led to 1 in 5 infected children needing medical attention, 1 in 65 getting hospitalized, and 1 in 293 dying, around the world ². Fortunately, two RV vaccines were approved in 2006 and this dire scenario was averted and instead the number of deaths associated with RV has declined, from 440,000 annually in pre-vaccine era to 128,500 in 2016 ¹. However, one fact that has not changed over the decades is that more than 80% of these deaths occur in the developing regions of the world. The most disheartening part is that the full potential of the currently approved vaccines has not yet been achieved which could have averted another 83,200 deaths in the year 2016 ¹. In spite of WHO recommending the use of RV vaccines in the national immunization programs in all parts of the world in 2009, the global coverage of RV vaccines was only about 28% by the end of 2017 ³. The two major reasons for the poor coverage or use of the current vaccines are high cost and inadequate supply in the developing countries where the burden of RV disease is highest ⁴. The focus of this work is to develop analytical tools and stable formulations for a recombinant subunit trivalent RV vaccine candidate which is currently in clinical trials. The goal is to produce this vaccine at an affordable cost and ensure a more sustainable supply to meet the demands of the poor and populous countries.

The first section of this introduction chapter will describe the basic biology and pathology of the RV from a vaccine development perspective. Emphasis will be given on the deficiencies of the current RV vaccines and the need for new generation vaccines. The trivalent subunit or non-replicating rotavirus (NRRV) vaccine candidate, the focus of this work, will be defined and discussed. The second section will focus on various types of analytical tools used to characterize and test recombinant protein subunit antigens which facilitate their development as well-defined

macromolecular vaccines, both physically and chemically. The last section of this introduction will discuss the challenges and opportunities involved with the formulation development of subunit vaccines for use in developing countries.

1.1 Rotavirus

1.1.1 Structure and strain classification

RVs are non-enveloped icosahedral viruses belonging to *Reoviridae* family. Structurally, the virus is composed of six viral proteins (VPs) and contains a segmented genome with 11 double stranded RNA segments (Figure 1.1). The viral genome is surrounded by the internal layer composed of VP1, VP2 and VP3 proteins. VP6 is the major structural protein and constitutes the middle layer of the RV. The outer layer/capsid is made of two surface proteins VP4 and VP7. Upon infection, six non-structural proteins (NSPs) are produced, NSP1 – NSP6. These structural and non-structural proteins serve a variety of roles during viral infection and replication ⁵.

Based on the antigenicity of the VP6 protein, RVs are divided into Groups A – H, Group A RVs are mostly involved in human infections. Serotype classification is based on the surface proteins; VP4 is a protease sensitive protein, called P type, and VP7 is a glycoprotein, called G type. These two proteins contain neutralizing epitopes and immune responses against either can provide protection ⁶. Matthijssens et al. proposed the genotype-based classification system using the 11 RNA segments that code for the six structural and 6 NSPs. In this classification system, VP7-VP4-VP6-VP1-VP2-VP3-NSP1-NSP2-NSP3-NSP4-NSP5/6 proteins are coded by G_x-P_[x]-I_x-R_x-C_x-M_x-A_x-N_x-T_x-E_x-H_x genes, respectively ⁷. Wa-like (G1/3/4-P[8]-I1-R1-C1-M1-A1-N1-T1-E1-H1) and DS-1-like (G2-P[4]-I2-R2-C2-M2-A2-N2-T2-E2-H2) are two major genotype constellations for human strains ⁸.

1.1.2 Burden and epidemiology

In 2016, RV infection was associated with an estimated 258 million diarrheal episodes resulting in 18.8 million clinical visits, 1.5 million hospitalizations, and 128,500 deaths around the world, among children below 5 years of age ¹. Regions with poor sanitation and personal hygiene, lack of healthcare infrastructure and safe drinking water are most susceptible to this illness due to high rate of transmission (see next section) and fecal-oral route of transmission. As a result, poor and developing countries bear the brunt of unhygienic conditions and over 80% of these deaths occurred in sub-Saharan Africa and another 13% occurred in South and Southeast Asia ^{1,9}. To date, 36 G and 51 P genotypes have been recorded around the world ¹⁰. Since the RV genome has segmented nature there are higher chances of strain reassortment during co-infections. Global distribution of RV strains detected in humans from 2007 to 2012 suggest G1P[8] as the most prevalent strain, and P[8] is the most common P genotype followed by P[4] (Figure 1.2A). In addition, P[6] genotype is of significant relevance in the African and Southeast Asian region with approximately 25% and 17% of the strains containing this genotype, respectively (Figure 1.2B, 1.2C) ¹¹. Hence it is essential to include P[6] genotype in the newer generation vaccines (for the developing countries) if homotypic protection is required against P[6] type.

1.1.3 Transmission and replication

RV is mainly transmitted through the fecal-oral route. An infected person sheds about 10^{10} viral particles per gram of fecal material. Only 10 particles are needed to infect another person which, in addition to its stable nature even under harsh environmental conditions, makes the virus highly contagious. Other domestic hygiene conditions such as contaminated drinking water, food, hands, or surfaces can also contribute to the viral transmission. Upon infection, the first step is the attachment of virus to the enterocytes of villi in the small intestine. This is mediated by the VP8*

protein (proteolytic cleavage product of VP4, $VP4 \rightarrow VP5^* + VP8^*$) that binds to sialic acid receptors or Histo blood group antigens (HBGA). Virus then enters the cell through endocytosis (or potentially other unknown mechanisms). Upon entry, outer capsid is removed, and a double layer particle is formed in the inclusion bodies called viroplasms and NSP2, NSP5 and NSP6 are involved in this step. Then transcription of the genetic material takes place in the viroplasms using VP1 (RNA dependent RNA polymerase) and VP3 (a methyltransferase). The newly synthesized RNA acts as a template for further replication and translation into structural VPs. Last step is the virion assembly using the new VPs and genetic material, and release of the newly produced infectious RVs from the cells via lysis. Since VP4 is involved in the first step of cell attachment, P genotype plays an important role in epidemiology. Similarly, host genetic differences could also play a role since HBGA expression can also affect RV cell attachment^{6,8}. Some studies have shown that RV infection is not just limited to intestines but has some extra-intestinal presence as well¹². Both viremia and antigenemia have been recorded in infected children and RV infection has been associated with neurological illness, biliary atresia, and diabetes mellitus^{6,12}. These findings require further research to better understand in the future, especially to explore the potential protective role of RV vaccines in this regard.

1.1.4 Symptoms and immunity

Upon infection, RV has an incubation period of 2 – 4 days. After this, symptoms include fever, vomiting, dry mouth, dizziness, decreased urination, and abdominal pain, followed by watery diarrhea for 3 – 8 days. This could result in severe dehydration and acute gastroenteritis ultimately leading to death. RV shedding continues for about 1 – 3 weeks in most children following a severe RV episode¹³. Mechanism of RV immunity is not completely understood but both natural infection and vaccines can elicit protection against future infections. With each

repeated infection the severity of disease decreases, and a complete protection could be achieved after three natural infections. Serum IgA, IgG and neutralizing antibodies along with fecal IgA have been detected in infected children but so far there is no satisfactory correlate of protection against RV disease. In addition, secretory IgA and IgG could play a protective role since intestinal antibodies specific to VP4 and VP7 may be required to prevent viral attachment and entry into the cell. Intestinal or mucosal immunity is considered important because small intestines are the local site of infection and viral replication causing gastrointestinal illness ¹³⁻¹⁸.

1.1.5 Treatment options

Oral rehydration solution (ORS) is the recommended treatment option by WHO to regain electrolyte balance and hydration. This has been successfully used to treat dehydration in most children, and under severe circumstances, intravenous fluids can be used. In addition, zinc supplementation, adequate food intake, breastfeeding and probiotics can also help under specific circumstances. There is no fully developed antiviral therapy for RV but a few drugs including nitazoxanide, racecadotril, smectite and anti-emetics have shown promising results in some studies in this regard ⁶.

1.1.6 Rotavirus Vaccines

As mentioned above, natural RV infection is known to reduce the disease severity with every subsequent infection and complete protection can be achieved after three infections ¹⁹. However, improvements in personal hygiene, domestic sanitation and quality of drinking water has not eliminated the risk of infection due to the highly contagious nature of RV. This situation has laid the foundational motivation for developing vaccines against this infectious pathogen.

1.1.6.1 First generation

Rotashield was the first RV vaccine approved by the US FDA in 1998 and licensed to Wyeth Lederle. It was an orally delivered, live attenuated, 3-dose, quadrivalent human-rhesus reassortant vaccine resulting from reassortment of G1, G2 or G4 gene from human RVs with 10 genes from a naturally attenuated rhesus RV-MMU G3 strain. The vaccine showed an estimated efficacy of 85% and 51% in the developed and developing regions, respectively, in the clinical trials. However, post-licensure, a vaccine associated adverse event, intussusception, was recorded in 1 in 10,000 vaccinated children (an elevated risk of 30-fold compared to the estimated natural intussusception occurrence). Consequently, Rotashield was withdrawn from the market within a year of its approval²⁰⁻²².

1.1.6.2 Second (Current) generation

Two orally delivered, live attenuated RV vaccines, RotaTeq (RV5) and Rotarix (RV1), were approved in 2006 and 2008, respectively, by the FDA, and since their introduction, RV associated mortality rate has significantly reduced worldwide as depicted in Figure 1.3. These vaccines were initially approved in developed nations but soon became a global success story. There has been a significant reduction in both morbidity and mortality in all the countries using these vaccines. In 2009, WHO recommended the addition of these two RV vaccines worldwide in the national immunization programs and currently they are available in over 100 countries to reduce the burden of RV infection. As noted in Figure 1.3, majority (>93%) of RV related deaths in the post-vaccine era occur in the developing regions of Sub-Saharan Africa, and South and Southeast Asia. Post-licensure data from 2006 – 2016 from 24 countries have estimated a vaccine effectiveness of 84% for RV1 and 90% for RV5 in the countries with low mortality. The vaccine effectiveness is, however, only about 57% for RV1 and 45% for RV5 in the countries with high

mortality²³. These results highlight that the current RV vaccines have lower efficacy in the poor and developing regions of the world where the need for these vaccines is most urgent. Furthermore, due to the history of intussusception with Rotashield, RV1 and RV5 underwent large-scale clinical trials involving over sixty thousand infants to confirm no significant increase in the risk of intussusception. Post-marketing surveillance studies have estimated a risk of 1 to 6 excess cases per 100,000 vaccinated children²⁴. Nonetheless, the clinical and societal benefits of these vaccines far outweigh their low risks²⁵.

In addition to these two global RV vaccines, there are four indigenously developed RV vaccines (Rotavac, Rotasil, Lanzhou Lamb Rotavirus, Rotavin-M1) approved for use in selected countries in the developing world. Recently, in 2018, Rotavac and Rotasil received WHO pre-qualification and will also be more widely available for procurement by UN and GAVI in the future. Table 1.1 provides a brief comparison of these six RV vaccines in terms of the manufacturer, year of approval, price per vaccination course, virus strains present, formulation presentation, vaccine vial monitor, storage requirements, route of administration, number of doses and dosing schedule, and licensure and availability status. All the approved RV vaccines are administered orally in 2-3 dose schedule and contain live, attenuated viruses. Oral administration has several advantages such as induction of both mucosal and systemic immunity, herd immunity due to reduced virus shedding and transmission, needle-free delivery (ease of administration), reduced medical waste and logistic requirements²⁶. However, oral vaccines tend to have an impaired efficacy in the developing countries as observed with the two global RV vaccines. Similar observations have been made with the oral cholera and oral polio vaccines²⁷. The reasons for reduced efficacy of the oral RV vaccines are not well understood but seems to be multi-factorial and inter-twined as shown in the schematic in Figure 1.4. A brief summary of how these factors

could impair the immune response or reduce the viral titer and the proposed solutions is provided in Table 1.2. It is important to note that for the majority of the listed factors, if not all, there are some contradicting studies showing lack of correlation with the vaccine efficacy ^{15,28-35}. Interestingly, some studies have shown that breastfeeding can provide protection against natural infection due to acquired RV specific IgA ^{32,36}.

1.1.6.3 Third (Future) generation

Based on the evidence for the lower efficacy of currently RV vaccines in the poor and developing countries, where the burden of RV illness is highest, there is an urgent need to develop new generation vaccines to minimize the RV associated childhood morbidity and mortality in the developing countries. In addition to the enhanced efficacy, the following attributes are desired of the future generation RV vaccines in low-resource settings to successfully improve vaccine coverage and availability.

1.1.6.3.1 Recombinant subunit vaccine with parenteral administration

Oral administration of the current RV vaccines is linked with their poor efficacy in the developing countries (as described above, Table 1.2). In addition, live, attenuated RV vaccines have been associated with the rare adverse event, intussusception. Intussusception is a medical condition in which a part of intestine slides into its adjacent part like shutting a telescope. This leads to obstruction of bowel movement, intense abdominal pain and reduced blood supply to that segment of the intestine. Replication of live viruses in the oral vaccines can trigger intussusception and thus there is some low associated risk with the current RV vaccines ⁶. In addition, there is always a risk of attenuated viruses reverting to the virulent form, especially in immunocompromised and prematurely born children ³⁷. Also, multiple live virus strains can potentially undergo reassortment with wild type strains in a common host and form new virulent

strains leading to an antigenic shift^{38,39}. Thus, based on these limitations of orally delivered, live attenuated RV vaccines, a recombinant subunit, parenterally administered RV vaccine would be an attractive alternative if it is able to provide comparable efficacy irrespective of the socioeconomic background of the child while devoid of any increased risk of intussusception or reversion^{14,29,40}.

1.1.6.3.2 Affordability and accessibility

The price of the two internationally available RV vaccines (oral, live attenuated) is very high (approximately 200 USD per course, CDC price list 2019) for resource limited countries to introduce them in their national immunization programs. Therefore, without the support from international organizations (such as Global Alliance for Vaccines and Immunization, GAVI), it is impossible for these countries to afford such expensive vaccines. Also, so far, GAVI support is available to low-income countries and not to lower-middle and middle-income countries which also face challenges in introducing RV vaccines. GAVI-eligible countries could get the vaccines at subsidized co-pay price of 0.40 – 10.5 USD per course⁴¹. This heavily subsidized price reflects the true price low-income countries can afford to accept these vaccines. Therefore, the new generation RV vaccines need to be produced at low cost so that they are available at affordable price to the developing countries which need them the most.

Rotasiil and Rotavac (recently WHO-prequalified) vaccines (oral, live attenuated) are priced at much lower cost (6.0 and 2.5 USD per course, respectively) and thus would be a valuable addition to the international market. These vaccines would provide relief to the GAVI-ineligible countries and countries about to graduate out of GAVI. In addition to the lower price, sustainable global supply of the childhood vaccines is a must to meet the demands of the countries with large birth cohorts. Some countries tend to hesitate from introducing new vaccines until supplies are

sufficiently abundant or a local manufacturer is available ⁴. Rotavac is a great example of an indigenously developed vaccine supplied at a more affordable cost in India (India is ineligible for RV vaccine support from GAVI). Successful introduction of this vaccine in the national immunization program of India is estimated to save 34,000 deaths annually and will also lead to significant decline in outpatient visits (21%) and hospitalizations (28%) due to RV ⁴². In addition, a thermostable vaccine, such as Rotasiil, can enhance the accessibility to more remote parts of the low resource countries since no extensive vaccine cold chain is required for storage and distribution.

1.1.6.3.3 Increased vaccine coverage

RV vaccines have been introduced in 91 countries (2017) including 41 countries supported by GAVI. Global RV vaccine coverage, however, is only about 28%. Troeger *et al.* estimated that full vaccine coverage could have averted 83,200 deaths due to RV in 2016 ¹. Apart from reducing the cost and maintaining consistent supply, vaccine coverage can be boosted by adding a compatible RV antigen to the current childhood combination vaccines. Combination vaccines have been in use for ~70 years and provide numerous benefits and value to society and the public healthcare system as described in Figure 1.5. Historically, DTaP and DTwP vaccines have been the cornerstone of combination vaccines, and recently a hexavalent vaccine, DTaP5-IPV-Hib-HepB, was approved in the US ⁴³. A pentavalent DTwP-Hib-HepB vaccine is available in the developing world. In the future, a recombinant protein-based RV vaccine could potentially be added with these types of combination vaccines to boost the RV vaccine coverage. Currently, there are numerous RV vaccine candidates in different stages of development with alternate routes of administration (oral, intramuscular, intradermal) and vaccine type (live attenuated, subunit

antigen, VLP) as listed in Table 1.3. Successful incorporation of these candidates in the immunization programs of developing countries will depend on the above-mentioned qualities.

Among all the promising new RV vaccine candidates in the pipeline, a trivalent subunit vaccine based on truncated VP8 proteins of P[4], P[6] and P[8] genotypes is the most advanced candidate offering alternate administration route (intramuscular) and vaccine type (non-replicating rotavirus vaccine, NRRV). The analytical characterization and formulation development of this trivalent non-replicating rotavirus vaccine (NRRV) candidate is the focus of this PhD dissertation work.

1.1.7 Trivalent non-replicating rotavirus (NRRV) vaccine candidate

This parenteral trivalent NRRV vaccine candidate was discovered at the NIH and is currently being developed by PATH and is being tested in clinical trials. The next few sections will describe the composition and nomenclature of the three antigens present in this candidate vaccine. Also, the key results from the pre-clinical work at NIH is highlighted along with the results from early stage clinical trials conducted by PATH. Finally, a perspective on the need for stable formulation development for this candidate vaccine is provided.

1.1.7.1 Composition and nomenclature

Each of the three antigens in this candidate vaccine is a fusion protein derived from the VP4, outer capsid protein of RV. As described above, viral infectivity is dependent on the cleavage of VP4 protein in the intestinal lumen into VP5* and VP8* proteins. VP8* protein is involved in the attachment of the virus to host cells and an immune response generating neutralizing antibodies against this protein antigen should provide protection. Wen *et al.* at NIH attempted to recombinantly express the individual VP5* and VP8* proteins in *E. coli* but were unsuccessful due to their insoluble nature. A truncated soluble version of VP8* with key epitopes intact was

successfully expressed and named as $\Delta VP8^*$ ⁴⁴. Further, a CD4⁺ T cell epitope (P2) from tetanus toxoid was fused at the N-terminus of $\Delta VP8^*$ via a GSGSG linker to create a fusion protein as shown in the schematic in Figure 1.6⁴⁵. The three recombinant antigens were named as P2-VP8-P[4], P2-VP8-P[6] and P2-VP8-P[8] where P2 is the carrier protein from tetanus toxoid, VP8 represents the $\Delta VP8^*$ segment of the VP8*, and P[4], P[6], P[8] denote the three genotypes from RV strains DS-1-like (G2P[4]), 1076-like (G2P[6]), Wa-like (G1P[8]), respectively.

1.1.7.2 Pre-clinical studies (NIH)

In the first study⁴⁴, guinea pigs hyperimmunized IM with each monovalent $\Delta VP8^*$ variant (250 μ g) elicited high levels of homotypic neutralizing antibodies (NAbs), and heterotypic NAb titers varied between the three antigens. $\Delta VP8$ -P[8] antigen elicited high levels of NAbs against P[4] and low levels against P[6] and P[10] genotypes. $\Delta VP8$ -P[4] elicited high levels of NAbs against P[8], and moderate to low levels against P[6] and P[10], respectively. $\Delta VP8$ -P[6] elicited low levels of NAbs against both P[8] and P[10] genotypes. In a dose-escalation (10–40 μ g/injection) study, guinea pigs immunized with $\Delta VP8$ -P[8] induced high levels of homotypic NAbs after 3 doses (NAbs levels were below detection after 2 doses). Aluminum based adjuvants were also tested with the $\Delta VP8$ -P[8] and no immunopotential effect was observed. $\Delta VP8$ -P[4] was also administered to mice mimicking the clinically relevant schedule and dose, high titers of homotypic IgG and NAbs were developed along with low levels of heterotypic IgG against P[8].

In the second study⁴⁵, Wen *et al.* showed that inclusion of a CD4⁺ T cell epitope (P2) at the N-terminus of the $\Delta VP8$ -P[8] and $\Delta VP8$ -P[6] antigens enhanced their immunogenicity in guinea pigs (IM immunization). Addition of an aluminum-based Adjuphos® (AP) adjuvant increased the immunogenicity of the P2-VP8-P[8/6] antigens. Also, in an oral challenge study with Wa-like G1P[8] RV strain, guinea pigs immunized with P2-VP8-P[8] vaccine containing AP

showed protection by delaying the onset and reducing the duration of diarrhea. Furthermore, P2-VP8-P[8] vaccine induced high levels of virus NAb in serum pre and post challenge, and RV specific serum IgA post challenge. Increasing trend in P[8] specific IgG titer was also observed post vaccination and post challenge. Increased levels of systemic and intestinal RV specific IFN- γ producing T cells (CD4⁺ and CD8⁺) were also observed post challenge.

1.1.7.3 Clinical studies (PATH)

PATH has conducted two clinical studies so far using the monovalent P2-VP8-P[8] antigen adsorbed to aluminum hydroxide (Alhydrogel, AH) adjuvant in South Africa. Phase I clinical trial (NCT01764256) was conducted in healthy adults and the vaccine was well tolerated with no adverse events. Increased (at least 4-fold) P2-VP8 specific IgA and IgG titers were observed in the serum. NAb response was found to be genotype specific as strong response was observed against P[8] strains compared to moderate and weak responses against P[4] and P[6], respectively. This result indicated that a multivalent vaccine containing all three antigens may be needed to provide broad serotype coverage. Intestinal mucosal immune response was also evaluated by measuring IgA and IgG titers in lymphocyte supernatant and a dose dependent increase in IgA was observed

46.

As the next trial, a Phase I/II descending age, dose-escalation study (NCT02109484) was conducted in infants and toddlers using AH bound monovalent P2-VP8-P[8] vaccine. Three dose levels of 10, 30 and 60 μ g were tested. Overall, the vaccine was well tolerated at all dose levels without notable adverse reactions. At each dose level, anti P2-VP8-P[8] IgG titers were high and IgA response was also recorded in most infants. Strong NAb response was observed against the P[8] type RV strains whereas moderate to no response was observed against P[4] and P[6] types, respectively. This is consistent with the findings of the Phase I trial and supports the rationale of

having all three P type antigens in the subunit NRRV vaccine. Reduced shedding of the Rotarix vaccine in feces was also observed which is indicative of some level of mucosal immunity. Based on the findings of this study, a Phase I/II descending age, dose-escalation study to test the safety and immunogenicity of the trivalent vaccine in adults, toddlers and infants is underway at three sites in South Africa ⁴⁷.

1.1.7.4 Need for vaccine formulation development

Apart from the clinical safety and efficacy of a vaccine candidate, pharmaceutical stability is equally important for its successful development and eventual commercialization. The goal of this dissertation work is to develop stable formulations for both the bulk drug substance and the final drug product of the NRRV vaccine candidate. In this work, drug substance refers to the three P2-VP8-P[4/6/8] NRRV proteins which will be stored as frozen monovalent bulk antigens, and drug product refers to the monovalent NRRV antigens individually bound to aluminum adjuvant (Alhydrogel) and stored as a liquid presentation at 2–8°C. The clinical presentation of the NRRV vaccine will be a trivalent, Alhydrogel-adjuvanted formulation containing all three of the P2-VP8-P[4/6/8] protein antigens in one vial, and this presentation was not evaluated in this work.

Successful formulation development of a recombinant protein subunit vaccine containing adjuvant typically involves the following five steps: (1) development of analytical tools to characterize key structural attributes of the antigen, (2) elucidation of the physicochemical degradation pathways of the antigen, (3) designing formulation composition to minimize degradation of the bulk drug substance during storage, (4) understanding the effect of adjuvant and other excipient(s) on the structural integrity and physicochemical stability of the antigen, and (5) evaluating the long-term storage stability of the vaccine drug product. The next section of this

introductory chapter will discuss various analytical tools to characterize and develop protein-based adjuvanted subunit vaccines.

1.2 Analytical tools to characterize and develop subunit vaccines

Vaccines are complex biological preparations with multiple components, and in the case of recombinant subunit vaccines, includes both antigens and adjuvants. Maintaining vaccine stability and quality (drug substance and drug product) during various stages of development (pre-clinical studies, clinical trials), and post approval (manufacturing and distribution) is challenging and requires a robust set of analytical tools to monitor the key structural attributes of a vaccine⁴⁸⁻⁵⁰. This analytical toolbox can, in general, be divided into two groups, potency assays to monitor antigenicity/immunogenicity and physicochemical assays to monitor structural integrity and adjuvant interactions as described in Table 1.4. It is important to appreciate that each subunit vaccine drug product (antigen, adjuvant, excipients) is unique and thus the list of analytical tools in Table 1.4 is not comprehensive and not all assays are applicable to every subunit vaccine candidate. These tools serve a variety of purposes as discussed below to ensure the safety and efficacy of a vaccine throughout its product development and post licensure life-cycle.

1.2.1 Potency assays

Potency is defined as “the measure of the biological activity using a suitably quantitative biological assay (also called potency assay or bioassay), based on the attribute of the product which is linked to the relevant biological properties”⁵¹. Potency assays are product specific release and stability tests that are also used to ensure batch to batch consistency in the manufacturing process⁵². However, it is important to point out that potency assay is not a measure of vaccine efficacy in humans, and thus potency assay results are not necessarily reflective of the protective mechanism of the vaccine. A potency assay can be either *in-vitro* and/or *in-vivo* with the following desirable

properties (1) can measure biological activity, (2) can provide quantitative comparison with a reference standard, (3) can be validated during development i.e. assay is “developable”, and (4) can be integrated in the quality control^{53,54}. Selection of a potency assay depends on the knowledge regarding the mechanism of action of the vaccine and how well the assay can be correlated to the efficacy while adhering to the principles of the 3R rule to minimize testing in animal models (Replace, Reduce, and Refine)^{55,56}.

1.2.1.1 In-vivo assays

Generally, the mechanism(s) of immune protection of a new vaccine candidate is not completely understood during early development and *in-vivo* animal studies are conducted to identify the correlate(s) of protection. Historically, these tests have also been used to assess the potency of a vaccine during lot release to ensure the consistency in the manufacturing process⁵⁷. In contrast to biological drugs such as antibodies or enzymes (which bind antigens and catalyze chemical reactions, respectively), many vaccine antigens lack an identifiable biological activity other than its ability to elicit an immune response, a property historically assessed in animal models. Among all the analytical tools available to study and characterize vaccines, *in-vivo* functional and immunogenicity assays are presumably most representative of the observed efficacy in humans as depicted in the Figure 1.7⁵⁸.

In-vivo potency assays can themselves be broadly categorized into two general groups, immunization-challenge studies and serological analyses. In an immunization-challenge study, the animal subjects are first immunized with the vaccine and then challenged with the relevant virulent strain of the pathogen. Potency of the vaccine is determined by comparing the relative number of immunized and non-immunized animals surviving the challenge⁵⁹. Among the currently licensed vaccines in the US, lethal immunization-challenge tests are used for potency determination of

rabies and anthrax vaccines. There is an ongoing push towards refinement of such tests to include other endpoints such as body weight, body temperature and biological marker levels instead of the crude endpoint of death to minimize animal pain and distress. To this end, serological analyses can serve as excellent alternatives to immunization-challenge tests and help in refinement of the use of animals in *in-vivo* potency assays. These assays measure different aspects of the immune response such as specific antibody titers, T cell counts, cytokine levels or other biological markers relevant to the potency of the vaccine ⁵⁷. A variety of high throughput assay formats such as ELISA, multiplex assays, and flow cytometry are available to carry out serological analyses, however, they do require a detailed understanding of the mechanism of action of the vaccine. Several US-licensed vaccines such as inactivated polio, acellular pertussis, diphtheria, and tetanus vaccines employ serological analyses as potency assays ^{55,57,60}.

Although animal studies are most relevant to the mechanism of action of a vaccine, they tend to be highly variable, time consuming (1-2 months), expensive, laborious, raise ethical questions, and pose risks to laboratory staff working with virulent strains. *In-vivo* tests were heavily used in the past because analytical technologies were not available or fully developed to perform a comprehensive characterization of the vaccine itself. Also, vaccines can be more complex in terms of their composition and often times protective antigen(s) in the vaccine are not well-defined (for example whole cell inactivated pertussis vaccine). With the advent of recombinant DNA technology, the recombinant protein vaccines against hepatitis B and human papilloma viruses were developed and produced as well-defined protein antigens (virus-like particles) with a better understanding of their antigenic composition. Hence many of the critical quality attributes (e.g., protective epitopes, structural integrity, size) are known and can be assessed by modern *in-vitro* potency assays and physicochemical analyses ^{58,60}.

1.2.1.2 In-vitro assays

There is always a goal to replace *in-vivo* potency assays with *in-vitro* potency assays for both currently used vaccines and new vaccine candidates in pipeline due to above mentioned reasons. Apart from not requiring the use of animals, *in-vitro* potency assays tend to be more consistent, higher throughput, more cost-effective and more robust. However, they may correlate less strongly with the biological activity compared to the *in-vivo* assays (e.g., ability to generate a specific immune response). Also, development of successful *in-vitro* potency assays requires a good understanding of the correlate(s) of protection of a vaccine, for example, *in vivo* antibody response vs. a known neutralizing epitope⁵⁶. Commonly used *in-vitro* potency assays for testing of subunit vaccine antigens can be grouped into two general categories: cell-based assays and immunochemical binding assays.

1.2.1.2.1 Cell-based assays

Cell-based *in vitro* potency assays are often employed to monitor the ability to generate a particular phase of an immune response and a specific biological marker(s). For example, these assays can be used to measure the frequency and functions of cellular responses (B cell and/or T cell) to a particular stimulus. Enzyme-linked immunospot (ELISpot), T cell proliferation, multiplex array techniques, flow cytometry, cytotoxic potential, tetramer staining are examples of various cell-based assay formats employed alone or in combination to study the immune response to antigens during subunit vaccine development⁶¹⁻⁶⁵. In particular, ELISpot assays can be used to measure antigen-specific B cells. The vaccine antigen is coated to a plate and B cells are added which upon antigen recognition would secrete antibody. The secreted antibody is detected by a secondary antibody which upon reaction with a substrate leads to visible precipitation as spots. ELISpot can also be used to measure frequency of T cells secreting a particular cytokine upon

antigen stimulation. T cell proliferation assay is another example of a cell-based assay which measures division of T cells upon activation by an antigen. A fluorescent dye or radioisotope can be introduced into the cell and loss in signal can be monitored which is indicative of cell division⁶³. Historically, cell-based potency assays have been more difficult to implement in regulatory fillings since extensive analytical validation is needed. Successful development of cell-based potency assays also requires thorough understanding of the disease pathology and correlate(s) of protection. Since such information is not always readily available during the early stages of vaccine development, these methods have to date found little application to vaccine quality control and are more often used as supportive analytical characterization assays⁵⁹.

1.2.1.2.2 Binding assays (immunochemical assays)

Enzyme linked immunosorbent assays (ELISA) are a commonly used *in-vitro* immunochemical method to measure either the identity, concentration, potency, antigenicity, or conformational integrity of the recombinant protein antigens, depending on the nature of the antibody used (e.g., specific vs. non-specific, neutralizing vs. non-neutralizing, linear vs. conformational epitopes). Affinity and avidity of the antibody reagent towards the target antigen determine the sensitivity and selectivity of the assay. Depending upon the size and nature of the antigen and available immunochemical reagents, different formats of this assay are used such as sandwich (direct or indirect) and inhibition/competition ELISA⁶⁶. An ELISA-based assay is used as an *in-vitro* potency test to quantify protective antigens in the approved subunit vaccines for hepatitis B and human papilloma viruses⁶⁰.

Single radial immune diffusion assay is another example of an *in-vitro* immunochemical method used to assess the potency (native antigen content) of influenza vaccines since 1978⁶⁷. The assay is based on the principle of diffusion of an antigen through antigen-specific antibody

present in an agarose gel plate. The size of the ring formed, due to an immunoprecipitation reaction when the antibody-antigen complex reaches a critical ratio during the antigen's migration through the gel, is proportional to the amount of antigen in the sample by comparison to standards of known antigen concentration. This is a relatively straightforward and user-friendly assay but comes with disadvantages of time consuming, low through-put and having a small linear range of quantitation⁶⁸.

Bio-layer interferometry (BLI) and surface plasmon resonance (SPR) are emerging label-free techniques which also work on the principle of formation of antibody-antigen complexes by binding reactions. In addition to their specificity and sensitivity, a key advantage of these methods lie in capturing the real-time binding kinetics of both association and dissociation steps, thus, enabling the determination of dissociation rate constant of binding (k_d). Lower k_d is reflective of higher avidity of the antibody and vice versa⁶⁹. These methods have short run times and are highly automated to provide higher throughput as compared to traditional ELISA assays. Also, the higher degree of reproducibility and ease of use make them suitable for *in-vitro* testing in vaccine research and development settings. BLI and SPR techniques have been used in numerous basic research studies involving multiple vaccine candidates and will soon likely enter the routine quality control laboratories^{70,71}.

1.2.2 Physicochemical Assays

As a complement to potency analysis of vaccines, modern physicochemical assays can define key structural attributes and stability parameters which in turn can potentially be linked to immune protection *in-vivo*⁷². Also, as part of routine vaccine release/stability QC tests, it is desirable to implement *in-vitro* physicochemical assays, to complement potency assays, due to practical advantages such as higher throughput, lower cost, better reproducibility and accuracy

(Figure 1.7). Many recombinant subunit protein vaccines are comprised of purified antigens which can be better characterized (both physically and chemically) as compared to many of the older generation vaccines containing intact viruses (e.g., live attenuated, inactivated). Thus, apart from maintaining consistent potency, regulatory expectations are high in terms of batch to batch monitoring of identity, purity, structural integrity of subunit vaccines ⁴⁹. A battery of physicochemical assays are often used to define critical quality attributes (CQAs, i.e., key aspects of structural integrity, stability, and immunological potency) of a protein-based antigen. The analytical testing of CQAs are then performed to ensure product quality and consistency during manufacturing.

During vaccine process and product development, analytical tools are employed to perform physicochemical characterization of the vaccine antigen(s) and forced degradation studies are conducted to deduce the degradation routes for each antigen. These analytical results are used as part of comparability studies that ensure product quality during process changes during development. Since only limited material is typically available during early development, it is important to identify the right set of analytical tools which are the most informative yet also consume minimal material. Further, stability-indicating methods are identified from forced degradation studies to perform formulation development for both vaccine bulk drug substance and final drug product (described in the next section). A large toolbox of physicochemical methods is available to facilitate characterization, pre-formulation evaluation, formulation development, comparability assessments and storage stability evaluations of subunit antigens (Table 1.4). The utility of these methods is described below in the context of drug substance and drug product vaccine development. It is important to note that only a subset of methods in Table 1.4 are employed (at each stage or during routine lot release testing) based on the information needed and

sensitivity, specificity, precision, transferability, robustness and throughput of the assay. In addition, regulatory requirements and cGMP compliance are also taken into consideration ^{57,73}.

1.2.2.1 Testing of bulk drug substance (DS)

For a protein-based subunit vaccine, bulk drug substance refers to the monovalent protein antigen(s) formulated in an optimized formulation buffer to ensure stability during long-term storage prior to subsequent formulation into a final vaccine drug product. Bulk protein antigens are typically stored frozen to minimize physical and/or chemical degradation due to environmental and mechanical stresses. Subsequently, the DS is thawed, formulated with excipients and adjuvants, diluted to the appropriate dose and then fill-finish is conducted under aseptic conditions to produce the final, sterile vaccine drug product in the appropriate container for clinical or commercial use. A variety of physicochemical techniques are used to characterize and compare the primary and higher-order structures, post-translational modifications, conformational stability and aggregation propensity of the antigen as shown in Table 1.4. In addition, forced degradation studies are performed to elucidate degradation pathways of chemically labile residues or “weak spots” and analytical tools are developed to monitor/quantify degradative changes and degradation products. The most informative physicochemical assays are applied to the formulation development of DS (and DP, see below) to ensure structural integrity and physicochemical stability of the vaccine throughout its manufacturing and during long term storage (shelf life).

In terms of the regulatory requirements, physicochemical tools are needed to ensure lot to lot consistency in terms of identity, purity, potency and quantity of the DS ⁵¹. Peptide mapping using mass spectrometry coupled with liquid chromatography (LC-MS) is the method of choice for not only identifying the protein antigens, but for monitoring primary structure and post translational modifications. Identity tests can be a combination of physicochemical and

immunochemical methods and can also be qualitative in nature. In terms of impurities, the nature and levels depend on the analytical methods used. Therefore, multiple orthogonal methods are used to assess the presence of product related impurities such as charge, mass, size, and other variants (Table 1.4). Process-related impurities such as host-cell DNA, host-cell proteins are also monitored and quantified using appropriate techniques. Finally, potency testing of the DS may or may not be routinely performed (depending if a potency assay is available for DP) and the quantity of DS is evaluated using total protein mass assays. In addition to the above attributes, it is also expected to demonstrate the overall structural integrity and stability of the bulk drug substance protein antigens during storage ⁵¹.

1.2.2.2 Testing of drug product (DP)

For a subunit vaccine, DP is defined as the pharmaceutical product in the appropriate final container which contains DS diluted to the appropriate dose, along with addition of adjuvant(s) and a formulation buffer containing suitable excipients (e.g., surfactant, preservatives). For an adjuvanted vaccine DP, it is very important to understand the antigen-adjuvant interactions and their effect on the antigen structure and physicochemical stability to ensure optimal vaccine safety and efficacy. Aluminum-based salts, for example aluminum oxyhydroxide (Alhydrogel®) and aluminum phosphate (AdjuPhos®), are the most commonly used adjuvants in commercially available vaccines. A key challenge in the analysis of DP is to develop analytical methods to assess the structural integrity and physicochemical stability of the antigen (typically at low protein mass levels) bound onto the surface of the aluminum adjuvant. There is a growing need to expand the repertoire of assays that can work with the antigen bound to the surface of aluminum since antigen desorption process can induce artifacts (see forced-desorbed antigen section below). As shown in Table 1.4, a combination of analytical tools is employed to assess some quality attributes of the

antigen in the bound state and some attributes are studied after forced desorption of the antigen from the aluminum surface.

1.2.2.2.1 Testing of protein antigen bound to aluminum adjuvant

Analysis of protein bound to aluminum adjuvant is challenging due to low doses of antigen present, the irreversibility of adsorption, and the turbid nature of aluminum adjuvant containing formulations⁷⁴. The extent of antigen binding and the strength of interaction between antigen and aluminum adjuvant are important parameters for storage stability as well as optimum immune response. This concept has more recently been shown to be antigen-adjuvant pair specific and thus needs to be evaluated during part of early vaccine development⁷⁵. Langmuir binding isotherms can be used to determine the adsorptive capacity (maximum amount of a protein that can bind as a monolayer on the surface of the adjuvant) and adsorptive strength (strength of interaction between an antigen and an adjuvant) of the aluminum adjuvant for an antigen in a particular formulation. Quantity of antigen (both bound to adjuvant and potentially free in solution) and *in vitro* potency of the formulated vaccine can be demonstrated using immunochemical methods as listed in Table 1.4. Structural integrity and conformational stability of the antigen in bound state can be determined by selected biophysical tools amenable to turbid samples (e.g., DSC). Moreover, characterization of adjuvant itself and its stability is also important in terms of particle size, surface charge, morphology and chemical composition. These adjuvant properties are also evaluated using the same physicochemical tools as mentioned above as part of the DP studies.

1.2.2.2.2 Forced-desorption studies to remove antigen from adjuvant

Many of the analytical methods used for characterizing protein antigens in solution are incompatible with the aluminum adjuvanted subunit vaccines as described above. Therefore, to employ such methods, antigen is forced-desorbed from the aluminum adjuvant surface and then

assayed. Forced desorption can be achieved by surface charge neutralization of the adjuvant (e.g., adding phosphate salts to aluminum oxyhydroxide) or by dissolving aluminum (using α -hydroxycarboxylic acids such as citric acid, lactic acid, and malic acid) ^{76,77}. However, potential problems with forced desorption include, (1) harsh components of the desorption buffer could still interfere with the analytical method, (2) desorption process could perturb the antigen structural integrity and induce artifacts, and (3) poor recovery after desorption might lead to misrepresentation of the analyte species. If successfully desorbed, the antigen can be analyzed using LC-MS peptide mapping (similar to DS) to monitor and quantify post translation modifications. Further, purity and heterogeneity can be assessed using a combination of spectroscopic and electrophoretic methods as listed in Table 1.4. Depending on the success of the desorption method, both at time zero and during storage (desorption can become more difficult over time due additional interactions between the antigen and adjuvant), a wide variety of analytical methods used for physicochemical characterization of proteins should be applicable as long as there is no matrix effect from the desorption procedure.

1.3 Formulation development of subunit vaccine candidates for developing countries

Apart from being safe and efficacious, a vaccine should be affordable and readily available to achieve success especially in the low-resource settings of developing countries. Development and progression of a vaccine from the concept to clinical trials to regulatory approval and large-scale immunization programs is a complex, long and multi-step process. Formulation is a key step in the development process which ensures the potency, structural integrity and stability of the DS during manufacturing and storage, and the DP during fill-finish, long term storage, transportation and administration ⁷⁸⁻⁸³. The focus of this section will be formulation development strategies (including bulk antigen and drug product manufacturing) for subunit vaccines with the aim to

minimize their cost. Also, the importance of establishing an interface between DS and DP formulation development efforts will be highlighted.

1.3.1 Vaccine bulk antigen (DS) manufacturing

Producing bulk drug substance antigen (DS) is the first step of producing a subunit vaccine followed by final drug product manufacturing (formulation, fill-finish, packaging), QC release testing, and distribution steps⁸⁴. Bulk antigen production is often the most complex, time consuming and expensive part of the overall vaccine manufacturing process. Depending upon the number of antigens present in a vaccine, especially for multi-valent vaccines, multiple bulk preparations could be needed to produce each required antigen separately. Historically, the process/method, equipment and facility used is antigen-specific and thus needs to be custom built in most cases. This leads to the high costs of bulk antigen production and thus overall high cost of the vaccine. So, in order to keep the cost of vaccine lower, it is imperative to choose the right manufacturing process, equipment and facility for bulk antigen production.

The antigen manufacturing process, e.g., the expression system, can have a profound impact on the facility and infrastructure requirements, cost of product and the ease of regulatory approval⁸⁴. The most commonly employed expression hosts for subunit vaccine antigen production are bacteria, yeast, insect, or mammalian cell culture-based systems. Each of these methods have their advantages and disadvantages in terms of production speed, yield, cost, post-translational modification ability and ease of regulatory approval as listed in Table 1.4⁸⁴. From a developing country standpoint, low cost is key while still ensuring quality. The overall cost per dose also needs to be evaluated by taking into account the yield, speed, complexity, scalability and flexibility of the process used at the required scale^{84,85}. Complex manufacturing processes for multivalent antigens (such as for acellular pertussis, human papilloma virus, meningococcus,

pneumococcus) tend to increase the cost and lower the production capabilities of a facility which in turn can disrupt the global supply of a vaccine ⁸⁶. Therefore, the production process needs to be simple and robust to consistently produce the bulk antigen(s) at a large scale with acceptable quality and affordable cost.

Due to the high demand for affordable vaccines in the developing countries, setting up local manufacturing sites can help to reduce the cost and provide sustainable supply. Local manufacturing facilities gain from lower cost associated with real estate, construction, labor, maintenance, and transportation ⁸⁵. This is supported by the fact that majority of low cost vaccines acquired and distributed by UNICEF are now manufactured in developing countries ⁸⁷. However, setting up a new facility in low-resource settings is challenging as it requires a large initial investment, high cost of operation, need for technology transfer and training from established manufacturers, and a considerable lead time before any revenue is generated. In addition, if the facility is located in a remote place, it could become difficult to acquire raw materials, secure reliable sources of water and electricity, get technical support and/or identify/train skilled workers. Furthermore, a single facility cannot produce all vaccines due to differences in fermentation and purification methods, formulation requirements, and safety considerations. Thus, multiple facilities are needed. Overall, the goal of a vaccine-specific local manufacturing facility is to produce optimal number of doses per year to keep the operational costs low and meet the local vaccine demand ⁸⁴.

1.3.2 Interface between DS and DP formulation development to improve efficiency

The DS formulation is ideally rationally designed after a series of studies in the early development phase including physicochemical characterization (to identify key structural attributes), pre-formulation characterization (forced degradation studies to identify residues and

epitopes susceptible to degradation), excipient screening (to identify additives to minimize degradation and maintain bulk antigen structural integrity and physicochemical stability), and freeze-thaw evaluations (to ensure stability during freeze-thaw) ^{72,74}. The goal of DS formulation is to provide optimum stability to the bulk antigens during storage and subsequent fill-finish operations. The purified bulk antigen is usually stored as a frozen liquid and this is useful since often times bulk manufacturing facilities can only handle one antigen at a time. This provides the operational flexibility to produce multiple batches of each antigen when manufacturing multiple antigens for multivalent vaccines.

The frozen bulk antigens are transported to a separate fill-finish facility where they are thawed, diluted to the appropriate dose while formulated with adjuvant and other excipients (e.g., preservative if making a multi-dose presentation). For subunit vaccines, aluminum-based salts are the most commonly used adjuvant (as described in the next section) ⁷⁵. It is important to characterize the physicochemical stability of the antigen in the presence of adjuvant as well as antigen-adjuvant interactions for optimal vaccine performance ^{74,75}. Thus, the formulation parameters (such as buffer type, salt, pH, ionic strength) often require some re-optimization when the adjuvant is introduced into the DP. This may lead to another buffer exchange step for the DS (after thawing) into a formulation buffer which is compatible with the adjuvant. This additional step can cause timeline delays, extra expenses, and compromise the integrity or stability of the bulk antigen. To avoid such a scenario and make more efficient utilization of time and resources, it is imperative that there is good communication between the DS and DP formulation teams. Therefore, the DS formulation should be designed keeping in mind the compatibility of the antigen with the additional components which will be introduced during DP formulation (e.g., adjuvants and preservatives).

1.3.3 Vaccine drug product (DP) formulation

A subunit vaccine DP formulation contains antigen(s) and adjuvant(s) at the appropriate dose levels, a preservative (if making multi-dose presentation), as well as the DS formulation components. Since cost is a major hurdle while introducing new vaccines in the developing countries, the next few sections will briefly describe three formulation strategies to either reduce the cost of a subunit vaccine (and/or increase the vaccine coverage), and the associated formulation development challenges with each strategy.

1.3.3.1 Low-cost aluminum adjuvants

Adjuvants are often added to subunit vaccines to enhance their immunogenicity (cellular and/or humoral) and provide a more robust protection. There are a variety of adjuvants available to use such as aluminum-based (e.g., Alhydrogel, AdjuPhos, AS04), emulsions (e.g., MF59, AS03, AF03), liposomes (e.g., ISCOMS, CAF01, AS01E, AS01B, AS15), polymeric particles (PLG microparticles), and immunostimulatory compounds (MPL, QS-2, CpG) as well as combinations of these adjuvants. Apart from immunopotential effect, adjuvants can lead to dose sparing, reduction in the number of booster shots, enhancement of immunogenicity in immunocompromised populations, improvement in antigen stability and delivery ⁸⁸. These adjuvant systems differ in terms of their effect on antigen stability and location of antigen w.r.t. the adjuvant, and poses a variety of advantages and challenges ⁸⁰.

Aluminum adjuvants have been used in human vaccines for over nine decades and have a long record of safety and immunopotential. The adjuvant property of aluminum containing compound was first realized in 1926 when diphtheria and tetanus toxoids were precipitated in the presence of alum (aluminum potassium sulfate) and improved immunogenicity was recorded compared to soluble toxoids ⁸⁹. Antigen co-precipitation with alum salts has been replaced with

antigen adsorption to physically and chemically well-defined, preformed aluminum based adjuvants (Alhydrogel®, aluminum oxyhydroxide and Adju-Phos®, aluminum phosphate)⁷⁵. The scientific community has recently gained a better understanding of these adjuvants in terms of their mechanism of action, physicochemical properties, storage requirements, stability challenges and interaction with antigens⁷⁵. Most importantly, these adjuvants are readily available worldwide and are inexpensive compared to other adjuvant types, and therefore, make a suitable candidate for incorporation into subunit vaccines for developing countries⁸⁰.

From a vaccine stability and efficacy perspective, it is very important to optimize the aluminum adjuvant containing DP formulation to obtain optimal results. This includes optimization of antigen-adjuvant interactions (extent and strength of adsorption), characterization of the physicochemical integrity and stability of the antigen on the surface of aluminum and correlation of these factors to the potency of the vaccine^{74,75}. One major stability challenge with the use of aluminum adjuvants is their sensitivity to freeze-thaw which causes agglomeration of the aluminum particles leading to the loss of vaccine potency and potential safety risks^{90,91}. Consequently, commercially available aluminum adjuvanted vaccines are stored at 2-8°C and accidental exposure to subzero temperatures can be identified by using temperature sensitive vaccine vial monitors and/or by conducting a ‘shake test’ in the field^{78,92}. Also, some studies have demonstrated the use of various excipients (such as freezing point depressants, carbohydrates, etc.) can help to prevent aluminum adjuvant agglomeration upon freezing⁹².

1.3.3.2 Multi-dose presentation

Using multi-dose presentation is an effective strategy to reduce the cost of vaccine per dose. Multi-dose vials offer numerous economic advantages over single dose formats; (1) lower overall vaccine cost which comprises of production, packaging and overfill adjustment, (2) lesser

cold-chain volume requirement in terms of storage and transport, and (3) the medical waste volume generated is lower^{93,94}. However, this strategy is not suited for all vaccination campaigns and economic benefits depend on the intrinsic cost of the vaccine, frequency of patients arriving for vaccination (i.e., vaccine demand) and vaccine wastage. Therefore, the number of doses that go into an individual vial needs to be carefully assessed to minimize the overall cost of the immunization program and could vary from one vaccine to another⁹⁵. In general, multi-dose formats would be cost-effective for mass vaccination campaigns which are popular in the developing countries. Since there is a risk of microbial contamination during withdrawal of multiple doses from the same vial, multi-dose drug product requires the addition of a preservative or an anti-microbial agent to prevent contamination⁹⁶.

Addition of a preservative to a subunit vaccine, however, is challenging as it can affect the physicochemical stability and/or potency of the vaccine. Addition of thimerosal, a commonly used preservative in vaccines in developing countries, is known to reduce the potency of HPV and IPV vaccines over time as measured by *in vitro* binding assays and *in vivo* immunogenicity studies^{97,98}. Furthermore, deleterious effects of thimerosal have been recorded with foot-and-mouth disease virus-like particles (dissociation of VLP) and hepatitis B vaccine (reduced immunogenicity)^{99,100}. Therefore, it is very important to assess the compatibility and stability of the vaccine antigens with various preservatives.

1.3.3.3 Combination vaccines

Another strategy to reduce the overall cost of immunization programs is to combine multiple vaccines into a single dose. Impact of combination vaccines can be divided into three groups, (1) societal and public health value, (2) economic value, and (3) value of innovation. Societal value includes benefits for children, parents, and healthcare providers. Increased

compliance and timeliness of vaccination provide better protection to children, and reduced number of shots cause less pain and discomfort. Fewer number of vaccination visits lead to better acceptance among parents and health care providers benefit from lower risk of needle stick injuries. Public health is improved with combination vaccines due to increased vaccine coverage, reduced risk of missed or delayed vaccination, and better opportunity for introduction of new vaccines in the childhood immunization schedules. Economic benefits of the combination vaccines include reduced cost of vaccine packaging, storage, handling and transportation ¹⁰¹⁻¹⁰³. However, formulating multiple vaccine antigens together in a single dose can be an immensely challenging task.

It is required in a combination vaccine that there are no deleterious physical/chemical interactions between the different antigens (or between any two formulation components) which reduce the safety or immunogenicity of any individual antigen/vaccine. More extensive laboratory testing and clinical trials are needed to ensure the safety and efficacy of the combination vaccines. Therefore, it takes a very long time before combination vaccines are developed, evaluated and approved by the national and international regulatory authorities ¹⁰². Nonetheless, due to their enormous societal and cost benefits, combination vaccines have evolved from initial trivalent DTwCP (whole cell inactivated pertussis) vaccine to recently approved hexavalent acellular pertussis containing vaccine DTaP-IPV-Hib-HepB ⁴³. The long-term goal of NRRV vaccine development is to introduce the NRRV vaccine antigens into the current childhood combination vaccines to enhance patient compliance, lower the immunization costs, and increase the RV vaccine coverage.

1.4 Tables

Table 1.1. Comparison of currently available RV vaccines. (Adapted and modified with permission from Ref. 4⁴)

Name	WHO Prequalified				Licensed for national markets	
	Rotarix	RotaTeq	Rotavac	Rotasiiil	LLR	Rotavin-M1
Manufacturer, country	GlaxoSmithKline Biologicals, Belgium	Merck, USA	Bharat Biotech International Limited, India	Serum Institute of India Limited, India	Lanzhou Institute of Biological Products, China	Center for Research and Production of Vaccines, Vietnam
Year of Approval	2006	2006	2014	2017	2000	2007
Price per vaccination course	From approximately US\$0.50 in GAVI-eligible countries up to US\$185–\$226 in the USA ¹		US\$ 2.50	US\$ 6.00 maximum	US\$ 72.00	US\$ 17.60
Strain(s) present in vaccine	Attenuated human G1P[8] strain	Human-bovine reassortant strain with G1, G2, G3, G4, and P[8] proteins	Human G9, P[11] strain	Human-bovine reassortant pentavalent (G1-G4, G9) strain	Lamb G10P[12] strain	Human G1P[8] strain
Formulation Presentation	1. Liquid vaccine in single-dose applicator or squeezable, polyethylene tube 2. Lyophilized vaccine, reconstituted with calcium carbonate buffer	Liquid vaccine in squeezable tube	Liquid vaccine in single- and multi-dose vial. Liquid antacid buffer given before the vaccine	Lyophilized vaccine, reconstituted with calcium carbonate buffer	Liquid vaccine with buffer	Liquid vaccine in single-dose vial
Vaccine vial monitor (VVM) on label	Yes, VVM 14	None	Yes, VVM 2	Yes, VVM 30	None	None
Storage requirements	2 to 8° C, not frozen and protected from light	2 to 8° C, not frozen and protected from light	Frozen at –20°C ± 5°C	Stable at 37°C for two years and 40°C for six months	2 to 8°C	Frozen at –20°C ± 5°C
Route of administration	Oral	Oral	Oral	Oral	Oral	Oral
Number of doses and dosing schedule	Two doses, given on same schedule as DPT vaccine	Three doses, given on same schedule as DPT vaccine	Three doses, four weeks apart, beginning at 6 weeks of age	Three doses, four weeks apart, beginning at 6–8 weeks of age	One dose every year for three years between 2 and 35 months of age	The first dose from 6 weeks of age. The second dose after 1–2 months. Should be given before 6 months of age.
Licensure and Availability	Internationally licensed, available in > 100 countries		Licensed in India, will soon be available for procurement by UN and GAVI		Licensed in China	Licensed in Vietnam

¹Price varies depending on the country

Table 1.2. Potential factors for the reduced efficacy of orally administered, live attenuated viral RV vaccines in developing countries.

Factor	Interference	Proposed solution
Breast milk composition and feeding ^{15,28-30}	RV specific IgA can reduce vaccine viral titer and glucoconjugates in milk can mimic the RV receptor in small intestines	<ol style="list-style-type: none"> 1. Higher vaccine dose 2. Withholding breastfeeding for some time before and after vaccine administration
Maternal immunity ^{29,31,32,104}	Transplacental acquired RV specific IgG can lower seroconversion	<ol style="list-style-type: none"> 1. Delay immunization till antibodies wane off 2. Add another booster shot 3. Increase vaccine dose
Co-vaccination ^{29,105}	Oral polio vaccine can reduce RV vaccine effectiveness	<ol style="list-style-type: none"> 1. Different immunization schedule
Co-infections ^{15,29,32,106}	High pathogen or co-infections (HIV, tuberculosis, malaria) burden can lead to diminished induction of mucosal immunity	<ol style="list-style-type: none"> 1. Maintaining community hygiene and environmental sanitation
Malnutrition ^{15,107-109}	Certain micronutrients have been found to be key regulators in gut immunity essential for both innate and adaptive responses	<ol style="list-style-type: none"> 1. Zinc supplementation 2. Vitamin A and D supplementation
Gut microbiota ^{31,106,109,110}	May directly or indirectly affect vaccine efficacy and the development of effective and durable mucosal immune responses	<ol style="list-style-type: none"> 1. Probiotic supplementation with individual and combinations of species, to alter the composition of gut microbiota
Environmental enteropathy ³⁰	Functional and anatomical alterations of the small intestines of the children living in poor settings with lack of hygiene and basic sanitary facilities	<ol style="list-style-type: none"> 1. Domestic sanitation 2. Personal hygiene
Others (Host genetic make-up, RV strains) ³²	<ol style="list-style-type: none"> 1. Expression levels of RV receptors (HBGAs) depend on genetic make-up 2. Prevalent RV strains could differ from ones present in the vaccines 	<ol style="list-style-type: none"> 1. Personalized vaccine approach similar to Hep B vaccine for people of specific HLA haplotypes 2. New generation vaccines with broader/relevant serotype coverage

HBGAs – Histo blood group antigens

HLA - Human leukocyte antigen

Table 1.3. RV vaccines currently in development with alternate routes of administration and vaccine types. (Reproduced with permission, from Ref. 29²⁹)

Stage of development	Name/type	Composition	Route of administration	Organization/company
Phase III	LLR reassortants	Live attenuated lamb-human reassortant rotavirus strains, G2, G3, G4	Oral	Lanzhou Institute of Biological Products, China
Phase III	RotaShield	Live attenuated rhesus-human reassortant rotavirus strains, tetravalent	Oral	International Medica Foundation and PATH, USA
Phase III	UK reassortants	BRV Tetravalent, G1–G4	Oral	Shantha Biotech, India
Phase IIb	RV3	Live attenuated neonatal rotavirus strain, G3P[6]	Oral	Murdoch Children’s Research Institute, Australia and Biofarma, Indonesia
Phase II	Subunit	Truncated VP8 of P4, P6, P8	Intramuscular	National Institutes of Health and PATH, USA
Phase I	UK reassortants	Bovine UK Human G1, G2, G3, G4, G9 reassortants 5V	Oral	Instituto Butantan, Brazil
Phase I	UK reassortants	Live attenuated bovine-human reassortant strains, tetravalent to hexavalent	Oral	Wuhan Institute of Biological Products, China and PATH, USA
Pre-clinical	IRV	Inactivated G1P[8], G2P[4]	Intramuscular or intradermal	US CDC
Pre-clinical	Subunit	Virus-like particles: VP 2/6/7 and VP 2/4/6/7	To be determined	Baylor College of Medicine, USA
Pre-clinical	Subunit	Truncated VP8 in norovirus P particles	To be determined	Cincinnati Children’s Hospital Medical Center, USA
Research	Subunit	VP6 combined with norovirus G1 and GII VLPs	To be determined	University of Tampere School of Medicine, Finland


BRV bovine rotavirus, *CDC* Centers for Disease Control and Prevention, *IRV* inactivated rotavirus vaccine, *LLR* Lanzhou Lamb Rotavirus

Table 1.4. Summary of analytical tools available to characterize recombinant protein subunit vaccines and to apply to their formulation development.

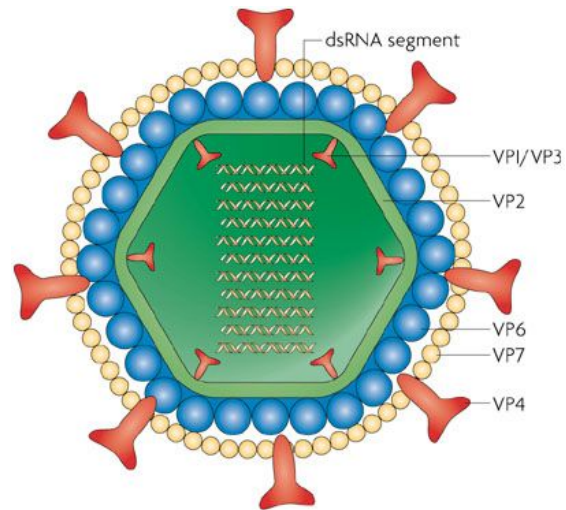
Potency Assays	In-vivo	Animal Studies	Immunization-Challenge Studies, Serological Analyses	
	In-vitro	Cell-based Assays	ELISpot, T Cell Proliferation, Multiplex Array Techniques, Flow Cytometry, Tetramer Staining	
		Binding Assays	ELISA, Single Radial Immune Diffusion, Bio-layer Interferometry (BLI), Surface Plasmon Resonance (SPR)	
Physicochemical Assays	Drug Substance	Quantity (Total Protein)	UV-Visible Spectroscopy (A280), Bradford/BCA/Lowry Assays	
		Purity	Native or SDS-PAGE Gels, Isoelectric Focusing Gels, Capillary Isoelectric Focusing, Chromatography-based methods (RP-HPLC, HIC, IEX)	
		Host-cell DNA	DNA Hybridization, Dot Blot, qPCR	
		Host-cell Proteins	ELISA	
		Identity	Mass Spectrometry (Peptide Mapping)	
		Primary Structure/PTMs	Mass Spectrometry (Peptide Mapping)	
		Secondary Structure	Far UV Circular Dichroism, Fourier Transform Infrared Spectroscopy	
		Tertiary Structure	Near UV Circular Dichroism, Intrinsic and Extrinsic Fluorescence Spectroscopy	
		Overall Conformational Stability	Differential Scanning Calorimetry	
		Size/Mass	Analytical Ultracentrifugation, Size-Exclusion Chromatography, Field-Flow Fractionation, Static/Dynamic/Multi-Angle Light Scattering (LS), Electron Microscopy (EM), Light Obscuration, Flow Imaging Microscopy	
	Drug Product	Bound State	Antigen-Adjuvant Interactions	Langmuir Binding Isotherms
			Adjuvant Characterization	Laser Diffraction, Electrophoretic LS, XRD, Transmission EM
			Protein Concentration/Conformation	ELISA, BLI, SPR
			Secondary Structure	Fourier Transform Infrared Spectroscopy
			Tertiary Structure	Intrinsic Fluorescence (Steady State And Time-resolved)
			Overall Conformational Stability	Differential Scanning Calorimetry
		Forced Desorbed	Primary Structure/PTMs	Mass Spectrometry (Peptide Mapping)
			Protein Concentration and Heterogeneity	UV-Visible Spectroscopy (A280), Reduced and Non-Reduced SDS-PAGE Gels

ELISpot - enzyme-linked immune absorbent spot
 ELISA - enzyme-linked immunosorbent assay
 RP-HPLC - reverse phase high pressure liquid chromatography
 HIC - hydrophobic interaction chromatography
 IEX - ion exchange chromatography
 XRD - X-Ray Diffraction

Table 1.5. Comparison of expression systems used for production of vaccine bulk antigens. (Reproduced from Ref. 84⁸⁴)

	Low  High			
Speed	Mammalian	BEVS/insect cell	Yeast	Bacteria
Cost	Bacteria	Yeast	BEVS/insect cell	Mammalian
Typical yield	Mammalian	BEVS/insect cell	Bacteria	Yeast
Post-translational modification	Bacteria	Yeast	BEVS/insect cell	Mammalian
Regulatory approval	BEVS/insect cell	Yeast	Bacteria	Mammalian

1.5 Figures



Nature Reviews | Microbiology

Figure 1.1. Schematic representation of a rotavirus virion highlighting the structural proteins. (Adapted with permission from Ref. 5⁵)

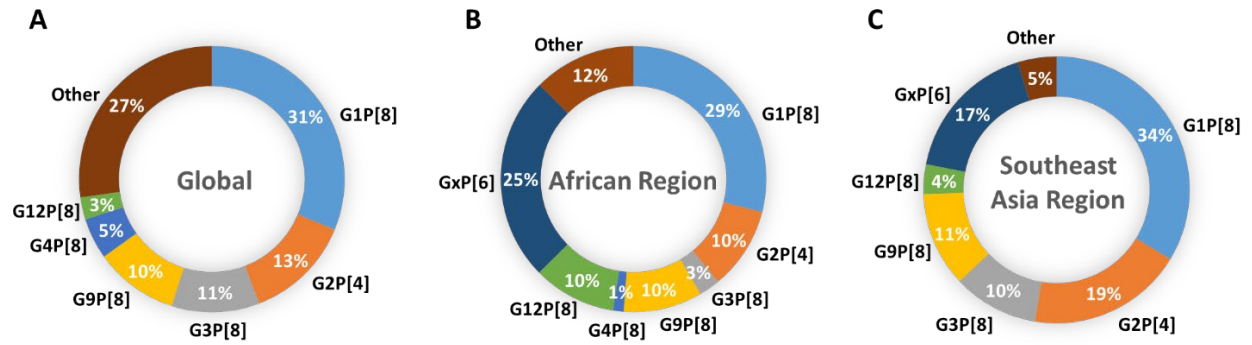


Figure 1.2. Distribution of medically important RV strains from 2007 - 2012. (A) Global distribution, and distribution in (B) African, and (C) Southeast Asia region. (Ref. 11¹¹)

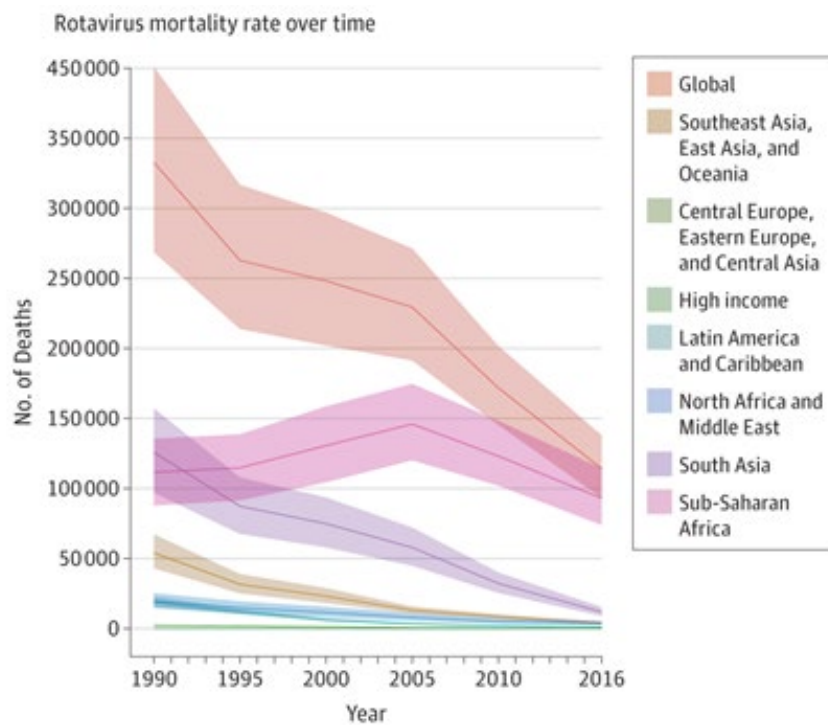


Figure 1.3. Change in RV associated mortality rate from 1990 to 2016. (Reproduced with permission from Ref. 1¹)

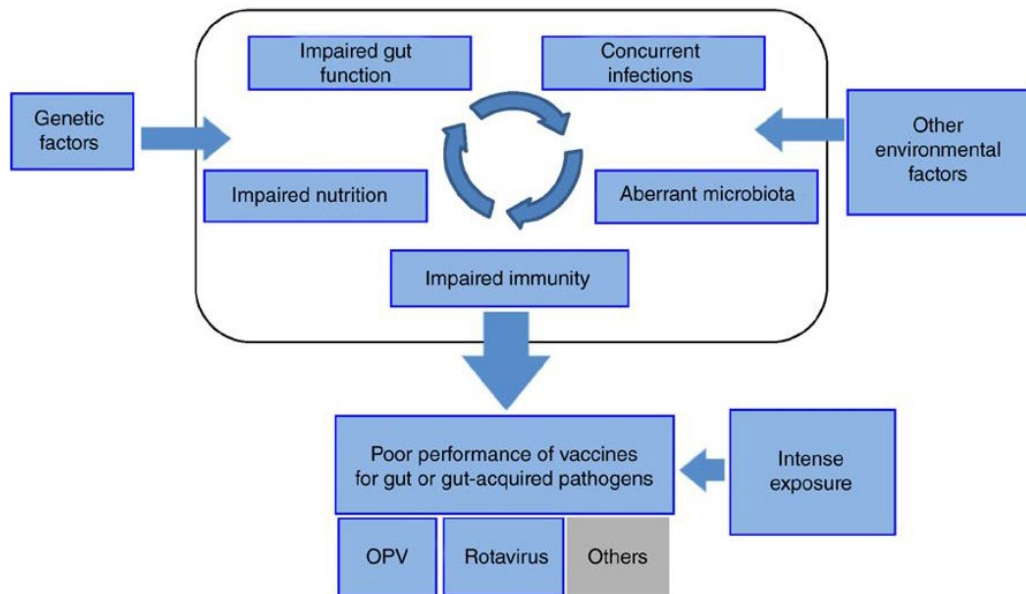


Figure 1.4. Potential factors for reduced efficacy of commercially available, orally delivered, live attenuated viral RV vaccines in developing countries. (Adapted with permission from Ref. 107¹⁰⁷)

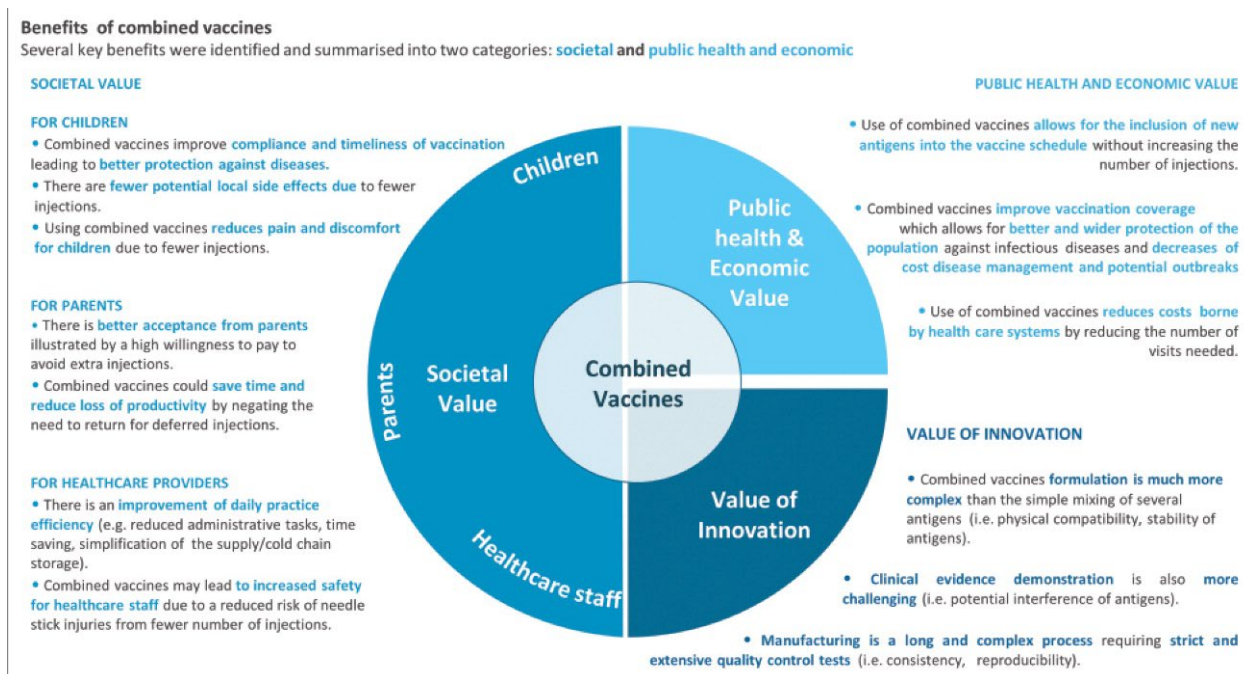


Figure 1.5. Societal and public health benefits of combination vaccines. (Reproduced with permission from Ref. 101¹⁰¹)

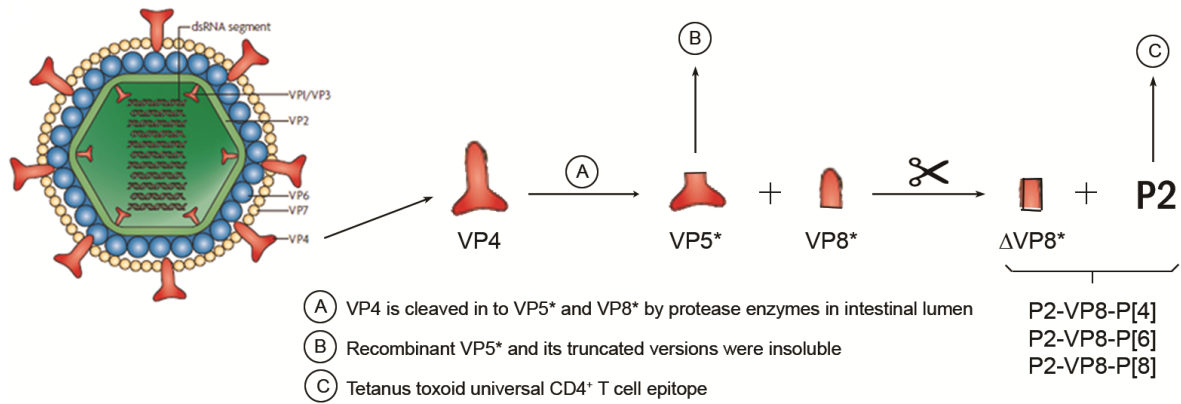


Figure 1.6. Composition and nomenclature of the three recombinant fusion protein antigens that comprise the NRRV candidate vaccine.

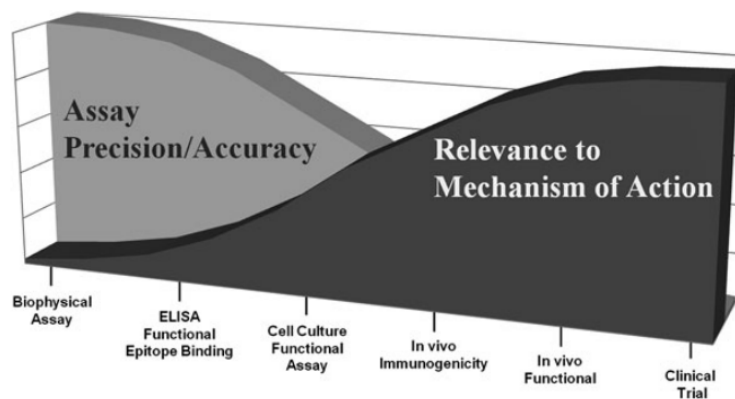


Figure 1.7. Analytical tools and their strengths vs. weaknesses in terms of assay properties vs. relevance to vaccine clinical performance. (Reproduced with permission from Ref. 60⁶⁰)

Chapter 2

Recombinant subunit rotavirus trivalent vaccine candidate: physicochemical comparisons and stability evaluations of three protein antigens

2.0 Introduction

Rotavirus (RV) is a leading cause of acute diarrhea and gastroenteritis among infants and young children across the world and approximately 128,500 children under five years of age died from RV infection in the year 2016 ¹. The majority of deaths occur in developing countries. Furthermore, millions of children worldwide require home care, ER visits, and hospitalization, which contribute significantly to the disease burden ². Improvements in sanitation, personal hygiene or food quality reduce but do not eliminate the risk of this infection ^{111,112}. Therefore, vaccination is the most cost-effective strategy to control the burden of RV-related illness.

Currently, four WHO pre-qualified, live attenuated oral RV vaccines (RotaTeq®, Rotarix®, Rotavac®, Rotasil®) are commercially available and combined cover more than 100 countries. In general, widely used RV vaccines (RotaTeq® and Rotarix®) show good efficacy (>85%) in developed countries, however, efficacy is reduced (40-60%) in the low-income countries where the need is most ^{13,23,29,30 109,113}. While the causes for their reduced efficacy are unknown, and are an active area of investigation, contributing factors possibly include lower viral titer (transplacentally acquired RV antibodies, components of breast milk and stomach acid) and/or impaired immune response (malnutrition, interfering microbes and other co-infections) ^{20,35,106}. From limited available data, lower efficacy in certain sub-populations of the developing world of other live, attenuated oral vaccines has also been observed against enteric pathogens such as Poliovirus and *Vibrio cholerae* ¹¹⁴. Thus, there is interest in developing recombinant subunit protein, injectable RV vaccine candidates to address some of the current deficiencies of live attenuated oral vaccination ¹¹⁵.

To this end, a candidate recombinant protein-based, parenterally administered rotavirus vaccine is under development (non-replicating rotavirus vaccine, NRRV). In a Phase 1 clinical trial conducted in infants and toddlers in South Africa, a monovalent NRRV vaccine was shown

to be well-tolerated and immunogenic, thus demonstrating a promising new approach to develop vaccine against RV^{46,47}. Moreover, a trivalent version of the NRRV vaccine has also been shown to be well-tolerated and immunogenic in infants and toddlers in early stage clinical trials in South Africa^{46,47}. The NRRV vaccine is composed of three recombinant protein antigens designed to protect against the most prevalent rotavirus strains in the developing world (P[4], P[6], and P[8]).

Each of these three antigens is a recombinant fusion protein based on the RV surface protein VP4. Upon host infection, VP4 is cleaved by proteases in the intestinal lumen into VP5* and VP8* leading to production of neutralizing antibodies¹¹⁶. Wen *et al.* at the NIH successfully expressed Δ VP8*, a truncated, soluble version of the VP8* protein, in *E. coli* while preserving its key epitopes. The tetanus toxoid CD4⁺ T cell epitope (P2) was added on the N-terminus via a GSGSG linker to create a fusion protein which enhanced the immunogenicity of Δ VP8* as demonstrated in guinea pigs⁴⁵. In terms of nomenclature, the three recombinant protein antigens are P2-VP8-P[4], P2-VP8-P[6], and P2-VP8-P[8] where P2 stands for the carrier protein, VP8 refers to the Δ VP8* part of VP8* protein, and P[4], P[6], P[8] represent the RV strain DS-1 (G2P[4]), 1076 (G2P[6]), Wa (G1P[8]), respectively⁴⁴. For simplicity, the protein antigens are referred to as P[4], P[6], or P[8], respectively, in this chapter.

Successful development and eventual commercialization of this recombinant subunit RV vaccine candidate will not only depend on clinical safety and efficacy results, but also the ability to produce the vaccine at low cost for use in the developing world. To this end, demonstrating a product candidate retains its critical quality attributes (CQAs, i.e., key aspects of structural integrity, stability, and immunological potency) as the manufacturing process is changed and scaled-up to ensure low cost production is a key aspect to its development. To ensure CQAs are retained pre- versus post- process change, it is important to develop analytical assays that are robust

and sensitive to detect changes in the physicochemical and immunological properties of the protein antigen. Thus, it is essential to develop a battery of analytical assays capable of monitoring structural and functional equivalence during comparability assessments¹¹⁷⁻¹¹⁹. In addition, these analytical characterization methods can be applied to the formulation development to ensure vaccine potency (and physicochemical stability) of the three NRRV antigens across the vaccine's shelf life^{50,72,78}.

In this work, a wide variety of physicochemical characterization techniques were employed to characterize and compare the primary and higher-order structures, post-translational modifications, conformational stability and aggregation propensity of each of the three NRRV antigens. In addition, forced degradation studies were performed to elucidate degradation pathways of chemically labile residues or "weak spots" and analytical tools were developed to monitor/quantify degradative changes. The most informative assays for each structural attribute were then applied to the development of candidate formulations to minimize protein aggregation during frozen storage of these NRRV antigens as a bulk drug substance (see chapter 3).

2.1 Materials and Methods

The P[4] and P[6] antigens were produced and purified from *E. coli* at Walter Reed Army Institute of Research, MD and provided in 0.5 mM sodium phosphate, 150 mM NaCl, pH 7.2. The P[8] antigen was produced and purified from *E. coli* by Blue Sky BioServices, MA and provided in 600 mM ammonium sulfate, 50 mM Tris, pH 7.5 buffer. Unless otherwise noted, each of the antigens was dialyzed overnight at 4°C in 10 mM sodium phosphate, 150 mM NaCl, pH 7.2 buffer which is referred as *formulation buffer* in the text hereafter. Sodium phosphate dibasic heptahydrate, and sodium chloride were purchased from Thermo Fisher Scientific (Waltham,

MA). All other buffer reagents and chemicals including sodium phosphate monobasic monohydrate, citric acid, and ammonium bicarbonate were purchased from Sigma-Aldrich (St. Louis, MO) and were of analytical grade or higher unless noted otherwise. The extinction coefficient of each NRRV antigen was calculated from the primary sequence using online ExPASy tool (Swiss Institute of Bioinformatics), resulting in values of $1.653 \text{ mg/ml}^{-1} \text{ cm}^{-1}$, $1.708 \text{ mg/ml}^{-1} \text{ cm}^{-1}$, and $1.733 \text{ mg/ml}^{-1} \text{ cm}^{-1}$ for P[4], P[6], and P[8] antigen, respectively, to determine protein concentration. It should be pointed out that the protein samples used in this study are bulk and by inference do not represent the aluminum adjuvanted drug product vaccine.

2.1.1 Intact Protein Mass Spectroscopy

Prior to intact mass analysis in formulation buffer, the NRRV samples were treated with either water or 100 mM dithiothreitol (DTT) and incubated for 60 min at 37°C. The intact masses of each sample (in duplicate) were measured using a Synapt G2 mass spectrometer (Waters, Milford, MA) and with the assistance of the Mass Spectrometry and Analytical Proteomics Laboratory at the University of Kansas.

For the high pH and temperature stress studies, the NRRV samples were treated with either 100 mM DTT or water. The samples with DTT were heated for 30 min at 37°C. All samples were then diluted 1/100 with water + 0.1% formic acid. Twenty pmol of each NRRV sample were subjected to intact mass analysis using a 1220 LC system (Agilent Technologies) connected in-line to a G6230B time-of-flight mass spectrometer (Agilent Technologies). The sample was desalted using a ZORBAX 300SB C3 column (Agilent Technologies, 820950-924). The LC gradient consisted of 20-70% B (A: water + 0.1% formic acid, B: acetonitrile + 0.1% formic acid) over 1 min at a flow rate of 1.5 ml/min. The electrospray ionization parameters consisted of: 290°C gas temperature, 4000V Vcap, and 275V fragmentor. Mass spectra were collected from 700-2800

m/z at 1 spectra/sec. Mass spectra were processed using MassHunter (Agilent Technologies) and the deconvolution range consisted of 5-50 kDa, with 1 Da mass steps.

2.1.2 LC-MS Peptide Mapping

For proteolysis under reducing conditions, the NRRV samples were incubated with 15 mM DTT for 30 min at 80°C, and then alkylated with 30 mM Iodoacetamide for 30 min at room temperature. Alkylation was quenched by 15 mM DTT. The samples were incubated for 2 hr at 37°C with 2.5 µg of chymotrypsin. Trifluoroacetic acid (0.05%) was added to quench the proteolysis and 15 µg of digested protein was subjected to LC-MS.

The peptides from the digested protein solution were separated by a liquid chromatography system (Thermo Scientific, Waltham, MA) prior to analysis. Peptides were injected onto a C18 column (1.7µm, 2.1 x 150 mm, Waters) and a 60 min 0-30% B gradient (A: H₂O and 0.05% trifluoroacetic acid; B: acetonitrile and 0.05% trifluoroacetic acid; 200 µl/min flow rate) for separation. MS was performed using a LTQ-XL ion trap (Thermo Scientific) and the Xcalibur 2.0 software (Thermo Scientific). The instrument was also tuned using a standard calibration peptide (Angiotensin II, Sigma) for maximal sensitivity before running any experiments. The mass spectra were acquired in the LTQ over a mass range of m/z 300-1900. The ion selection threshold was 12,000 counts and the dynamic exclusion duration was 5 sec. The raw data files were processed using *PepFinder 2.0* software (Thermo Scientific). Potential Cys carbamidomethylation, Asn deamidation, and Met oxidation were included during the analysis.

2.1.3 Fourier-Transform Infrared (FTIR) Spectroscopy

FTIR spectroscopy were performed (in triplicate) of the filtered protein samples at their stock concentrations (1.29 mg/mL for P[4], 0.82 mg/mL for P[6], and 1.5 mg/mL for P[8]) using a Bruker Tensor-27 FTIR spectrometer (Bruker Optics, Billerica, MA) equipped with a KBr beam

splitter. The MCT detector was cooled with liquid N₂ for at least 30 min prior to use and the interferometer was constantly purged with N₂ gas. Two hundred fifty-six scans were recorded from 4000 to 600 cm⁻¹ with a 4 cm⁻¹ resolution using a Bio-ATR cell. Sample spectra were corrected for the background signal, followed by atmospheric and baseline corrections using OPUS V6.5 (Bruker Optics, Billerica, MA) software. Fourier self-deconvolution was initiated using a 50% Lorentzian and 50% Gaussian function, with a deconvolution factor of 2 and the noise reduction filter was set to 0.5. Following the deconvolution, five peaks were fitted to the absorbance spectrum in the Amide I region (1700-1600 cm⁻¹) for P[4], similarly, six peaks were fitted each for P[6] and P[8] antigens. The areas of the peaks were used to calculate the relative percentage of secondary structure components in each protein sample.

2.1.4 Far-UV Circular Dichroism (CD) Spectroscopy

Far-UV CD spectra of the NRRV antigens were recorded at 0.2 mg/mL in quartz cuvettes (0.1 cm path length) sealed with a Teflon stopper (Starna Cells Inc., Atascadero, CA) using a Chirascan-plus CD spectrometer (Applied Photophysics Ltd, Leatherhead, UK) equipped with a 6-cuvette sample holder and a Peltier temperature controller (Quantum Northwest, Liberty Lake, WA) and a high performance solid-state detector. The lamp (150 W air-cooled Xe arc) housing, monochromator and sample compartment were continuously purged with N₂ gas. The wavelength range was 280-200 nm for data collection using 1 nm step size and a 0.5 s sampling time, temperature was ramped at 1°C/min from 10 to 90°C in 2.5°C intervals with 2 min equilibration at each temperature point. All data were corrected for the background signal from the formulation buffer, followed by a 3-point Savitzky-Golay smoothing filter using the Chirascan software (Applied Photophysics).

2.1.5 Intrinsic Tryptophan Fluorescence Spectroscopy and Static Light Scattering (SLS)

The emission spectra of 0.2 mg/mL antigen were collected in 1cm path length quartz cuvettes from 310 to 410 nm with step size of 1 nm and integration time of 1 s using an excitation wavelength of 295 nm. Data were collected from 10 to 90°C in 2.5°C intervals with 2 min equilibration at each temperature point using a dual emission PTI QM-40 Spectrofluorometer (Photon Technology International (PTI), Inc., Birmingham, NJ) equipped with a 4-position cell holder, Peltier temperature control device, a high power continuous 75 W short-arc Xe lamp (Ushio), and a Hamamatsu R1527 photomultiplier tube. Aggregation propensity was monitored as a function of increasing temperature by collecting scattered light intensity at 295 nm concurrently with the fluorescence spectra by employing a second detector (90° to the incident light and 180° to the fluorescence detector). The excitation and emission slits were both set such that the initial signal at 10°C had an emission maximum of ~800,000 counts per second for fluorescence spectra and an emission maximum of ~5,000 counts per second for light scattering spectra. Peak intensity was determined at each temperature using a mean spectral center of mass (MSM) method applied using in-house software (MiddaughSuite), after correcting for formulation buffer, this analysis algorithm increases the signal to noise ratio. The T_{onset} values were estimated by monitoring baseline deviation from linearity and the T_m were calculated by first derivative analysis of the thermal melt curve using Origin software (Northampton, MA).

2.1.6 SDS-PAGE

For the reduced samples, 10 µg of the protein stock were mixed with 4X LDS loading dye (Life Technologies, Grand Island, NY), 20 mM iodoacetamide (Life Technologies), and formulation buffer and incubated in dark for 10 min at room temperature. Then the samples were boiled at 90°C for 10 min to cause protein unfolding and lithium dodecyl sulfate (LDS) binding.

Samples were then reduced by adding 10 mM DTT and incubating at 37°C for 10 min. The reduced samples were separated by electrophoresis using NuPAGE 4-12% Bis-Tris (Life Technologies) gels and a MES running buffer (Life Technologies). A similar procedure was followed for non-reduced protein samples except the reduction step using DTT. The NuPAGE gels were run for 60 min at 150V and protein bands were visualized by staining with coomassie blue R250 (Teknova, Hollister, CA) and destained with a mixture of 40% methanol, 10% acetic acid, and 50% ultrapure water. Gels were digitized using an Alphaimager (Protein Simple, Santa Clara, CA) gel imaging system.

2.1.7 Size Exclusion Chromatography (SEC)

SEC analysis of the NRRV antigens was performed using a TSK-Gel BioAssist G2SWxl column (7.8 x 300 mm, TOSOH Biosciences, King of Prussia, PA) on a Shimadzu Prominence UFLC HPLC system equipped with a diode array detector (with absorbance detection at 214 nm). Prior to sample injection, the column was equilibrated with at least 10 column volumes of mobile phase (formulation buffer) and then 30 µg of protein was injected at a flow rate of 0.7 mL/minute. Both the analysis and the corresponding guard column (TOSOH Biosciences) were operated at ambient temperature and the run time was 30 minutes. To ensure column and HPLC system integrity, a suitable gel filtration standard (Bio-Rad, Hercules, CA) was run and analyzed at the beginning and after every three sample runs. In addition, the samples were subjected to SEC without the guard and main columns attached to better determine if insoluble aggregates are present in the samples or if the sample binds to the column (i.e., sample recovery). Data analysis was completed using LC solutions software (Shimadzu, Kyoto, Japan).

2.1.8 Sedimentation Velocity Analytical Ultracentrifugation (SV-AUC)

Sedimentation velocity profiles of the NRRV antigens were obtained on a Proteome Lab XL-I (Beckman Coulter, Fullerton, CA) Analytical Ultracentrifuge using ultraviolet-visible optical detection system. Rotor was equilibrated for ≥ 1 h to ensure that it has reached the set temperature of 20°C, then the protein samples at 0.5 mg/mL were subjected to centrifugal force at a rotor speed of 40,000 RPM and the species undergoing sedimentation were detected at 280 nm. Beckman charcoal-epon two sector cells with a 12 mm centerpiece (either sapphire or quartz windows) were used for loading protein samples and the formulation buffer.

The partial specific volume of 0.73 mL/g was used for each antigen and the buffer density (1.0058 g/mL) and viscosity (1.0195 cPoise) were calculated using Sednterp (Professor Thomas Laue, University of New Hampshire and BITC). A continuous $c(s)$ distribution was used in the Sedfit (Dr. Peter Schuck, NIH) program to monitor the size related species in the protein samples. Sedimentation data of 200 scans were used with a range of 0 to 15 Svedbergs, resolution and confidence level were 300 and 0.95, respectively during data analysis. Meniscus and the bottom positions were set manually by careful observation and the baseline, radial independent noise, and time independent noise were floated. The $c(s)$ distributions were imported into Origin (OriginLab, Northampton, MA) and peaks were integrated to get percent distribution of multiple species in the samples.

2.1.9 Reversed-Phase Ultra High Performance Liquid Chromatography (RP-UHPLC)

NRRV antigens in formulation buffer were subjected to RP-UHPLC (in triplicate) using a Ultimate 3000 UHPLC system (Thermo Scientific) and a 2.6 μm , 2.1 x 150 mm C-4 column (Thermo Scientific). The flow rate was set at 0.2 ml/min and the column and auto-sampler temperatures were set at 60°C and 5°C, respectively. The elution of proteins was monitored using

the absorbance at 214 nm and mobile phase (A) consisted of water with 0.1% trifluoroacetic acid (TFA) and mobile phase (B) consisted of acetonitrile with 0.1% TFA. A mobile phase gradient of 10% B (0-5 min), 10→99% B (5-15 min), 99% B (15-20 min), 99→10% B (20-22 min), and 10% B (22-27 min) was used. In addition, the samples were run without the guard and main columns attached to better determine if insoluble aggregates are present in the samples or if the proteins bind to the column (i.e., sample recovery). Data were analyzed using Chromeleon software (Thermo Scientific).

For the high pH and temperature stress, a 1.7 μm , 1 μm x 50 mm C-4 column (Waters Corporation) was used with the Ultimate 3000 UHPLC system. One microgram of each antigen sample (in triplicate) were subjected to RP-UHPLC analysis. Protein elution was monitored by absorbance at 214 nm. The column temperature was set at 60°C and the flow rate was 0.2 ml/min. The mobile phase A was water with 0.05% trifluoroacetic acid (TFA) and mobile phase B was acetonitrile with 0.05% TFA. The gradient consisted of 0% B (5 min), 0-25%B (3 min), 25-45% B (50 min), 45-60%B (2 min), 60% B (3 min), 60-0% B (2 min), and 0%B (5 min). From 8-58 min, the elution from the RP-UHPLC column was directed into a LTQ-XL ion trap (Thermo Scientific). Mass spectra were acquired in the LTQ over a mass range of m/z 600-1800. MS¹ peaks corresponding to NRRV protein were deconvoluted manually.

2.1.10 Hydrophobic Interaction Chromatography (HIC)

HIC was performed on a Shimadzu Prominence UFLC HPLC system equipped with a diode array detector (detection at 214 nm) using a TSKgel BioAssist Phenyl-5PW (7.8 mm X 5 cm, 10 μm) column (TOSOH Biosciences). Thirty μg of each antigen was injected onto the column for each run, mobile phase A was composed of 2M ammonium sulfate, 0.5 mM sodium phosphate, pH 6.8 and mobile phase B was 0.5 mM sodium phosphate, pH 6.8. The flow rate was 0.5 mL/min

and the gradient consisted of 50% B (0-5min), 50→100% B (5-15 min), 100% B (15-20 min), 100→50% (20-22 min), and 50% B (22-30 min). Sample recovery and insoluble aggregates were also tested similar to SEC and RP-UHPLC methods.

2.1.11 Differential Scanning Calorimetry (DSC)

DSC thermograms were obtained for each sample in formulation buffer at 0.4 mg/mL in triplicate using an Auto-VP capillary differential scanning calorimeter (MicroCal/GE Health Sciences, Pittsburgh, PA) equipped with Tantalum sample and reference cells. Scan were recorded from 10 to 90°C at 60°C/h scanning rate, 15 min pre-equilibration time, and cleaning was done after every scan. Formulation buffer scan was subtracted from the sample scan and data were normalized for the protein concentration and baseline correction were performed using Origin software (OriginLab, Northampton, MA).

2.1.12 Extrinsic ANS Fluorescence Spectroscopy

Extrinsic ANS fluorescence measurements were performed using Photon Technology International (PTI) spectrofluorometer (Lawrenceville, NJ) equipped with a turreted four-position Peltier-controlled cell holder and a xenon lamp. Samples contained 0.2 mg/ml protein in a total sample volume of 700 μ l in quartz cuvettes. Stock solution of ANS (1-Anilino-naphthalene-8-sulfonic acid) dye purchased from Sigma, Inc. (St. Louis, MO) was made at 25 mM in DMSO. Finally, a ratio of 25:1 (dye: protein) was maintained during fluorescence measurements. An excitation wavelength of 372 nm was used, and emission spectra were collected from 400-600 nm with a step size of 1 nm and an integration time of 1 s. Temperature was increased from 10 to 90°C at 2.5°C intervals with a 2 min equilibration time at each temperature. The data analysis was performed using *Middaugh Suite* developed in-house at KU. The emission peak position and peak intensity were determined using a mean spectral center of mass method (MSM) executed in

Middaugh Suite after correcting for the buffer alone signal. The T_m values were determined by a first derivative method using Origin software (v. 8.0) and the T_{onset} values were determined by identifying the point at which the baseline deviated from linearity.

2.1.13 OD₃₅₀ (turbidity) analysis

Turbidity measurements were performed using a Cary 100 UV-Visible spectrophotometer (Varian medical Systems, Inc., Palo Alto, California) equipped with a 12-cell holder with a Peltier type temperature controller. A total sample volume of 225 μ L in 1 cm path length quartz cells was used during the experiments. Optical density at 350 nm (OD₃₅₀) was monitored as the temperature was raised in increments of 2.5°C from 10 to 90°C with a heating rate of 60°C/h and equilibration of 2 min at each temperature. Protein samples were run in triplicate and corresponding buffer blanks were run and subtracted from each sample. The OD₃₅₀ value was plotted vs temperature using Origin and T_m were determined using first derivative analysis.

2.1.14 Physical stability profile comparisons using data visualization tools

Each of the three antigens were dialyzed into 20 mM citrate phosphate buffer containing 150 mM NaCl at pH 3, 4, 5, 6, 7, and 8 using Slide-A-Lyzer mini dialysis device (ThermoFisher) overnight at 4°C. Biophysical stability data sets were collected in triplicate at each pH condition at 0.2 mg/mL protein concentration from 10 to 90°C every 1.25°C intervals using Far-UV CD spectroscopy, Intrinsic Tryptophan Fluorescence spectroscopy, SLS, and extrinsic ANS fluorescence as described above. For simplified visual representation and to facilitate comparison of the large biophysical data sets collected for the three antigens, Radar Charts were constructed using in-house developed *Middaugh Suite* program as described in detail elsewhere¹²⁰ Mean residue ellipticity at 216 nm from CD experiments, intrinsic tryptophan fluorescence peak position and peak intensity, static light scattering signal at 295 nm, and extrinsic ANS fluorescence peak

intensity data sets as a function of pH and temperature were used in the construction of the Radar Charts.

2.1.15 Chemical stability profile comparisons at elevated temperature and solution pH and in presence of H₂O₂

For elevated temperatures and pH, each of the three NRRV proteins were dialyzed into two different buffers overnight at 4°C: (a) 10 mM sodium phosphate, 150 mM NaCl, pH 7.2, and (b) 25 mM ammonium bicarbonate, 150 mM NaCl, pH 9.0. The protein samples at 0.70 mg/mL were incubated in triplicate at pH 7.2 and pH 9.0 at 4°C and at pH 9.0 25°C for 4 days in the two buffers. Samples were then subjected to intact mass analysis, peptide mapping, SDS-PAGE, and RP-HPLC analysis as per the methods described above.

For the forced oxidation studies, each of the NRRV antigens in formulation buffer, was incubated in triplicate for one hour at ambient temperature at the following H₂O₂ concentrations: 0%, 0.01%, 0.025%, 0.05%, 0.1%, 0.25% and 0.5% v/v. Reactions were quenched with D-Met and all samples were subjected to intact mass analysis, peptide mapping, and RP-UHPLC as per the methods described above.

2.1.16 Modeling of NRRV antigen structure

I-TASSER algorithm was used to predict the structure of the three NRRV antigens which are recombinant fusion proteins. For a detailed description of how I-TASSER generates protein structure prediction from amino acid sequence, readers are advised to refer to the published literature and Zhang group's web page ¹²¹⁻¹²³. Briefly, first the structure templates are identified from the protein data bank (PDB) library by using a threading approach. Second, the identified continuous fragments from templates are combined into full length models using Monte Carlo simulations and ab initio modelling. A clustering program is then used to cluster all the models and up to five models are reported which correspond to the lowest free energy state of the protein.

In this work, out of the five predicted models for each antigen, model with the highest confidence score (i.e., better quality) was adopted to highlight the location of amino acids (using PyMOL) which are most susceptible to degradation. It is important to point out that the crystal structures of VP8-P[8] (PDB ID: 2AEN) and VP8-P[4] (PDB ID: 2DWR) proteins were employed as templates during structure prediction of the NRRV antigens by the I-TASSER program.

2.2 Results

2.2.1 Physicochemical characterization and comparisons of the three NRRV antigens

The primary structure of the three fusion proteins was initially assessed by intact mass analysis. As shown in Figure 2.1, panels A, B, C, predominantly a single peak was observed for each antigen and the average molecular weight results (20517.6 ± 0 , 20732.0 ± 0 , 20433.7 ± 0.1 Da for P[4], P[6] and P[8], respectively, $n = 3$) correspond to the expected native protein mass based on the amino acid sequence plus an additional +132 Da (similar results were obtained for non-reduced samples, see Supplemental Fig. S2.1A). As confirmed by LC-MS peptide mapping results described below, an additional Met residue is present on the N-terminus of these antigens, as would be expected for a foreign protein expressed in *E. coli*.

LC-MS peptide map analysis was conducted to confirm each antigen's primary sequence and identify any post translational modifications. Each antigen displayed a unique peptide elution profile as shown in Figure 2.1 panels D, E, F, demonstrating the ability to distinguish the three proteins as a potential identity test. Using intact (MS^1) and fragmentation (MS^2) mass analysis, 44 peptides were identified in the [P4] digest, 50 peptides in P[6], and 37 peptides in P[8], which covered 100% of each of the protein's primary sequence (Supplemental Fig. S2.1B). Moreover, the peptide mapping results suggested deamidation at several Asn residues in P[4] and P[8], and

at one Asn residue in P[6]. For P[4], Asn⁷, Asn⁴⁷ and Asn¹⁷⁹ were ~3-4% deamidated. For P[6], Asn⁷ was ~2-3% deamidated. For P[8], Asn⁷ was ~20%, Asn⁴⁶ ~6% and Asn¹⁷⁸ ~3% deamidated. Thus, the peptide mapping method was shown to be useful not only as an overall fingerprint analysis for the structural integrity and identity of each NRRV antigen, but also as charge heterogeneity test for Asn deamidation (also see chemical stability section below).

The overall higher-order structure (HOS) of the three proteins was assessed by a combination of different biophysical tools. The secondary structure composition was measured by FTIR by monitoring the absorbance in the amide I region (1600 - 1700 cm⁻¹). All three antigens were primarily β -sheet in structure with main peak at ~1642, ~1639, and ~1640 cm⁻¹ for P[4], P[6], and P[8], respectively as shown in Figure 2.2, panels A, B, C. The secondary structure composition by Fourier self-deconvolution (see Figure 2.2D) correlated very well with the secondary structure assignments from X-ray crystal structures of P[4] and P[8] antigens in the literature^{124,125}. Far UV circular dichroism spectroscopy was employed to confirm the findings from FTIR analysis and a peak minimum around 215-216 nm was observed for each antigen indicating β -sheet structure in solution (Figure 2.2E). The overall tertiary structure was compared using intrinsic tryptophan fluorescence emission spectrum from 305 – 405 nm. Peak position or λ_{\max} for P[4], P[6], and P[8] was 334 ± 0 , 333.7 ± 0.6 , and 335.3 ± 0.6 , respectively (Figure 2.2F). This result suggests the average Trp residue for each of the three antigens is located in a similar environment (each NRRV antigen has 4 Trp residues).

A combination of SV-AUC and SE-HPLC were used to probe the size of the three protein antigens and to assess the presence of soluble aggregates (monomer, dimer, etc.). Each antigen had monomeric composition $\geq 99\%$ and about 1% higher molecular weight (HMW) species based on the peak areas from sedimentation coefficient (s) distribution (Figure 2.3A). Similar s value of

2.09 ± 0.01 were recorded for P[4] and P[8], whereas for P[6], s value was 2.03 ± 0.01 suggesting smaller hydrodynamic size for P[6] compared to P[4] and P[8] (which show similar size). These observations were supported by SE-HPLC as an orthogonal tool. The retention time for P[4] and P[8] was 16.28 ± 0.01 and 16.24 ± 0.01 min respectively, whereas P[6] eluted at 17.08 ± 0.06 min consistent with a smaller hydrodynamic size for P[6] (Figure 2.3B). As expected based on the size results from intact mass analysis (see above), P[6] antigen band migrated at a somewhat higher molecular weight on SDS-PAGE gels as compared to P[4] and P[8] (which were at similar mass level, Figure 2.3C).

From hydrophobic interaction chromatography (HIC) analysis (Figure 2.3D), all three antigens appeared heterogeneous when eluted from phenyl column with the major species accounting for >92% for each protein. Out of the three antigens, P[4] was most homogeneous at $98.3 \pm 0.3\%$ followed by P[8] at $92.8 \pm 0.4\%$ and P[6] at $92.3 \pm 0.3\%$ (n= 3). P[6] was most hydrophobic of the three antigens as it eluted at a relatively later retention time as compared to P[4] or P[8] (Figure 2.3D). Similarly, through reversed-phase high pressure chromatography analysis (RP-HPLC), the major peak accounted for >93% of each protein. Out of the three antigens, P[4] was most homogeneous at $\sim 100 \pm 0\%$ followed by P[6] at $96.5 \pm 0.2\%$ and P[8] at $93.4 \pm 0.1\%$ (n= 3). P[6] eluted later than P[4] or P[8] as shown in Figure 2.3E. These RP-HPLC results are consistent with the HIC results (Figure 2.3D). No difference in the total area was observed with and without the column in HIC and RP-HPLC assays indicating excellent recovery (i.e., no notable levels of protein were lost due to column adsorption).

2.2.2 Physical stability profiles and comparisons of the three NRRV antigens as a function of temperature and pH

The HOS and conformational stability of each NRRV antigen was measured and compared as a function of temperature (10-90°C) in the formulation buffer. Secondary and tertiary structure

stability was evaluated by monitoring CD molar ellipticity at 216 nm and intrinsic Trp fluorescence emission peak intensity, respectively. As shown in Figures 2.4A and 2.4B, a single transition event was noted for each antigen and P[8] showed highest onset (T_{onset}) and apparent melting temperature (T_m) as shown in the bar graphs on right. This result suggests that the HOS of the P[8] antigen is the most stable of the three antigens against thermal stress. Similar rank order of conformational stability was observed between the three antigens with P[8] being most stable (and P[4] was slightly more stable than P[6]) as measured by DSC and DSF (Figures 2.4C and 2.4D), respectively.

Two light scattering methods (SLS and OD_{350}) were used to assess thermally-induced aggregation. Results indicate P[8] is most stable (highest T_{onset} value) as shown in the bar graphs on right panels of Figures 2.4E and 2.4F. The P[4] and P[6] antigens showed similar thermal induced aggregation profiles. It is interesting to note the substantially lower T_{onset} values (by $\sim 20^\circ\text{C}$) by SLS as compared to OD_{350} method for each of the three antigens. These differences in SLS vs. OD_{350} results likely reflects the higher sensitivity of SLS towards formation of smaller aggregates compared to OD_{350} method which is likely more sensitive to the formation of larger aggregates/particles in solution.

Physical stability of each antigen as a function of both solution pH (from 3.0 to 8.0) and temperature (from 10 to 90°C) was then monitored to measure changes in secondary structure, tertiary structure, and aggregation behavior. Overall, a pH-dependent destabilization was observed in secondary structure for each antigen (Supplemental Figure S2.2, A – C). For tertiary structure analysis, intrinsic Trp fluorescence MSM peak position showed some subtle changes in the thermal melt profiles, but in general, was not sensitive enough to monitor any potential differences between the antigens (Supplemental Figure S2.2, D – I). In contrast, DSF showed a clear pH-dependent

destabilization with lower pH being less stable as the temperature was increased (Supplemental Figure S2.2, J – L). Aggregation propensity vs solution pH was assessed by monitoring the intensity of total scattered light at 295 nm at 90 degrees. P[8] showed highest intensity values at pH 6.0 and pH 7.0 before precipitation occurred (Supplemental Figure 2.2O). In summary, all three antigens showed a pH dependent destabilization at lower pH values (with P[6] being least stable at pH 4.0 and pH 5.0).

To better visualize and compare the entire biophysical stability data sets of each antigen as a function of pH and temperature, a radar chart, data visualization analysis ¹²⁰ was utilized (Figure 2.5). Each radar chart has 5 axes corresponding to the five biophysical measurements and the data are mapped to a pentagon such that smaller area of polygon indicate native-like state of protein and relatively larger area represents structural alterations. For each antigen, four distinct regions were observed (Regions I, II, III/IV, V). Region I correspond to a native-like structure of the antigen, Region II represent partially structurally altered state, Region III denote low pH structurally altered state, Region IV shows an aggregation prone region identified specifically for P[8] antigen, and Region V represent more extensively aggregated and structurally altered state. Data for each technique can be read in the radar charts by following a particular axis. For instance, SLS signal is mapped to axis ‘a’ (Figure 2.5, radar chart key) and if we follow axis ‘a’ for P[8] antigen in radar charts I to V; I – low signal indicate native-like or monomeric state, II – low to medium signal indicate low levels of aggregation, IV – high signal i.e. significant aggregation, V – low signal due to precipitation of aggregated protein. If the total relative area of native-like state (i.e., Region I) of each antigen is compared; P[8] was most stable with an area of 39%, followed by P[4] with 33%, and P[6] was least stable (27%). Also, a specific aggregation prone region (Region IV) was identified for P[8] suggesting it might be prone to aggregation in that range of

pH and temperature (note that P[4] and P[6] are also structurally altered and/or aggregated in Region IV).

2.2.3 Chemical stability profiles and comparisons of the three NRRV antigens

After subjecting the three NRRV antigens to elevated pH and temperature stress (pH 9.0, 25°C for 6 days), an increasing trend in molecular mass was observed for each protein by intact mass analysis compared to pH 7.2, 4°C control samples (Figure 2.6A). Peptide mapping analysis was conducted to further probe the nature of the mass increase. Representative data for P[4] is shown in Figure 2.6B and similar data for P[6] and P[8] antigens are shown in Supplemental Figures S2.3A and S2.3B, respectively. Under no stress conditions (pH 7.2, 4°C), deamidation was observed at Asn⁷ in each antigen and at each of the Asn-Gly (NG) sites (P[4] and P[8] antigens have two NG sites, whereas, P[6] has none). Upon incubation at pH 9.0 25°C for 6 days, P[4] antigen showed increased levels of deamidation at Asn⁷ and Asn-Gly residues (Asn⁴⁷ and Asn¹⁷⁹) as shown in Figure 2.6C. For P[6] antigen, Asn⁷ showed increased levels of deamidation under the same stress conditions. The P[8] antigen also showed increased levels of Asn⁷ deamidation and an increasing trend of deamidation was observed for the Asn-Gly residues (Asn⁴⁶ and Asn¹⁷⁸) under similar stress, although it was not statistically significant under these conditions (more notable levels of Asn⁴⁶ and Asn¹⁷⁸ deamidation were observed in P[8] when subjected to more aggressive stress condition of pH 9.0 40°C for 6 days, however, P[4] and P[6] antigens could not be tested for deamidation under this condition due to aggregation (data not shown). Overall, forced deamidation studies demonstrated the susceptibility of Asn⁷, Asn⁴⁷, Asn¹⁷⁹ in P[4], Asn⁷ in P[6], and Asn⁷, Asn⁴⁶, Asn¹⁷⁸ in P[8] towards deamidation under basic conditions at elevated temperature with the Asn⁷ residue being the most labile across all three antigens.

SDS-PAGE analysis (under non-reducing conditions) of the same elevated pH and temperature stressed P[6] samples showed an additional band corresponding to dimeric species which was absent/less abundant under reducing condition as shown in Figure 2.7A. This result suggests the dimeric species were linked with inter-molecular disulfide bond since each NRRV antigen has single Cys residue. A faint dimeric band was also present under non-reducing condition for P[6] pH 9.0, 4°C stressed samples. RP-UHPLC analysis showed an additional peak (~34.5 min) eluting at later retention time than the monomer peak (~30 min) as shown in Figure 2.7C. This additional peak was identified as P[6] dimer species by MS¹ analysis (right panel, Figure 2.7C) which correlates with SDS-PAGE results. However, the dimeric species were not observed by intact mass analysis presumably due to their low abundance and a single peak corresponding to monomeric protein was observed in control and stressed samples (Figure 2.7B). For the P[4] antigen, a very faint HMW smear was observed at pH 9.0, 25°C (but not at pH 9.0, 4°C) under non-reducing conditions in SDS-PAGE analysis as shown in Supplemental Figure S2.4A. The P[4] dimer species also eluted at later retention time on reversed-phase chromatography as confirmed by the MS¹ analysis of the eluting peaks (see Supplemental Figure S2.4C). For the P[8] antigen, no additional HMW species was observed under the tested conditions suggesting higher stability of this antigen to non-native disulfide formation as compared to P[4] and P[6] (see Supplemental Figure S2.5). Overall, the chemical stability profile demonstrates that P[6] is more susceptible to this non-native disulfide bond reaction compared to P[4] and P[8] antigens.

In terms of oxidative stress reactions, the three NRRV antigens were subjected to different amounts of H₂O₂. Figures 2.8A and 2.8B show representative data for P[6] antigen, a prominent peak for native species and low level of oxidized species were observed in the control sample (without H₂O₂) as measured by intact mass spectrometry and LC-MS peptide mapping,

respectively. With the increasing amount of H₂O₂ the relative abundance of native species decreased, and the number and abundance of oxidized species increased. Peptide mapping analysis was conducted to identify the amino acids undergoing oxidation and also to quantify the oxidation relative to the control sample. As shown in Figure 2.8C, for P[6] antigen which has two Met residues, Met¹ was most susceptible to oxidation followed by Met¹⁰⁰. Similar observations were made for the two Met residues in P[8] antigen (Met¹ more susceptible than Met⁹⁹), as shown in Figure 2.8C and Supplemental Figure S2.8. The P[4] antigen has three Met residues and their susceptibility to oxidation can be rank ordered as Met¹ > Met¹⁰⁰ > Met¹²⁴ (Figure 2.8C). Oxidized Met¹⁰⁰ in P[4], P[6], and Met⁹⁹ in P[8] were only detectable when samples were incubated with ≥ 0.1% H₂O₂ (≥ 1000 ppm) as described in Figure 2.8C. Similarly, Met¹²⁴ in P[4] was oxidized only when exposed to ≥ 0.25% H₂O₂ (data not shown). No detectable change in the elution profile of digested peptides was observed until exposure to 0.1% H₂O₂, at which point the elution profile was altered and sequence coverage was reduced from 100% to ~80% for all three antigens (Supplemental Figure S2.6 – S2.8). In addition, the elution profiles of each sample (stressed or control) of a particular antigen were similar on a reversed-phase column, in which the primary peak eluted at ~9.5 min (P[4]), ~9.7 min (P[6]), and ~9.5 min (P[8]) as shown in Figure 2.8D and Supplemental Figure S2.9. Also, the area of the peak corresponding to native species did not change substantially between samples (Figure 2.8D) indicating no measurable loss of protein. In summary, intact protein mass measurement and peptide mapping by LC-MS methods are assays of choice to detect and monitor oxidation. The Met¹ residue in each NRRV protein antigen was most susceptible to H₂O₂ induced oxidation, and oxidation was also observed at other Met residues under more aggressive stress conditions (≥ 1000 ppm H₂O₂).

2.2.4 Structural modeling and comparisons of the three NRRV antigens

As a first step to facilitate the analysis of the physicochemical data generated in this work, a schematic is provided in Figure 2.9A which describes the composition and nomenclature of the three NRRV antigens studied in this work (refer to Introduction section for more details). The X-ray crystal structures for VP8-P[4] (i.e., Δ VP8* from DS-1 (G2P[4]) strain) and VP8-P[8] (i.e., Δ VP8* from Wa (G1P[8]) strain) have been determined. These proteins bind to carbohydrates on target epithelial cell receptors and are involved in host cell recognition and attachment during RV infection^{124,125}. We used I-TASSER modelling to model the 3-D structure of the complete NRRV antigen, i.e. including the P2 epitope, by using the available crystal structures of the Δ VP8* protein from DS-1 and Wa strains of human rotavirus as template. As described in the methods section, I-TASSER modelling predicted five structures with the lowest energy state for each antigen and the major difference between the five predicted structures is the unstructured/random orientation of the P2 epitope indicating its flexible nature. Figure 2.9B shows the predicted 3-D structure of each NRRV antigen including the three key structural elements: the P2 epitope (black), GSGSG linker (cyan) and Δ VP8* protein (grey). The chemically labile residues or “weak spots” identified for each antigen in this work are highlighted on the structural models (Met – magenta, Asn – green, Cys - red) in Figure 2.9B.

2.3 Discussion

In this work, the primary and higher-order structures, post-translational modifications, and product-based impurities (e.g., charge heterogeneity, aggregates) of the three recombinant NRRV protein antigens were measured and compared using a wide variety of physicochemical characterization tools. In addition, degradation pathways of each of these proteins were elucidated

via forced degradation studies to identify “weak spots” in terms of physical and chemical stability profiles. Although the potential impact of physicochemical structural alterations on immunogenicity is unknown at this time, developing such stability-indicating analytical tools and applying the structural knowledge gained in this work will be useful to (1) set critical manufacturing process parameters to ensure consistency, (2) monitor key structural attributes during comparability assessments, and (3) develop stable formulations for the bulk drug substance and adjuvanted final drug product. The pharmaceutical stability profiles encountered during manufacturing and storage are not only dependent on such intrinsic properties (e.g., primary sequence/post-translational modifications ¹²⁶, conformational stability ¹²⁷, solubility ¹²⁸), but also extrinsic stress factors (e.g., storage temperature, freeze-thaw, agitation) ^{81,129}.

Primary structure, post-translational modifications and chemical stability profile

An additional Met residue identified at N-terminus of each antigen was not unexpected since these antigens were expressed in *E. coli* and the efficiency of methionine aminopeptidase (MetAP), enzyme responsible for excision of N-terminal methionine during translation, is about 30–60% depending on the host ¹³⁰. Residue next to the N-terminal Met for each NRRV antigen is Glu with a bulky side chain which could also hinder the efficiency of MetAP by steric effects as noted in the literature ^{131,132}. Peptides generated after chymotrypsin digestion during peptide mapping analysis of each antigen showed distinct and very reproducible elution profile on a RP column which could be used as an identity test during future development of these antigens.

Oxidation via reactive oxygen species is a commonly observed chemical degradation pathway for protein biotherapeutics/vaccine antigens which can affect product quality, stability, and raises immunogenicity concerns ^{133,134}. Peroxides are an example of reactive oxygen species which can come in contact with vaccine drug products through various means such as the use of

vaporized H₂O₂ as a sterilizing agent, as contaminants in formulation excipients like polysorbates, and potentially even as trace quantities present in water depending upon its source¹³⁵⁻¹³⁸. Under forced degradation conditions (100 – 5000 ppm H₂O₂), the Met¹ residue was most sensitive to oxidation in each of the three NRRV antigens. Interestingly, the Met¹⁰⁰ or Met⁹⁹ residue in each antigen, and Met¹²⁴ in P[4] antigen were less prone to H₂O₂ induced oxidation compared to Met¹ (which could be due to their reduced solvent accessibility within the 3D structure of the protein; see below).

Forced deamidation studies confirmed that Asn⁷ in each NRRV antigen is susceptible to deamidation under conditions of basic pH and elevated temperature. Asn⁷ in these proteins is followed by Ser residue which is the second most susceptible sequence for deamidation after NG sequence⁸¹. The P[4] and P[8] antigens each have two NG sites (P[6] has none) in their primary sequence, and the Asn residues at these sites also showed increasing trend in deamidation levels for stressed samples (Figure 2.7C). It is known that Asn deamidation in proteins and peptides depends on a combination of factors including their primary sequence, three dimensional (3D) structure (i.e., flexibility and solvent accessibility of these sites) and solution conditions (i.e., pH, buffer type, temperature)^{139,140}. Overall, the peptide mapping method was able to detect and quantify the Asn deamidation in each NRRV antigen and thus will be a valuable tool during future formulation development and analytical comparability assessments.

The labile Met¹ and Asn⁷ residues are both located in the P2 epitope region of these antigens which is highly flexible and unstructured as predicted by I-TASSER modelling (Figure 2.9B) and some preliminary hydrogen deuterium exchange mass spectrometry studies (data not shown). Higher flexibility of this P2 region would explain the higher propensity of Met¹ to

oxidation and Asn⁷ to deamidation due to their relatively higher solvent accessibility compared to other Met and Asn residues which could be buried inside the protein structure.

In addition, the one free Cys residue in each NRRV antigen is also a “weak spot” in each antigen. Under stressed conditions of elevated pH and temperature, we observed reducible dimeric/multimeric species which were linked with intermolecular disulfide bonds. The P[6] antigen showed the highest susceptibility to this degradative reaction, followed by P[4], while dimeric/multimeric species were not observed for P[8] under the tested conditions. This result is in agreement with the physical stability data which showed higher conformational stability of P[8] antigen suggesting some sort of conformational alteration is needed for the Cys residue to get more solvent exposed allowing it to form non-native intermolecular disulfide bonds. Susceptibility of Cys¹⁷³ in P[4] and P[6] to non-native disulfide formation could be due to lower conformational stability of the helical domain containing this Cys residue, thus exposing the free Cys to solvent and promoting the degradative reaction. Although the P[8] antigen was more stable to this degradative reaction under these conditions, disulfide linked covalent aggregates were formed with all three NRRV antigens when subjected to agitation stress (see chapter 3).

Size, higher-order structure (HOS), and physical stability profile

Each antigen was primarily monomeric in size and P[6] eluted at later retention times on a SEC column compared to P[4] and P[8]. The smaller overall size of P[6] was in agreement with the sedimentation coefficient values. These results are consistent with P[6] being more globular or compact in its overall conformation. In addition, GRAVY analysis indicated P[6] is most hydrophobic out of the three antigens with a GRAVY score of -0.466, as compared to P[4] and P[8] with scores of -0.573 and -0.569, respectively. This could also explain in part its relatively

more compact three-dimensional structure. The more hydrophobic nature of P[6] was also confirmed by the observed longer retention times on HIC and RP columns to P[4] and P[8].

The HOS of each NRRV antigen was primarily β -sheet in composition as suggested by available crystallographic information on Δ VP8* (PDB ID: 2AEN, 2DWR) and predicted by I-TASSER modelling (Figure 2.9B). The FTIR and far-UV CD spectroscopic results in this work are consistent with this secondary structure composition. Some minor differences in environment around Trp residues were observed between the three antigens; the average Trp residues appeared to be more buried for P[4] and P[6] antigens compared to P[8].

Differences in structural integrity and physical stability of the three NRRV antigens (with 66 – 80% sequence homology) highlight the importance of differences in the primary and HOS structures of otherwise “similar” antigens that can govern their pharmaceutical stability profiles and developability as a vaccine candidate. Solution pH plays an important role in controlling the ionization state of different residues which keep the molecule in its marginally stable HOS, native conformation^{141,142}. Each NRRV antigen underwent structural alterations at pH 3.0. The P[6] antigen was least stable at pH 4.0 and 5.0 followed by P[4] and P[8]. Radar chart analysis is a data visualization tool that has been employed to summarize and compare large biophysical data sets to study the effect of various stresses (e.g., pH, temperature) on physical stability of a wide variety of macromolecules including vaccine and protein drug candidates^{127,143-149}. Radar chart analysis in this work showed that the structural integrity and conformational stability of three NRRV antigens as a function of pH and temperature. P[8] was the most stable, followed by P[4], and P[6] was least stable. In addition, non-native dimer formation was observed for P[6] and P[4] antigens, no dimeric species was recorded for P[8]. Interestingly, the P[8] antigen showed relatively lowest

stability against shaking (i.e., colloidal stability) and freeze-thaw stresses resulting in the highest levels of particle formation when comparing the three NRRV antigens (see chapter 3).

Ongoing and Future Work

In terms of ongoing and future work, both physical and chemical degradation processes elucidated in this work (leading to structural alterations, chemical changes and/or aggregate formation) could be detrimental to the development of NRRV antigens as a candidate vaccine without appropriate formulation development. The analytical characterization tools developed in this work were applied to the development of candidate formulations to minimize protein aggregation during frozen storage of these NRRV antigens as bulk drug substance (see chapter 3). These assays can also be adopted and modified to characterize and assess the physicochemical stability of the final drug product which will be formulated with an aluminum-based adjuvant to further enhance the immunogenicity of this vaccine (see chapter 4). However, it is essential as part of future work to better correlate these physicochemical changes with *in vitro* potency using immunochemical (binding) assays (e.g., ELISA, bio-layer interferometry, or surface plasmon resonance) utilizing antibody reagents which are specific to each antigen and bind to neutralizing epitope(s). Eventually the results from physicochemical and *in vitro* potency assays need to be correlated with *in vivo* immunogenicity (animal studies) in order to determine their true impact on biological potency of the vaccine. Finally, the physicochemical analytical tools described in this work can be used during future comparability assessments of different lots of each of the NRRV antigens made from scaled-up manufacturing processes. It is not uncommon to introduce changes in the manufacturing processes during scale-up or switching to a different manufacturing site to keep the cost of vaccine production low, which is a key focus for the success of this subunit rotavirus vaccine candidate for use in the developing world.

2.4 Figures

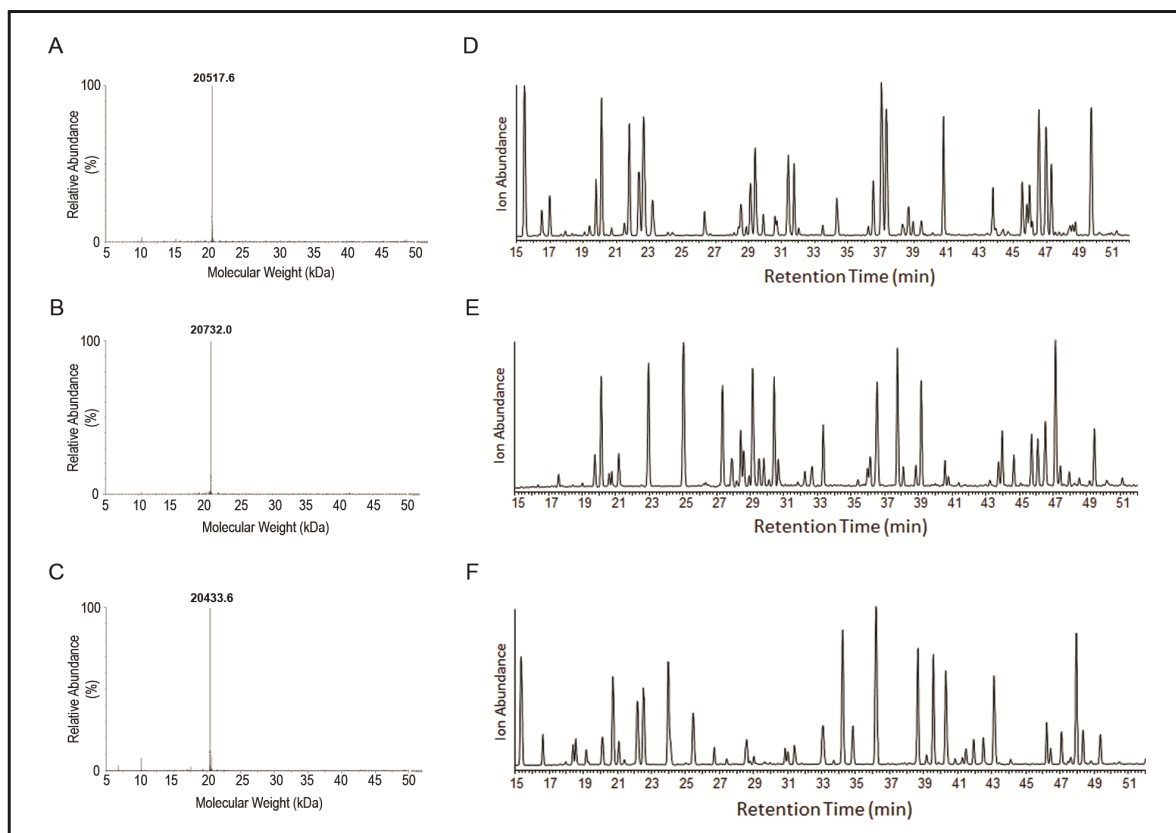


Figure 2.1. Primary structure analysis of the three NRRV antigens. Representative deconvoluted mass spectra for analysis of intact proteins under reducing condition for (A) P[4], (B) P[6], and (C) P[8]. Representative UV_{214nm} chromatogram from peptide map analysis of reduced, alkylated, and chymotrypsin digested proteins for (D) P[4], (E) P[6], and (F) P[8]. See Supplemental Figure S2.1 for intact mass analysis data under non-reducing condition and sequence coverage (100% for both reducing and non-reducing conditions) from peptide map analysis.

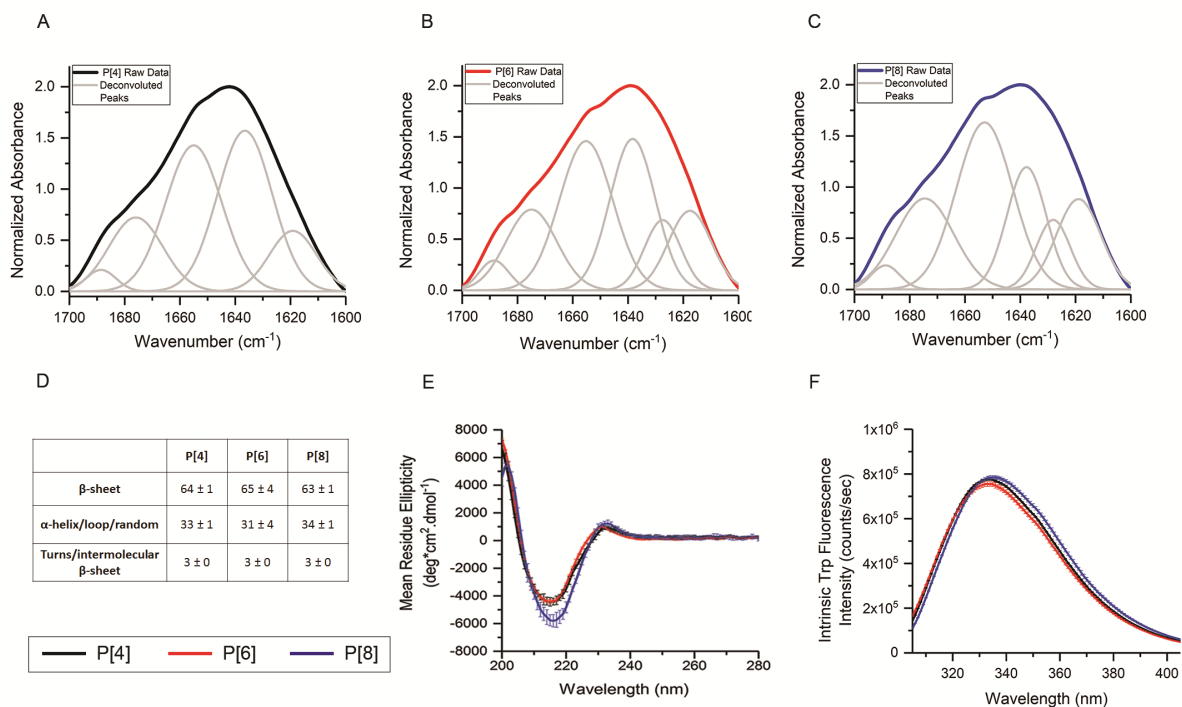


Figure 2.2. Higher order structure (HOS) analysis of each of the three NRRV protein antigens at 10°C in 10 mM PBS, pH 7.2. Representative FTIR absorbance spectrum of the amide I region and Fourier self-deconvoluted peaks for (A) P[4], (B) P[6], (C) P[8] antigens, and (D) secondary structure composition of each antigen obtained from Fourier self-deconvolution of FTIR spectrum. (E) Far-UV CD spectra, and (E) intrinsic Tryptophan fluorescence emission spectra overlay for the three antigens. Error bars denote 1SD from triplicate measurements.

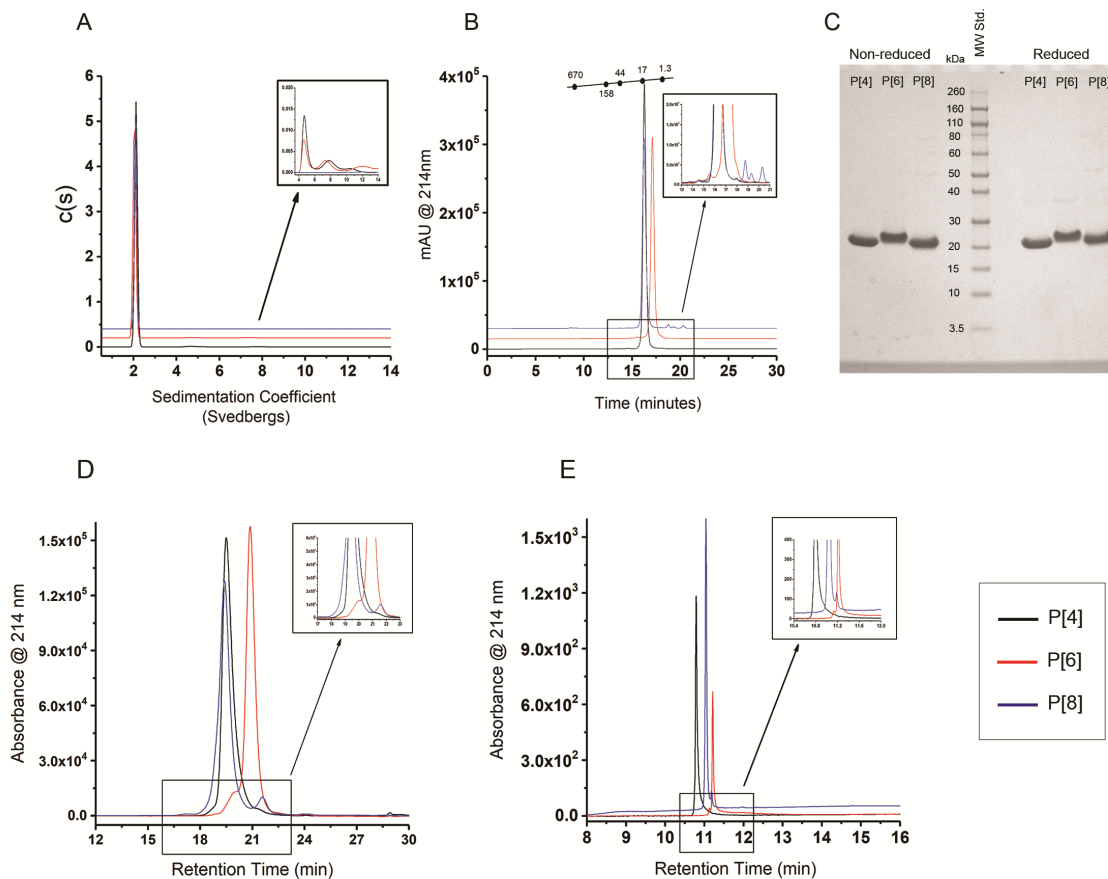


Figure 2.3. Size, aggregation, and heterogeneity analysis of each of the three NRRV antigens in 10 mM PBS, pH 7.2. (A) Representative SV-AUC sedimentation coefficient distribution profiles from 0 to 14 Svedbergs, inset shows $c(s)$ distribution from 4 to 14 Svedbergs for better visualization of aggregate species peak(s). (B) Representative SE-HPLC chromatograms for three antigens with inset showing the peaks corresponding to fragments and/or aggregate species. (C) SDS-PAGE analysis under non-reducing and reducing (+ DTT) conditions. (D) Representative HIC chromatograms, and (E) representative RP-HPLC chromatograms of the three antigens overlay with inset showing the minor peaks for better visualization. DTT, dithiothreitol.

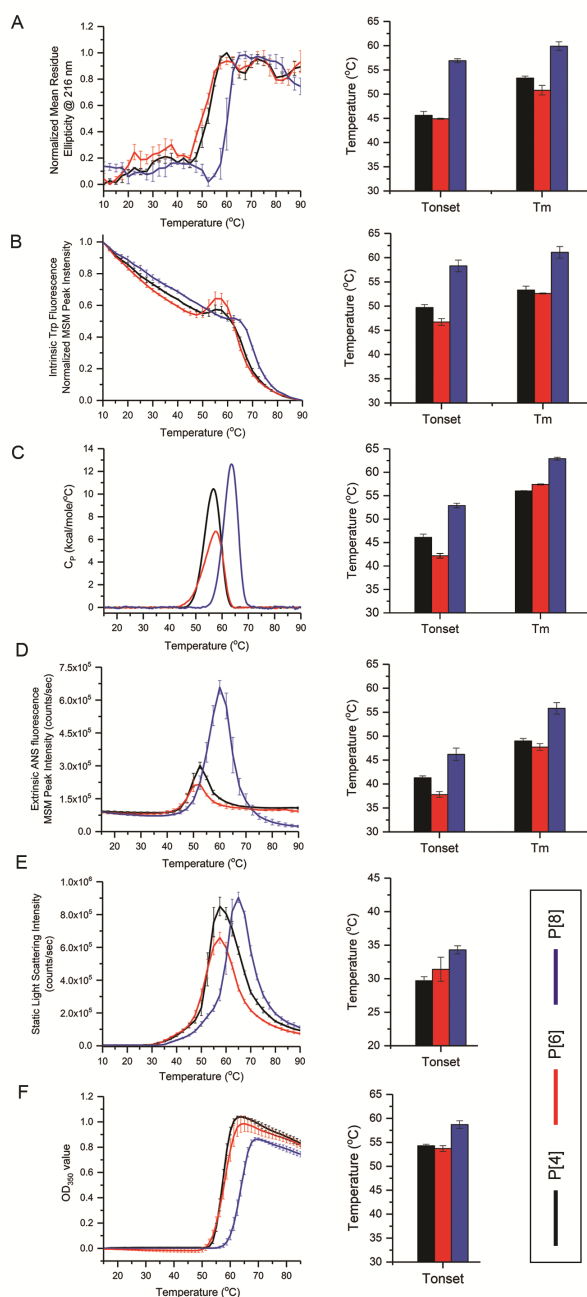


Figure 2.4. Higher-order structure (HOS) stability and aggregation propensity of the NRRV antigens in formulation buffer at pH 7.2 as a function of thermal stress (10°C to 90°C). (A) Far-UV CD normalized mean residue ellipticity at 216 nm, (B) intrinsic tryptophan fluorescence normalized MSM peak intensity, (C) representative DSC thermograms of each antigen, (D) extrinsic ANS fluorescence MSM peak intensity, (E) static light scattering intensity at 295 nm, and (F) OD₃₅₀ values for P[4] (black), P[6] (red), and P[8] (blue) antigens. Bar graphs on the right side of each panel show thermal onset and melting temperature values for each antigen. Error bars represent 1 SD from triplicate measurements.

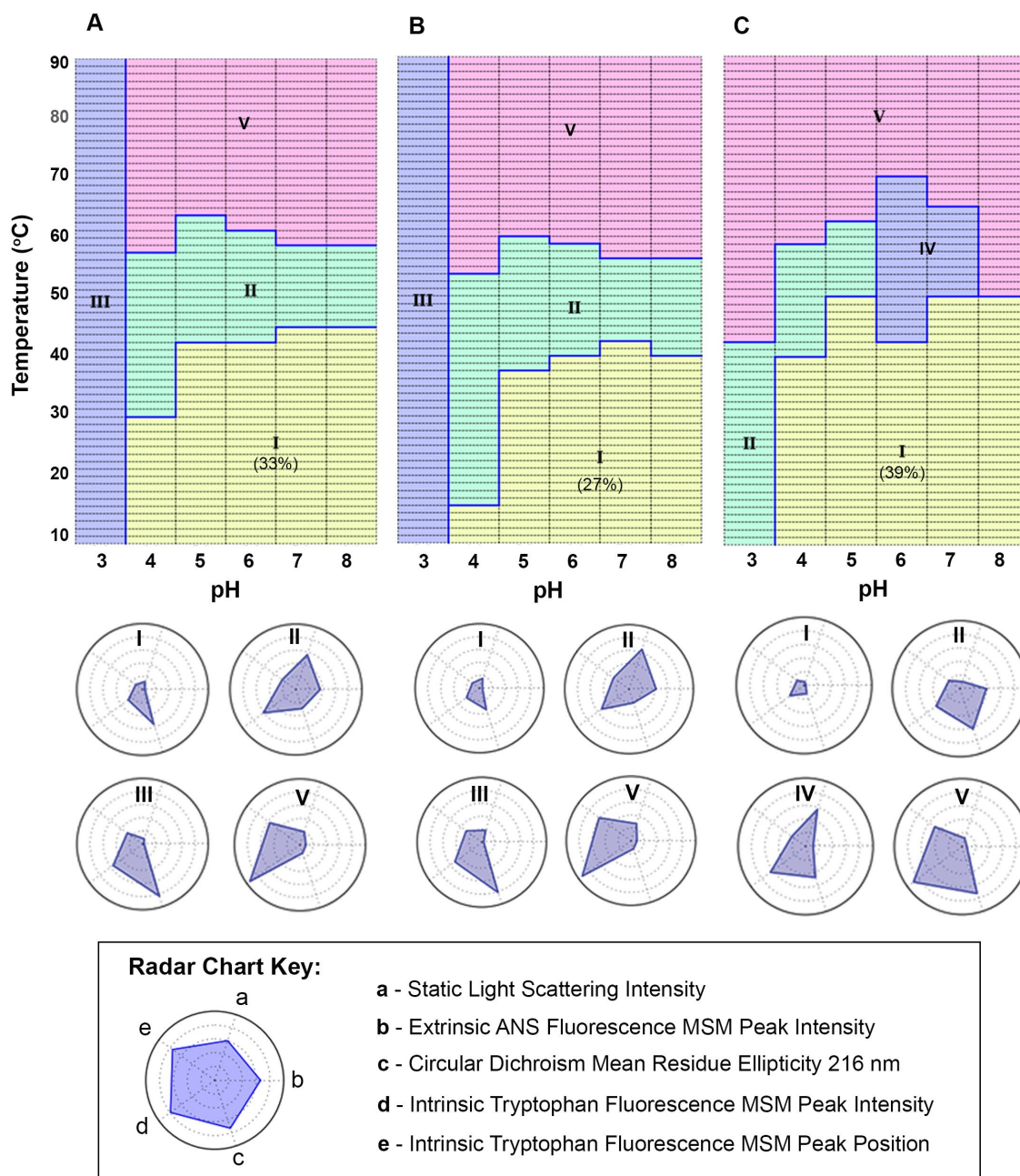


Figure 2.5. Biophysical stability profile from radar chart analysis of each NRRV antigen versus temperature across the pH range of 3.0 to 8.0. Sample buffer is 20 mM citrate phosphate buffer containing 150 mM NaCl at indicated pH value. Panel (A) P[4], (B) P[6], and (C) P[8] show radar charts generated from multivariate stability data sets shown in Supplemental Figure 2.2. Radar chart key is provided in the bottom panel (see text for further explanation).

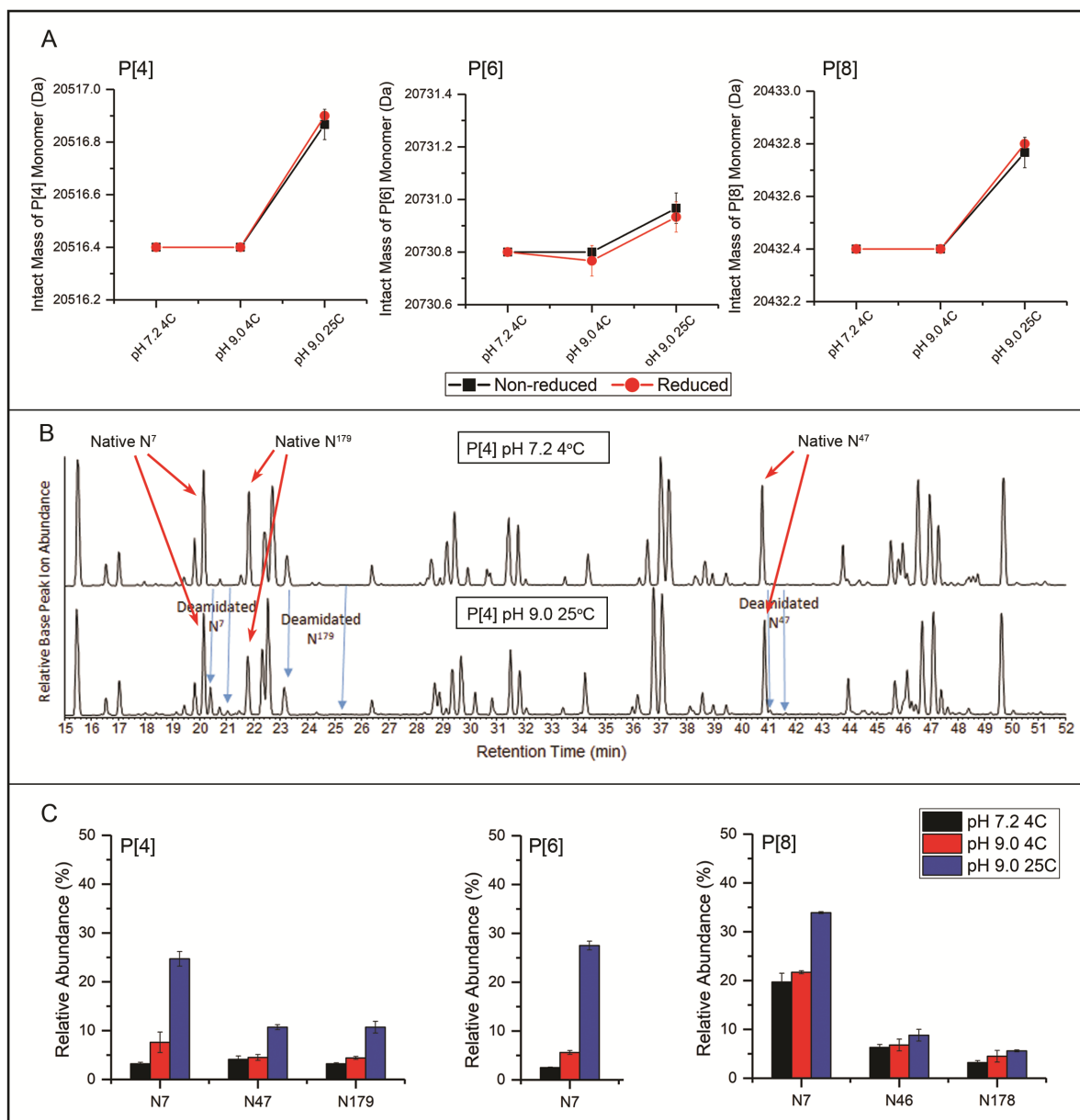


Figure 2.6. Forced degradation (Asn deamidation) studies of each antigen after incubation at pH 9.0 25°C for 6 days. (A) Monomer species mass from intact mass analysis of reduced (red) and non-reduced (black) samples for each antigen. (B) Representative total ion chromatogram from peptide map analysis of reduced, alkylated, and chymotrypsin digested P[4] samples, pH 7.2 4°C (top) and pH 9.0 25°C (bottom), native Asn peaks are pointed by red arrows and deamidated Asn peaks are pointed out by blue arrows (see Supplemental Figure S2.3 for peptide map data with P[6] and P[8] antigens). (C) Percent deamidation of different Asn residues in each antigen obtained from the peptide mapping analysis under reducing conditions. Error bars represent 1SD from triplicate vials.

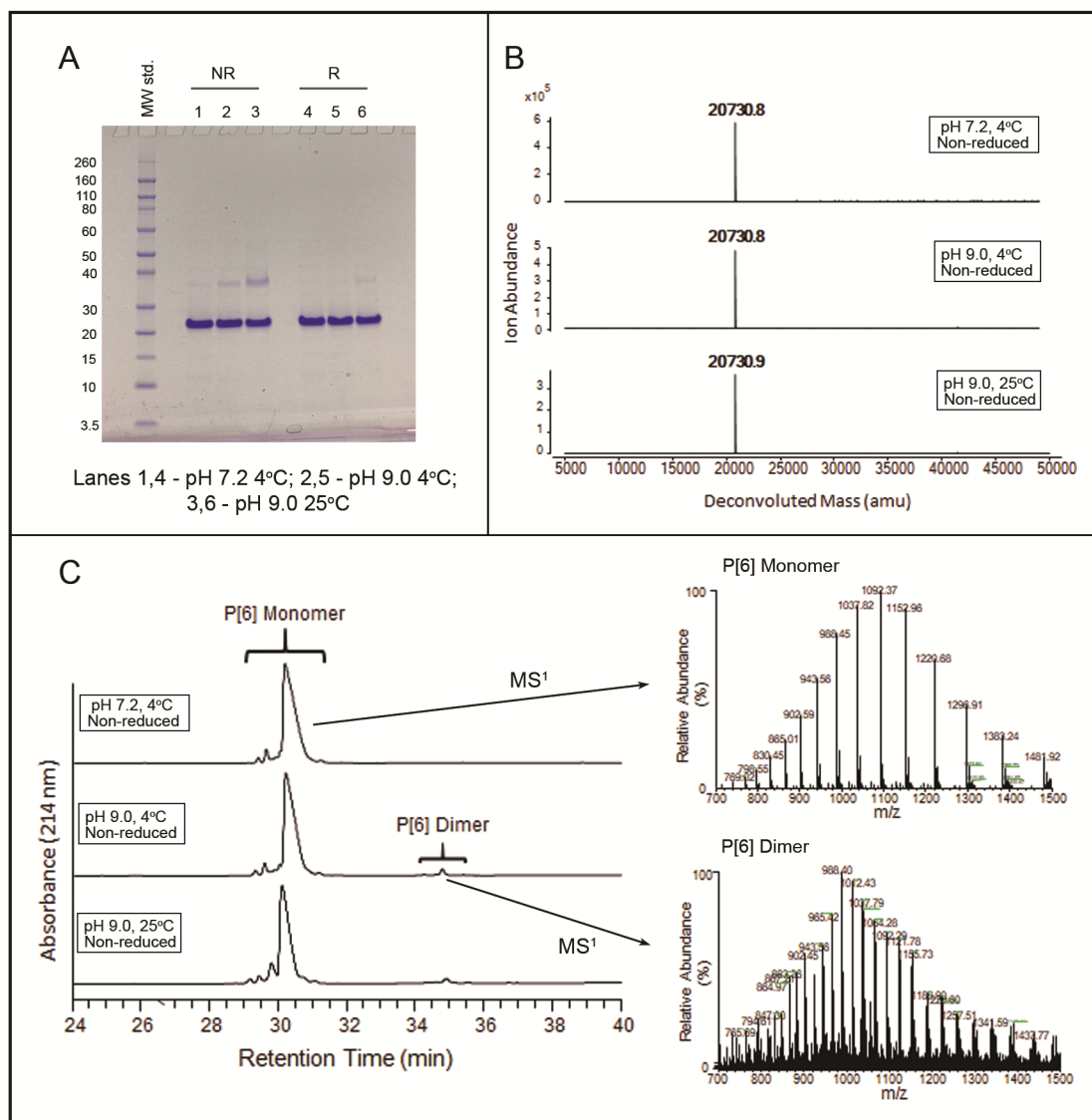


Figure 2.7. Forced degradation (non-native disulfide formation) studies with P[6] antigen after incubation at pH 9.0 25°C for 6 days. (A) SDS-PAGE analysis, (B) intact mass analysis, and, (C) RP-UHPLC analysis of the stressed and control samples, further, MS¹ spectra confirming the molecular masses of the eluting peaks to the P[6] monomer and dimer species are shown. Refer to Supplemental Figures S2.4 and S2.5 for similar data with P[4] and P[8] antigens, respectively.

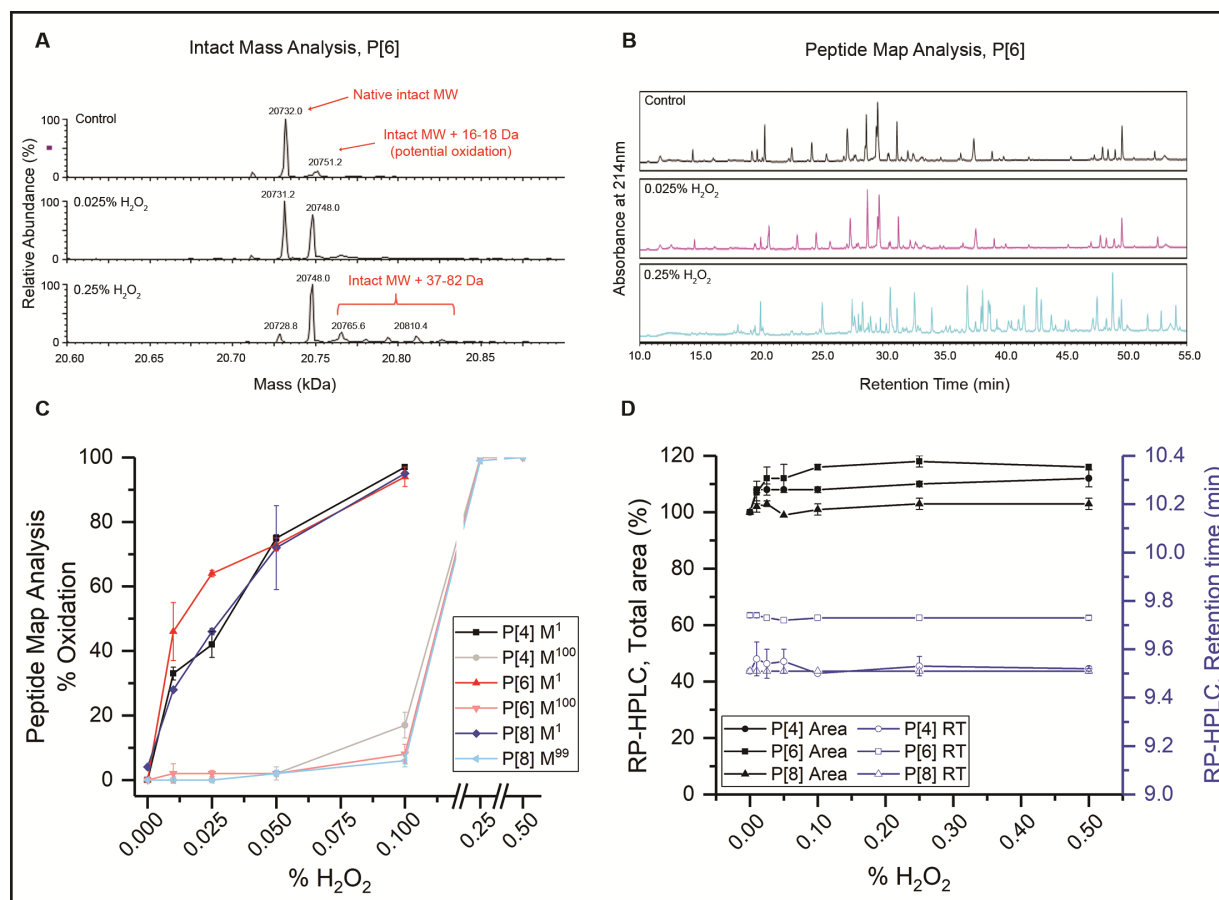


Figure 2.8. Forced oxidation studies as a function of hydrogen peroxide concentration. Representative (A) deconvoluted mass spectra for intact mass analysis, and (B) peptide map analysis of P[6] antigen under reducing (+DTT) condition. See Supplemental Figures S2.6 – S2.9 for the complete data sets of the three antigens. (C) Hydrogen peroxide effect on the relative percent oxidation of 2 out of 2 methionine residues for P[6], P[8], and 2 out of 3 methionine residues for P[4]. (D) % total area and retention time of main peak in RP-HPLC chromatograms of each antigen, see Supplemental Figure S2.9 for individual chromatograms. Error bars represent 1SD from triplicate measurements.

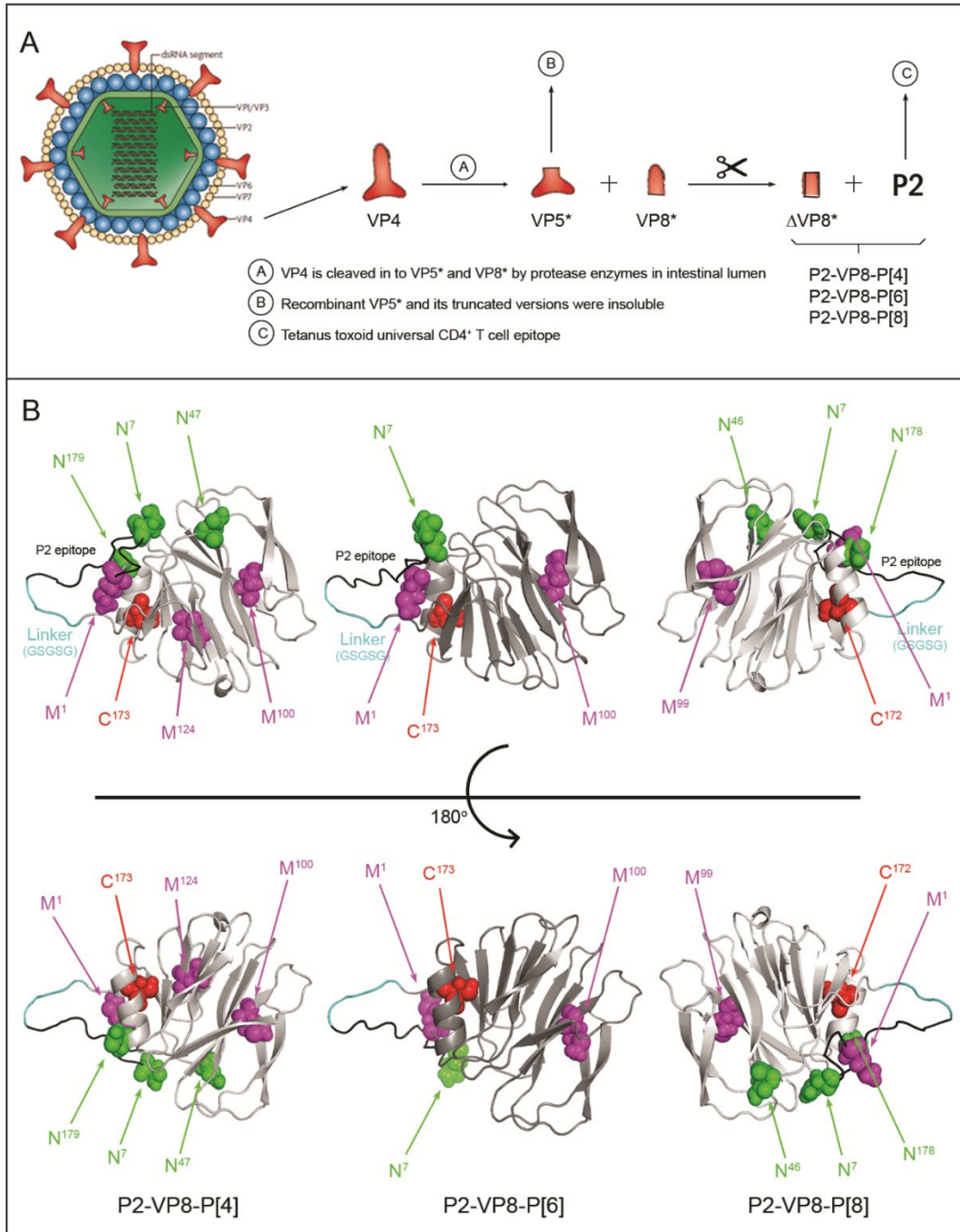
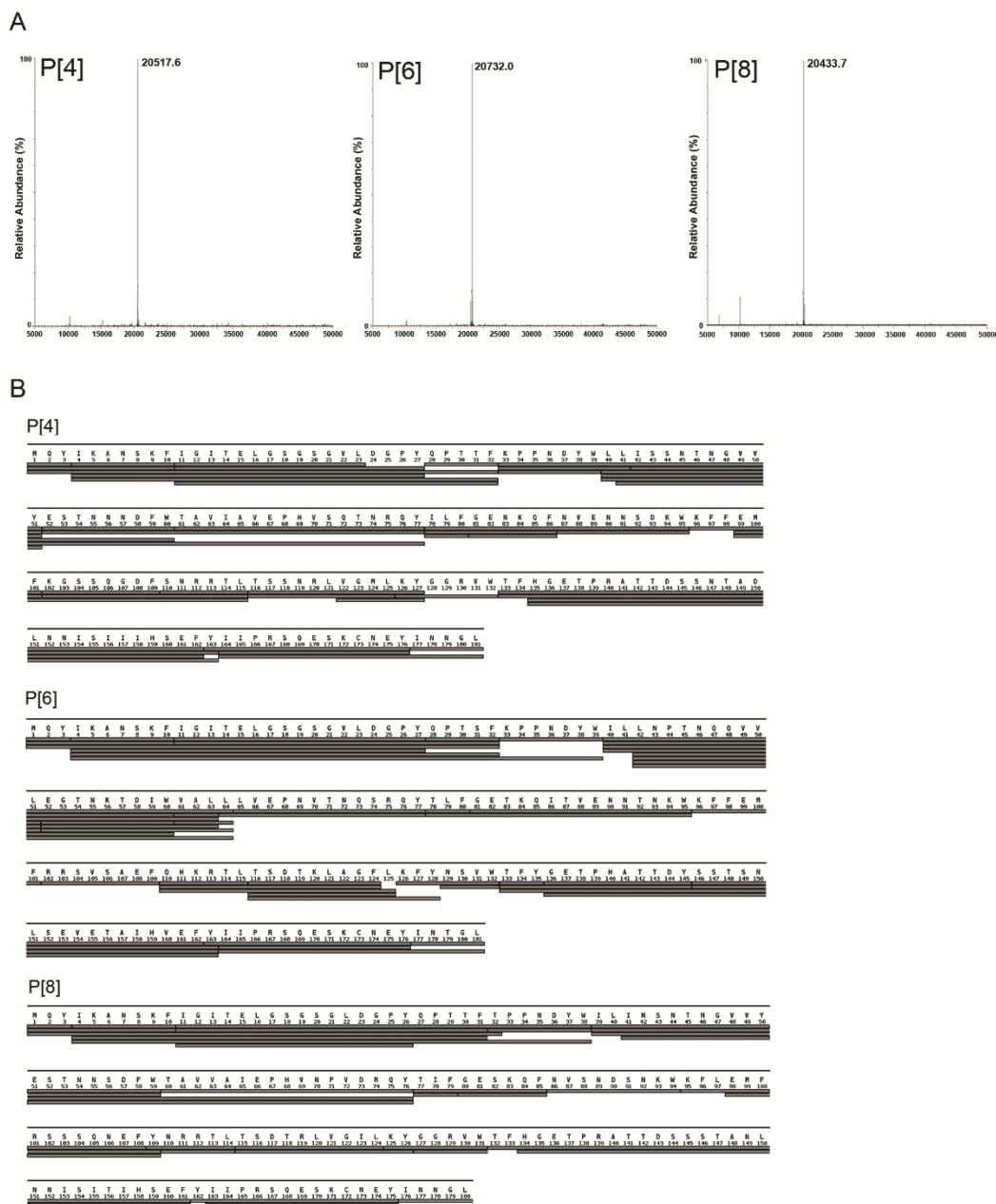
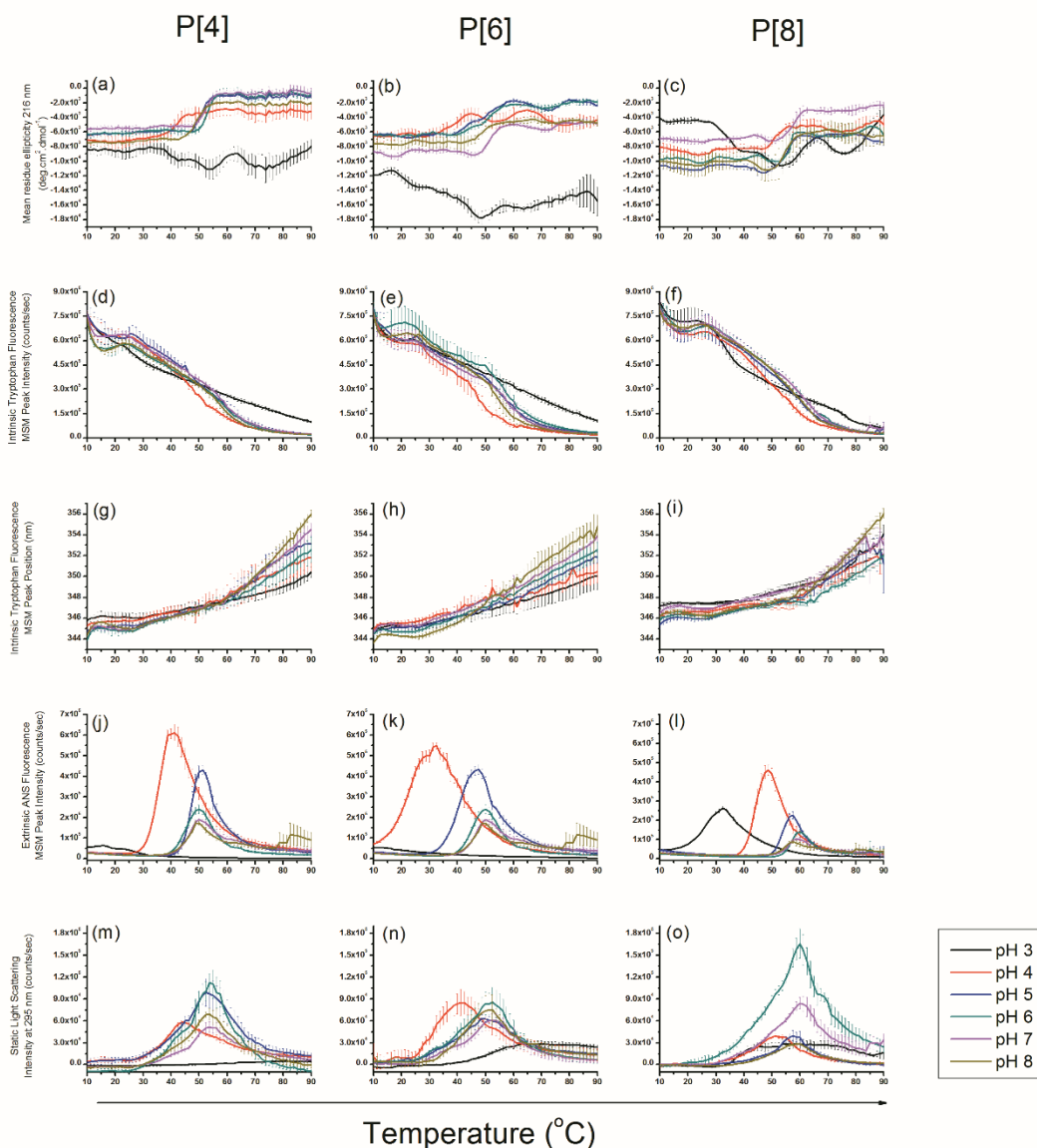


Figure 2.9. Structural modeling of the three NRRV protein antigens. (A) Schematic description of the protein composition and nomenclature of each NRRV antigen, and (B) 3-D structure prediction of each NRRV antigen using I-TASSER modelling; Δ VP8* protein is shown in grey, GSGSG linker in cyan, and P2 epitope in black. Residues susceptible to chemical degradation under stressed conditions are highlighted (Cys - red, Asn - green, Met - magenta).

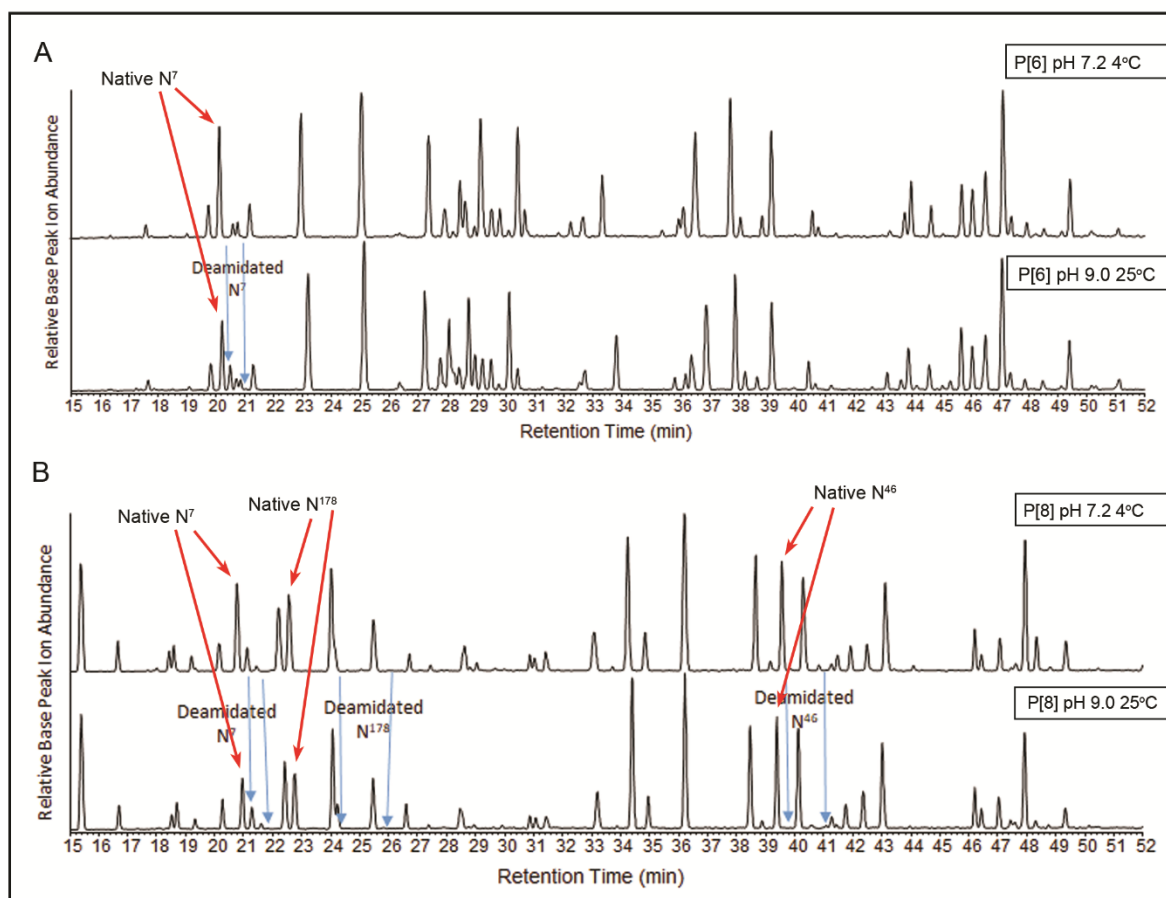
2.5 Supplemental Figures



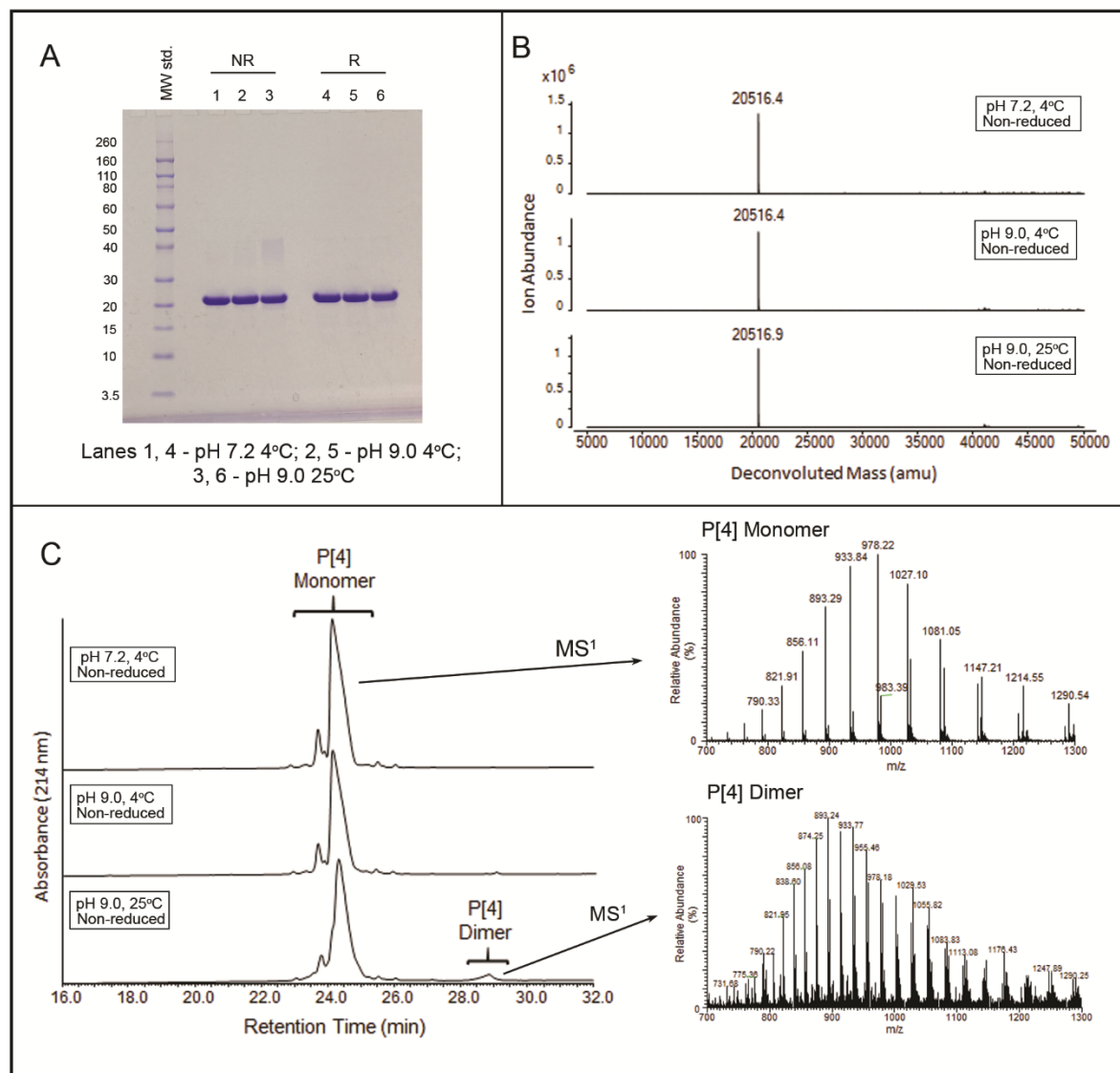
Supplemental Figure S2.1. Primary structure analysis of the NRRV antigens. (A) Representative deconvoluted mass spectra for analysis of intact proteins under non-reducing condition, and (B) sequence coverage of each antigen from peptide map analysis of reduced, alkylated, and chymotrypsin digested proteins.



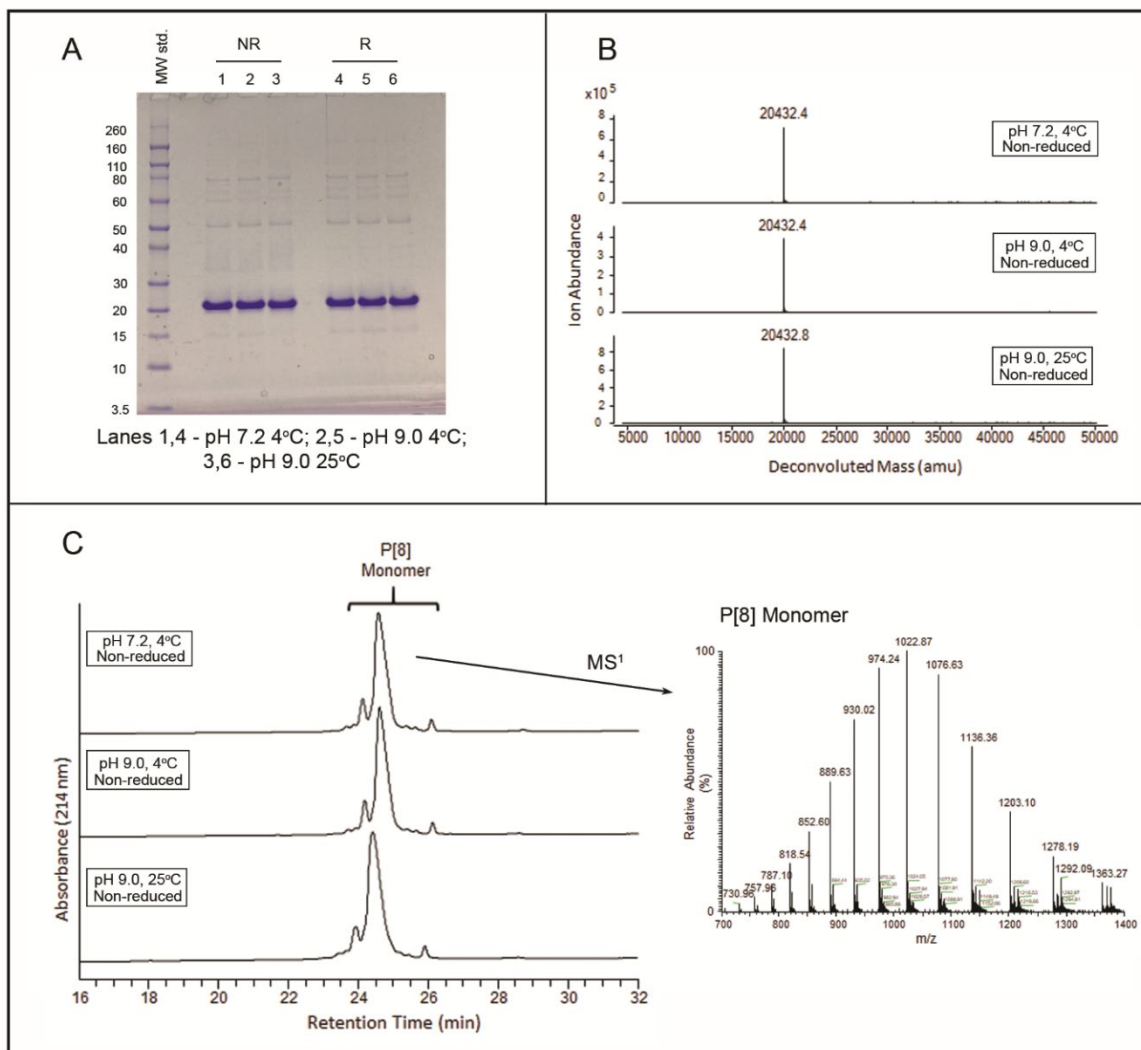
Supplemental Figure S2.2. Biophysical stability profile and data for radar chart analysis of the three NRRV antigens versus temperature across the pH range of 3.0 to 8.0 in 20 mM citrate phosphate buffer containing 150 mM NaCl. Biophysical measurements include (a – c) far-UV CD normalized mean residue ellipticity at 216nm, (d – f) intrinsic tryptophan fluorescence MSM peak intensity, (g – i) intrinsic tryptophan fluorescence MSM peak position, (j – l) extrinsic ANS fluorescence MSM peak intensity, and (m – o) static light scattering intensity at 295 nm for each of the three antigens. Error bars represent 1SD from triplicate measurements.



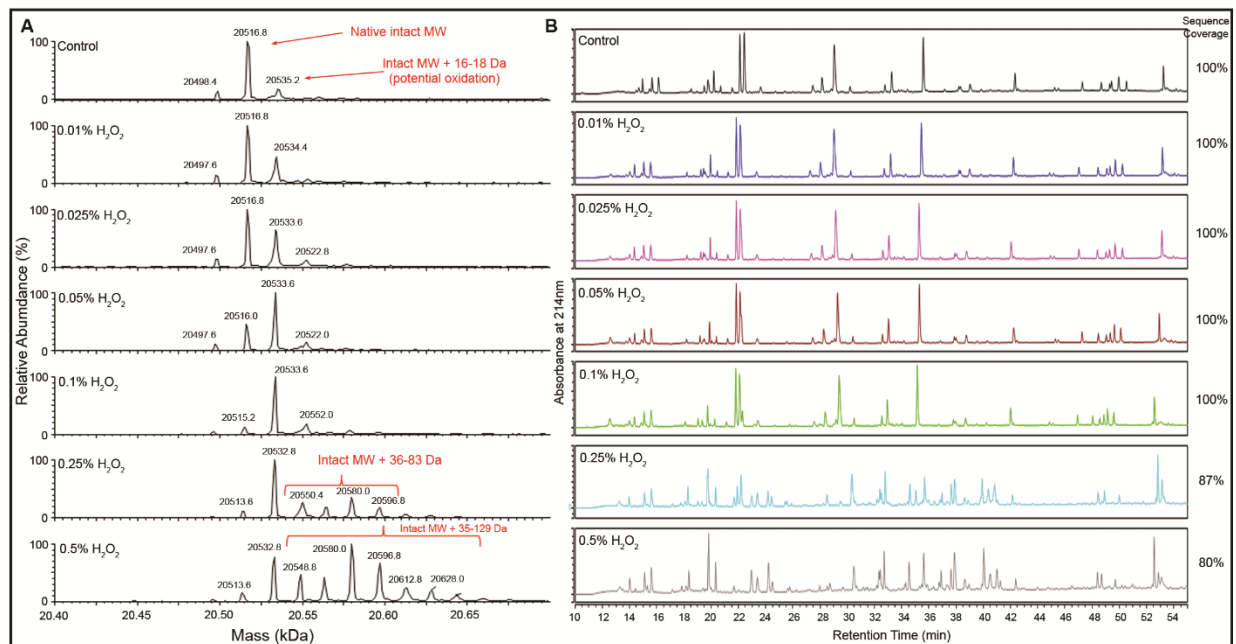
Supplemental Figure S2.3. Forced degradation (Asn deamidation) studies as a function of pH and temperature. Representative UV_{214nm} chromatogram from peptide map analysis of reduced, alkylated, and chymotrypsin digested (A) P[6], and (B) P[8] samples at pH 7.2 4°C (top) and pH 9.0 25°C (bottom). Native Asn peaks are pointed out by red arrows and deamidated Asn peaks are pointed out by blue arrows. Refer to Figure 6 in main text for % deamidation quantitation.



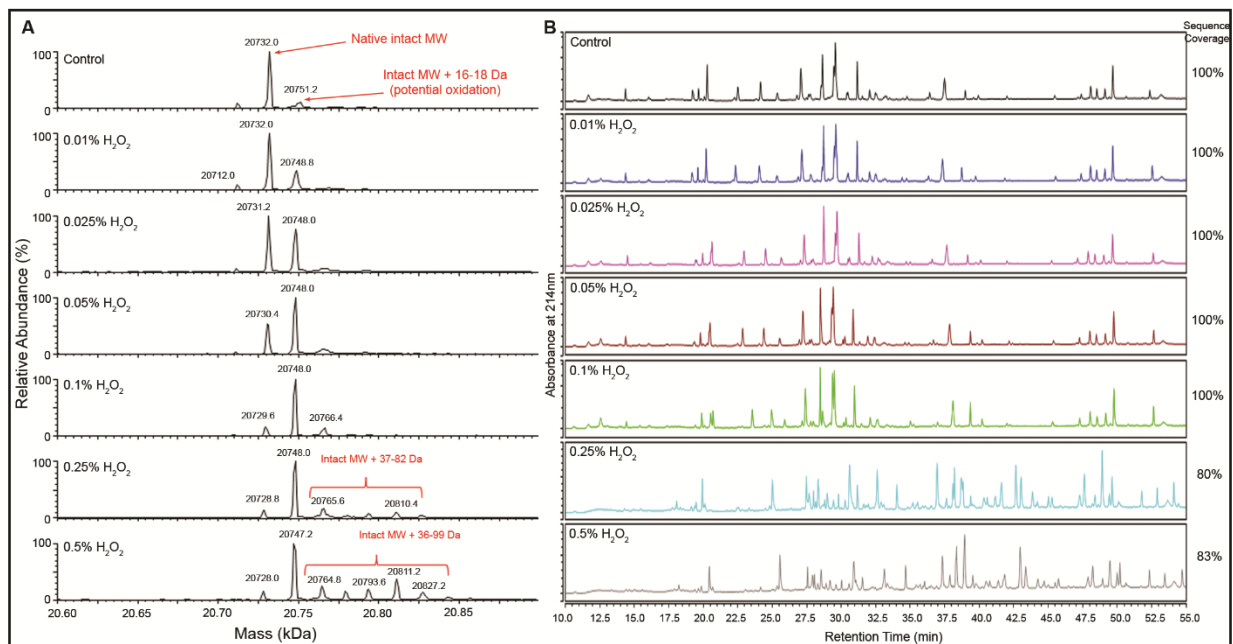
Supplemental Figure S2.4. Forced degradation (non-native disulfide formation) studies with P[4] after incubation at pH 9.0 25°C for 6 days. (A) SDS-PAGE analysis, (B) intact mass analysis, and, (C) RP-UHPLC analysis of the stressed and control samples, further, MS¹ spectra confirming the molecular masses of the eluting peaks to the P[4] monomer and dimer species are shown.



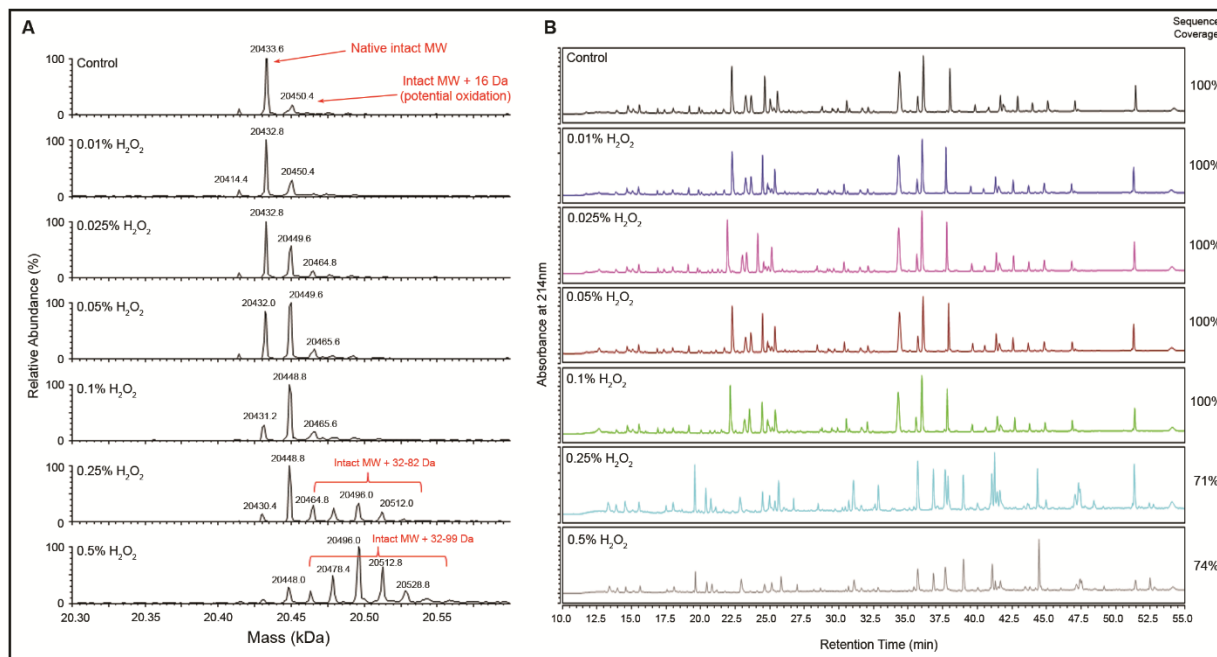
Supplemental Figure S2.5. Forced degradation (non-native disulfide formation) studies with P[8] antigen after incubation at pH 9.0 25°C for 6 days. (A) SDS-PAGE analysis, (B) intact mass analysis, and, (C) RP-UHPLC analysis of the stressed and control samples, further, MS¹ spectra confirming the molecular masses of the eluting peaks to the P[8] monomer species are shown.



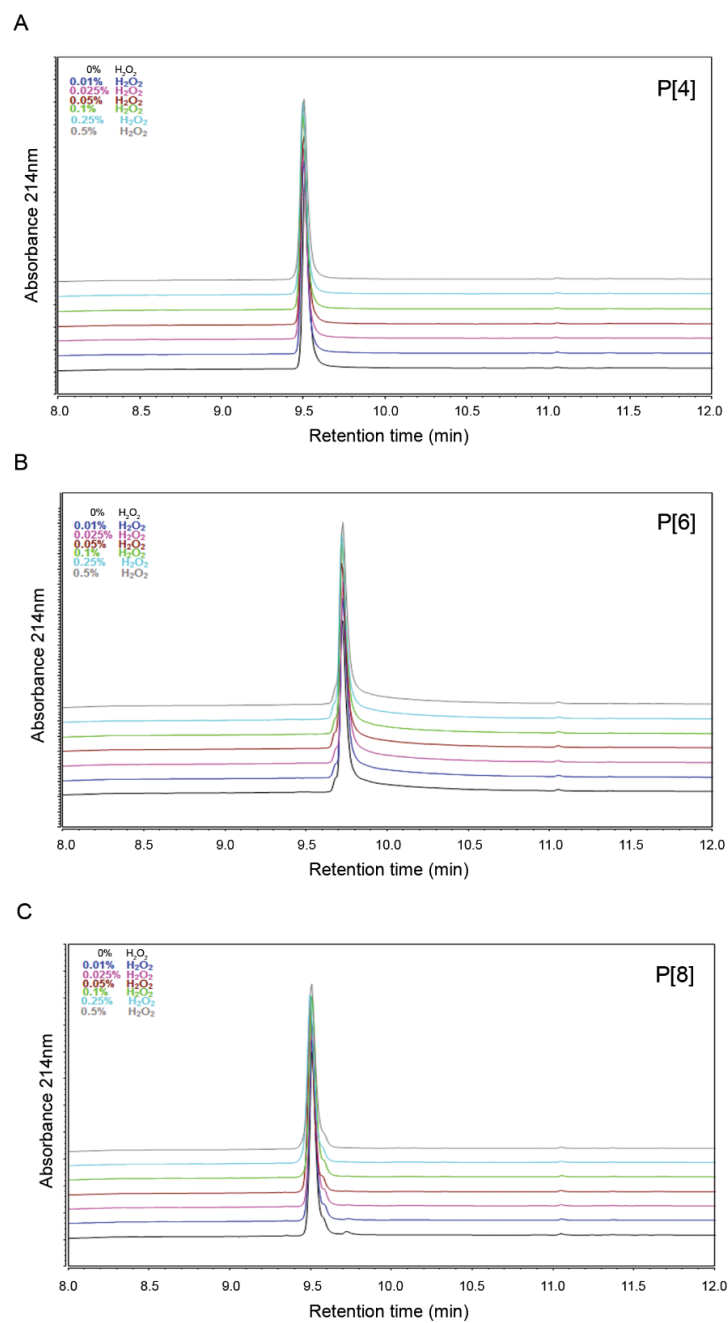
Supplemental Figure S2.6. Forced oxidation studies of P[4] antigen as a function of hydrogen peroxide concentration. (A) Deconvoluted mass spectra for intact mass analysis, and (B) peptide map analysis under reducing (+DTT) condition.



Supplemental Figure S2.7. Forced oxidation studies of P[6] antigen as a function of hydrogen peroxide concentration. (A) Deconvoluted mass spectra for intact mass analysis, and (B) peptide map analysis under reducing (+DTT) condition. Part of this data is also shown in Figure 2.9 of the main text as representative data for this antigen.



Supplemental Figure S2.8. Forced oxidation studies of P[8] antigen as a function of hydrogen peroxide concentration. (A) Deconvoluted mass spectra for intact mass analysis, and (B) peptide map analysis under reducing (+DTT) condition.



Supplemental Figure S2.9. Forced oxidation studies of the three NRRV antigens as a function of hydrogen peroxide concentration. Representative RP-HPLC chromatograms of (A) P[4], (B) P[6], and (C) P[8] at different hydrogen peroxide concentrations.

Chapter 3

Developing stable frozen liquid bulk formulations to minimize aggregation and particle formation of three recombinant protein vaccine antigens for use in a trivalent rotavirus vaccine candidate

3.0 Introduction

Essentially every child before reaching 5 years of age gets infected by Rotavirus (RV) which can cause gastroenteritis and diarrhea²⁹. There are currently four WHO pre-qualified RV vaccines (RotaTeq®, Rotarix®, Rotavac® and Rotasil®) which combined cover over 100 countries to reduce the burden of this viral infection⁴. In addition, there are several other live, attenuated oral RV vaccines approved for local use and approximately five more candidates are in clinical trials¹⁵⁰. Vaccine efficacy of live, orally administered RV vaccines varies considerably, however, between developing (~40-60%) vs. developed countries (~80-90%)^{31,35,106,151}. Thus, there is growing interest in a recombinant protein subunit vaccine with parenteral administration capabilities to address these differences and provide similar efficacy irrespective of the socio-economic background of a child^{40,115}. Success or failure of a vaccine also relies on its global coverage, and unfortunately, global coverage of rotavirus vaccines is currently only about 28%¹⁵². Development of a recombinant subunit RV vaccine will hopefully also improve affordability, allow for a more constant vaccine supply, and improve coverage by addition to widely used pediatric combination vaccines. For example, a subunit RV vaccine could eventually be combined with the current childhood combination vaccines such as hexavalent DTaP-IPV-HepB-Hib or the pentavalent DTwCP-HepB-Hib vaccines to improve compliance with the immunization schedule and encourage wider vaccination coverage¹¹⁵.

Although vaccine effectiveness is mainly guided by its composition (e.g., antigen and adjuvant), development of a stable vaccine formulation is equally important to ensure the safety and efficacy during manufacturing, long term storage, transport and administration^{72,153}. Live, attenuated viral vaccines contain weakened versions of the pathogens and are often sensitive to elevated temperatures and thus vulnerable to potency loss due to cold chain break down, especially in the developing world⁷⁸. In contrast, recombinant protein subunit vaccines are in general

considered safer and more stable (although often require adjuvants to enhance immune responses)¹⁵⁴. Considerable efforts have been employed towards development of subunit RV vaccine candidates (e.g., soluble antigens, virus-like particles) that are being evaluated in pre-clinical and early clinical studies¹⁵⁵⁻¹⁵⁹. One such candidate (referred to NRRV) containing a trivalent mixture of recombinant truncated VP8* fusion proteins is in Phase 1/2 clinical trials. Previously, one of the three antigens (P2-VP8-P[8]) was shown to be safe in healthy adults as well as to be well tolerated and immunogenic in infants and toddlers thus establishing the proof of concept^{46,47}. See companion paper for detailed structural composition of the three NRRV antigens¹⁶⁰. Briefly, each antigen is composed of a universal tetanus toxoid CD4⁺ T cell epitope, P2, fused with a truncated Δ VP8* protein using a GSGSS linker. Δ VP8* is a soluble truncated version of the VP8* protein which is a proteolytically cleaved product of RV surface protein VP4. The three NRRV antigens are produced recombinantly in *E. coli* as fusion proteins and are named as P2-VP8-P[4], P2-VP8-P[6] and P2-VP8-P[8] where P2 refers to the tetanus toxoid epitope and VP8-P[x] represents the Δ VP8* protein derived from human RV strain DS-1 (G2P[4]), 1076 (G2P[6]) or Wa (G1P[8])^{44,45}. The three antigens are abbreviated as P[4], P[6] and P[8], respectively, in this chapter.

For successful formulation development of a new recombinant protein antigen, the following steps including (1) analytical characterization of key structural attributes, (2) understanding of the physicochemical degradation mechanisms, and (3) rational design of formulation composition to minimize degradation are performed to maintain a vaccine antigen's potency during storage over the intended period of use⁷⁸. Since protein molecules are only marginally stable in their native folded conformation, it is necessary to identify optimal solution conditions (e.g., buffer, pH, ionic strength, excipients, etc.) to ensure their integrity and stability at every step of the manufacturing process as well as during long term storage^{82,161}. The vaccine

formulation development effort becomes even more challenging when multiple protein antigens are combined into a multivalent vaccine candidate^{50,78}.

During the course of manufacturing protein antigens for multivalent vaccines, it is convenient and often necessary for the manufacturer to separate the manufacturing of the purified antigen (Bulk Drug Substance) from subsequent formulation and fill-finish operations (Vaccine Drug Product). This is very useful and often necessary in a more limited manufacturing environment (such as in some developing countries) when the production and purification are carried out in a setting which can handle only one product at a time. In particular for multivalent vaccines it is therefore advantageous to campaign each antigen and store the purified drug substance, typically in a frozen state. The purpose of this work described herein, is to develop stable frozen liquid formulations for bulk storage of the three NRRV antigens. The aggregation propensity (i.e., colloidal instability) of the antigens was identified as a major degradation mechanism, especially during thawing of the frozen bulk drug substance at large scale (data not shown). Thus, a better understanding of the conditions leading to physical instability of the three protein antigens was pursued and candidate frozen liquid formulations were developed. Since the NRRV antigens are already in clinical trials, the selection of final formulation components was constrained such that minimal changes are needed to the current formulation. Also, the new candidate formulations must be compatible with subsequent formulation steps with aluminum adjuvants.

3.1 Materials and Methods

The P[4] and P[6] used for colloidal stressed stability studies were produced and purified from *E. coli* at Walter Reed Army Institute of Research, MD and formulated in 0.5 mM sodium

phosphate, 150 mM NaCl, pH 7.2. The P[4] and P[6] used for the bulk formulation studies, and P[8] used for all the studies in this work, were produced and purified from *E. coli* by Blue Sky BioServices, MA and provided in 600 mM ammonium sulfate, 50 mM Tris buffer at pH 7.5. Sodium phosphate dibasic heptahydrate, and sodium chloride were purchased from Thermo Fisher Scientific (Waltham, MA). All other buffer reagents and chemicals including sodium phosphate monobasic monohydrate, citric acid, and ammonium bicarbonate were purchased from Sigma-Aldrich (St. Louis, MO) and were of analytical grade or higher unless noted otherwise. Protein concentration for each antigen was determined using extinction coefficient as described in the chapter 2.

3.1.1 Colloidal Stability Studies Using Agitation Stress

Each of the three NRRV recombinant protein antigens was dialyzed overnight at 4°C in 10 mM sodium phosphate, 150 mM NaCl, pH 7.2 buffer, which is referred as “base buffer” in the text hereafter. The buffer-exchanged proteins samples in base buffer were subjected to shaking stress in 2 ml Fiolax clear, Schott (Lebanon, PA) glass vials with rubber stoppers (West Pharmaceutical, PA). The vials were filled with 0.4 ml of 0.15 mg/ml protein sample and were shaken sideways at 250 RPM for 6 hr. at RT. Stressed samples (6 hr.) in triplicate for each antigen and control samples (unstressed, 0 hr.) were assessed for the presence of aggregate/particles by OD₃₅₀ value and the total number of sub-visible particles were counted by Micro-flow imaging (MFI) as described below.

For characterization studies of aggregates/particles, the samples were generated in the base buffer for each of the three NRRV antigens similar to colloidal stressed stability study described above. The vials were filled with 0.6 ml of 0.2 mg/ml protein sample and were shaken sideways at 250 RPM for 90 min at RT. These parameters were optimized to attain similar level of

degradation in each antigen. The generated aggregates/particles were analyzed for their size, appearance, secondary structure, tertiary structure, and chemical composition by various analytical tools mentioned below.

3.1.2 Visual Appearance and Turbidity

Samples were visually assessed for visible particles under Adelphi Apollo II liquid viewer (Adelphi Co., UK). Turbidity measurements were performed in triplicate using a Hach 2100 AN Laboratory Turbidimeter. Instrument calibration was achieved using standards in the range of <0.1 to 2,000 Nephelometric Turbidity Unit (NTU), and the turbidity values of the samples were corrected for the turbidity of the empty tube and base buffer.

3.1.3 UV-Visible spectroscopy

The UV-Visible absorption spectra of the NRRV samples were recorded before and after centrifugation (13,000 X g for 5 min) from 190-1100 nm using a 0.5 s integration time and 1 cm path length quartz cuvettes using an HP-8453 photodiode array detector (Agilent Technologies, Santa Clara, CA) equipped with Deuterium (D2) and Tungsten (W) lamps. The Beer-Lambert law was used to calculate the protein concentration using the extinction coefficient of a 0.1% solution of each antigen. Light scattering correction was applied to all the collected absorbance spectra using the manufacturer's data analysis software (Chemstation UV-Vis analysis software, Agilent Technologies). The optical density value at 350 nm (OD350) was recorded from the uncorrected spectra.

3.1.4 Micro-Flow Imaging (MFI)

Sub-visible particles (1-100 μm) were measured and quantified using DPA-4200 flow microscope (Protein Simple, Santa Clara, CA) system equipped with a 100 μm silane coated flow cell. The instrument was calibrated using 10 μm polystyrene particle standards (Thermo Scientific)

prior to analysis. The samples were carefully drawn up in a low protein binding, filter-tip pipette (Neptune Scientific, San Diego, CA) and analyzed using a flow rate of 0.17 ml/min. The purge volume for each measurement was 0.2 ml and measurements were made at ambient room temperature. Particle free water was used to optimize illumination prior to each measurement.

3.1.5 Resonance Mass Measurement (RMM)

Archimedes particle metrology system (Affinity Biosensors, Santa Barbara, CA), equipped with Hi-Q microsensors was used to assess the total number and distribution of sub-micron particles (200 nm to 1 μm) in the samples. Prior to each sample run, clean baseline was obtained by cleaning the flow cell and sensor with 20% Contrad 20 and then flushing with particle free water. The accuracy of the sensor was determined by analysis of 1 μm polystyrene beads (Thermo-Scientific). Particle density of 1.37 g/ml was used, limit of detection was set to 0.03 Hz and measurements were made at ambient room temperature. Samples were run for either 10 min or till the total particle count reached 300.

3.1.6 Sedimentation Velocity Analytical Ultracentrifugation (SV-AUC)

SV-AUC experiments were performed on the unstressed and stressed samples as per the method described in chapter 2.

3.1.7 Size Exclusion Chromatography (SEC)

Stressed and unstressed samples were subjected to SEC analysis as per the method described in chapter 2.

3.1.8 Fourier Transform Infrared Spectroscopy (FTIR)

FTIR spectra were collected for each of the stressed and unstressed sample as per the previous method in chapter 2. Qualitative comparisons (number of peaks and their position) were

made between the in-solution protein FTIR spectra vs the FTIR spectra of filtered particles from same sample obtained using FTIR microscopy technique (described below).

3.1.9 Fourier Transform Infrared Microscopy

The samples were filtered using 3 μm gold filters (Pall Corporation) which were pre-equilibrated by washing with 0.1 M NaOH. After filtration, samples were washed with ultrapure water, and dried overnight. A Bruker Hyperion FTIR Microscope with a 15X objective was used to image individual particles. Two-hundred-fifty-six scans were recorded from 600-4000 cm^{-1} with a viewing area of about 100 $\mu\text{m} \times 100 \mu\text{m}$. OPUS (V6.5) software was used for baseline and atmospheric correction. The second derivative spectra were obtained using OPUS software and applying a nine-point Savitzky-Golay smoothing function.

3.1.10 Extrinsic (ANS) Fluorescence Spectroscopy

Samples were centrifuged at 13,000g for 5 min to separate the soluble and insoluble fractions. The pellet was re-suspended in base buffer. The final protein concentration in each of these supernatant and pellet components was 0.15 mg/ml. 8-Anilino-1-naphthalene sulfonate (ANS) was used as an extrinsic fluorescence probe with the A PTI QM-1 spectrofluorometer (Brunswick, NJ) equipped with a turreted four-position Peltier-controlled cell holder and a xenon lamp. The stock solution of ANS (1-Anilinonaphthalene-8-sulfonic acid) dye purchased from Sigma, Inc. (St. Louis, MO) was made at 25 mM in DMSO. Finally, a ratio of 25:1 (dye:protein) was maintained in the protein samples during fluorescence measurements. An excitation wavelength of 372 nm was used and emission spectra was collected from 400-600 nm at a 1 nm/s collection rate in 0.2 cm path length cuvette. Spectra for all the samples (supernatant and pellet of stressed and unstressed samples) of a particular antigen were collected by keeping the light intensity constant and this constant intensity was set using the supernatant of the unstressed sample

at RT. The obtained emission spectra were corrected for the buffer blank and data were plotted using Origin (v 7.0) software.

3.1.11 SDS-PAGE

Prior to SDS-PAGE analysis, samples were centrifuged for 5 min at 13,000 X g, and the resulting supernatant and pellet were separated. Approximately, 2.5 µg of protein (supernatant or pellet) (+/-shaking) was mixed with 4X NuPAGE LDS sample buffer (Life Technologies). Nonreduced samples were incubated in dark for 10 min with 20 mM iodoacetamide and then boiled at 95°C for 10 min. For reducing conditions, 10 mM dithiothreitol (DTT) was added followed by incubation at 37°C for 10 min. The samples were then separated using NuPAGE 12% Bis-Tris gel (Life Technologies) and MES running buffer by running at 150 V for 60 min. Staining of protein bands was done using Coomassie blue R250 (Teknova, Hollister, CA), followed by destaining with a mixture of 40% methanol, 10% acetic acid, and 50% ultrapure water. Gels were digitized using an Alphaimager (Protein Simple, Santa Clara, CA) gel imaging system.

3.1.12 Ammonium Sulfate (AS) Precipitation Assay

AS precipitation assay was performed for each antigen in base buffer at RT. Stock solution of 3.5 M AS was prepared in the same buffer and pH was adjusted to 7.2. Samples were prepared in a 96-well plate to a final protein concentration of 0.18 mg/mL by mixing appropriate amounts of protein stock solution, AS stock solution and buffer to a final volume of 125 µL. Samples were mixed and incubated at RT for 10 min before filtering through a 0.2 µm polystyrene filter plate (Corning #3504; Corning Life Sciences, NY) by centrifugation at 3000 RPM for 10 min. Thereafter, 80 µL of the filtrate was transferred to a 384-well UV Star microplate (Greiner #781801; Greiner Bio-one, NC) and absorbance was measured at 280 nm on a SpectraMax M5 UV-Visible plate reader. Protein concentration (mg/mL) versus AS molar concentration (M) data

were fit to a Boltzmann sigmoidal curve function as described by Yamniuk et al using Origin 2017 to obtain AS mid-point value (AS_{midpt}) for each antigen ¹⁶².

3.1.13 Excipient Screening for NRRV Antigens under Agitation, Thermal and Freeze-thaw Stresses

Excipient screening studies using both thermal and agitation/shaking stresses - Frozen P[8] protein samples were thawed and buffer exchanged in base buffer. Stock solutions (2x) of 35 pharmaceutical excipients were prepared in base buffer, and a stock solution of NaCl (salt) (10x) was also prepared which consisted of 10 mM sodium phosphate, 1.5 M NaCl, pH 7.2 buffer. For each sample for excipient screening, an excipient of interest, protein stock solution, salt stock solution, and base buffer were combined to achieve the desired concentration of each excipient. A final protein concentration of 0.15 and 0.10 mg/mL was used for shaking and thermal stress, respectively. Assays were then performed on these samples in triplicate. For shake stress studies, 2 mL Fiolax clear, Schott (Lebanon, PA) glass vials were filled with 0.4 mL of 0.15 mg/mL protein and stoppered with sterile and coated stoppers (Part# 19700302, West Pharmaceutical, PA). The vials were then shaken sideways at 300 RPM for 6 hr. at room-temperature. Additionally, control vials were filled with 0.4 mL of each base buffer without protein and shaken under similar conditions. The following techniques were used in excipient screening experiments: (a) OD_{350} as a function of temperature (Thermal stress), (b) UV-Visible Spectroscopy (Shaking stress), and (c) Micro-flow imaging (MFI) (Shaking stress). The OD_{350} method is described in chapter 2 and methods for (b) and (c) are described above. The excipients that showed stabilizing effect on P[8] antigen either during thermal or shaking stress were tested for their effect on P[4] and P[6] antigens. Not all of the excipients could be tested with P[4] and P[6] antigens due to limited material available for these antigens.

Concentration optimization of lead excipients for their stabilizing effect: concentration of the identified lead excipients (Thermal stress - Sucrose, Trehalose, Mannitol, Sorbitol, Pluronic F-68 (Figure 3.6A); Shaking stress – PS-80, 2-OH propyl β -CD, Pluronic F-68 (Figure 3.6B)) was optimized using P[8] antigen under thermal and shaking stress, using OD₃₅₀ and MFI assays, respectively, as described above.

Salt and candidate excipient(s) combination optimization: increasing concentrations of salt (NaCl) from 0 to 150 mM were screened with different combinations of lead excipients for their stabilizing effect on the P[8] antigen. Different combinations (C1 – C14) selected for the lead excipients at their optimized concentration are mentioned in table below Figures 6C and 6D, OD₃₅₀ and MFI assays were used to assess the stability against thermal and shaking stress, respectively in each combination.

pH and buffer optimization studies: selected combination of excipients (0.025% PS80 + 10% Sucrose) was further tested in different buffers (1 mM sodium phosphate, 10 mM sodium phosphate, 10 mM histidine, and 10 mM HEPES) at different pH conditions 6.5, 6.8, 7.2, and 7.5 to study their effect on P[8] under thermal and shaking stress. Based on the effect of these buffer conditions on P[8] antigen, a subset of conditions (1 mM sodium phosphate pH 6.5 and 7.2, 10 mM sodium phosphate pH 6.5 and 7.2, 10 mM HEPES pH 6.5 and 7.2, and 10 mM sodium phosphate with 150 mM NaCl pH 7.2) were down selected to test with P[4] and P[6] antigens.

Thermal, shaking, and freeze-thaw (FT) stress studies of candidate bulk formulations: based on the information gained from the above studies, 8 candidate bulk formulations were designed (Sup. Table S3.3) and tested for the stability of the three antigens under forced thermal, shaking, and FT stress conditions. Thermal and shaking studies were conducted as previously described here. For FT study, stress consisted of five cycles of freezing each sample at -80°C and thawing at room-

temperature. 200 μ L of protein samples at 0.15 mg/mL in 1.5 mL Eppendorf tubes were used in this study and protein loss after five FT cycles was determined by measuring absorbance at 280 nm.

Further optimization of PS80 concentration: based on the protein loss data during FT study with 8 candidate bulk formulations, three different concentrations of PS80; 0.025%, 0.05% and 0.1% were further tested against FT stress (5 cycles) at protein concentration of 0.15 and 0.40 mg/mL for each of the three antigens in 1mM sodium phosphate 150 mM NaCl pH 7.2 buffer (current formulation buffer). We also evaluated these different PS80 concentrations (0.025%, 0.05% and 0.1%) against shaking stress for each antigen in current formulation buffer with the same method as described above.

Additional FT studies with candidate bulk formulations for the three NRRV antigens: each of the three NRRV antigens in the current formulation and two candidate formulations (1 mM sodium phosphate 150 mM NaCl 0.05% PS80 pH 7.2, 10 mM histidine 150 mM NaCl 0.05% PS80 pH 6.8) were subjected to 1 and 5 FT cycles in Eppendorf tubes at \sim 1 mg/mL concentration. Samples were subjected to visual inspection, SEC, UV-Visible spectroscopy, MFI, and DSC.

3.2 Results

3.2.1 Colloidal stability assessments and characterization of aggregates and particles

As shown in Figure 3.1A, as a result of shake/agitation stress, high OD₃₅₀ value of \sim 0.45 was observed for P[8] antigen which indicates substantial protein aggregation compared to P[4] and P[6]. The P[6] protein appeared to be least susceptible to aggregation when subjected to shaking stress under the tested conditions (with OD₃₅₀ value below 0.01). Since all three antigens showed similar turbidity values after shake stress (7.8-12.9 NTU; see Supplemental Table S3.1),

this result is likely a reflection of the formation of larger aggregates and particulates. Consistent with this, the total number of sub-visible particles in the stressed samples was highest for P[8] and lowest for P[6] antigen as measured by MFI (Figure 3.1B). Visible particles were observed by visual assessment in some of the stressed samples, and A_{280} values after centrifugation and light scattering correction decreased by ~30% for P[4] and P[8], and ~35% for P[6] antigen indicating notable loss in protein mass. No detectable soluble aggregates were recorded by SEC and SV-AUC for each antigen; however, substantial monomer loss was observed (consistent with UV-visible spectroscopy results), suggesting the formation of larger, insoluble aggregates (Supplementary Table S3.1). Figure 3.1C-3.1F show representative aggregate and particle size distribution data for P[8] antigen; no soluble aggregates were detected and only a major peak corresponding to monomer was observed by both SEC chromatograms and SV-AUC $c(s)$ distribution analysis (Figures 3.1C and 3.1D). Substantial increases in the larger subvisible particles in size ranges 1.3 – 1.8 μm and 2 – 40 μm were observed, however, in stressed P[8] samples by RMM (Figure 3.1E) and MFI (Figure 3.1F) measurements, respectively.

The aggregates/particles generated from shake stress were then further evaluated in terms of morphology, higher-order structure (FTIR analysis and hydrophobic exposure by ANS fluorescence), and chemical composition (non-native disulfide formation). The results for P[8] antigen are described in Figure 3.2 and similar results were obtained for P[4] and P[6] antigens with some minor differences as shown in Sup. Figure S3.1. First, analysis of the MFI images revealed that the micron size particles formed were opaque and fibrillar in morphology (Figure 3.2A). The optical microscope was used to visualize the isolated particle (Figure 3.2B). FTIR analysis was then utilized to examine the overall secondary structure content of the unstressed sample in solution and FTIR microscopic analysis was used to examine the secondary structure of

protein within the isolated particles generated by shake-stress. Second derivative of amide I FTIR spectra were notably different for isolated P[8] particles vs. control protein in solution (Figure 3.2C). Many of the peaks in the control sample FTIR spectra were not retained in the stressed sample spectra suggesting loss of native structure. In addition, an additional primary peak ($\sim 1625 \text{ cm}^{-1}$) for protein within the isolated particles indicated the formation of inter-molecular β -sheet sheets (i.e., aggregates). Alterations in higher-order structural integrity of the P[8] protein present in the isolated particles (vs control protein in solution) was assessed by measuring the fluorescence of ANS dye binding. As shown in Figure 3.2D, substantial increase in the fluorescence intensity of ANS was recorded for the pellet of the agitation stressed samples as compared to the supernatant of stressed samples as well as compared to the supernatant/pellet of control protein samples. The higher fluorescence intensity of the protein derived from the pellet suggested increased hydrophobic surfaces, due to structural alterations and/or aggregated formation due to shaking stress. SDS-PAGE analysis of the protein from the pellet generated after shaking indicated the presence of oligomeric species ranging from 38 to 68 kDa in addition to the monomeric protein under non-reducing conditions (Figure 3.2E). The oligomeric species were not present in the reducing gel (Figure 3.2F) suggesting they were linked through non-native inter-molecular disulfide bonds (each NRRV antigen has single Cys residue). Single monomeric band was observed by SDS-PAGE for the control samples and for supernatant of the stressed samples under non-reduced and reduced conditions. Overall, the particles or aggregates generated for each NRRV antigen were opaque and fibrillar in morphology, showed increased inter-molecular β -sheet content and hydrophobic exposure, and were partially cross linked with inter-molecular disulfide bonds.

To assess if these agitation stress results, in terms of relative aggregate/particle formation of each antigen, are correlated with their relative solubility, the relative apparent solubility of each antigen was determined using an ammonium sulfate (AS) precipitation assay. Decreases in protein concentration were observed with the increasing amounts of AS added to the solution presumably due to the known salting-out mechanism of kosmotropic salts (Figure 3.2G). The AS_{midpt} value was calculated for each antigen which is a measure of relative solubility by comparing the amount of AS needed to precipitate 50% of the protein out of solution. A similar AS_{midpt} value of 1.35 ± 0.01 M was observed for P[4] and P[8], whereas AS_{midpt} was 1.29 ± 0.01 M for P[6] suggesting an overall similar, albeit somewhat lower relative solubility of P[6]. This result is consistent with the relatively more hydrophobic nature of P[6] compared to the other two NRRV antigens (refer to chapter 2). The more notable agitation induced aggregate/particle formation of the P[8] antigen is thus not consistent with rank ordering of relative apparent solubility (compared to the P[4] and P[6] antigens as measured by AS_{midpt} values), and is likely therefore due to other causes (e.g., differences in colloidal or interfacial properties; see discussion).

3.2.2 Screening stabilizing excipients to minimize shaking and thermal induced aggregation of NRRV antigens

Due to the susceptibility of NRRV antigens toward aggregation by shaking stress (see above) and thermal stress (see chapter 2), these two stress conditions were used to screen 35 pharmaceutical excipients. Figure 3.3A shows total sub-visible particles by MFI analysis (2 – 100 μm after 6 h of shaking minus time zero results per milliliter of 10x diluted sample) for P[8] in base buffer \pm excipients. Many of the tested excipients mitigated particle formation during shaking stress (to varying extents) while the remaining excipients had no effect or were perhaps mildly destabilizing (Figure 3.3A). Figure 3.3B shows the OD_{350} values (6h – 0h) in an increasing order obtained from the spectra of P[8] antigen in the base buffer \pm excipients. Overall, both the MFI

and OD₃₅₀ methods showed that many detergents (e.g., Triton X-100, Pluronic F-68, Brij-35, PS-20, and PS-80) were able to mitigate shaking induced aggregation of P[8] antigen. In addition, 2-OH propyl β -CD, PEG-3500, and MgCl₂ also showed stabilizing effects. Due to limited availability of P[4] and P[6] antigens, a subset of excipients that showed stabilizing effect on P[8] were tested with P[4] and P[6]. Of this subset, each of the tested excipients had stabilizing effect on P[4] antigen, and with 2-OH propyl β -CD and PS-80 having the most positive effect (Sup. Figures S3.2A and S3.2B). With P[6] antigen, the goal was to probe the compatibility of these excipients and look for significant detrimental effects since P[6] antigen (without any excipient) showed minimal aggregation under the tested shaking stress condition. As shown in Sup. Figures S3.2D and S3.2E, addition of the six excipients did not show any dramatic destabilization of P[6] antigen. Thus, 2-OH propyl β cyclodextrin, Pluronic F-68, and PS-80 were chosen for further optimization of their concentration with P[8] antigen under shaking stress.

For excipient screening to stabilize NRRV antigens in the liquid state when exposed to thermal stress, OD₃₅₀ was measured as a function of temperature and the same set of 35 pharmaceutical excipients was screened with P[8]. Figure 3.4 inset shows representative OD₃₅₀ vs temperature plot for P[8] antigen alone and in the presence of a stabilizing and destabilizing excipient. The T_{onset} value for aggregation was defined as the temperature to reach OD₃₅₀ value of 0.1, and $\Delta T @ OD_{350}$ of 0.1 value was defined as the difference between T_{onset} value for P[8] antigen with vs without excipient (thus, a positive ΔT shows a stabilizing effect of the excipient and a negative ΔT shows destabilization). As expected, carbohydrates and polyols showed stabilizing effect against thermal stress, and Pluronic F-68 showed dramatic stabilization of the P[8] antigen (Figure 3.4). Similar to shaking stress, a subset of most stabilizing excipients were tested with P[4] and P[6] (Sup. Figures S3.2C and S3.2F). Each of the tested excipients showed a

similar stabilizing effect with the exception of 0.1 M aspartic acid (which did not stabilize P[4] or P[6]). Based on these results, sucrose, trehalose, mannitol, sorbitol, and Pluronic F-68 were selected for their concentration optimization with P[8] antigen under thermal stress.

3.2.3 Optimizing lead stabilizers to further minimize shaking and thermal induced aggregation of NRRV antigens

First, the concentration of each of the lead excipients was titrated down from the maximum concentration used in the screening study to find the minimal effective concentration. As shown in Figure 3.5A, reducing the concentration of carbohydrates or polyols reduced their effectiveness in inhibiting P[8] aggregation with 10% (w/v) showing the maximum thermal stability. Conversely, 0.025% (w/v) Pluronic F-68 showed higher thermal stability or delayed onset of aggregation as compared to 0.05% and 0.01% levels. For shaking stress study, each of the selected excipients at lower concentrations were also able to mitigate protein aggregation (Figure 3.5B). PS-80 was found to be most effective at 0.025% level out of the three tested concentrations. For 2-OH propyl β -CD and Pluronic F-68, all concentrations examined were equally effective.

As the next step, three stabilizing excipients against thermal and shaking induced aggregation of P[8] were selected for additional studies. Sucrose at 10% w/v was preferred over trehalose, mannitol and sorbitol (even though all three showed similar or slightly better thermal stability profiles compared to sucrose) because of cost or the known tendency of these additives to crystallize out during freezing and thawing¹⁶³⁻¹⁶⁵. Also, equal amounts (% w/v) of the two polyols (vs. sucrose or trehalose) impart higher solution osmolality which is less desirable for parenteral administration due to their hypertonic nature^{166,167}. Pluronic F-68 at 0.025% was also selected since it was excellent in minimizing P[8] antigen aggregation due to thermal and shaking stresses. PS-80 is well known to reduce protein aggregation due to interfacial interactions as this non-ionic detergent can outcompete protein molecules for the interfaces when added above their critical

micelle concentration ¹⁶⁸. In this study, 0.025% PS-80 concentration was found to be effective in minimizing shaking induced aggregation of P[8] antigen. Finally, the effect of different amounts of salt (sodium chloride) was also evaluated in this study. Different combinations of above selected excipients were studied to probe for synergistic effects in stabilizing the P[8] antigen. As shown in Figures 3.5C and 3.5D, all the tested combinations outperformed the base formulation (C-14 in the figure which shows the highest P[8] aggregation propensity). It can be seen that each combination of selected excipients was effective in limiting thermal induced aggregation of P[8] in the absence of salt (C1 – C8 in Figure 3.5C). The effect of sucrose on thermal stability was also evaluated at different salt concentrations (50, 100, 150 mM) and lower salt resulted in better stability profile (Figure 3.5C; samples C-9, C-11, C-13). The higher aggregation propensity of P[8] by addition of 50 mM NaCl could be due to surface charge screening resulting in neutralization of short-range protein-protein repulsive electrostatic interactions ^{169,170}. Agitation stress results suggested that addition of 0.025% non-ionic detergent either alone or in combination with 10% sucrose were able to mitigate aggregation (Figure 3.5D; C-1 – C-4, C8). Interestingly, detectable aggregates were observed in the stressed P[8] samples containing all three excipients (C-6). As expected, sucrose alone or in combination with different amounts of salt (C-13, C-11, C-9) was not able to minimize shaking induced aggregation of P[8].

3.2.4 Optimizing buffering agent and solution pH to minimize shaking and thermal induced aggregation of NRRV antigens

Three different buffering agents (sodium phosphate, Histidine, and HEPES) were evaluated at four pH values (6.5, 6.8, 7.2, and 7.5) for their effect(s) with the P[8] antigen in the C-2 formulation (10% Sucrose, 0.025% PS-80) during both thermal and agitation induced aggregation. As shown in Figure 3.6A, phosphate and HEPES buffers had similar effects and were better than histidine (10 mM phosphate was marginally better than 1 mM phosphate buffer) after

shaking stress. No apparent effect of pH was observed. In thermal stress study (Figure 6B), a clear pH-dependent trend was observed as higher pH was more stabilizing ($7.5 > 7.2 > 6.8 > 6.5$) and different buffers could be rank ordered as Phosphate > HEPES > Histidine. Phosphate buffer at 1 mM was most effective in limiting aggregation at all tested pH conditions with or without excipients.

Based on the results described above with P[8] antigen, pH conditions and buffer systems were down-selected to test with P[4] and P[6] antigens (due to their limited availability). Surprisingly, for the majority of conditions tested, OD₃₅₀ value after shaking for 6 hr. elevated (was above 0.01) even in the presence of 0.025% PS-80 suggesting some undesirable level of aggregation (Sup. Figures S3.3A and D3.3D). However, when the same set of conditions were tested in the presence of 150 mM NaCl and 10% sucrose + 0.025% PS-80, aggregation was significantly reduced in all the samples containing P[4] antigen (Sup. Figure S3.3B). Due to limited availability of P[6] antigen, only one condition (10 mM PBS pH 7.2) could be tested for the effect of salt and results were comparable to P[4] (Sup. Fig. S3.3D). Overall, these results demonstrated that addition of salt in formulation (containing PS-80) might be necessary for the bulk storage of these antigens to mitigate shaking or agitation induced aggregation. Similar results were obtained for thermal stress study with P[4] and P[6] antigens as seen with P[8] antigen (Su. Fig. S3.3C and S3.3E). In summary, P[4] and P[6] samples at pH 7.2 were more stable than pH 6.5, and Phosphate was better than HEPES in the presence of excipients in terms of NRRV antigen stability. In addition, thermal induced aggregation was lowest in 1 mM phosphate (vs 10 mM phosphate) which is consistent with the P[8] data.

3.2.5 Evaluation of candidate formulations for frozen liquid bulk drug substance of three NRRV antigens

Eight candidate formulations (F2 – F9) listed in Table 3.1 were designed based on the above results. The osmolality values for each formulation were within an acceptable range, and low concentration buffer conditions (1 or 5 mM) were selected due to improved thermal stability profiles for each of the antigens (see Figure 3.7A; F2 vs. F4, F6 vs. F7). The candidate formulations (F2 – F9) were then tested along with the current formulation (F1) for their ability to mitigate aggregation due to thermal, shaking, and freeze-thaw (FT) stress as shown in Figure 3.7. Each candidate formulation containing sucrose showed better thermal stability as compared to the current formulation F1 (Figure 3.7A). For shaking stress study, 0.025% PS80 was able to reduce particle/aggregate formation for P[8] antigen but was not so effective for the other two antigens and warranted further examination (Figure 3.7B). Addition of PS-80 to the candidate formulations was able to mitigate protein loss for each antigen due to FT stress (albeit to a lesser extent with F9) as shown in Figure 3.7C.

Different PS-80 concentrations (0.025, 0.05, and 0.1%) were examined at 0.15 mg/mL protein concentrations for each NRRV antigen to optimize the final PS-80 amount. As shown in Figure 3.8A, addition of 0.025% PS-80 was able to significantly reduce aggregation for P[4] and P[8] antigens (P[6] antigen was already least prone to aggregation). No notable increase in OD₃₅₀ was observed with 0.05 or 0.1% PS-80 for each NRRV antigen. FT stress of 5 cycles caused low levels but measurable protein loss for each antigen at 0.15 mg/mL even in the presence of 0.1% PS-80 in the formulation (Figure 3.8B). Since part of this loss could potentially be attributed to protein adsorption to the plastic tubes used in the study, we repeated the FT study at a higher protein concentration (0.4 mg/mL). A notable reduction in the percent protein loss was observed at 0.4 mg/mL in the control (without PS-80) as well as PS-80 containing samples (Figure 3.8C).

For example, 0.05% PS-80 was most effective in mitigating protein loss for P[6] and P[8] antigens, and minimized loss for P[4] antigen. Thus, 0.05% PS-80 was added to candidate drug substance formulations.

The next goal was to test the selected candidate formulations to minimize/mitigate particle formation during FT stress under conditions which are more likely to occur during manufacturing and storage of the bulk drug substance materials. Figure 3.8 (D-F) shows sub-visible particle distribution for P[8] antigen after 0, 1, or 5 FT cycle(s) in the current formulation (Figure 3.8D) and two candidate formulations (Figure 3.8E – current formulation + 0.05% PS-80, Figure 3.8F – 10 mM Histidine 150 mM NaCl 0.05% PS-80 pH 6.8). Majority of the subvisible particles formed were in the size range 2 - 5 μ m and as expected the number of particles increased from 0 to 5 FT cycle. The two candidate formulations containing PS-80 helped in reducing subvisible particle formation by about 10 – 30-fold. Similar observations were made for P[4] and P[6] antigens and least number of particles were observed for P[4] out of the three antigen in the current formulation (Sup. Figure S3.4). Visual assessment of FT stressed and control P[8] samples in the current and candidate formulations revealed no visible particle formation in these small scale experiments (data not shown). Finally, minimal to no changes were observed between the three formulations of each NRRV antigen upon FT stress with regards to mass loss, soluble aggregate distribution (from SEC analysis), overall conformational stability, or chemical modifications (data not shown).

3.3 Discussion

The major goal of this work was to mitigate aggregation and particle formation of the three NRRV protein antigens during freeze-thaw (FT) and agitation, and to develop stable frozen liquid bulk formulations for long term storage (prior to formulation and fill-finish to manufacture the

final vaccine drug product in vials). Formation of visible particles leading to precipitation was a concern associated with these antigens during early process development, especially during FT in larger volumes (data not shown). Since these antigens are already in clinical trials a major constraint during formulation development was to minimize the change to current formulation to ensure the NRRV program's progress is not hindered while ensuring optimal protein stability. Aggregates are widely studied as product-related impurities in biopharmaceutical drug candidates since they can be associated with potential immunogenic characteristics known to reduce the efficacy, for example, by generating anti-drug antibody (ADA) responses¹⁷¹⁻¹⁷⁴. In the case of vaccine protein antigens, aggregates or particles can lead to protein loss during process development (e.g., during filtration) thus affecting the productivity and cost of vaccine production.

The P[8] antigen was found to be most prone to aggregation under shaking/agitation stress. This result was consistent with physical stability studies as a function of pH and temperature in the pH range 6 – 7 where aggregation was observed (see chapter 2). It is interesting to note that although the P[8] antigen showed highest conformational stability (compared to P[4] and P[6]), it is also the most susceptible of the three antigens to shaking or agitation induced aggregation. This is likely due to lower colloidal stability of the P[8] antigen. It is possible that the thermal stress vs. shaking stress (i.e., exposure to air-liquid interface, bubble entrapment, etc.) generate different types of partially unfolded protein states. For example, species generated under shaking stress could potentially have higher levels of exposed hydrophobic residues or regions with a greater tendency to interact and form multimers.

As noted above, it was interesting to compare the higher colloidal stability of P[4] and P[6] vs. the P[8] antigen, although they share 66 – 80% sequence homology. This result highlights the potential use of point mutations and protein engineering to improve pharmaceutical properties and

developability of candidates without compromising their biological activity¹⁷⁵. Comparative second virial coefficient (B_{22}) measurements can be made in the future, when sufficient material is available of each antigen, which would potentially be a good qualitative indicator of the differences in colloidal stability of these protein antigens^{176,177}. With limited material, however, we were able to compare the relative solubility ranking of the three antigens using AS_{midpt} values from the AS precipitation assay. The PEG precipitation assay (using a macromolecular crowding agent polyethylene glycol), which is widely used to screen monoclonal antibody candidates to assess their relative solubility under different formulation conditions^{128,178}, did not lead to notable precipitation with these three protein antigens (likely due to interaction between the protein and PEG, data not shown). We observed salting-out of each antigen in similar range of AS and interestingly lowest AS_{midpt} was observed for P[6] which is also most hydrophobic among the three antigens (see chapter 2). Similar AS_{midpt} values were observed for P[4] and P[8] antigens. The relative rank ordering of solubility obtained from AS precipitation assay reflects the propensity of native state of a protein to self-associate. Thus, for these three protein antigens, the aggregate/particle formation pathway (during FT, thermal or shaking-induced stresses) is likely governed by formation of structurally altered/partially unfolded protein states of the protein and not by protein-protein interactions in the native state (i.e., as described above in the AS precipitation assay)¹⁷⁹.

To this end, we then characterized the nature and composition of the NRRV protein within aggregates/particles. We utilized a limited shake stress test to evaluate the aggregates/particles when they just started to form, but majority of the protein was still in native-like state. This enabled us to capture the initial formation of protein aggregates/particles for each antigen. The results showed overall similar characteristics for the three antigens in isolated aggregates/particles. For

example, most aggregates were fibrillar in morphology with opaque nature, showed increased levels inter-molecular β -sheet content, and some loss of native secondary structure content was recorded. Increased exposure of apolar regions was observed by ANS fluorescence studies and formation of aggregates containing non-native disulfide bonds (which were reducible in nature) were seen by SDS-PAGE analysis. Interestingly, the physicochemical characteristics of protein within the isolated aggregate/particle were similar in nature to the protein within aggregates generated for an IgG under different stress conditions as reported previously in our laboratories¹⁸⁰. These results further support the aggregation pathway of the NRRV antigens proceeds via formation of structurally altered protein intermediates (as described above by a combination of FTIR, ANS fluorescence and SDS-PAGE analyses).

During excipient screening and optimization studies with P[8], 0.025% PS-80 or Pluronic F-68 were effective in preventing shaking induced aggregation either alone or in combination with sucrose and no NaCl containing formulations (Figure 3.5D). Non-ionic surfactants such as PS-80 and Pluronic F-68 are known to out-compete protein molecules for air-liquid, liquid-solid interfaces thus preventing protein structural alterations due to surface adsorption leading to non-native aggregate formation¹⁸¹. Sucrose, on the other hand, is known to stabilize proteins against thermal stress by the well-known mechanism of preferential exclusion; the sugar molecules increase the free energy of the unfolded state (as compared to the native state of the protein), and thus, the native state of the protein is favored¹⁸². Due to limited material, only a subset of the stabilizing excipients identified with P[8] were tested with P[4] and P[6]. This challenge is not uncommon during early formulation development when only a few milligrams of material is available. Since P[8] was available in larger quantities, and since the three bulk antigens will be

co-formulated with aluminum adjuvant as a trivalent vaccine drug product, it was a reasonable and efficient approach to avoid screening each excipient with each of the three antigens.

Buffering agents can be regarded as a key excipient added to protein-based formulations, apart from maintaining the desired solution pH, they can affect the physical stability and solubility of proteins by variety of mechanisms ¹²⁹. Higher physical stability against thermal induced aggregation was observed at higher pH ($7.5 > 7.2 > 6.8 > 6.5$) in each of the buffer systems studied (Phosphate, Histidine, HEPES) for each antigen. This result is consistent with the calculated theoretical pI of each antigen, 6.3 for P[4], and 5.9 for P[6] and P[8]. Since the net charge on a protein molecule will be closer to zero at pH condition near its pI, the aggregation propensity is expected to be higher due to poor colloidal stability.

Eight candidate frozen liquid bulk formulations (Table 3.1) were designed for the NRRV antigens ranging from minimal changes (such as addition of PS-80 to the current formulation, F1) to more major changes (such as changing the buffering and tonicifying agents). Each of these new formulations improved NRRV antigen stability against thermal, shaking and FT stresses (Figure 7). Formulations F3, F5 and F8 showed notable improvements in thermal stability in the liquid state for each antigen. We further optimized the concentration of PS-80 and found 0.05% to be optimum concentration for each NRRV antigen to minimize shaking-induced aggregation and protein loss due to FT stress (Figure 3.8). Notable levels of aggregation were observed for P[4] and P[6] antigens after shaking stress as well as significant protein loss was observed for each of these two NRRV antigens after 5 FT cycles (Figure 3.7). It is important to note that the antigens were subjected to accelerated conditions (5 FT cycles) versus what they would normally encounter (1-2 FT cycles) during routine preparations. Also, some protein loss during FT can be attributed to protein adsorption to plastic tubes used in the study (and % loss appears higher since the study

was conducted at only 0.15 mg/mL protein concentration to conserve material). Lower percent levels of protein loss were observed at higher protein antigen concentrations (> 0.4 mg/mL) that will be targeted for future batches of the protein antigens.

Liquid formulations of bulk drug substance can be kept frozen (-80°C) during long term storage to avoid degradation by reducing the mobility of molecules and mitigating transportation stress (shaking/agitation stress), for example, between the vaccine bulk and drug product manufacturing sites. Thus, stabilization of the three antigens against FT stress is critical since such treatments expose proteins to ice-water interfaces, cryo-concentrations (concentration gradients of protein and excipients across the container), pH shifts, and temperature fluctuations, which could lead to both physical and chemical degradation of the protein antigens¹⁸³⁻¹⁸⁶. Addition of 0.05% PS-80 to the current formulation was able to mitigate sub-visible particle formation till 5 FT cycles for each antigen. Formation of visible particles and precipitation upon thawing of frozen NRRV antigen bulk solutions were observed in larger volumes in a suboptimal buffering system (data not shown). This was the major concern with the current formulation for bulk storage of these NRRV antigens since bulk drug substance typically undergoes one FT cycle before formulation steps (e.g., dilution, mixing with other antigens and adsorption to aluminum adjuvant to prepare the trivalent vaccine) and subsequent fill-finish into vials to produce a final vaccine drug product. No visible particles were observed for P[8] antigen in our scaled-down study in glass vials which might not be the most accurate representation of FT process in larger volume containers where freezing and thawing rates, surface-area to volume ratio, container type, head space, etc. can be substantially different¹⁸⁷⁻¹⁸⁹.

It is important to note that the studies presented in this work were aimed at developing candidate frozen liquid formulations for bulk storage of drug substance (i.e., monovalent antigens).

The formulated final vaccine drug product, however, will be a trivalent vaccine drug product containing an adjuvant (Alhydrogel®) to enhance the immune response and potentially a preservative to enable multi-dose presentations. Chapter 4 of this dissertation focuses on the assessment of interaction of the NRRV antigens with adjuvant, physicochemical and immunochemical stability profiles of the antigens bound to adjuvant, and compatibility with antimicrobial agents. Thus, a key additional consideration for final selection of the frozen liquid bulk drug substance formulation during development will be compatibility with the drug product, both in terms of manufacturing and long-term stability of the trivalent, aluminum adjuvanted vaccine candidate at various antigen doses.

3.4 Tables

Table 3.1. Composition and osmolality values of 8 candidate frozen liquid formulations for each NRRV antigen for their individual bulk storage. Osmolality values are from triplicate measurements and error bars represent 1 SD.

F #	Formulation Components (pH 7.2)	Osmolality (mOsm)
1	1mM Sodium Phosphate + 150mM NaCl (Current Bulk Formulation)	270 ± 1
2	1mM Sodium Phosphate + 150mM NaCl + 0.025% PS-80	268 ± 1
3	1mM Sodium Phosphate + 10% w/v Sucrose + 0.025% PS-80	328 ± 2
4	5mM Sodium Phosphate + 150mM NaCl + 0.025% PS-80	297 ± 4
5	5mM Sodium Phosphate + 10% w/v Sucrose + 0.025% PS-80	330 ± 8
6	1mM Sodium Phosphate + 7.5% w/v Sucrose + 50mM NaCl + 0.025% PS-80	343 ± 4
7	5mM Sodium Phosphate + 7.5% w/v Sucrose + 50mM NaCl + 0.025% PS-80	308 ± 4
8	5mM HEPES + 10% w/v Sucrose + 0.025% PS-80	308 ± 4
9	5mM HEPES + 7.5% w/v Sucrose + 50mM NaCl + 0.025% PS-80	331 ± 2

3.5 Figures

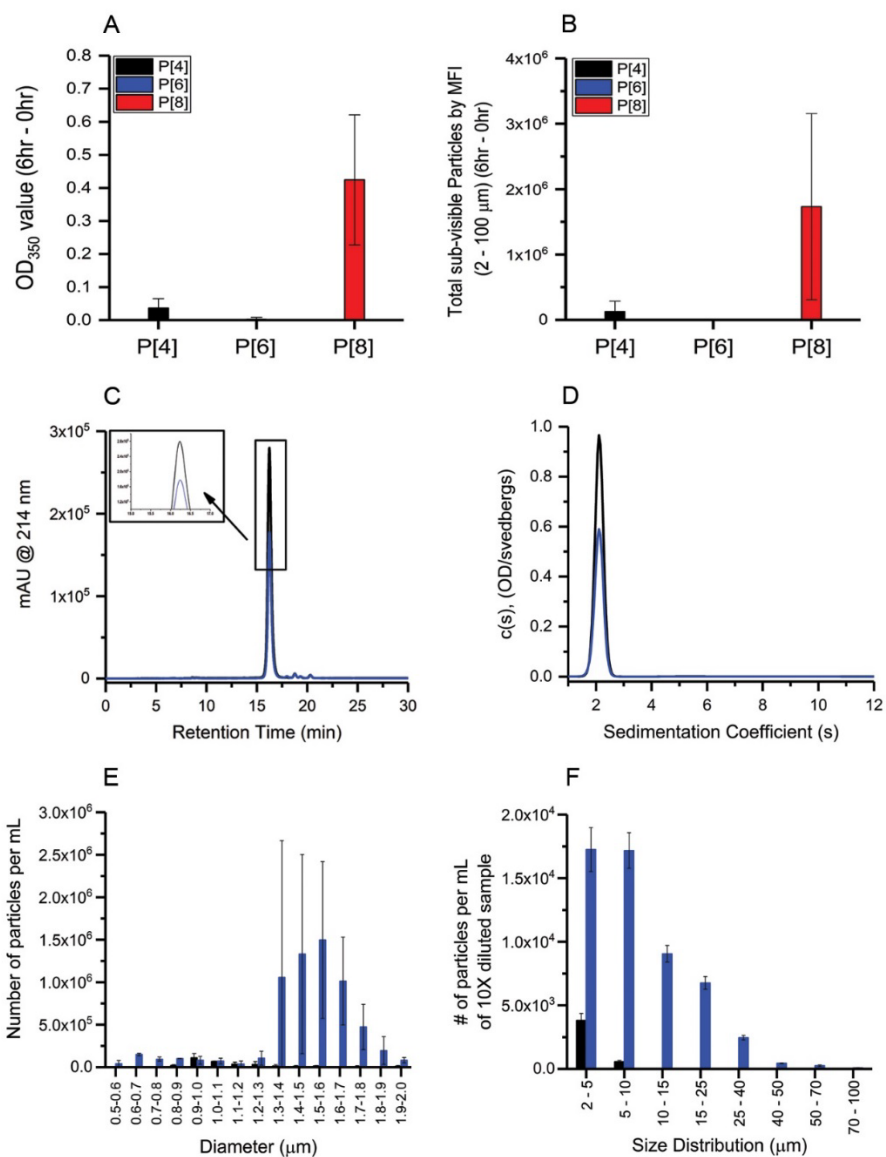


Figure 3.1. Colloidal stability assessment and comparison of the three NRRV antigens after shake stressed for 6 h. (A) light scattering as measured by OD₃₅₀ values, and (B) total sub-visible particles (2 – 100 μm) per mL by MFI. Results from unstressed samples (0 h) are subtracted from stressed samples (6 h). Size-distribution analysis of shake stressed P[8] antigen in base formulation (10 mM PBS pH 7.2) were then monitored as soluble aggregates/fragments and protein loss quantification by (C) SEC, and (D) SV-AUC analysis. Sub-micron and sub-visible particle analysis by (E) resonant mass measurement, and (F) micro-flow imaging microscopy, respectively. Error bars represent 1 SD from three separate measurements. Refer to Supplemental Table S1 for data of similar studies with P[4] and P[6] antigens.

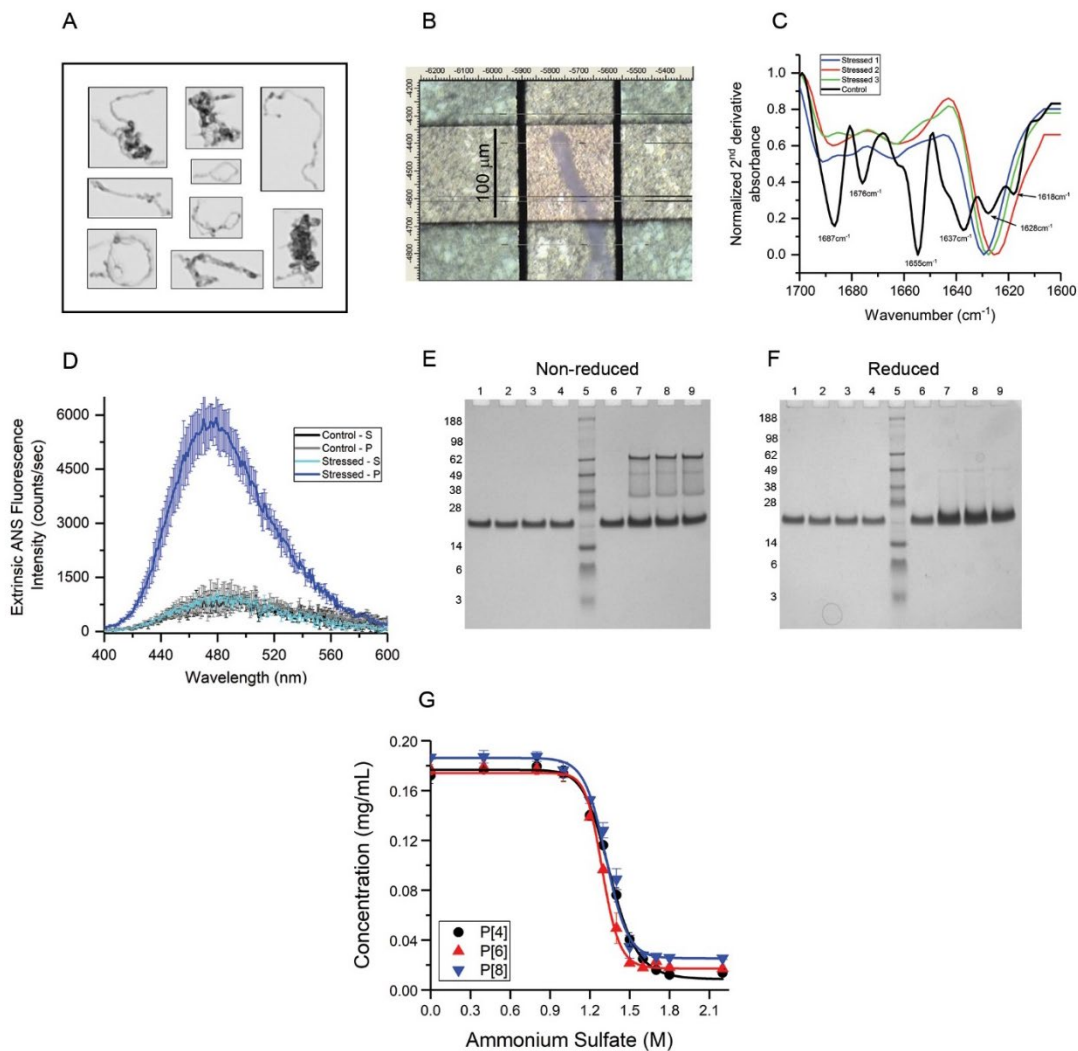


Figure 3.2. Morphology and structural analysis of protein within aggregates/particles formed for P[8] antigen after shake stress in base formulation. (A) Representative particle images recorded by micro-flow imaging microscopy, (B) optical microscopic image of an isolated protein particle/aggregate, (C) secondary structure analysis of protein in isolated insoluble protein particles/aggregates by FTIR microscopy, (D) higher order structure integrity analysis of unstressed and stressed protein in the supernatant (S) and pellet (P) fractions by ANS fluorescence spectroscopy, and chemical modification analysis of unstressed and stressed protein in S and P fractions by (E) non-reduced and (F) reduced SDS-PAGE (Lane 1 – S unstressed, lanes 2,3,4 – S stressed, lane 5 – MW marker, lane 6 – P unstressed, and lanes 7,8,9 – P stressed). Refer to Supplemental Figure S1 for data sets of similar studies with P[4] and P[6] antigens. (G) Relative solubility assessment of three NRRV antigens using ammonium sulfate precipitation assay, error bars represent 1SD from triplicate experiments.

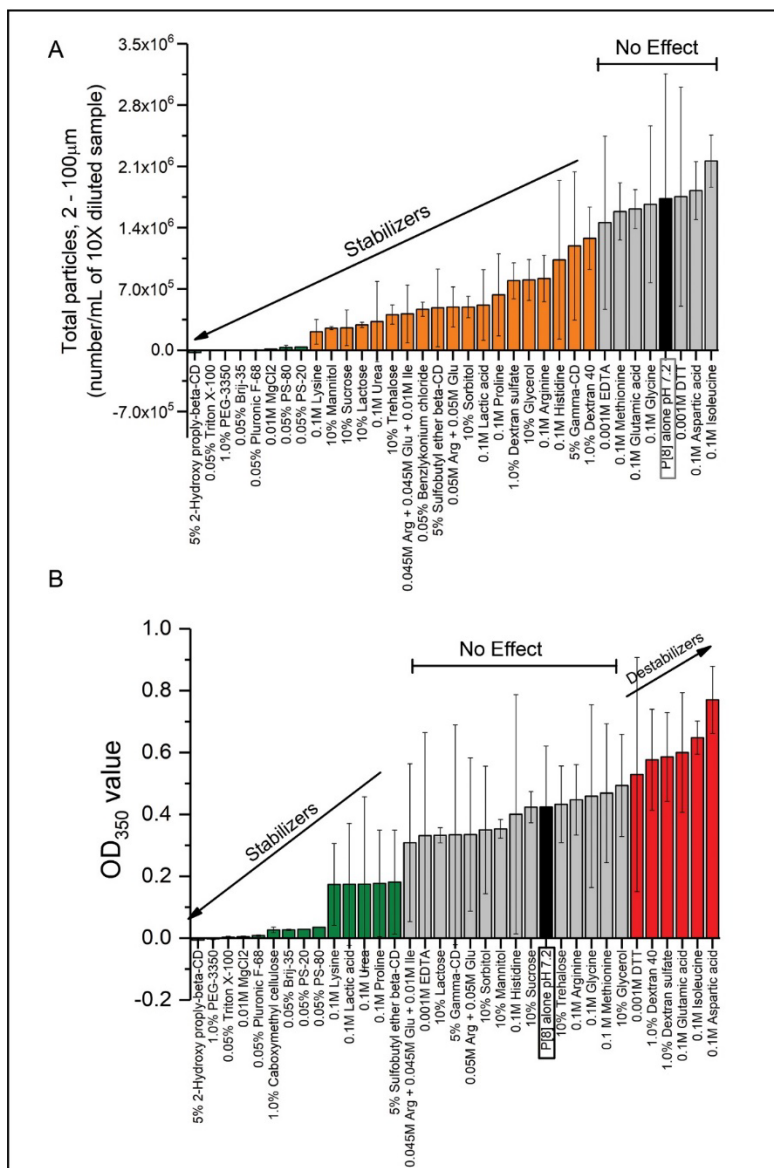


Figure 3.3. Excipient screening against agitation stress of P[8] protein antigen. (A) Total sub-visible particles, and (B) OD₃₅₀ values of 0.15 mg/mL P[8] solution after shake stressed for 6 h in base buffer (10 mM PBS pH 7.2; black bar, highlighted in box) and in base buffer containing different excipients. Excipients are rank ordered from lowest to highest total sub-visible particles or OD₃₅₀ value suggesting highest to lowest stability. Excipients in green, orange, grey, and red resulted in large increase, moderate increase, no effect, and decrease in stability, respectively. Error bars represent 1 SD from triplicate experiments. Refer to Supplemental Figure S2 for similar studies with down-selected excipients for P[4] and P[6] antigens.

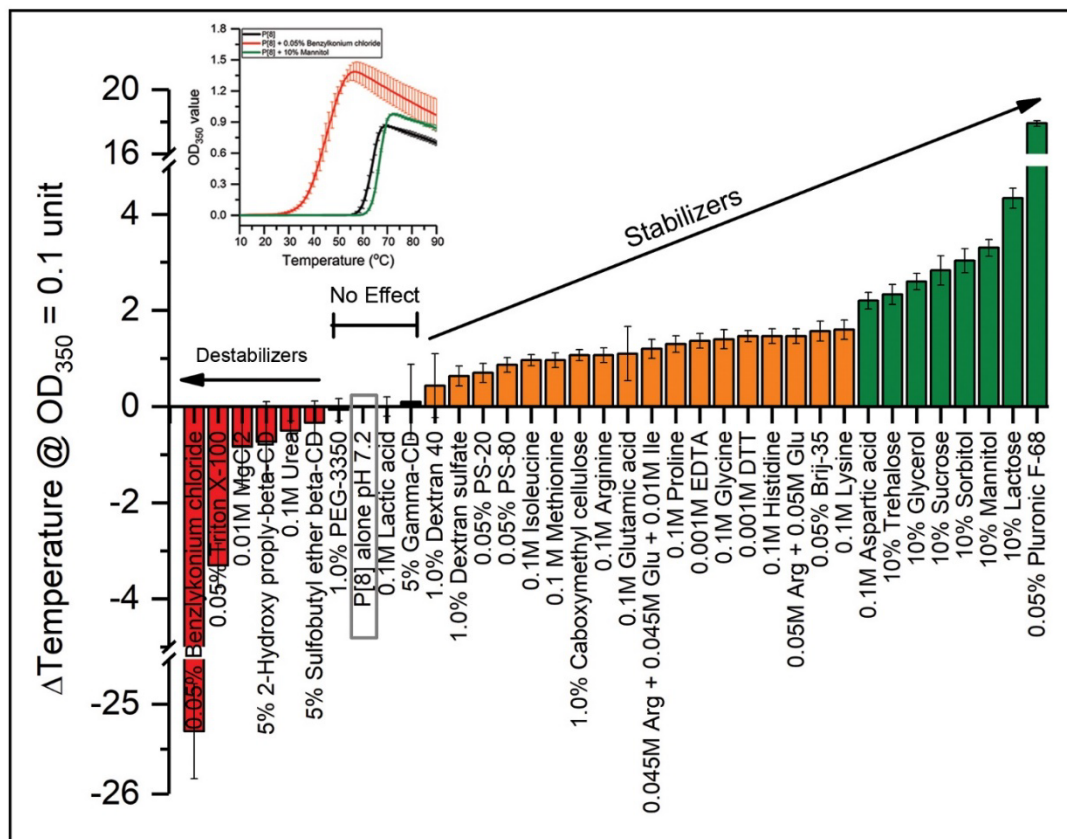


Figure 3.4. Excipient screening against thermal stress of P[8] protein antigen. OD₃₅₀ studies of 0.1 mg/mL P[8] solution subjected to thermal stress from 10 to 90°C in base buffer (10 mM PBS pH 7.2) and in base buffer containing different excipients. Average delta temperature (Δ T) value at which OD₃₅₀ reaches 0.1 absorbance unit is shown and error bars represent 1SD from triplicate experiments. Excipients are rank ordered from lowest to highest Δ T value suggesting lowest to highest stability. Excipients in green, orange, grey, and red resulted in large increase, moderate increase, no effect, and decrease in stability, respectively. The inset shows OD₃₅₀ vs. temperature plots of a representative stabilizing (green line) and destabilizing (red line) excipient as compared to P[8] alone (black line) in base buffer. Refer to Supplemental Figure S3 for similar studies with down-selected excipients for P[4] and P[6] antigens.

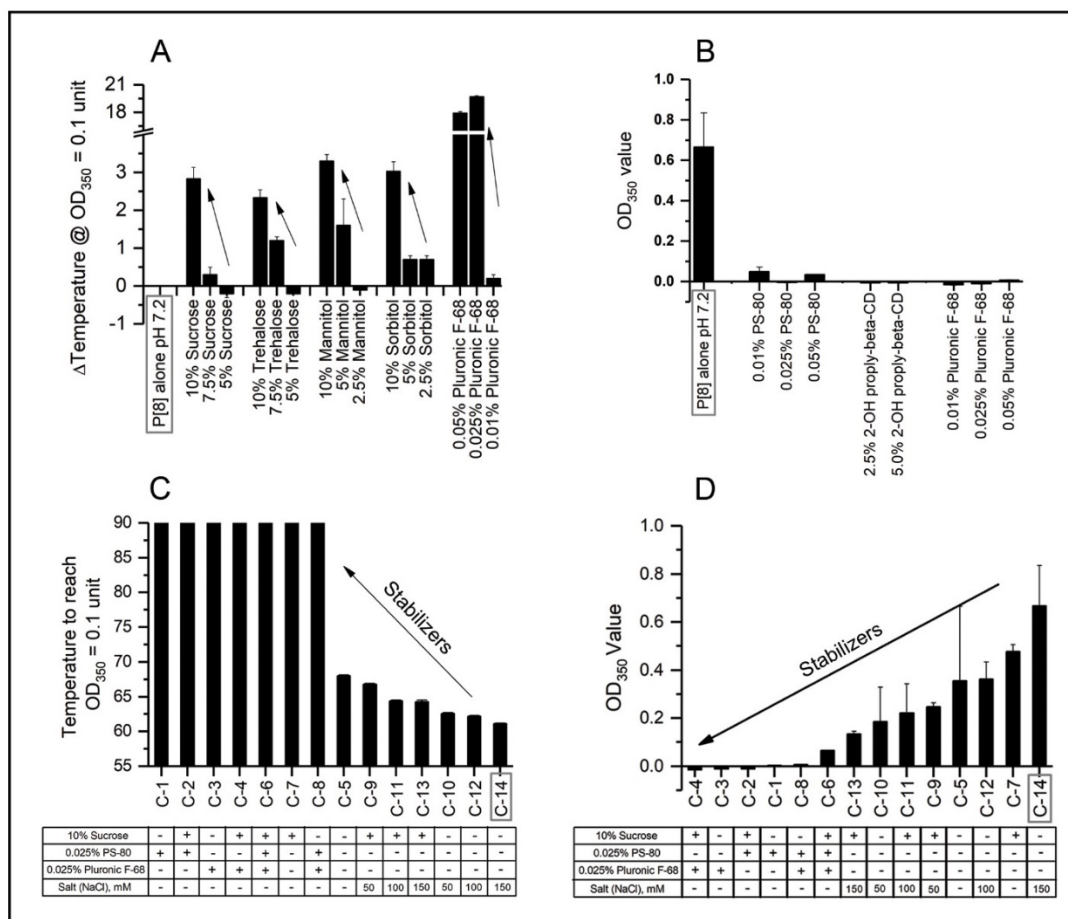


Figure 3.5. Effect of excipient concentrations and combinations on thermal and shaking induced aggregation propensity of P[8] in base buffer (10 mM PBS pH 7.2). (A) ΔT to reach $OD_{350} = 0.1$, and (C) temperature to reach $OD_{350} = 0.1$ during thermal stress studies. OD_{350} value of P[8] samples stressed for 6 h minus time zero samples with different (B) excipients concentrations, and (D) excipients combination studies. Error bars represent 1 SD from triplicate experiments. Tables below panels C and D indicate which excipients were present in each combination.

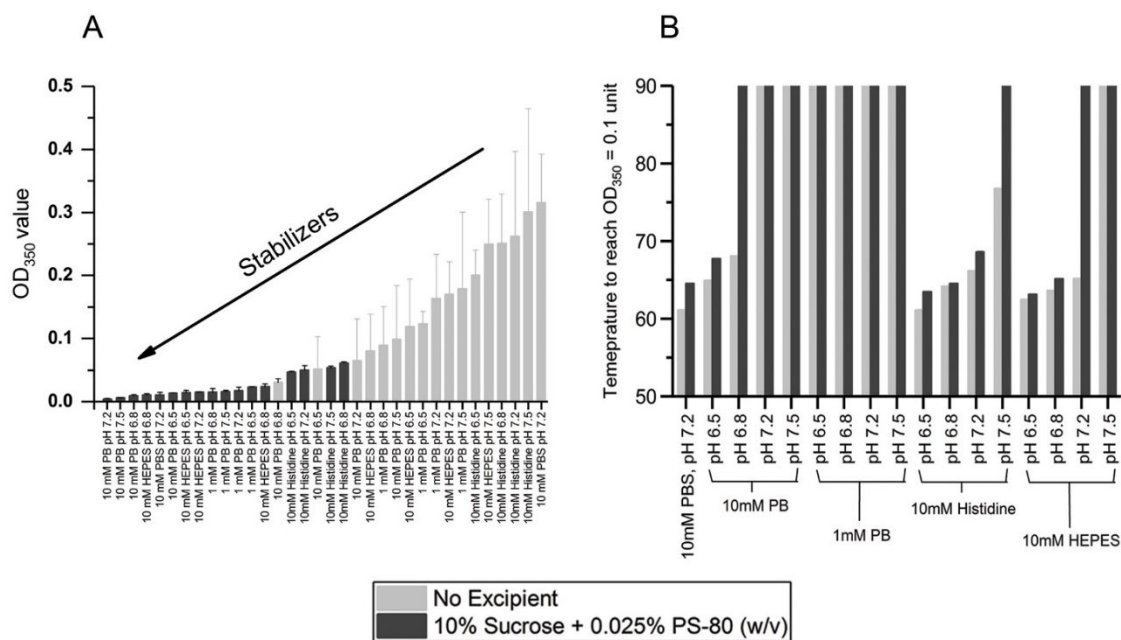


Figure 3.6. Effect of different buffer types and pH conditions on (A) thermal induced, and (B) shaking induced aggregation propensity of P[8]. In panel A, solution conditions are rank ordered from highest to lowest stabilizing effect, and, in panel B, buffer types are grouped together for easier data interpretation. Error bars represent 1 SD from triplicate experiments. Refer to Supplemental Figure 3.S4 for similar studies with down-selected conditions for P[4] and P[6] antigens.

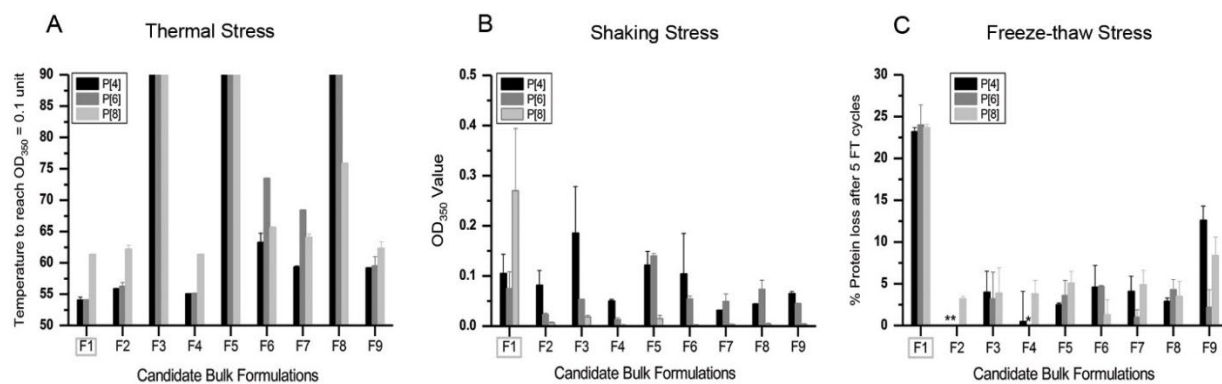


Figure 3.7. Comparison of candidate bulk formulations (F2 – F9) versus current formulation (F1), of individual NRRV antigens against (A) thermal stress, (B) shaking stress, and (C) freeze-thaw stress. Error bars represent 1 SD from triplicate experiments. Refer to Table 3.1 for the composition and osmolality of each candidate formulation.

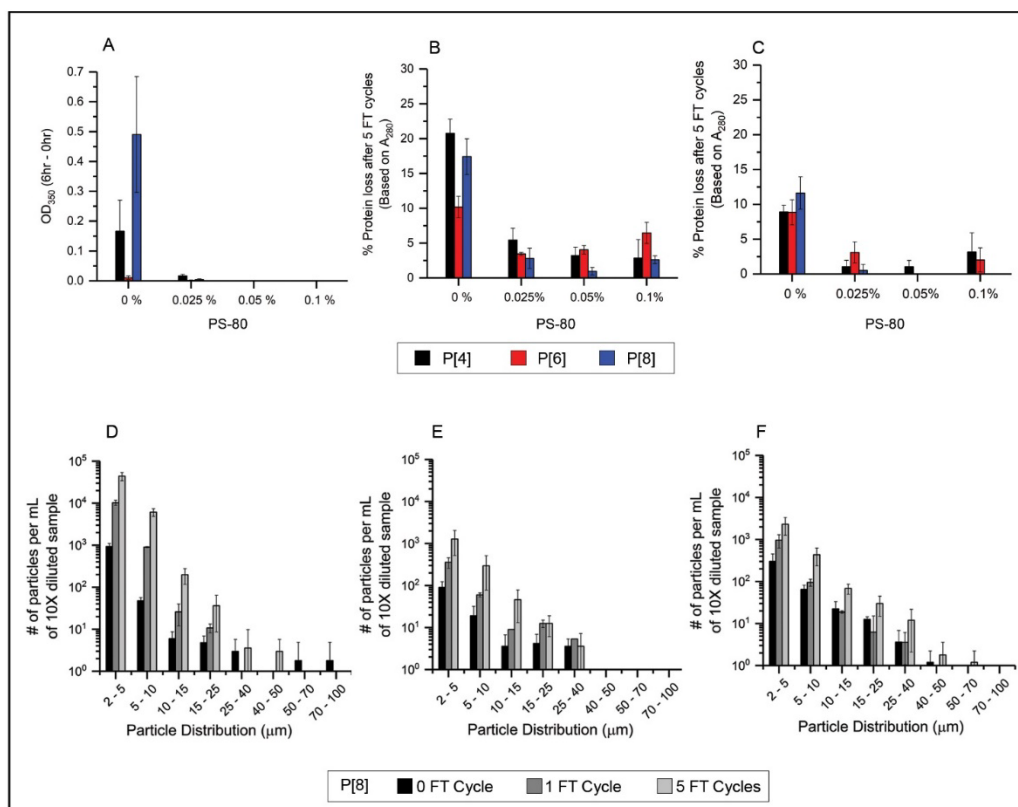


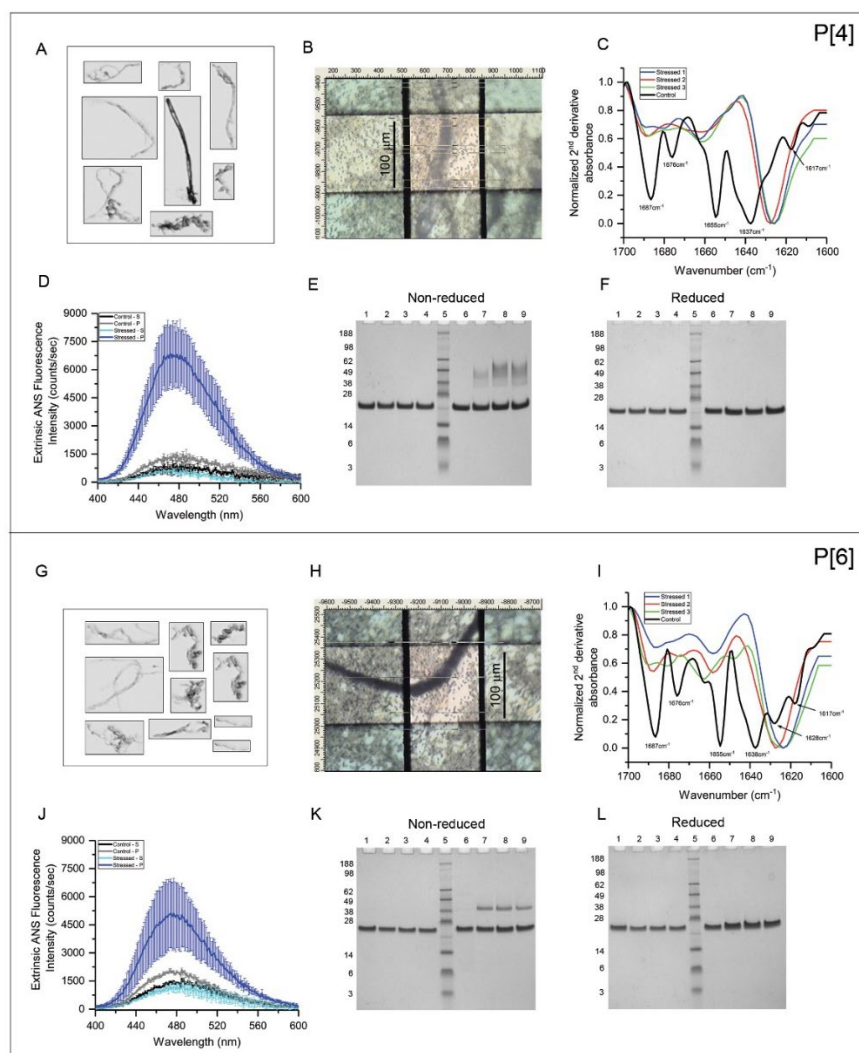
Figure 3.8. Effects of PS-80 concentration during freeze-thaw and shaking stresses on physical stability of NRRV antigens in current formulation. (A) OD₃₅₀ value after shaking each antigen for 6 hours at 0.15 mg/mL protein concentration. Percent protein loss after 5 FT cycles at (B) 0.15 mg/mL and (C) 0.4 mg/mL protein concentration. Sub-visible particle distribution analysis of P[8] antigen after 0, 1, and 5 FT cycles in (D) current (1mM sodium phosphate 150 mM NaCl pH 7.2) formulation and two candidate formulations, (E) 1mM sodium phosphate 150 mM NaCl 0.05% PS80 pH 7.2, and (F) 10 mM histidine 150 mM NaCl 0.05% PS80 pH 6.8. Error bars represent 1 SD from triplicate experiments.

3.6 Supplementary Tables

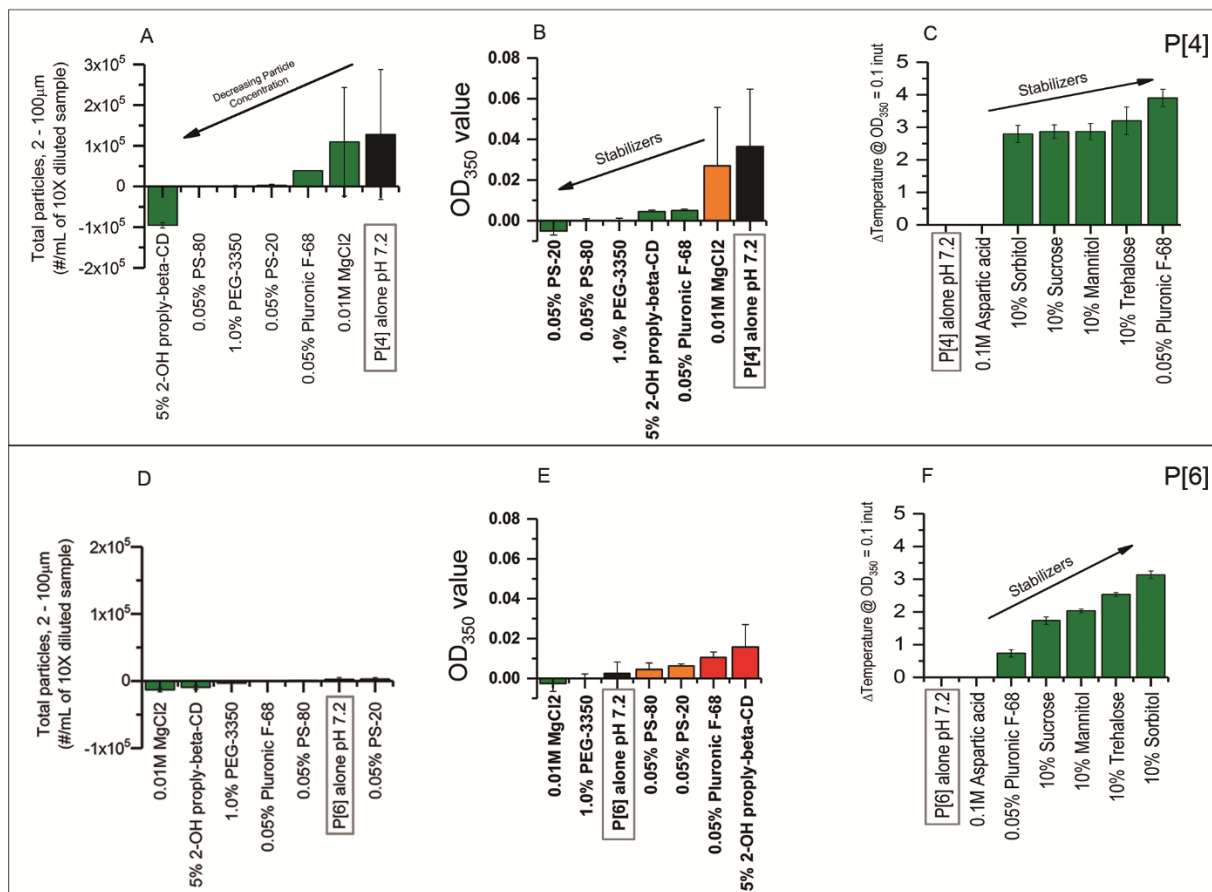
Supplementary Table S3.1. Comparison of aggregate and particle formation in different size ranges for the three NRRV antigens. Stressed samples were generated under forced degradation conditions of shaking stress for 1.5 hr. at 250 RPM at room temperature in base formulation (see main text). Error bars represent 1 SD from triplicate measurements. ('-' particles not observed, '+' particles observed)

Size Range	Analytical Methods	P[4]		P[6]		P[8]		
		T = 0 h	T = 1.5 h	T = 0 h	T = 1.5 h	T = 0 h	T = 1.5 h	
>100 μm	Visual assessment	-	-	-	+	+	+	
1 nm – 100 μm	UV-visible absorption spectroscopy	A280	0.35 \pm 0.0	0.25 \pm 0.01	0.35 \pm 0.0	0.23 \pm 0.0	0.37 \pm 0.0	0.26 \pm 0.0
		OD350	0.01 \pm 0.0	0.46 \pm 0.07	0.01 \pm 0.0	0.35 \pm 0.02	0.01 \pm 0.0	0.40 \pm 0.04
	Turbidimetry (NTU)	0.5 \pm 0.0	12.9 \pm 0.8	0.5 \pm 0.0	7.8 \pm 0.5	0.5 \pm 0.0	9.9 \pm 0.3	
2 – 100 μm	Micro-flow imaging (Total particles/mL of 10X diluted sample)	1.38 \pm 0.37	$\times 10^3$ 1.0 \pm 0.18 $\times 10^5$	3.32 \pm 0.52	$\times 10^3$ 0.8 \pm 0.06 $\times 10^5$	4.43 \pm 0.70	$\times 10^3$ 0.53 \pm 0.04 $\times 10^5$	
1 – 2 μm	Resonant mass measurement (Total Particles/mL)	2.09 \pm 0.06	$\times 10^5$ 1.20 \pm 0.96 $\times 10^6$	1.01 \pm 0.12	$\times 10^6$ 3.29 \pm 2.23 $\times 10^7$	3.24 \pm 0.92	$\times 10^5$ 6.34 \pm 3.88 $\times 10^6$	
1 – 100 nm	SV-AUC	Monomer (%)	100 \pm <1	70 \pm 2	100 \pm <1	74 \pm 1	100 \pm <1	67 \pm 2
		Soluble aggregates (%)	0 \pm <1	0 \pm <1	0 \pm <1	0 \pm <1	0 \pm <1	0 \pm <1
	SEC	Monomer (%)	99.4 \pm 0.1	71.4 \pm 4.2	98.5 \pm 0.3	74.7 \pm 0.8	96.7 \pm 0.1	65.2 \pm 3.6
		Fragments (%)	0.3 \pm 0.0	1.3 \pm 0.4	0.2 \pm 0.2	2.6 \pm 0.4	3.3 \pm 0.1	3.9 \pm 0.1
		Soluble + Insoluble aggregates (%)	0.3 \pm 0.0	27.4 \pm 4.3	1.3 \pm 0.1	21.9 \pm 1.2	0.0 \pm 0.0	30.8 \pm 3.8

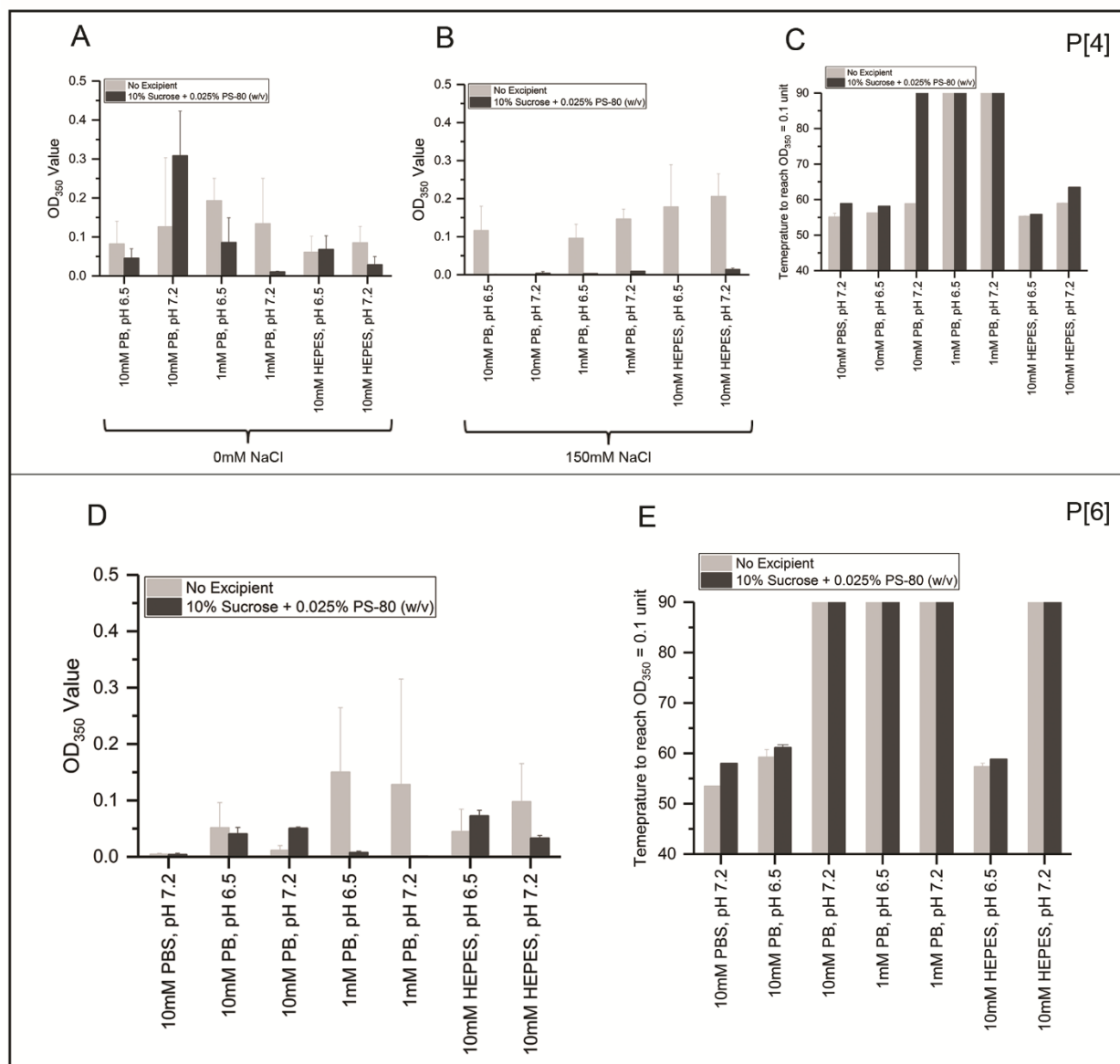
3.7 Supplementary Figures



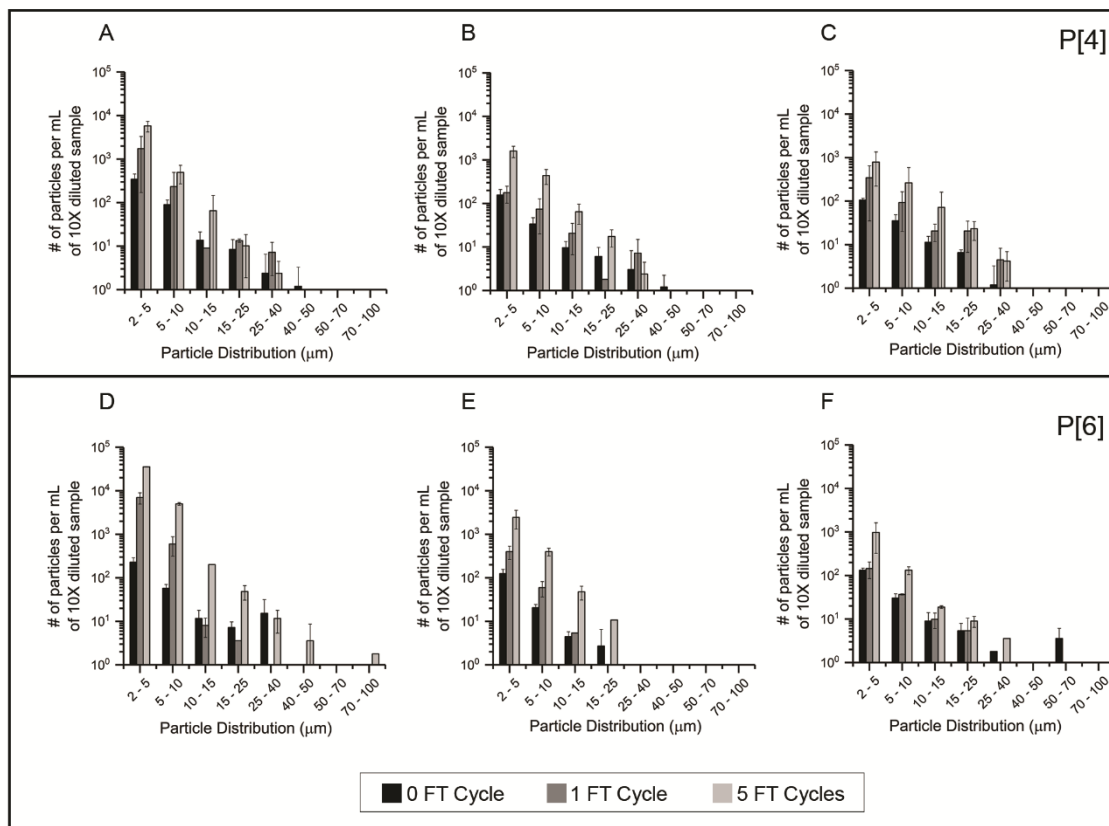
Supplementary Figure S3.1. Morphology, higher order structure and chemical composition of aggregates/particles formed for P[4] (top panel) and P[6] (bottom panel) antigens after shake stress in base formulation. (A, G) Representative particle images recorded by micro-flow imaging microscopy, (B, H) representative optical microscopic image of an isolated protein particle, (C, I) secondary structure analysis of unstressed protein in solution (control) and isolated particle from stressed sample by FTIR microscopy, (D, J) higher order structure integrity analysis of unstressed and stressed protein in the supernatant (S) and pellet (P) fractions by ANS fluorescence spectroscopy. Chemical modification analysis of unstressed and stressed protein in S and P fractions by (E, K) non-reduced and (F, L) reduced SDS-PAGE (Lane 1 – S unstressed, lanes 2,3,4 – S stressed, lane 5 – MW marker, lane 6 – P unstressed, and lanes 7,8,9 – P stressed).



Supplementary Figure S3.2. (A, D) Total sub-visible particles, and (B, E) OD₃₅₀ value of 0.15 mg/mL P[4] and P[6] solutions after shake stressed for 6 h. (C, F) Average ΔT value at which OD₃₅₀ reaches 0.1 absorbance unit of 0.1 mg/mL solution subjected to thermal stress from 10 to 90°C. Studies were conducted in base buffer (black bar, highlighted in box) and in base buffer containing different excipients. Excipients are rank ordered from lowest to highest total sub-visible particles or OD₃₅₀ value suggesting highest to lowest stability. For OD₃₅₀ melt data, higher ΔT suggests higher stability. Excipients in green, orange, and red resulted in large increase, no effect, and decrease in stability, respectively. Top row shows data for P[4] and bottom row for P[6] antigen, error bars represent 1 SD from triplicate measurements.



Supplementary Figure S3.3. Effects of down-selected buffer types and pH conditions on (A, B, D) shaking induced, and (C, E) thermal induced aggregation propensity of P[4] and P[6] antigens. Top panel shows data for P[4] and bottom for P[6] antigen. Error bars represent 1 SD from triplicate experiments.



Supplementary Figure S3.4. Sub-visible particle distribution analysis of P[4] and P[6] antigens after 0, 1, and 5 FT cycles as measured by MFI. Samples in (A, D) current formulation (1mM sodium phosphate 150 mM NaCl pH 7.2) and two candidate formulations, (B, E) 1mM sodium phosphate 150 mM NaCl 0.05% PS80 pH 7.2, and (C, F) 10 mM histidine 150 mM NaCl 0.05% PS80 pH 6.8. Top row shows data for P[4] and bottom for P[6] antigen. Error bars represent 1 SD from triplicate experiments.

Chapter 4

Effect of aluminum adjuvant and preservatives on structural integrity and physicochemical stability profiles of three recombinant subunit rotavirus vaccine antigens

4.0 Introduction

Rotavirus (RV) is a leading cause of childhood gastroenteritis and severe diarrhea worldwide with ~128,500 deaths (children below 5 years of age) in 2016¹. Majority of RV-related mortality occurs in developing countries where rehydration therapy is more difficult to obtain and efficacy of currently available live-attenuated, oral RV vaccines is lower compared to the developed world²⁹. Reasons behind the lower efficacy are multi-factorial and not well understood¹⁰⁹. There is thus a great need for a new generation RV vaccine with enhanced efficacy for the developing world at affordable costs with consistent supply to improve vaccine coverage⁴. A trivalent subunit RV vaccine (non-replicating rotavirus vaccine, NRRV) contains three recombinant protein antigens (belonging to rotavirus genotypes P[4], P[6] and P[8]; see below) and is currently in clinical trials in South Africa¹². These three antigens not only provide broad worldwide serotype coverage to RV infections, but the P[6] genotype is much more prevalent in the African and Southeast Asian regions¹¹. Previously a monovalent NRRV vaccine adsorbed to Alhydrogel® was shown to be safe and immunogenic in infants and toddlers in early stage clinical trials⁴⁷.

Each of the three NRRV protein antigens is a recombinant fusion of the truncated VP8* protein (a cleavage product of the RV outer capsid protein VP4) linked to CD4⁺ T cell epitope (P2) from tetanus toxoid using a GSGSG linker^{44,45}. The three antigens are named P2-VP8-P[4], P2-VP8-P[6] and P2-VP8-P[8] where P2 is the tetanus toxoid epitope, VP8 the truncated VP8* protein, and P[x] denotes the P genotype from the human RV strains DS-1-like (G2P[4]), 1076-like (G2P[6]) and Wa-like (G1P[8]). The three NRRV antigens are referred to as P[4], P[6] and P[8] in this work. Wen *et al.* showed that addition of an aluminum-based adjuvant to P2-VP8-P[6/8] containing monovalent vaccines increased the neutralizing antibody titers against RV in guinea pigs, however, the binding of antigens to adjuvant (aluminum phosphate) was not taken

into consideration ⁴⁵. The clinical NRRV vaccine is formulated with aluminum hydroxide (Alhydrogel) to keep the NRRV antigens bound to adjuvant ^{46,47}.

Affordability and accessibility are major hurdles during successful incorporation of a new vaccine in the national immunization programs of developing countries ⁴. Using multi-dose formulations is an effective strategy to reduce the cost of vaccine per dose in terms of manufacturing, packaging, storage, transport, and medical waste ⁹³. However, the suitability of a multi-dose formulation strategy is vaccine-specific depending on inherent cost, patient demand and vaccine wastage ⁹⁵. Since there is potential risk of microbial contamination due to multiple withdrawals from the same vial, a multi-dose vaccine drug product requires the addition of a preservative ⁹⁶. Combining multiple vaccines into a single vial (combination vaccines) also provides many economic benefits such as fewer vaccination visits and reduced manufacturing costs (fewer doses, less packaging, and streamlined storage and handling). In addition, societal benefits of combination vaccines include improved vaccine coverage, fewer missed or delayed vaccinations as well as fewer needle stick injuries ^{101,102}.

The long-term goal of NRRV vaccine development is to introduce the NRRV vaccine into the pentavalent childhood combination vaccine (e.g., pentavalent diphtheria, tetanus, wc-pertussis, Hib and HepB) to lower costs, enhance patient compliance and improve RV vaccine coverage. Pediatric combination vaccines in the developing world typically contain whole cell pertussis (wcP) and thimerosal, used both as a preservative and inactivating agent during wcP production ¹⁹⁰. Therefore, it is important to assess the compatibility and stability of NRRV antigens with thimerosal, an ethyl mercury containing compound that has been used in multi-dose injectable vaccines since 1930s to protect against potential microbial contamination. The addition of

thimerosal to certain vaccines, e.g., HPV and IPV, is known however to reduce their *in vitro* potency and *in vivo* immunogenicity^{97,98}.

In this work, we determined the adsorptive capacity and strength of the P[8] antigen to aluminum adjuvant (Alhydrogel, AH) as well as the protein's structural integrity, physicochemical stability and antibody binding during stability studies (+/- the preservatives thimerosal and 2-phenoxyethanol). The physicochemical stability of the NRRV antigens on the surface of the Alhydrogel were examined by immunochemical (ELISA), biochemical (SDS-PAGE combined with LC-MS peptide mapping) and biophysical (DSC, fluorescence spectroscopy) methods. Due to limited availability of P[4] and P[6] antigens, a subset of key results obtained with P[8] were assessed with these two aluminum-adsorbed NRRV antigens. These results are discussed in the context of future formulation development efforts to be undertaken to develop a more stable multi-dose formulation of the trivalent NRRV vaccine.

4.1 Materials and Methods

The NRRV antigens (P[4], P[6], and P[8]) were produced and purified from *E. coli* at Blue Sky BioServices, MA and provided frozen in 600 mM ammonium sulfate, 50 mM Tris buffer at pH 7.5. Alhydrogel® (aluminum hydroxide adjuvant) was purchased from Accurate Chemical Scientific Corporation (Westbury, NY). Sodium chloride and sodium phosphate dibasic heptahydrate, were purchased from Thermo Fisher Scientific (Waltham, MA). Sodium phosphate monobasic monohydrate, Histidine, HEPES, Tris and all other reagents and chemicals were purchased from Sigma-Aldrich (St. Louis, MO) and were of analytical grade or higher. Extinction coefficient used for concentration determination of each antigen have been reported previously¹⁶⁰.

4.1.1 Measuring Zeta Potential

Zeta potential of AH was measured in different buffers using ZetaPALS Zeta Potential Analyzer (Brookhaven Instruments Corporation, NY). AH samples were prepared at 1.5 mg/mL of aluminum at varying concentrations of the buffering agent (0, 0.5, 1.0, 2.5, 5.0, 10, 20, 50, 100 mM), 150 mM NaCl and 0.025% PS-80. The different buffering agents tested were sodium phosphate, HEPES and Tris at pH 7.2, and Histidine at pH 6.5, 6.8 and 7.2. Samples were incubated overnight at RT and 1.5 mL of the diluted AH sample was used for the measurement in a disposable plastic cuvette and appropriate electrode. Each buffer condition was measured in duplicate and for each measurement 10 runs were collected with 10 cycles per run. All measurements were conducted at 25°C and parameters such as viscosity, refractive index and dielectric constant were chosen for water. Electrophoretic mobility was used by the instrument software to calculate zeta potential using Smoluchowski approximation. Finally, the average and 1SD of the 20 runs were reported for each buffer condition as the measured Zeta potential value of AH.

For the preservative containing samples, AH samples were prepared at 1.5 mg/mL of aluminum in formulations F1, F3 and F5 (see Table 1 in main text for formulation composition) with increasing amounts of thimerosal (0, 0.002, 0.005, 0.01, 0.02, 0.05% w/v). Samples were incubated overnight at room temperature and analyzed the following day in similar way as described above.

4.1.2 Antigen-Adjuvant Binding Study

Binding of NRRV antigens to AH was studied at their clinical concentration (i.e., 60 µg of antigen and 560 µg aluminum as AH per 0.5 mL) in different buffering agents in the presence of 150 mM NaCl and 0.025% PS-80. Each protein sample at 2X concentration was mixed 1:1 with 2.24 mg/mL AH (in 150 mM NaCl) to achieve the final desired concentration of protein, aluminum

and buffer in the final formulation. After mixing, the antigen adsorbed samples were incubated overnight at 4°C and then centrifuged at 5,000 X g for 10 min. The amount of unbound protein in the supernatant was measured by UV-Visible spectroscopy using an Agilent 8453 UV-Visible Spectrophotometer (Palo Alto, CA).

4.1.3 Langmuir Binding Isotherms

Appropriate volume of antigen stock, PS-80 stock and buffer were mixed in an Eppendorf tube to a final volume of 250 μ L containing 0, 20, 50, 75, 100, 150, or 200 μ g of antigen and 0.05% PS-80. These protein solutions were mixed 1:1 with AH solution (0.2 mg/mL aluminum in saline) to get the desired amount of antigen (i.e. 0, 10, 25, 37, 50, 75, or 100 μ g), buffering agent, and PS-80. Samples were incubated overnight at 4°C and then centrifuged at 5,000 X g for 10 min to pellet the adjuvant and bound antigen fraction. UV-visible spectroscopy was used to measure the concentration of free/unbound antigen in the supernatant.

Once the concentration of free antigen (C_e) had been determined for each total added amount of antigen (C_o) in the antigen-adjuvant mixture, the amount of bound antigen could be calculated ($C_o - C_e$). Then the amount of bound P[8] per mg of aluminum (Q_e) can be calculated by dividing $C_o - C_e$ by the amount of aluminum used (i.e., 50 μ g). Finally, Langmuir isotherm was generated by plotting Q_e vs C_e and linear form of the isotherm can be obtained by plotting C_e/Q_e vs C_e . Linear form of the Langmuir isotherm was further analyzed to obtain the adsorptive capacity (Q_m) from the slope and adsorptive/Langmuir coefficient (K_L) from the y intercept of the fitted straight line. For the studies in the presence of thimerosal, 0.01% w/v thimerosal was added after binding the antigen to adjuvant, and samples were incubated overnight at 4°C prior to the generation of isotherms. Micro-BCA assay (ThermoFisher Scientific, MA) was used to measure

the concentration of free/unbound antigen due to interference from thimerosal absorbance in the UV region.

4.1.4 Steady State Intrinsic Tryptophan Fluorescence

The intrinsic tryptophan fluorescence of NRRV antigens was measured in solution and on AH using a Photon Technology International (PTI) spectrofluorometer (Lawrenceville, NJ) equipped with a turreted four-position Peltier-controlled cell holder and a xenon lamp. For in solution samples, spectra could be collected in a conventional way by pouring 0.7 mL of sample in 1 X 1 cm path length quartz cuvette. However, for adjuvant bound samples, 0.2 mg/mL of antigen stock was mixed 1:1 with 4 mg/mL of aluminum. Two milliliters of this sample were added to the 1 X 1 cm quartz cuvette and then the samples were allowed to settle overnight at 4°C (or centrifuged at 100 X g for 1 min to pellet the adjuvant bound protein). Following day, the fluorescence emission spectra were recorded as a function of temperature (10 – 90°C) as described previously¹⁶⁰. For studies in the presence of preservative, 0.01% thimerosal was added after binding the antigen to adjuvant and samples were incubated overnight at 4°C.

4.1.5 Differential Scanning Calorimetry (DSC)

DSC was performed for the NRRV antigens at 0.12 mg/mL in solution and on AH using an Auto-VP capillary differential scanning calorimeter (MicroCal/GE Health Sciences, Pittsburgh, PA) as described before¹⁶⁰.

4.1.6 Time-resolved Intrinsic Tryptophan Fluorescence

Intrinsic tryptophan fluorescence lifetime for NRRV antigens bound to AH \pm 0.01% w/v thimerosal was obtained using a fluorescence plate-reader (Fluorescence Innovations, Minneapolis, MN) equipped with a tunable pulsed dye laser, a high-speed digitizer and a temperature controlled 384-well sample holder (Torrey Pines Scientific, Carlsbad, CA). This

fluorometer has two detectors: a charge coupled device (CCD) spectrometer and a photomultiplier tube (PMT), permitting recording of steady-state fluorescence and time-resolved intrinsic fluorescence, respectively. The emission signal was collected at 180° (front face geometry) and then sent through a 300 nm long pass filter (Thorlabs Inc., Newton, NJ). For time-resolved fluorescence recording, the signal was further passed through a 360 nm (\pm 23 nm) band-pass filter before reaching the PMT. Samples were loaded (10 μ L) into a 384 well plate (Hard-Shell 384-well PCR plates) and 2 μ L silicon oil (ThermoFisher Scientific) was added on top to avoid sample evaporation. Excitation wavelength of 295 nm was used and temperature ramp was set from 10-90°C with step size of 1.25°C and 2 min equilibration at each temperature. Time-resolved intrinsic fluorescence was performed by recording the fluorescence lifetime decay waveforms within a time scale of 100 ns. Life-time moment (ns) was obtained from the fluorescence lifetime decay waveform which is defined as the center of the waveform which vertically divides the peak area in two halves. Moment is similar to mean spectral mass in steady state intrinsic Trp fluorescence experiments. The lifetime moment represents the intensity-averaged lifetime of the waveform plot and its mathematical definition has been previously described ¹⁹¹.

4.1.7 SDS-PAGE Analysis + LC-MS Peptide Mapping, of desorbed protein

Antigen-adjuvant sample (500 μ L, 60 μ g antigen + 560 μ g aluminum) was centrifuged at 4,000 X g for 5 min to pellet the adsorbed antigen and adjuvant. Then 460 μ L the supernatant was removed, and the pellet was re-suspended in a mixture of 0.2M sodium phosphate + LDS buffer (Life Technologies) + 20 mM Iodoacetamide (Thermo Scientific), and incubated in dark for 15 min at RT. Then the samples were heated at 90°C for 10 min, followed by centrifugation at 4,000 X g for 5 min. Supernatant was recovered and divided in two parts to prepare non-reduced and reduced samples for SDS-PAGE analysis. For reduced samples, supernatant was mixed with 10

mM DTT (Thermo Scientific) and, for non-reduced samples, equal volume of ultra-pure water was added and then the samples were incubated at 37°C for 15 min. Finally, the reduced/non-reduced samples were separated by SDS-PAGE gel electrophoresis using NuPAGE 4-12% Bis-Tris (Life Technologies) gels and a MES running buffer (Life Technologies). A theoretically equivalent amount of protein was also loaded on the gel as in-solution control (i.e., protein that was never exposed to adjuvant). The purpose of running in-solution control was to quantify % desorption under forced desorption condition of phosphate + LDS sample buffer + boiling at 90°C for 10 min by comparing the band intensities between in-solution control and desorbed samples by ImageJ (NIH, US) analysis. Gels were run for first 10 min at 120V followed by 50 min at 150V. Protein bands were visualized by staining with coomassie blue R250 (Teknova, Hollister, CA) for 1 hr and destained with a mixture of 40% methanol, 10% acetic acid, and 50% ultrapure water. Gels were digitized using an Alphaimager (Protein Simple, Santa Clara, CA) gel imaging system.

For LC-MS peptide mapping, each monomer band and selected dimeric bands were excised from the SDS-PAGE gel and cut into small pieces. The Coomassie stain in the gel pieces was removed through two 45 min washes at 37°C with 0.2 M ammonium bicarbonate pH 7.5 + 50% acetonitrile. The gel pieces were then dehydrated using a SpeedVac (Eppendorf, Hamburg, Germany) for ~30 min at 30°C and then rehydrated with 50 mM ammonium bicarbonate pH 7.5. Chymotrypsin (3.5 µg, Promega, Madison, WI) was added and the samples were incubated overnight at 37°C. The following day the solution in each sample was removed and 0.05% trifluoroacetic acid was added to inactivate proteolysis. The samples were then subjected to LC-MS peptide mapping.

The peptides from each digested protein solution were separated by a liquid chromatography system (Thermo Scientific, Waltham, MA) prior to analysis. Peptides were

injected onto a C18 column (1.7 μ m, 2.1 x 150 mm, Waters) and a 55 min 5-50% B gradient (A: H₂O and 0.04% trifluoroacetic acid; B: ACN and 0.04% trifluoroacetic acid; 200 μ l/min flow rate) for separation. MS was performed using a LTQ-XL ion trap (Thermo Scientific) and the Xcalibur 2.0 software (Thermo Scientific). The instrument was also tuned using a standard calibration peptide (Angiotensin II, Sigma) for maximal sensitivity before running any experiments. The mass spectra were acquired in the LTQ over a mass range of m/z 350-1900. The ion selection threshold was 10,000 counts and the dynamic exclusion duration was 8 sec.

Raw experimental files were initially evaluated manually to determine if the ion counts and fragmentation of each peptide were sufficient for further analysis. The raw data files were then processed using PepFinder 2.0 software (Thermo Scientific). The database used for this experiment consisted of the [P8] and chymotrypsin primary sequences. Potential post-translational modifications (Asn deamidation and Met oxidation) were included during the analysis. Peptide assignments of MS/MS spectra were validated using a confidence score of $\geq 95\%$.

4.1.8 Inhibition ELISA

The details of the inhibition ELISA assay used in this work, including the antibodies used and the nature of their interaction with NRRV antigens, is described elsewhere (McAdams et al., manuscript in preparation). Briefly, the AH bound NRRV antigen samples were first incubated with a blocking buffer, then serial dilutions were made and incubated with a fixed amount of NRRV P[x] antigen specific antibody (primary antibody) overnight. Samples were centrifuged and the supernatant containing free antibody was transferred to a 96 well plate coated with the NRRV P[x] antigen standard. The plate was incubated at room temperature for two hours and then the amount of primary antibody bound on the plate was determined with a horseradish peroxidase labeled secondary antibody using a tetramethylbenzidine substrate. OD450 values were recorded

using a SpectraMax® plate reader (Molecular Devices). The NRRV P[x] antigen levels in the test samples were calculated by comparing results to OD450 values of a NRRV P[x] antigen reference standard using multi-parameter fitting of the standard curve.

4.1.9 Accelerated/Real Time Storage Stability Study

Monovalent NRRV vaccines were prepared in five formulations for P[8] with and without 0.01% thimerosal as illustrated in the schematic shown in Sup. Figure S4.1. Total ten formulations (F1 – F5, \pm 0.01% w/v thimerosal) were tested with P8 antigen bound to AH and details of formulation composition is provided in Table 4.1 in main text. Due to limited availability of P[4] and P[6], four formulations (F1, F2, \pm 0.01% w/v thimerosal) were tested with these antigens. Adsorption was achieved by adding the 2X antigen stock (sterile filtered through a 0.22 μ m filter) to the 2X AH stock with gentle mixing and final concentrations of protein and aluminum were 0.12 mg/mL and 1.12 mg/mL, respectively. Two milliliter aliquots of vaccine were dispensed into 3 mL Fiolax Clear glass vials (West Pharmaceutical Services, PA) and rubber stoppered (NovaPure®, West Pharmaceutical Services, PA). Vaccine vials were sealed with flip off caps and were incubated at 4°C and 25°C storage temperatures for 4 and 12 weeks, and at 37°C for 2, 4, and 12 weeks. At each time point, samples were pulled from the incubator and assayed for different physicochemical characteristics. As shown in the schematic in Sup. Figure S4.1, HOS integrity, conformational stability and antibody binding were studied with antigen in the bound state, whereas, chemical stability, monomer quantitation and desorption quantitation analysis were carried out after forced desorption of the antigen. For the storage stability assessment of monovalent P[8] vaccine in the presence of 1.0% w/v 2-Phenoxyethanol, vaccine vials were stored at 4°C and 37°C for 1, 7, 14 and 84 days.

4.2 Results

4.2.1 P[8] Antigen-Alhydrogel Adjuvant Interactions

The pretreatment of aluminum hydroxide (Alhydrogel, AH) with phosphate ions lowers the net surface charge due to replacement of hydroxyl groups on AH with phosphate ions⁷⁷. As expected, pretreatment of AH with increasing concentrations of phosphate buffer at pH 7.2 altered the zeta potential (ZP) values from +30 mV (0 mM phosphate) to -30 mV (100 mM phosphate). The ZP of AH did not change substantially (positive ZP >20mV) when incubated with 100 mM HEPES, Tris, or histidine buffers at pH 7.2 (Figure 4.1A). Similar results were obtained with AH and 100 mM histidine at pH 6.5 or 6.8 (data not shown). At pH 7.2, the P[8] antigen (pI ~5.9) is negatively charged resulting in net attractive electrostatic forces for binding to AH (100% P[8] bound in histidine, Tris or HEPES buffer). At low phosphate buffer (0.5 mM), P[8] was 100% bound to AH (Figure 4.1B), but the levels of AH-bound P[8] decreased with increasing concentrations of phosphate buffer (e.g., ~40% of P[8] bound at 10 mM).

Langmuir binding isotherms were generated in six different formulations (see Table 4.1 for composition), at pH 7.2 or 6.8, to determine the adsorptive strength and capacity values of P[8]-AH interactions. As shown in Figure 4.2A and Table 4.1, the adsorptive strength values of P[8]-AH interactions were substantially lower in phosphate formulations (F1, F3) vs. non-phosphate containing formulations (F5, F6, F7, F8). The adsorptive capacity in each formulation, however, was still substantially higher than the targeted clinical doses (i.e., up to 60 µg of each NRRV antigen per 0.56 mg of aluminum).

The structural integrity of solution vs AH-bound P[8] was assessed by intrinsic Trp fluorescence spectroscopy and DSC. As shown in Figure 4.2B, the intrinsic Trp fluorescence emission spectra of P[8] at 10°C in F1 are overall similar, demonstrating overall similar

microenvironments for the average Trp residues of P[8] upon binding to AH (albeit a small red shift of $\sim 1 - 2$ nm in the lambda-max peak position for P[8] was noted bound to AH compared to solution, potentially indicating very subtle structural differences). Upon heating, solution vs. AH-bound P[8] showed similar thermal onset values, albeit the subsequent thermal transitions differed in terms of extent and direction of intensity changes, likely due to the P[8] protein aggregating in solution vs. on the AH surface (Sup. Figure S4.2-A2), across various formulations (no effect of buffer type or 0.025% PS-80). The conformational stability of solution vs. AH-bound P[8] showed similar thermal melting values (T_m) and apparent enthalpy ($\Delta H'$) of unfolding values by DSC (Figure 4.2C), although the T_{onset} value decreased by $\sim 1.5^\circ\text{C}$, the T_m value was $\sim 1^\circ\text{C}$ higher and the apparent enthalpy ($\Delta H'$) was $\sim 30\%$ higher in the bound state (Sup. Table S4.1), likely indicating subtle differences in aggregation of solution vs AH-bound P[8] during heating.

4.2.2 P[8] Antigen-Alhydrogel Adjuvant-Thimerosal Interactions

The ZP of AH in three formulation buffers (F1, F3, F5) after pretreatment with 0.002 – 0.05% (w/v) thimerosal did not change (values of +22 to + 28 mV) indicating no interaction of AH with thimerosal (data not shown). P[8] was 100% bound to AH in the presence of 0.01% thimerosal at the clinical concentration (i.e., 60 μg antigen and 560 μg adjuvant per 0.5 mL dose) in each of the three formulations. Langmuir binding isotherms showed no significant changes in the adsorptive or capacity values of AH-P[8] interactions due to thimerosal addition (Table 4.1). However, 0.01% w/v thimerosal dramatically reduced the conformational stability of the bound P[8] as measured by DSC where the T_{onset} and T_m values decreased $\sim 10^\circ\text{C}$ and apparent enthalpy decreased by $\sim 20\%$ (Figure 4.3A and Sup. Table S4.1 for formulation F1 and Figure 34.B for formulations F3, F5). Similar to DSC results, a reduction of $\sim 9^\circ\text{C}$ in T_m values and $\sim 12^\circ\text{C}$ in

T_{onset} values was observed by thimerosal addition for aluminum-adsorbed P[8] as measured by time-resolved fluorescence (Figure 4.3C and 4.3D).

4.2.3 Storage stability of monovalent P[8]-Alhydrogel drug product

The effect of thimerosal was evaluated during a 12-week stability study with monovalent P[8] antigen bound to AH at different storage temperatures (4°C, 25°C, 37°C) in different formulations (see Table 4.1 for composition). A schematic describing the vaccine preparation work-flow and physicochemical attributes evaluated is provided in Sup. Figure S4.1. Overall, ten formulations were tested for their effects on antigen-adjutant interactions as well as P[8] physicochemical stability and antigen binding capacity during storage. As described below, although clear destabilizing effects of thimerosal were observed, the different buffering agents (phosphate or histidine) or surfactant concentration (0.025% or 0.006% w/v polysorbate-80) had no notable effects on the stability of aluminum-adjutant bound P[8]. The results from all ten P[8] formulations are presented, nonetheless, to demonstrate the reproducibility of the destabilizing effects of temperature and thimerosal.

Inhibition ELISA was used to measure the ability of aluminum-bound P[8] to bind a specific antibody. Figure 4.4A shows representative data for P[8] antigen (formulation F1+thimerosal) after 12 weeks storage at different temperature. A clear shift in the OD450 curve is observed which is indicative of reduced antibody binding. During 4°C storage, no notable differences were observed between P[8] formulations and time points with good antibody binding observed (Figure 4.4B). At 25°C, the stability of P[8] formulated without thimerosal was similar to T0, . In contrast, a decreasing trend in antibody binding was observed in P[8] formulations containing thimerosal (Figure 4.4C). At 37°C, P[8] rapidly lost the ability to bind antibody in the

presence of thimerosal with a slower but notable decreasing trend in P[8] formulations without thimerosal (Figure 4.4D).

To better understand thimerosal-induced loss of ELISA activity, the structural integrity of the P[8] antigen on the surface of AH was monitored by time-resolved fluorescence and DSC. As shown in Figure 4.5A, a faster decay of Trp fluorescence was observed in P[8]-AH samples stored at higher temperatures in the presence of thimerosal. Mean spectral mass peak position of the waveform (i.e., lifetime moment) was calculated and monitored over time. During storage at 4°C, 25°C and 37°C (Figure 4.5B), Alhydrogel-bound P[8] undergoes structural alterations at elevated storage temperatures which is accelerated by thimerosal. Overall, good stability was observed at 4°C in all formulations. For DSC analysis of the same samples, the total area of the thermogram (i.e., the apparent enthalpy of unfolding, $\Delta H'$) reduced at T0 in the presence of thimerosal (Figure 4.5C), however, no further notable losses were recorded during storage at 4°C (Figure 4.5D). At 25°C and 37°C, P[8] formulations with thimerosal were much less stable with a decreasing trend in $\Delta H'$ values over time (Figure 4.5D). Overall, an excellent correlation was observed between P[8] stability trends comparing the ELISA antibody binding data with the biophysical measurements.

The interaction of P[8] antigen with the AH adjuvant over time was monitored by reduced SDS-PAGE with densitometry (Figure 4.5E). Desorption of the AH-bound P[8] was carried out by adding SDS-PAGE sample buffer (with 0.2M phosphate and dithiothreitol (DTT) added), heating the sample at 90°C for 10 minutes, and subjecting the supernatant to SDS-PAGE. Essentially complete P[8] desorption from AH (~80-100%) was achieved throughout 12 weeks of incubation at 4°C or 25°C in all formulations (Figure 4.5F and see Sup Figure S4.3 for gels). At 37°C, however, a decreasing trend in % desorption was observed in thimerosal containing

formulations over time (Figure 4.5F, dashed traces) indicating strong binding of P[8] to AH. To better understand this observation, non-reduced SDS-PAGE analysis coupled to peptide mapping was also performed and the formation of multimeric P[8] species during storage of the aluminum adsorbed antigen was observed (Figure 4.6A and 4.6B). Overall, multimer formation was temperature dependent and the rate/extent is increased in the presence of thimerosal (see Figure 4.6C and Sup. Figure S4.3 for all gels). The multimer species were not observed under reducing conditions indicating disulfide bond crosslinking between the P[8] monomers (see Sup. Figure S4.3), and this was confirmed peptide mapping analysis (described below).

Non reduced SDS-PAGE analysis coupled with in-gel chymotrypsin digestion and LC-MS peptide mapping identified two chemical changes in the AH-bound P[8] antigen during storage (non-native disulfide bond formation at Cys¹⁷² and deamidation at Asn⁷). First, the P[8] monomeric vs multimeric bands were analyzed (Figure 4.6B). At 37°C, 2 weeks, the chymotrypsin peptide chromatograms were overall similar to the chromatograms of non-stressed (control without thimerosal) except for peptides containing IAM-labeled Cys¹⁷² (observed in the unstressed control and the monomer band of the F1+TH P[8], but lacking in F1+TH P[8] multimer band). These results show the observed P[8] multimer band on non-reduced SDS-PAGE was formed through a disulfide bond between single Cys¹⁷² of two P[8] monomers. Second, the levels of other PTMs in the P[8] monomer bands were evaluated at Asn⁷ and Met⁹⁹ (Figure 4.6D and Sup. Figure S4.4). Although some degradation of Asn⁷ and Met⁹⁹ in P[8] occurred during SDS-PAGE and in-gel digestion analysis rather than during storage (data not shown), a stability trend for Asn⁷ deamidation was noted over 12 weeks of storage with highest levels in the samples stored at 37°C (~80%), intermediate in the 25°C samples (~60%), and lowest in 4°C samples (40-50%).

4.2.4 P[4] and P[6] Antigen-Alhydrogel-Thimerosal interactions

Due to limited availability, only three formulations (F1, F3, F5; see composition in Table 4.1) were selected to examine the stability of the monovalent Alhydrogel-bound P[4] and P[6] antigens. Similar to P[8]-AH interaction results, the strength of adsorption was significantly higher in histidine formulations for P[4] and P[6] antigens compared to the phosphate containing formulations (Table 4.1). The adsorptive capacity of AH was similar for P[4] in the three formulations, whereas, some differences were observed for P[6] antigen (Table 4.1). Similar to P[8] results, P[4] and P[6] antigens also showed overall similar tertiary structures in solution or bound to AH by intrinsic fluorescence spectroscopy (Figures 4.7A and 4.8A). From DSC analysis (Figures 4.7B and 4.8B, and Sup. Table S4.1), the T_m values of solution vs aluminum bound P[4] and P[6] were comparable, while T_{onset} values were $\sim 5^\circ\text{C}$ lower when bound to adjuvant. The addition of 0.01% thimerosal significantly reduced the conformational stability of P[4] and P[6] antigens.

During 12 weeks of storage (see Figures 4.7 and 4.8, and Sup Figures S4.5-S4.9), the stability of aluminum adsorbed monovalent P[4] and P[6] antigens were monitored by DSC, ELISA and SDS-PAGE coupled to LC-MS peptide mapping. Similar to P[8] results above, P[4] and P[6] showed good stability in the absence of thimerosal at 4°C up to 12 weeks as measured by conformational stability (Figures 4.7C and 4.8C), ELISA antibody binding (Figures 4.7E and 4.8E) and chemical stability (Figures 4.7G and 4.8G). In the presence of thimerosal, notable destabilization of the P[4] and P[6] antigens was observed overall, albeit with differences between antigens noted depending on the method, temperature and time-point (see Figures 4.7 and 4.8). For example with P[4]-AH samples, thimerosal and temperature induced loss of ELISA antibody binding showed an excellent correlation with loss of conformational stability data from DSC (Figure 4.7C-F, and Sup. Fig.S4.5A). In contrast, no apparent effect of thimerosal was observed

on P[6] antibody binding and the ELISA results did not correlate well with the DSC data. Polysorbate containing formulations showed better antibody recognition compared to no polysorbate formulations, see Figure 4.8C-F and Sup. Figure S4.5B). Finally, as observed with P[8] antigen, non-native disulfide linked multimeric species were observed for aluminum adsorbed P[4] and P[6] antigens (see Sup. Figures S4.6 and S4.7 gels), and the abundance of monomer species decreased as a function of storage temperature as shown in Figures 4.7G, 4.8G and Sup. Figure S4.8. Overall, the P[6] antigen was most prone to this degradation pathway. Finally, increased levels of Asn⁷ deamidation in aluminum-adsorbed P[4] and P[6], and Asn⁹⁰ deamidation in P[6], were recorded under accelerated storage temperatures (Figures 4.7H, 4.8H and Sup. Figures S4.8, S4.9).

4.2.5 Comparison of Thimerosal vs. 2-Phenoxyethanol on P[8]-AH storage stability

Since thimerosal showed a detrimental effect on the storage stability of the three AH-bound monovalent NRRV antigens, the compatibility of another commonly used vaccine (preservative 2-Phenoxyethanol (2-PE)) was examined with AH-bound P[8]. During storage at 4°C (Figure 4.9A and 4.9C), no notable changes were observed in P[8] stability as measured by conformational stability (DSC) or antibody binding (by ELISA), except P[8]-AH-thimerosal sample at 12 weeks which displayed some conformational instability by DSC. During storage at 37°C, a notable instability trend was observed for each of the P[8]-AH formulations, and the rate of degradation was fastest in the presence of thimerosal, followed by addition of 2-PE and then the no preservative control formulation (Figure 4.9B and 4.9D). The DSC and ELISA results showed good agreement consistent with structural destabilization of AH-bound P[8] correlating with loss of antibody binding to the P[8] antigen.

4.3 Discussion

In this work, the compatibility and stability of three recombinant fusion protein antigens (NRRV antigens P[4], P[6], P[8]; see introduction) were assessed with two key components of a multi-dose subunit vaccine formulation, an aluminum adjuvant (Alhydrogel, AH) and two antimicrobial agents (thimerosal and 2-phenoxyethanol). The effect of formulation excipients/buffers on antigen-adjuvant interactions, antigen-preservative interactions and storage stability of AH-bound NRRV antigens were also examined. The aim was to determine the feasibility of developing a multi-dose formulation of the NRRV vaccine candidate, and it was demonstrated that there are significant formulation and stability challenges for the NRRV antigens formulated with commonly used vaccine preservatives.

NRRV antigen-aluminum adjuvant (Alhydrogel) interactions

Adjuvants enhance vaccine immunogenicity and effectiveness by boosting components of the immune response (i.e., cellular and/or humoral) against the pathogen. Adjuvants can also facilitate dose sparing and reduce the number of shots⁸⁸. Aluminum based adjuvants have been widely used in human vaccines for over 90 years and have a long record of safety and immunopotential⁸⁹. Antigen co-precipitation with formation of aluminum salts has been replaced with antigen adsorption to preformed aluminum adjuvant⁷⁵, and Alhydrogel® (aluminum oxyhydroxide, AH) and Adju-Phos® (aluminum phosphate, AP) are the two most commonly used aluminum adjuvants¹⁹². NRRV antigens have isoelectric point of ~6.0 and AH has point of zero charge (PZC) ~11.4. Thus, at physiological pH, AH is positively charged and the NRRV antigens are negatively charged. The interaction between P[8] antigen and AH was shown to be mediated by noncovalent electrostatic attractions as the amount bound decreased upon pretreatment of AH with phosphate (which altered the net surface charge of AH from positive to negative; Figure 4.1A). The current clinical NRRV vaccine formulation contains 0.5 mM phosphate ensuring

antigen binding to AH^{46,47}. Since 0.5 mM phosphate provides only a low buffering capacity, we evaluated other buffering agents (histidine, HEPES, Tris) at higher concentration (10 mM) and demonstrated 100% antigen binding (Figure 1B). Lower binding strength was also observed for each NRRV antigen in phosphate buffer compared to histidine buffer (Table 4.1).

The binding of antigen to aluminum adjuvant has historically been considered important for generating immune responses, although that has more recently been shown to be antigen specific. Studies with poxvirus L1-protein antigen in our laboratories demonstrated AH binding is important for immunopotentiality¹⁹³, and others have reported similar observations with pneumococcal protein antigens¹⁹⁴. The WHO recommends greater than 80% of the diphtheria and tetanus toxoids to be adsorbed to aluminum adjuvants. Since many vaccine antigens require low microgram doses, unbound antigens can adsorb to various interfaces during fill-finish manufacturing⁷⁵, so aluminum adjuvant binding can circumvent this and thus help reduce the cost of vaccine manufacturing. On the other hand, Hem *et al.* have shown that antigens formulated as unbound to aluminum adjuvant can elicit equal or better immune response compared to adjuvant-bound antigens¹⁹⁵⁻¹⁹⁷. Hem and colleagues have shown that several model proteins that bind AH due to electrostatic attractions elute readily upon contact with interstitial fluid¹⁹⁸, a potentially better parameter to predict immune responses¹⁹⁹. Finally, the strength of antigen adsorption to AH is another important parameter for immune responses. For example, inverse relationships have been reported for Hepatitis B surface antigen^{200,201}, HIV gp140 antigen²⁰², and anthrax recombinant protective antigen²⁰³. Using a model protein, alpha casein, it has been shown that tighter aluminum adjuvant binding can diminish both T cell and B cell activation, by impairing antigen processing in dendritic cells and reducing antigen availability for B cell recognition, respectively²⁰⁴. It will be of interest as part of future work to better characterize the effect of extent

and strength of adsorption of NRRV antigens to AH in terms of immune response in animal models.

Analytical challenges to evaluate NRRV antigen stability bound to Alhydrogel

Historically, animal based immunogenicity tests have been used to assess the potency and stability of aluminum-adsorbed, inactivated/recombinant based vaccines^{58,78}. There is great interest in replacing these *in vivo* assays with surrogate *in vitro* assays to monitor antigenicity and stability of vaccines. ELISA is a commonly used *in-vitro* immunochemical method to measure either the concentration, antigenicity or conformational integrity of protein antigens, depending on the nature of the antibody used (e.g., neutralizing vs. non-neutralizing, linear vs. conformational epitopes, etc.). In this work, a competitive ELISA format was employed to measure the antibody binding ability of the aluminum adsorbed NRRV antigens (each of the three antibodies are antigen-specific but likely non-neutralizing in nature; data not shown). The correlation of ELISA antibody binding results with NRRV antigen structural integrity is discussed below.

The use of physicochemical methods to monitor the structural integrity and stability of protein antigens in bound state to aluminum adjuvant is challenging due to low antigen doses, irreversibility of adsorption, and the turbid nature of the formulations. Examples of decreased^{205,206}, no effect^{207,208} or even enhanced structural stability^{209,210} of various model proteins and recombinant vaccine antigens upon adsorption to aluminum adjuvant have been reported. We have previously reported the development of a wide variety of analytical tools to monitor key structural attributes of the three NRRV antigens in solution and applied these methods to identify key degradation pathways^{160,211}. This work established that only a subset of these analytical methods could be applied to NRRV antigens bound to Alhydrogel (AH), and only a subset of possible degradation pathways are observed in the bound state. The chemical stability of AH-bound NRRV

antigens was monitored by SDS-PAGE coupled with LC-MS peptide mapping. We noted that formation of non-native, intermolecular disulfide bond at Cys (at position 173 – P[4], P[6] and 172 – P[8]) and deamidation of Asn⁷ are the two major chemical alterations for the NRRV antigens when bound to AH. The degree of Asn deamidation in protein antigens could potentially be enhanced on the surface of AH due to higher pH of the microenvironment²¹²⁻²¹⁴ including Asn deamidation induced loss of potency with a recombinant protective antigen vaccine. Estey *et al.* have reported for three recombinant botulinum protein antigens elevated levels of oxidation and deamidation in the adjuvant bound vs. solution state²¹⁵.

The higher-order structure (HOS) of the three NRRV antigens bound to Alhydrogel was evaluated by a combination of fluorescence spectroscopy and DSC. Although NRRV antigens unfold and aggregate upon heating in solution, when adsorbed to the surface of Alhydrogel, the NRRV antigens undergo structural alterations but do not aggregate (due to spatial distances between the surface-bound protein molecules and inability to colloiddally associate). Interestingly, this resulted in the apparent enthalpy of unfolding values for the NRRV antigens being higher on AH with a broader transition as well as a loss in the apparent enthalpy of unfolding (reduced area of thermograms) during storage (see below). The AH- bound P[6] was most unstable of the three NRRV antigens, and this result aligns with the previous in solution characterization work with the three NRRV antigens¹⁶⁰. The addition of thimerosal showed a clear destabilizing effect (8–14°C) on the conformational stability of each NRRV antigen as measured by DSC and fluorescence spectroscopy. To better understand the effect of preservatives on the stability of aluminum adsorbed NRRV antigens, a stability study was setup as described below.

Formulation and stability challenges with NRRV antigens in the presence of preservatives

These studies are a first step in the longer-term goal of NRRV vaccine development to combine it with pentavalent childhood combination vaccines (e.g., diphtheria, tetanus, and pertussis, Hep B, Hib) to enhance RV vaccine coverage and further lower costs. The most commonly used pediatric combination vaccine in the developing world contains both whole cell pertussis (wcp) and thimerosal, used both as a preservative and inactivating agent during wcp production¹⁹⁰. A 12-week accelerated, and real-time stability study was performed with each monovalent NRRV antigen bound to AH as evaluated by ELISA and physicochemical assays (see above). Overall, no notable effect of buffer type or surfactant concentration was observed on NRRV antigen stability while thimerosal (and 2-phenoxy ethanol) demonstrated a temperature dependent detrimental effects on the stability of each aluminum adsorbed NRRV antigen.

One measure of the prominent destabilizing effect of thimerosal on the conformational stability of AH adsorbed NRRV antigens was measured by DSC with a dramatic reduction in $\Delta H'$ of unfolding values during storage at elevated temperatures. This result implies some population of the AH bound protein remains in native state, while others lose structural integrity thus forming conformationally heterogeneous populations over time. Similar loss in DSC signal or $\Delta H'$ of unfolding have been reported for recombinant botulinum neurotoxin adsorbed to AH after storage at 30°C for 9 weeks²¹⁶. Further, protein structural changes on the surface of aluminum could lead to stronger adsorption over time, which in fact was observed for the thimerosal containing P[8]-AH samples stored at 37°C for 12 weeks. For AH-bound P[8] and P[4] antigens, an overall good correlation was observed between the ELISA antibody binding and DSC results, suggesting the conformational nature of the antibody binding epitopes. In the case of aluminum-adsorbed P[6] antigen, such a correlation is less convincing and additional work is in progress to better understand

the conformational vs linear nature of this antibody binding epitope (McAdams *et al.*, manuscript in preparation).

Chemical stability assessment by SDS-PAGE and LC-MS peptide mapping analyses revealed the susceptibility of each AH-bound NRRV antigen to non-native intermolecular disulfide formation via a single Cys residue. The extent/rate of this degradation was temperature dependent ($37^{\circ}\text{C} > 25^{\circ}\text{C} > 4^{\circ}\text{C}$) and P[6] was most susceptible. Addition of thimerosal clearly exacerbated disulfide formation for the P[8] antigen, whereas, for P[4] and P[6], disulfide formation was unaffected or perhaps somewhat prevented by addition of thimerosal. Thimerosal is an organometallic compound which degrades in aqueous solution into thiosalicylic acid and ethyl mercury²¹⁷. Ethyl mercury can bind to free Cys in proteins which leads to ethyl mercury adduct formation^{218,219}. Ethyl mercury adducts were observed for NRRV antigens in the presence of thimerosal by preliminary intact mass analysis (data not shown). We hypothesize that the interaction between free Cys and ethyl mercury leads to structural/conformational perturbation of the surrounding domains in the protein which ultimately leads to protein structural alterations. Also, the degree of adduct formation could depend on the accessibility of the free Cys with each NRRV antigen's three-dimensional structure, which in turn could increase at elevated storage temperatures due to increase protein dynamics. In contrast, no effect of thimerosal was seen on the extent of Asn⁷ deamidation in each antigen which could be due to the spatial distance of this residue from the thimerosal affected Cys containing domain of the protein. As expected, the extent of Asn deamidation increased at higher storage temperatures in each antigen.

Finally, we also tested the compatibility of a second commonly used vaccine preservative 2-PE with the P[8] antigen and unfortunately we observed similar destabilizing trends as seen with thimerosal as measured by ELISA and DSC. This result implies the inactivation of NRRV antigens

by preservatives is more complex mechanistically than direct interaction with the free Cys residue of the NRRV antigen (since 2-PE lacks the sulfhydryl chemistry described above for thimerosal). Ongoing work in our laboratories is focused on elucidating the molecular mechanism of thimerosal induced destabilization of the NRRV antigens, evaluating other preservatives, and reengineering the NRRV antigens through point mutations to produce NRRV antigens that are more compatible with preservatives. The goal is to facilitate development of multi-dose formulations of NRRV vaccine, ideally as part of currently available pediatric combination vaccines, to produce a lower cost RV vaccine with wider vaccine coverage for use in the developing world.

4.4 Tables

Table 4.1. Summary of NRRV antigen (P[8], P[6], and P[4]) and aluminum adjuvant (Alhydrogel, AH) binding parameters in different formulations. Data were fitted to linear form of Langmuir adsorption equation as described in Methods. See Figure 4.2A for representative binding isotherms with P[8]. Values represent Mean \pm Range from two measurements. Second part of the table describes the composition of the different formulations (F1-F8) described in this work.

	Formulation	Adsorptive Strength (mL/mg)	Adsorptive Capacity (μg/mg)	R²
P[8]	F1	13 \pm 5	1000 \pm 0	0.97
	F3	14 \pm 4	774 \pm 119	0.98
	F5	112 \pm 77	718 \pm 103	0.99
	F6	338 \pm 96	572 \pm 33	0.99
	F7	105 \pm 89	607 \pm 37	0.99
	F8	87 \pm 87	750 \pm 167	0.99
	F1 + TH	10 \pm 2	839 \pm 140	0.97
	F3 + TH	54 \pm 23	670 \pm 89	0.95
	F5 + TH	81 \pm 67	611 \pm 111	0.96
P[6]	F1	7 \pm 5	940 \pm 342	0.97
	F3	10 \pm 2	646 \pm 42	0.90
	F5	66 \pm 55	917 \pm 167	0.97
P[4]	F1	11 \pm 7	749 \pm 321	0.94
	F3	10 \pm 0	742 \pm 55	0.92
	F5	346 \pm 120	750 \pm 167	0.99
Formulation Composition				
Formulation #	Buffer	Salt (NaCl)	PS-80 (w/v)	pH
F1	0.5 mM Sodium Phosphate	0.15 M	--	7.2
F2	0.5 mM Sodium Phosphate	0.15 M	0.006%	7.2
F3	0.5 mM Sodium Phosphate	0.15 M	0.025%	7.2
F4	5 mM Histidine	0.15 M	0.006%	6.8
F5	5 mM Histidine	0.15 M	0.025%	6.8
F6	5 mM Histidine	0.15 M	0.025%	7.2
F7	5 mM HEPES	0.15 M	0.025%	7.2
F8	5 mM Tris	0.15 M	0.025%	7.2

TH – 0.01% Thimerosal

4.5 Figures

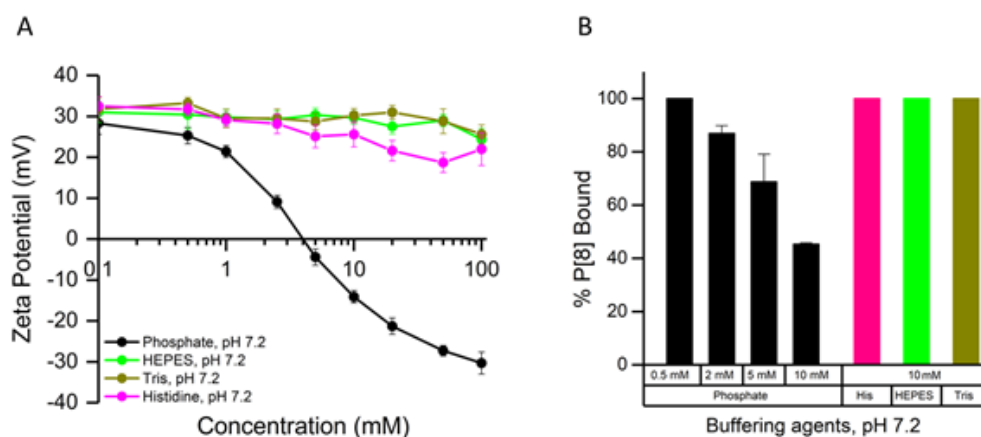


Figure 4.1. Surface charge and percent P[8] antigen binding to Alhydrogel (AH) in different buffers. (A) Zeta potential of AH at pH 7.2 after pretreatment with increasing concentrations of different buffering agents. (B) Percent P[8] bound to AH at pH 7.2 in different buffering agents (60 μ g P[8] antigen added to 0.56 mg of aluminum as AH in the presence of 0.15 M NaCl at pH 7.2). Error bars represent the range from duplicate measurements.

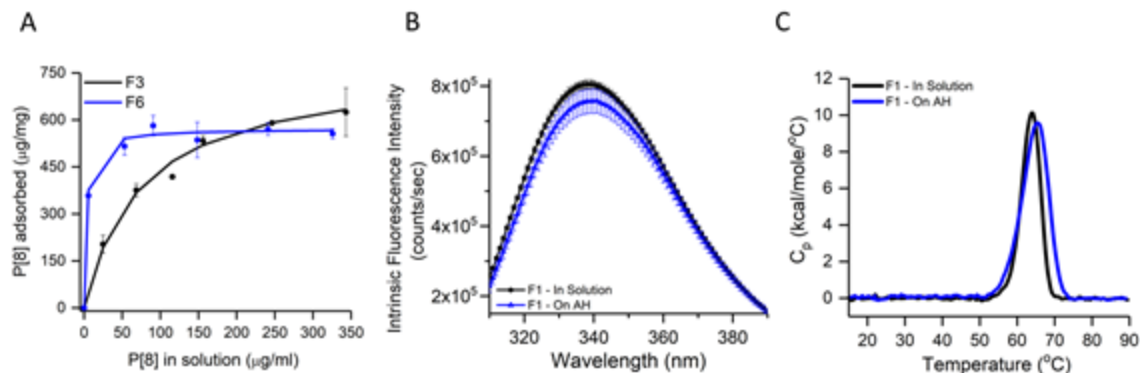


Figure 4.2. P[8] antigen interactions with the aluminum adjuvant Alhydrogel (AH) in different formulations. (A) Langmuir binding isotherms of P[8] antigen with AH in formulations F3 and F6. (B) Tertiary structure integrity analysis using intrinsic tryptophan fluorescence emission spectra at 10°C in solution (black) and bound to AH (blue) in F1 (see Sup. Figure S4.2 for data in F3 and F5 formulations). (C) Conformational stability analysis with representative DSC thermograms of P[8] in solution (black) and bound to AH (blue) in formulation F1 (see Sup. Table S4.1 for T_{onset} , T_m and $\Delta H'$ values). See Table 4.1 for composition of the different formulations. Error bars represent 1SD from triplicate measurements.

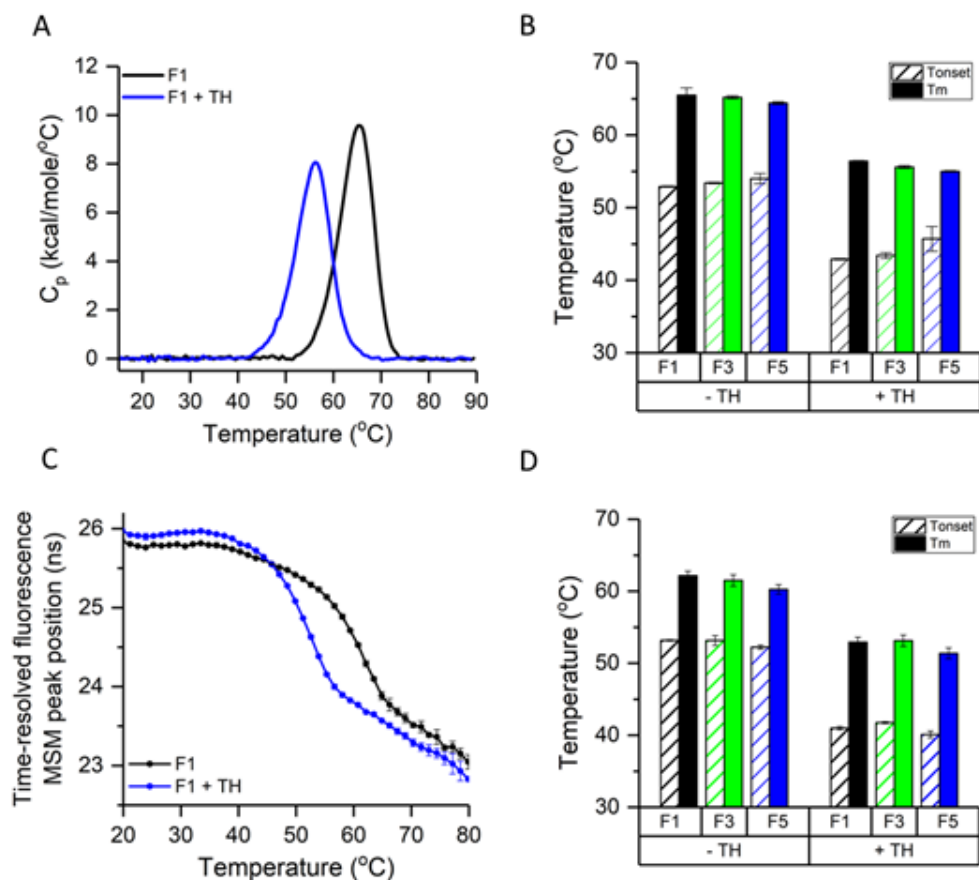


Figure 4.3. Effect of thimerosal on the conformational stability of Alhydrogel-bound P[8] antigen. (A) Representative DSC thermograms for P[8]-AH samples in formulation F1 with (blue) and without (black) thimerosal. (C) Time-resolved intrinsic fluorescence spectroscopy vs. temperature of P[8]-AH samples in formulation F1 with (blue) and without (black) thimerosal. Thermal onset (T_{onset}) and melting (T_m) temperatures of (B) conformational stability (DSC) and (D) tertiary structure (intrinsic fluorescence) in formulations F1, F3 and F5. Error bars represent 1 SD from triplicate measurements. See Table 4.1 for composition of the different formulations.

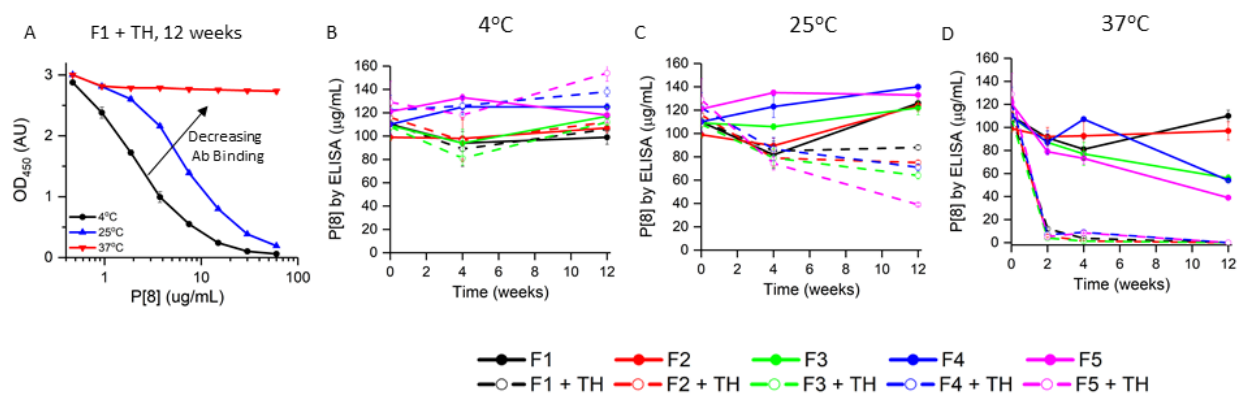


Figure 4.4. ELISA antibody binding for AH-bound P[8] antigen during storage stability studies at different temperatures in ten different formulations. (A) Schematic description of the inhibition ELISA assay. (B) Representative OD₄₅₀ inhibition ELISA curves for P[8]-AH samples in F1+TH formulation after 12 weeks at different storage temperatures, (C-D) Aluminum adsorbed P[8] binding to antibody as determined from the inhibition ELISA assay over 12 weeks of storage. Error bars represent 1 SD from triplicate vials. See Table 4.1 for composition of the different formulations. TH – 0.01% thimerosal.

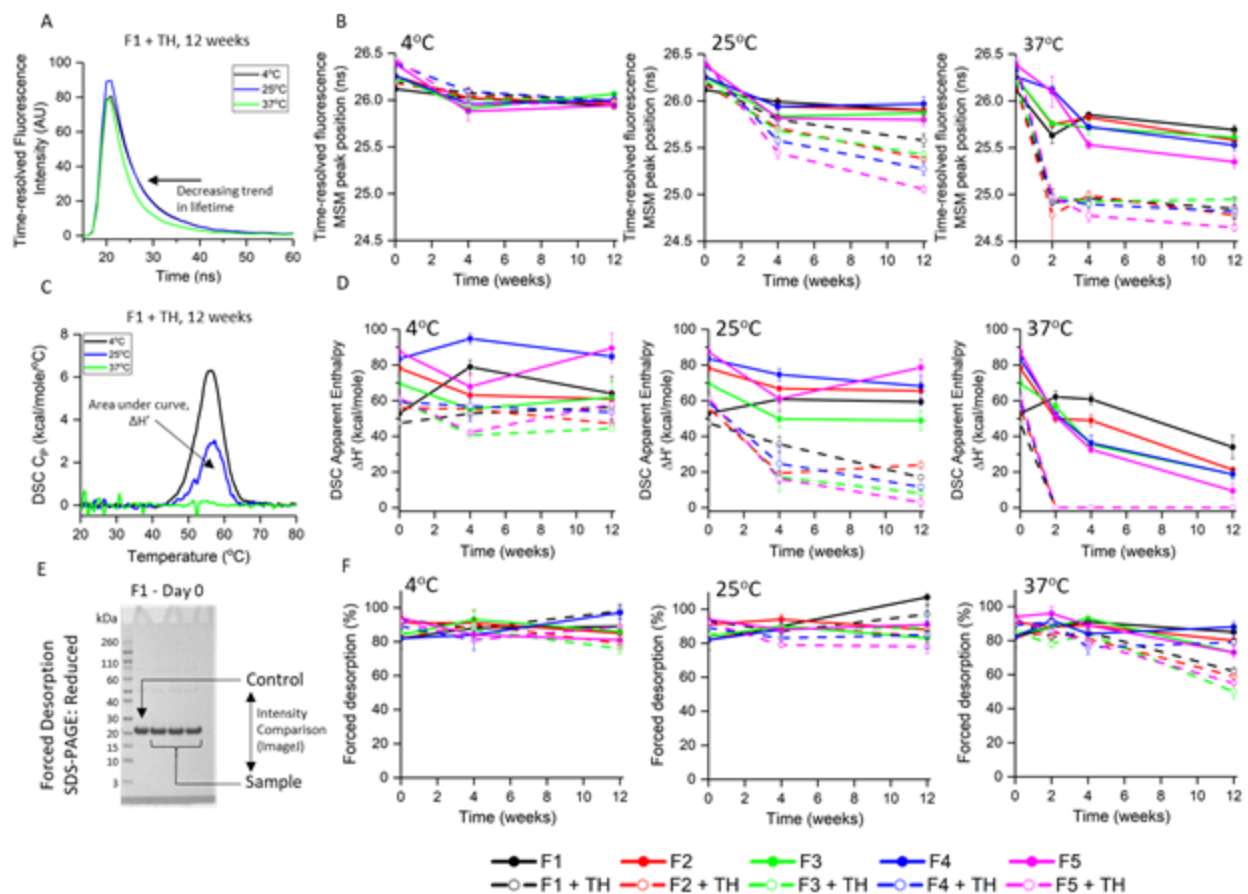


Figure 4.5. Physical stability profiles of AH-bound P[8] antigen during storage stability studies at different temperatures in ten different formulations. Overall tertiary structure stability of P[8]-AH as measured by time-resolved fluorescence spectroscopy: (A) Representative fluorescence decay waveform data for P[8]-AH samples in formulation F1+TH after 12 weeks, (B) fluorescence lifetime MSM peak position or moment values for P[8]-AH samples stored in different formulations and at different temperatures. Conformational stability of P[8]-AH as measured by DSC: (C) Representative DSC thermograms for P[8]-AH sample in formulation F1+TH, (D) apparent enthalpy of unfolding ($\Delta H'$) values (or area under thermograms) over 12 weeks of storage. Ability to desorb P[8] from AH as measured by SDS-PAGE: (E) Representative SDS-PAGE gel under reducing condition for P[8]-AH sample in formulation F1 at time zero, % desorption was calculated by comparing the intensity of desorbed P[8] band to control band by densitometry analysis, (F) % P[8] desorbed under forced desorption conditions. Error bars represent 1 SD from triplicate vials. See Table 4.1 for composition of the different formulations. TH – 0.01% w/v thimerosal.

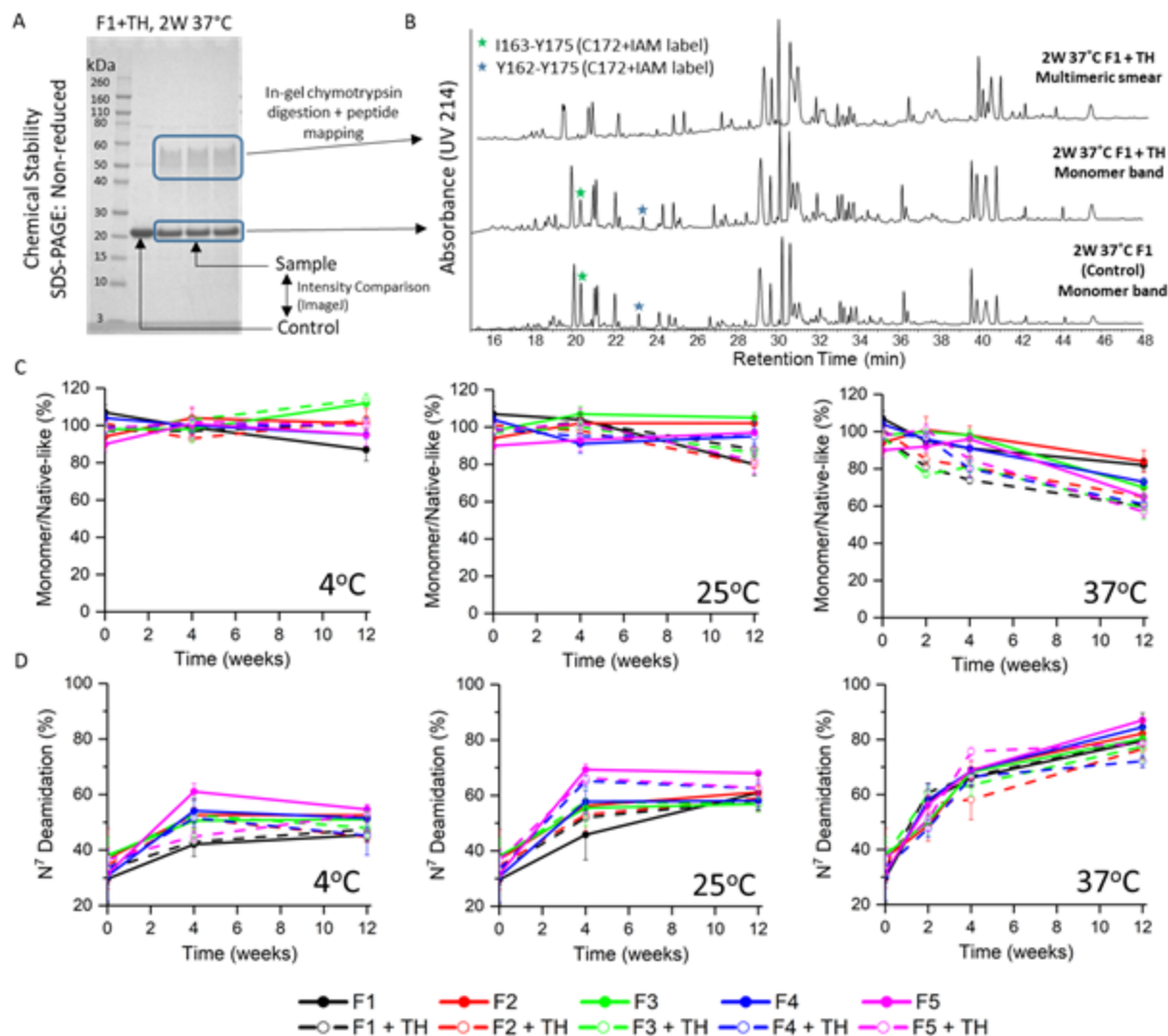


Figure 4.6. Non-native disulfide formation at Cys172 and deamidation at Asn7 of the AH-bound P[8] antigen during 12 weeks of storage at different temperatures in ten different formulations. (A) Representative SDS-PAGE gel under non-reducing condition for P[8]-AH sample in formulation F1+TH after storage for 2 weeks at 37°C, % monomer/native-like was calculated by comparing the intensity of desorbed P[8] monomer band to control band by densitometry analysis. (B) Representative peptide mapping chromatogram comparison of chymotrypsin-digested P[8] monomer and multimer bands from non-reduced SDS-PAGE gels for for P[8]-AH sample in formulations F1 (control) and F1+TH, 2 week 37°C sample. The green and blue stars indicate UV₂₁₄ peaks composed of two peptides containing IAM-labeled Cys¹⁷². (C) Percent monomer/native-like species from non-reduced SDS-PAGE analysis, and (D) relative deamidation of Asn⁷ over 12 weeks of storage. See Table 4.1 for composition of the different formulations. Error bars represent 1 SD from triplicate vials. TH – 0.01% w/v thimerosal.

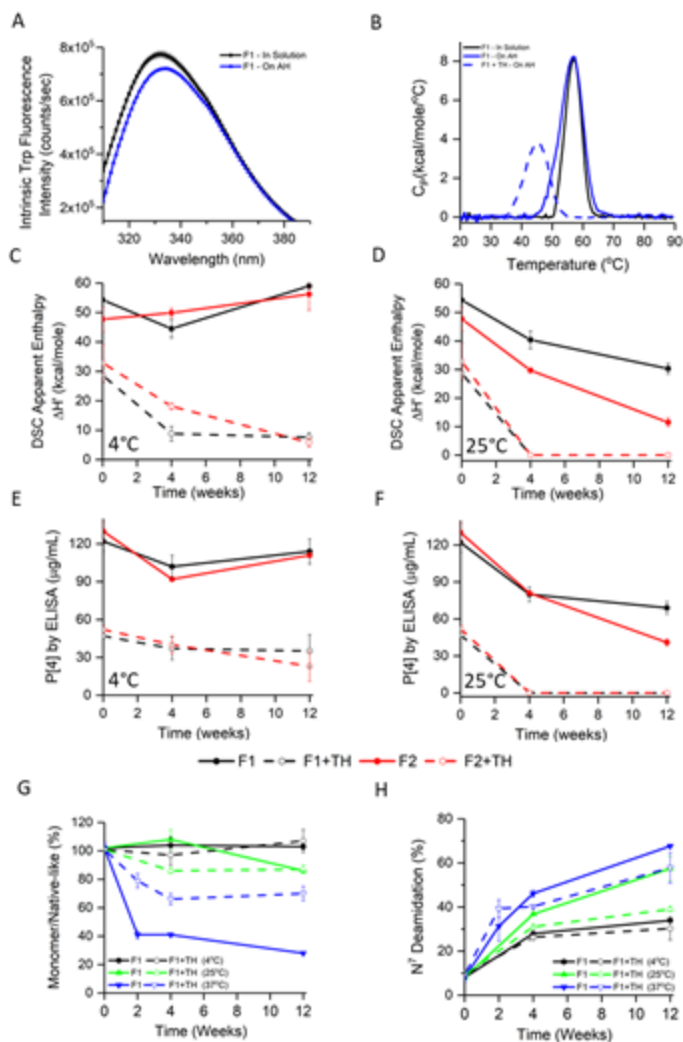


Figure 4.7. Effect of adjuvant (Alhydrogel, AH) and preservative (thimerosal) on physicochemical stability of P[4] antigen. (A) Tertiary structure integrity analysis using intrinsic tryptophan fluorescence emission spectra at 10°C in solution (black) and on AH (blue) in formulation F1 (see Sup. Figure S4.2C for data in formulations F3 and F5). (B) Conformational stability analysis with representative DSC thermograms of P[4] in solution (black) and bound to AH (blue) in F1 (see Sup. Table S4.1 for T_{onset} , T_m and $\Delta H'$ values). Apparent enthalpy of unfolding ($\Delta H'$) values of P[4]-AH from DSC at (C) 4°C and (D) 25°C storage temperatures over 12 weeks (see Sup. Figure S4.5-A1 for 37°C data). Aluminum adsorbed P[4] binding to antibody as determined from the inhibition ELISA assay over 12 weeks of storage at (E) 4°C and (F) 25°C (see Sup. Figure S4.5-A2 for 37°C data). (G) Percent monomer/native-like P[4] species from non-reduced SDS-PAGE analysis (see Sup. Figure S4.6 for gels), and (H) relative deamidation of Asn⁷ from peptide mapping analysis, over 12 weeks of storage at different temperatures in F1 and F1+TH (see Sup. Figure S4.8A for data in formulations F2 and F2+TH). Error bars represent 1 SD from triplicate vials. See Table 4.1 for composition of the different formulations. TH – 0.01% w/v thimerosal.

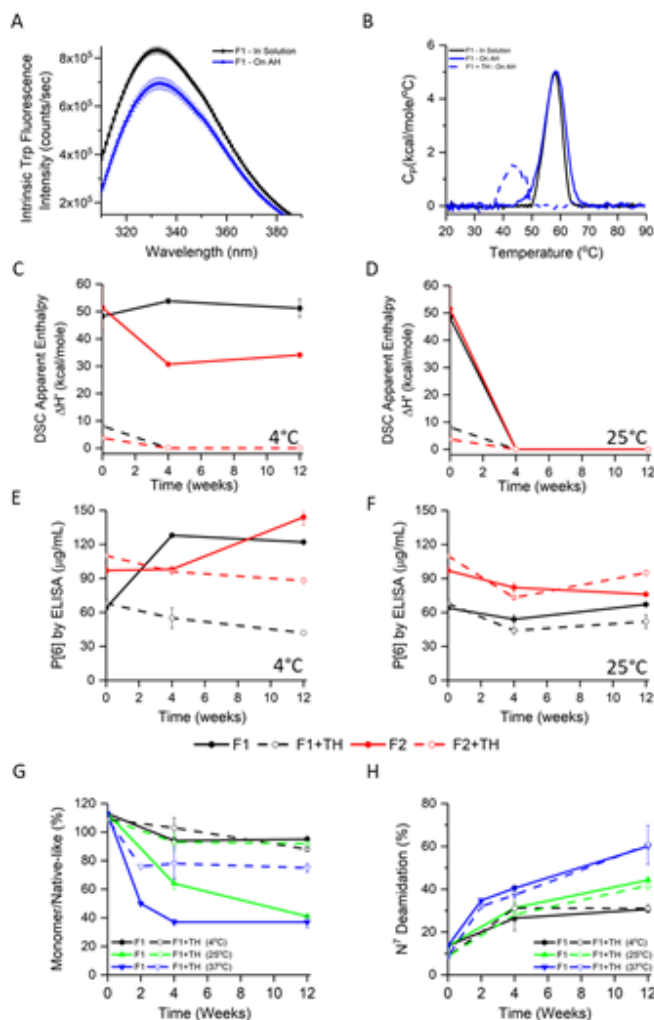


Figure 4.8. Effect of adjuvant (Alhydrogel, AH) and preservative (thimerosal) on physicochemical stability of P[6] antigen. (A) Tertiary structure integrity analysis using intrinsic tryptophan fluorescence emission spectra at 10°C in solution (black) and on AH (blue) in formulation F1 (see Sup. Figure S4.2B for data in formulations F3 and F5). (B) Conformational stability analysis with representative DSC thermograms of P[6] in solution (black) and bound to AH (blue) in F1 (see Sup. Table S4.1 for T_{onset} , T_m and $\Delta H'$ values). Apparent enthalpy of unfolding ($\Delta H'$) values of P[6]-AH from DSC at (C) 4°C and (D) 25°C storage temperatures over 12 weeks (see Sup. Figure S4.5-B1 for 37°C data). Aluminum adsorbed P[6] binding to antibody as determined from the inhibition ELISA assay over 12 weeks of storage at (E) 4°C and (F) 25°C (see Sup. Figure S4.5-B2 for 37°C data). (G) Percent monomer/native-like P[6] species from non-reduced SDS-PAGE analysis (see Sup. Figure S4.7 for gels), and (H) relative deamidation of Asn⁷ from peptide mapping analysis, over 12 weeks of storage at different temperatures in F1 and F1+TH (see Sup. Figure S4.8B for data in formulations F2 and F2+TH, and see Sup. Figure S4.9 for data showing deamidation of Asn⁹⁰). See Table 4.1 for composition of the different formulations. TH – 0.01% w/v thimerosal.

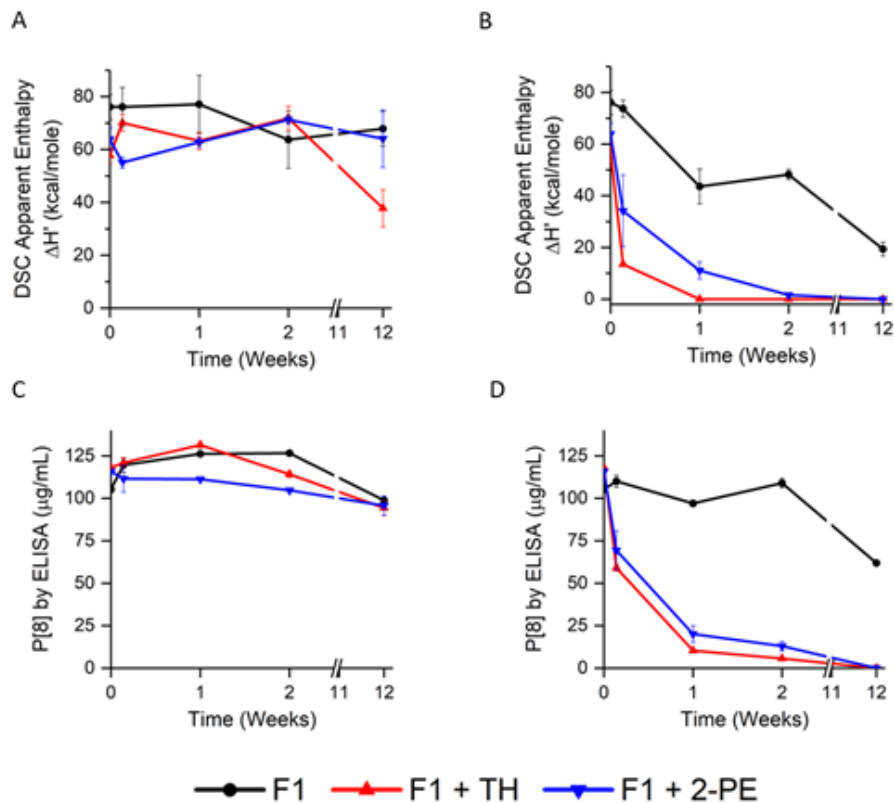


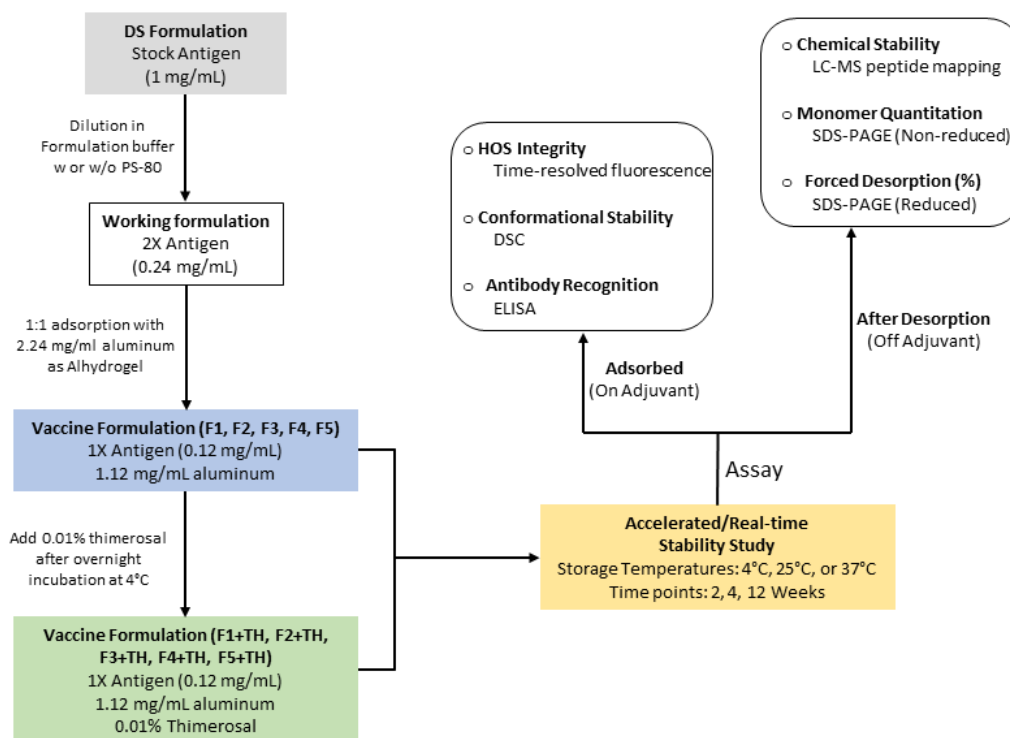
Figure 4.9. Destabilizing effect of in-use concentrations of thimerosal (0.01% w/v) vs. 2-phenoxyethanol (1.0 %) on conformational stability and antibody binding ability of AH-bound P[8] antigen. Stability study was over 12 weeks of storage at different temperatures in formulation F1. Apparent enthalpy of unfolding (ΔH°) from DSC at (A) 4°C and (B) 37°C storage temperatures. Aluminum adsorbed P[8] binding to antibody as determined from the inhibition ELISA assay over 12 weeks of storage at (C) 4°C and (D) 37°C. Error bars represent 1 SD from triplicate vials. See Table 4.1 for composition of F1. TH – 0.01% w/v thimerosal, 2-PE-1.05 2-phenoxyethanol.

4.6 Supplementary Tables

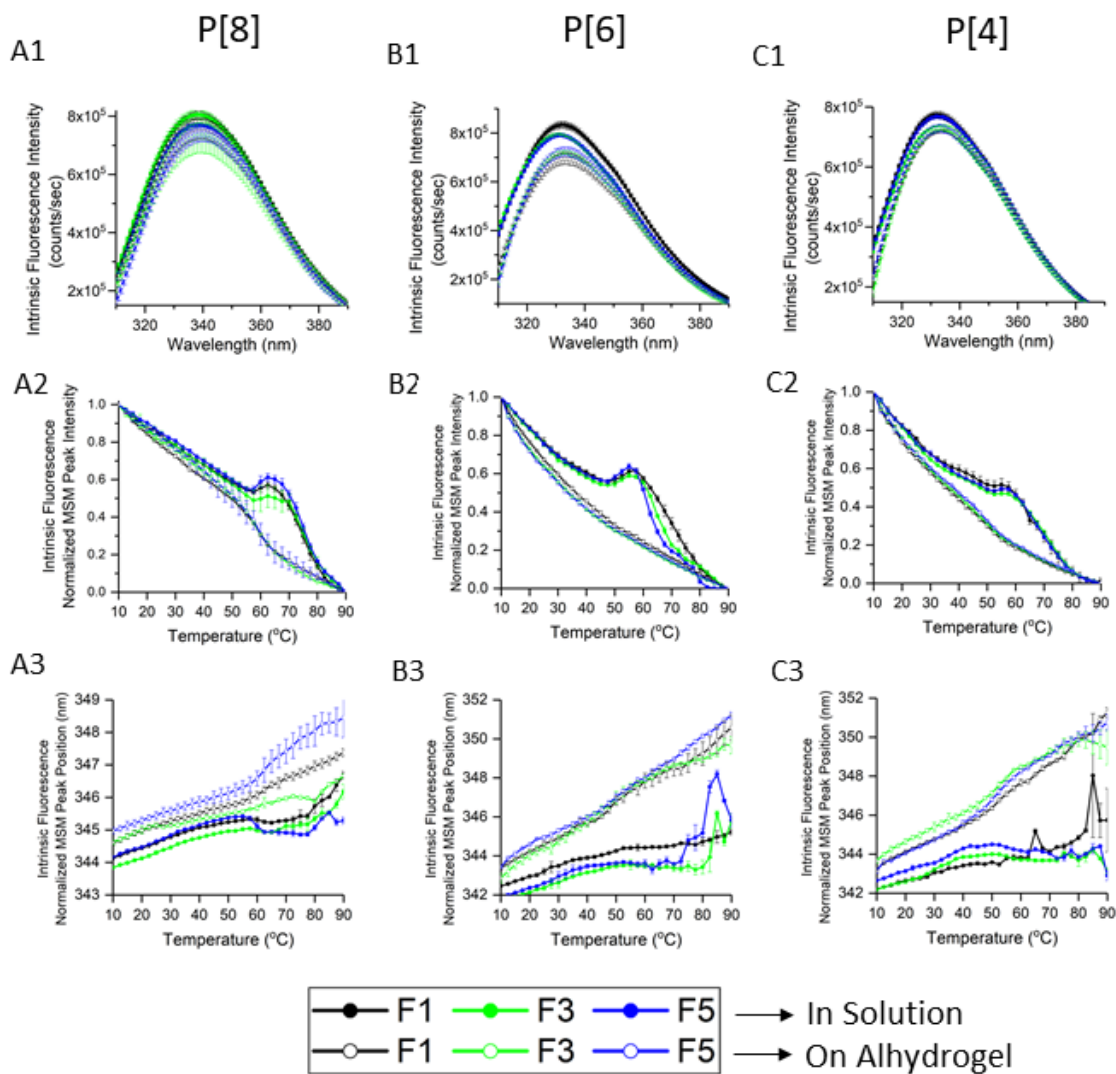
Supplementary Table S4.1. Summary of onset temperature (T_{onset}), melting temperature (T_m) and apparent enthalpy of unfolding ($\Delta H'$) from conformational stability analysis by DSC for the three NRRV antigens in solution and when bound to Alhydrogel adjuvant (AH) in the presence and absence of 0.01% w/v thimerosal. Data shown is for F1 formulation, 0.5 mM Sodium Phosphate 0.15 M NaCl, pH 7.2. Error bars represent 1 SD from triplicate measurements.

		In Solution		On Adjuvant	
		No Preservative	0.01% Thimerosal	No Preservative	0.01% Thimerosal
T_{onset} (°C)	P[4]	49.8 ± 0.3	39.2 ± 1.1	44.6 ± 1.1	35.8 ± 1.1
	P[6]	49.9 ± 0.1	38.3 ± 0.3	45.4 ± 0.8	36.8 ± 0.1
	P[8]	54.2 ± 0.4	46.5 ± 0.1	52.9 ± 0.1	42.9 ± 0.1
T_m (°C)	P[4]	57.0 ± 0.0	47.8 ± 0.1	56.9 ± 0.1	45.1 ± 0.1
	P[6]	57.9 ± 0.1	47.7 ± 0.0	58.3 ± 0.3	43.9 ± 0.2
	P[8]	63.9 ± 0.1	56.2 ± 0.1	65.5 ± 0.1	56.4 ± 0.1
$\Delta H'$ (kcal/mole)	P[4]	51.5 ± 0.6	33.8 ± 1.7	75.0 ± 1.3	29.6 ± 9.4
	P[6]	36.6 ± 2.2	18.9 ± 0.6	45.5 ± 6.9	10.4 ± 0.8
	P[8]	66.4 ± 0.4	51.7 ± 3.5	86.0 ± 0.6	71.0 ± 5.5

4.7 Supplementary Figures

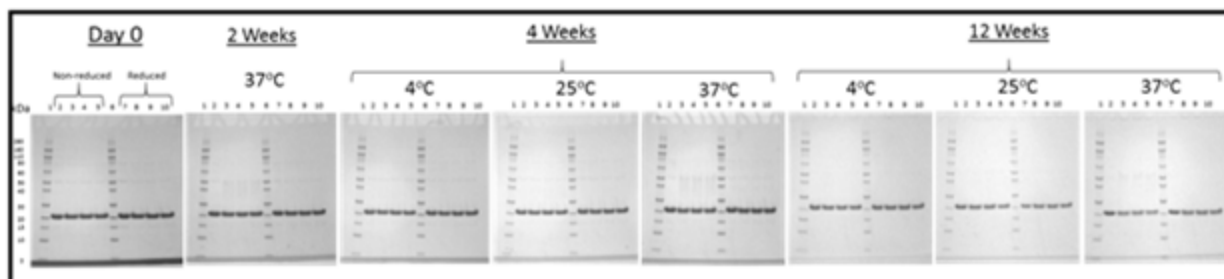


Supplementary Figure S4.1. Schematic description of the vaccine sample preparation work-flow in ten formulations with and without 0.01% w/v thimerosal for 12-week storage stability study. Different analytical methods used for structural integrity and physicochemical stability assessment with either antigen bound to aluminum adjuvant or after forced desorption. Refer to Table 4.1 in the main text for the composition of each formulation.

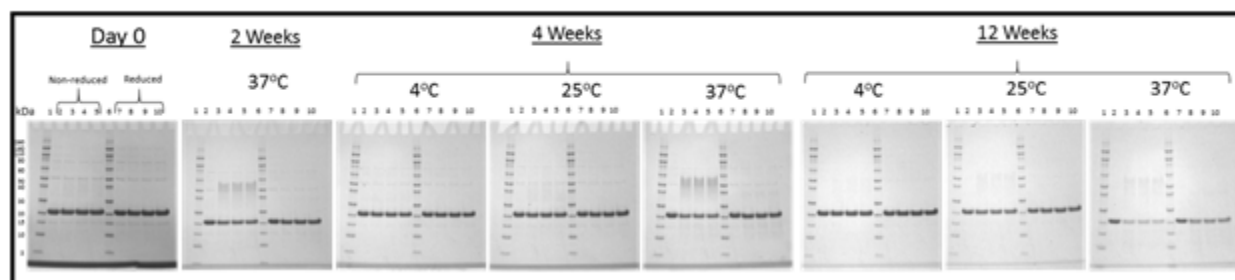


Supplementary Figure S4.2. Tertiary structure integrity and stability analyses of NRRV antigens bound to aluminum adjuvant Alhydrogel, AH (○) compared to in solution controls (●) in three different formulations. Intrinsic Trp fluorescence (A1, B1, C1) emission spectra at 10°C, and (A2, B2, C2) MSM peak intensity, and (A2, B2, C2) MSM peak position vs. temperature for the three antigens. Error bars represent 1 SD from triplicate measurements. Refer to Table 4.1 in the main text for the composition of each formulation.

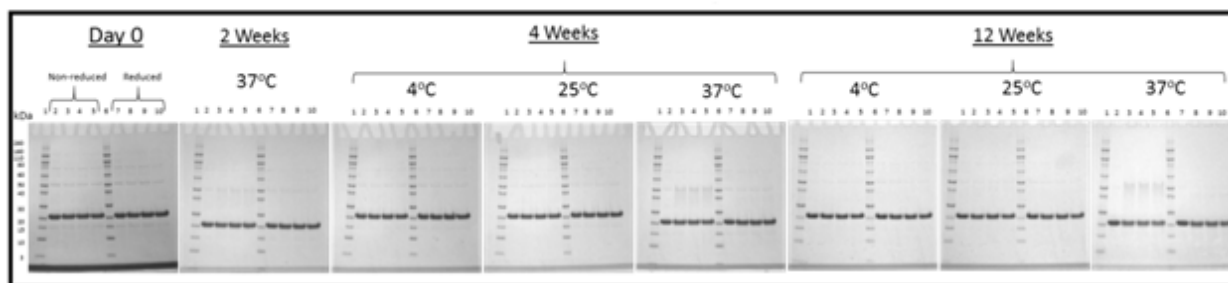
F1



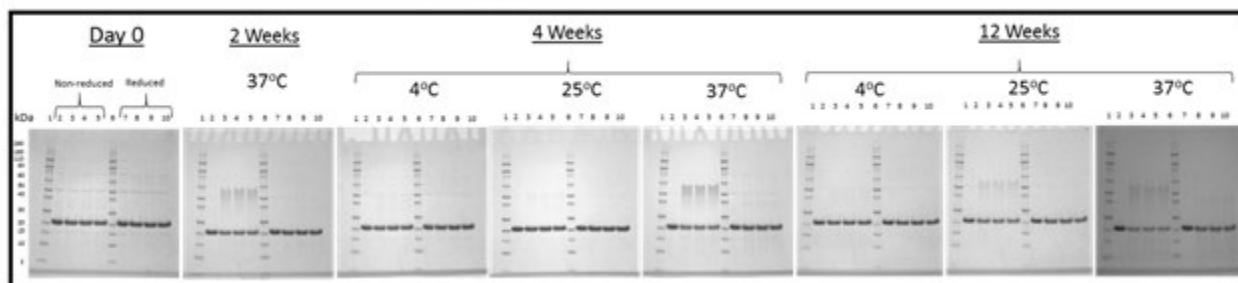
F1 + TH



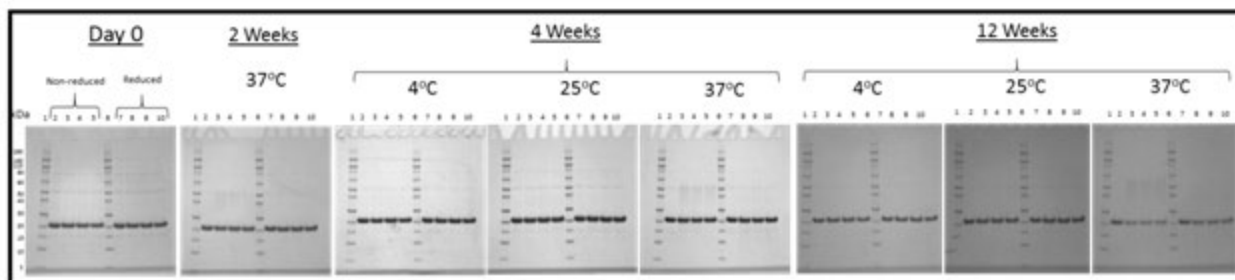
F2



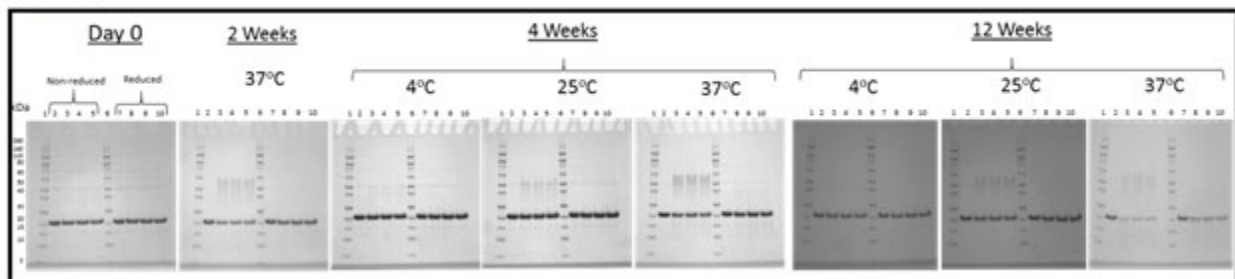
F2 + TH



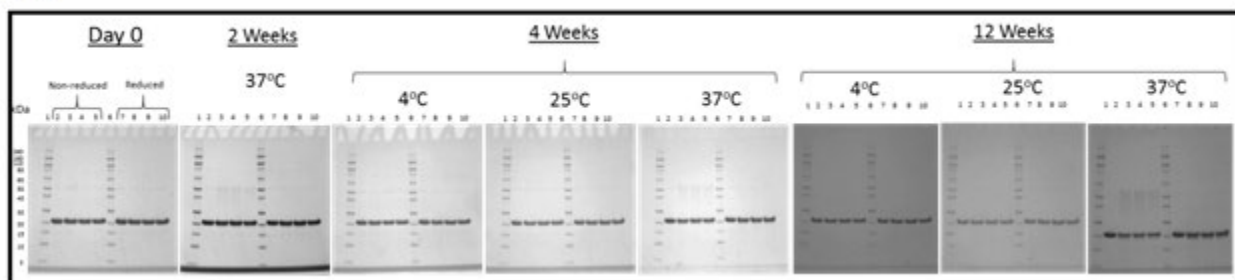
F3



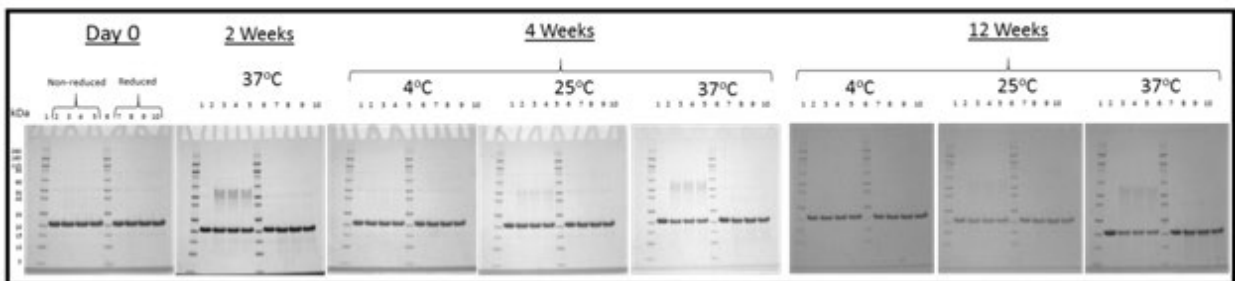
F3 + TH



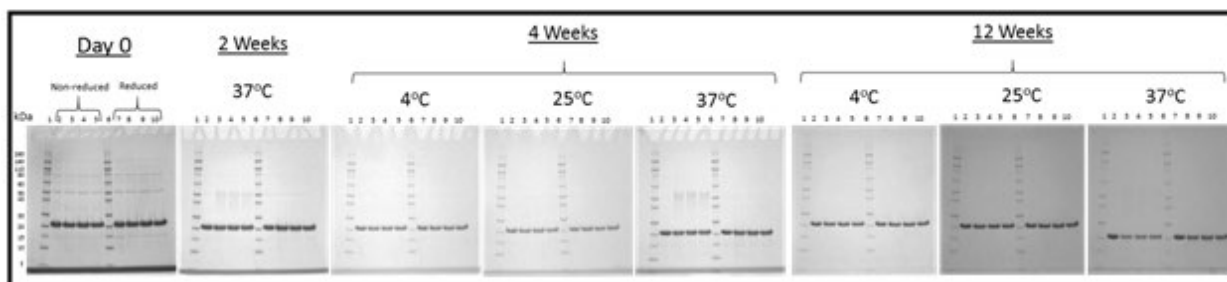
F4



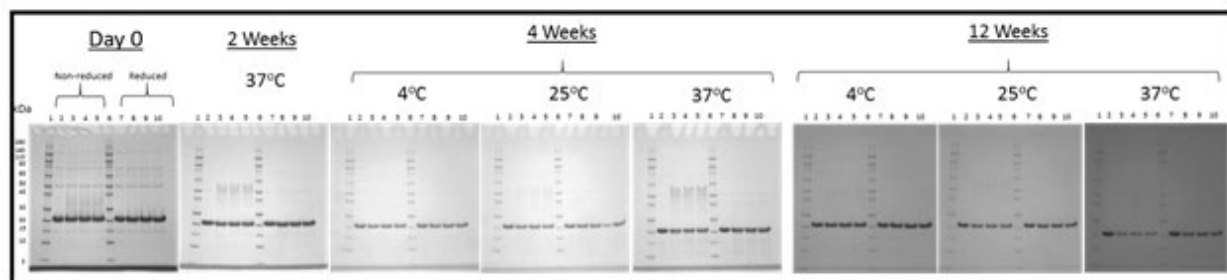
F4 + TH



F5

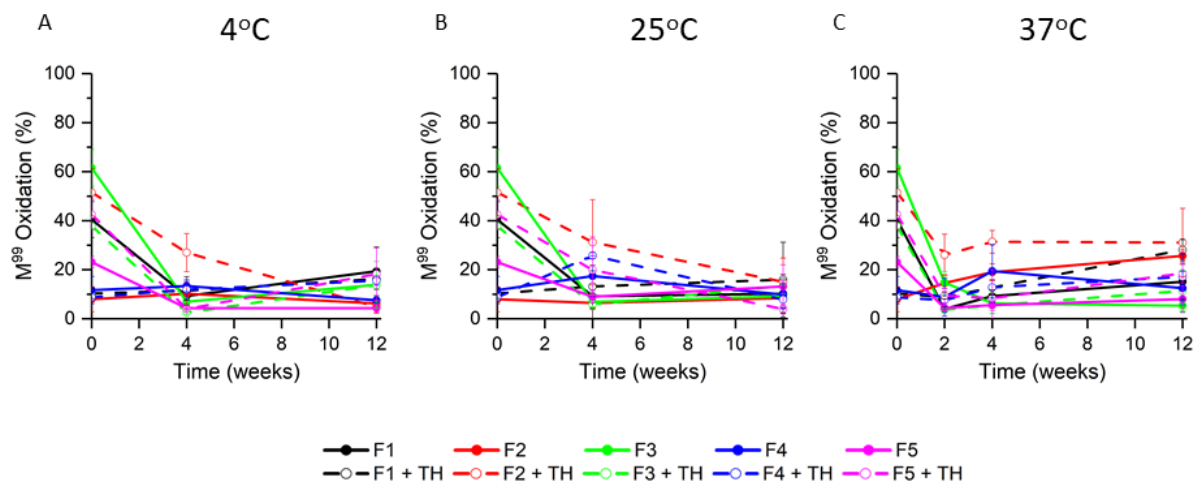


F5 + TH

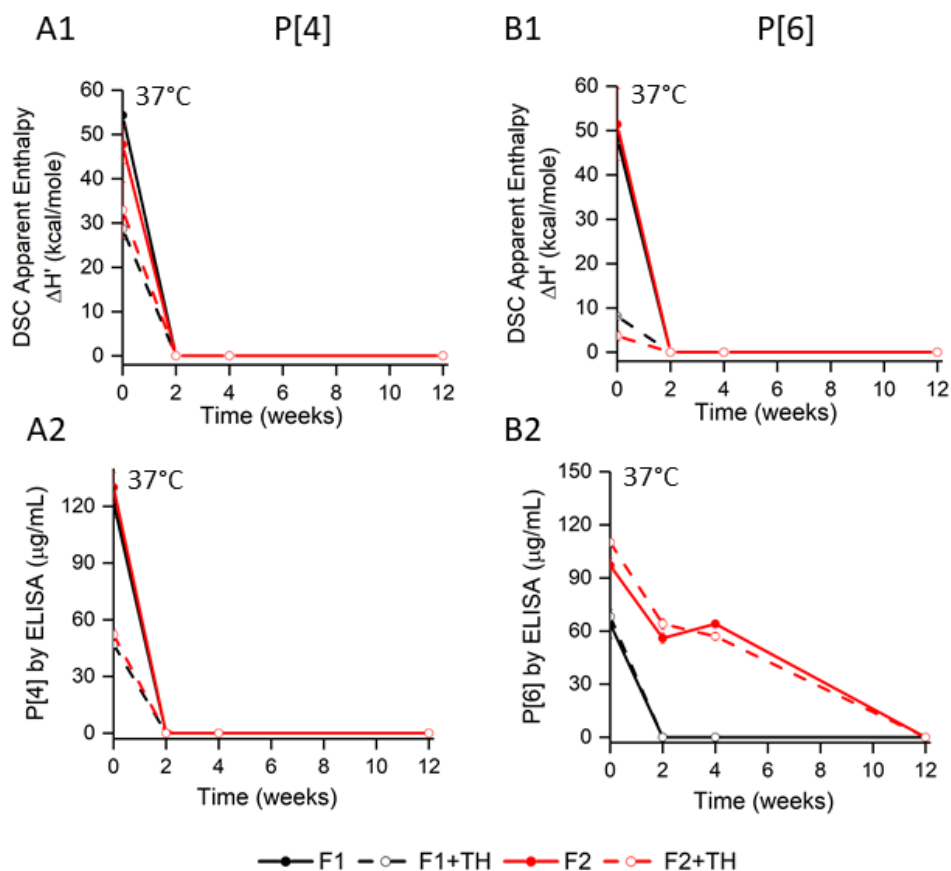


Lane 2, 7 – In solution control; Lane 3, 4, 5 – Desorbed and non-reduced P[8] in triplicate; Lane 8, 9, 10 – Desorbed and reduced P[8] in triplicate

Supplementary Figure S4.3. SDS-PAGE analysis of P[8] antigen under non-reducing and reducing conditions after forced desorption from Alhydrogel adjuvant at different time points during 12 week storage at different temperatures. TH – 0.01% w/v thimerosal. Refer to Table 4.1 in the main text for the composition of each formulation.

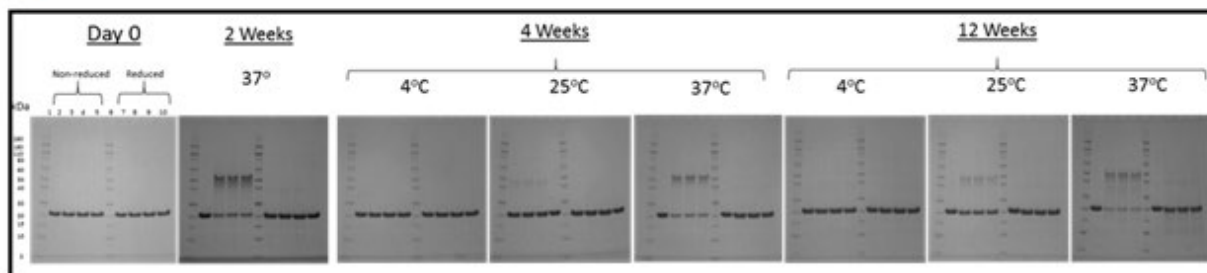


Supplementary Figure S4.4. Oxidation propensity of Met⁹⁹ of the P[8] antigen bound to Alhydrogel adjuvant during 12 weeks of storage at different temperatures in ten different formulations. Relative oxidation values from peptide mapping analysis. Error bars represent 1 SD from triplicate vials. Refer to Table 4.1 in the main text for the composition of each formulation. TH – 0.01% w/v thimerosal.

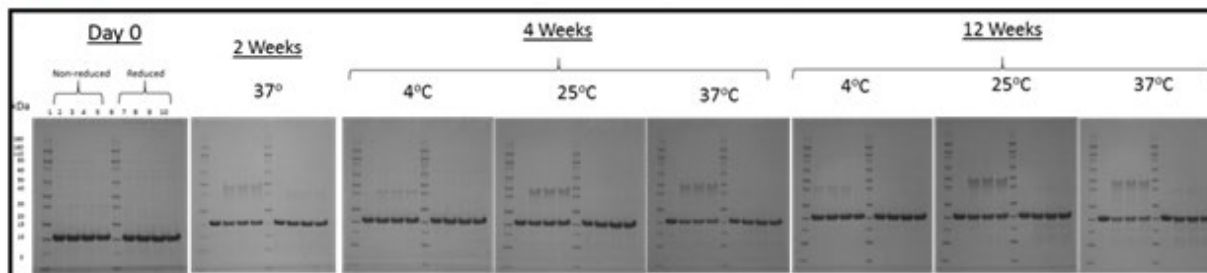


Supplementary Figure S4.5. Conformational stability and antibody binding of monovalent P[4] and P[6] antigens bound to Alhydrogel adjuvant during 12 weeks of storage at 37°C. (A1, B1) Apparent enthalpy of unfolding ($\Delta H'$) from DSC, and (A2, B2) antigen binding to antibody as determined from the inhibition ELISA assay. Refer to Table 4.1 in the main text for the composition of each formulation. TH – 0.01% w/v thimerosal.

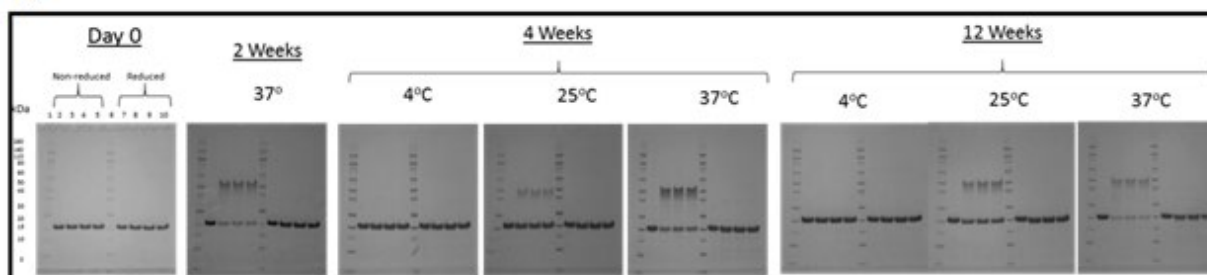
F1



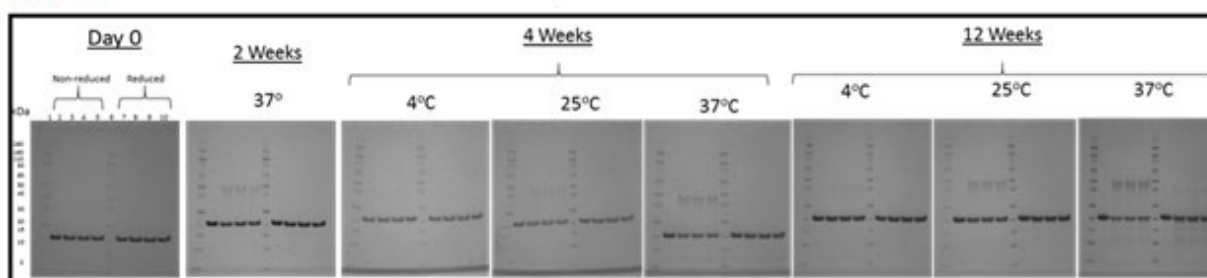
F1 + TH



F2



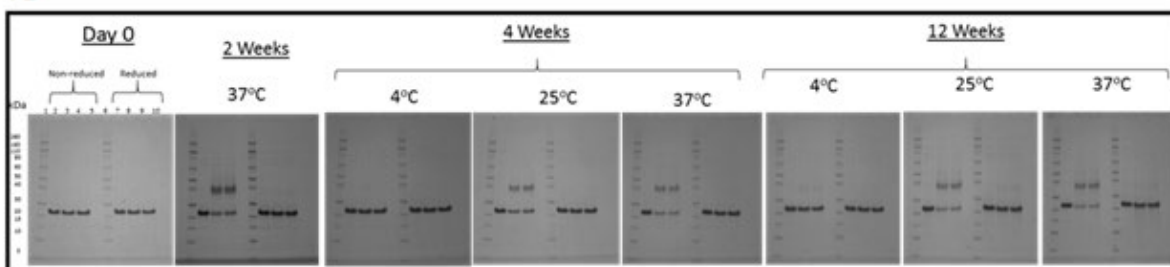
F2 + TH



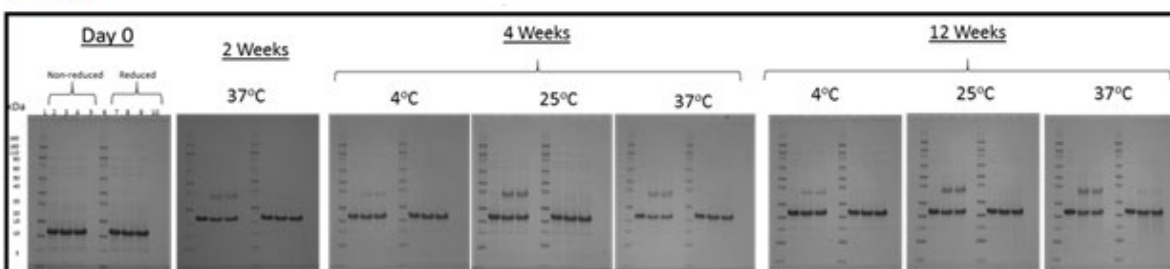
Lane 2, 7 – In solution control; Lane 3, 4, 5 – Desorbed and non-reduced P[4] in triplicate; Lane 8, 9, 10 – Desorbed and reduced P[4] in triplicate

Supplementary Figure S4.6. SDS-PAGE analysis of P[4] antigen under non-reducing and reducing conditions after forced desorption from Alhydrogel adjuvant at different time points during 12 week storage at different temperatures. TH – 0.01% w/v thimerosal. Refer to Table 4.1 in the main text for the composition of each formulation

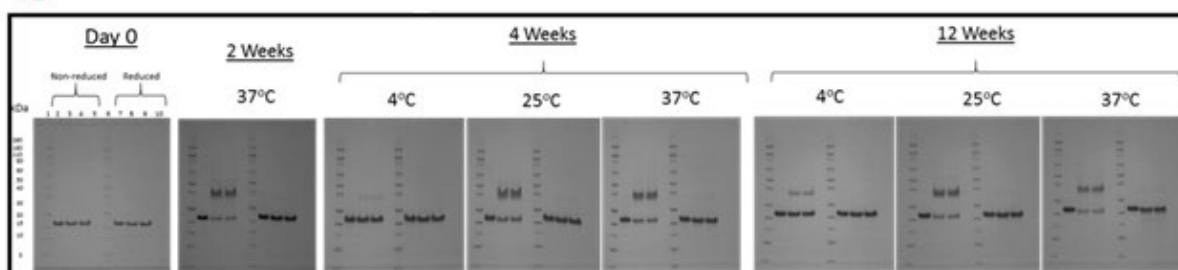
F1



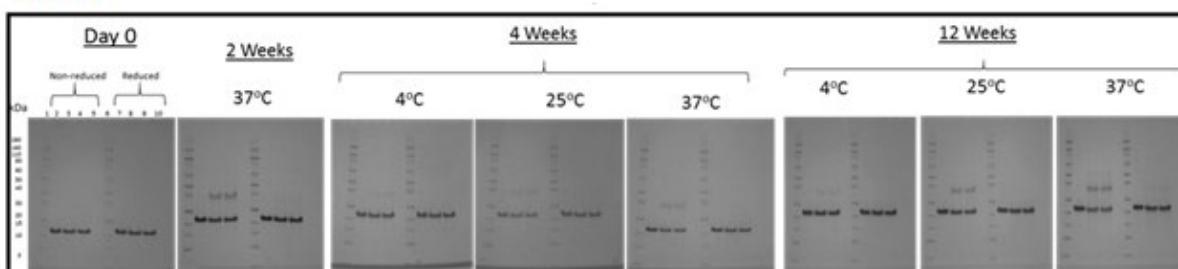
F1 + TH



F2

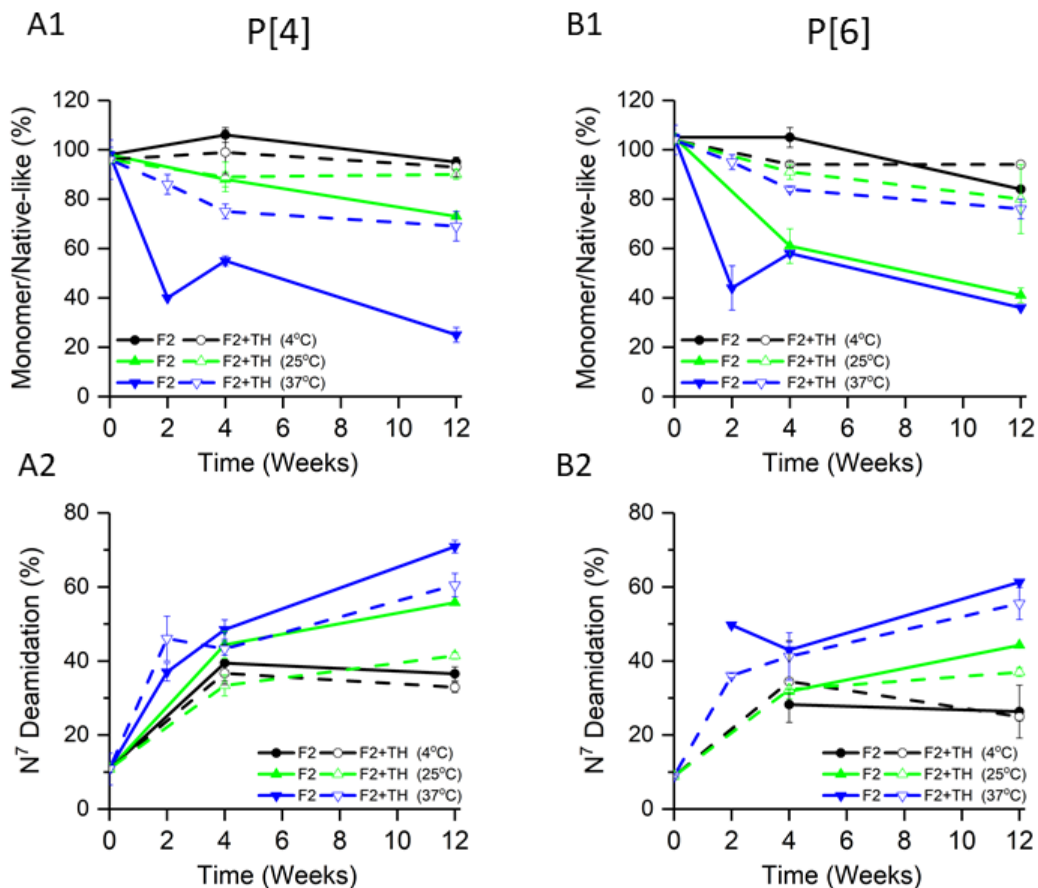


F2 + TH

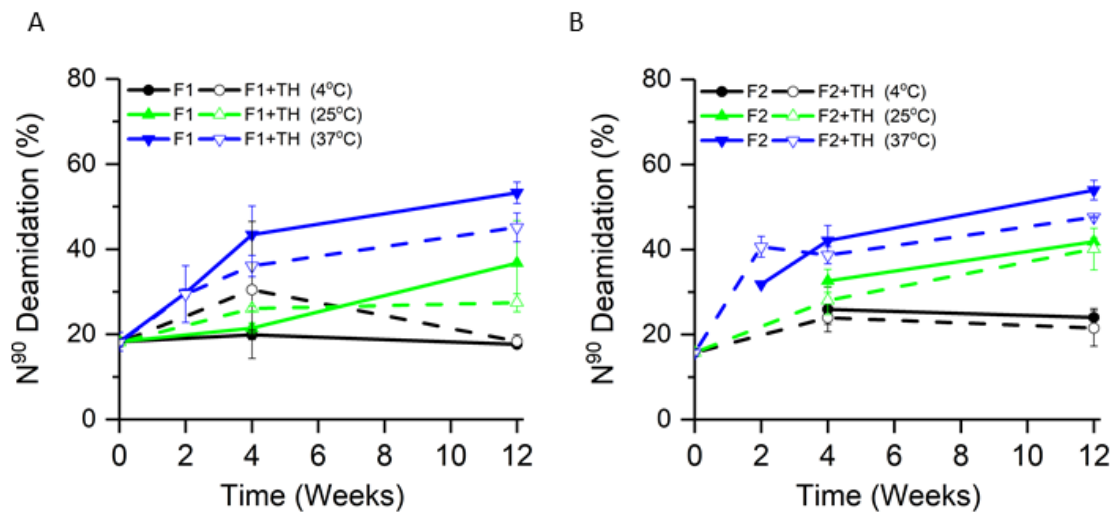


Lane 2, 7 – In solution control; Lane 3, 4 – Desorbed and non-reduced P[6] in duplicate; Lane 8, 9 – Desorbed and reduced P[6] in duplicate

Supplementary Figure S4.7. SDS-PAGE analysis of P[6] antigen under non-reducing and reducing conditions after forced desorption from Alhydrogel adjuvant at different time points during 12 week storage at different temperatures. Refer to Table 4.1 in the main text for the composition of each formulation. TH – 0.01% w/v thimerosal.



Supplementary Figure S4.8. Non-native disulfide formation at Cys¹⁷² and deamidation at Asn⁷ of the monovalent P[4] and P[6] antigens bound to Alhydrogel adjuvant during 12 weeks of storage at different temperatures in four different formulations. (A1, B1) Percent monomer/native-like species from non-reduced SDS-PAGE analysis, and (A2, B2) relative deamidation of Asn⁷ over 12 weeks of storage in formulations F2 and F2+TH. Error bars represent 1 SD from triplicate and duplicate vials for P[4] and P[6], respectively. Refer to Table 4.1 in the main text for the composition of F2. TH – 0.01% w/v thimerosal.



Supplementary Figure S4.9. Deamidation analysis of Asn⁹⁰ of the P[6] antigen bound to aluminum adjuvant Alhydrogel during 12 weeks of storage at different temperatures in four different formulations. Error bars represent 1 SD from duplicate vials. Refer to Table 4.1 in the main text for the composition of each formulation. TH – 0.01% w/v thimerosal.

Chapter 5

Chapter summaries and future directions

5.0 Overview

Rotavirus is a major cause of childhood diarrhea and acute gastroenteritis. About 128,500 children died from RV related illness worldwide in the year 2016 and the majority of these deaths occurred in the developing regions of the sub-Saharan Africa, South Asia and Southeast Asia ¹. Reasons for lower efficacy of the current live attenuated, orally administered RV vaccines in these settings are multi-factorial and are not completely understood ¹⁰⁹. There is an urgent need for new generation vaccines that can provide similar level of protection irrespective of the socioeconomic background of the child. A trivalent non-replicating rotavirus (NRRV) vaccine comprising of P2-VP8-P[4], P2-VP8-P[6] and P2-VP8-P[8] antigens adsorbed to Alhydrogel adjuvant is an emerging candidate. The three subunit antigens are truncated VP8 proteins from RV surface protein VP4 fused to the CD4⁺ T cell epitope P2 from tetanus toxoid (P2-VP8-P[4/6/8]) ^{44,45}. In early phase clinical trials, a monovalent P2-VP8-P[8] NRRV vaccine was found to be safe and immunogenic in infants and toddlers ^{46,47}. Apart from the clinical safety and efficacy, successful development and commercialization of this vaccine candidate will depend on the ability to produce this vaccine at affordable cost and ability to meet the demands of the developing countries. Affordable cost and ease of accessibility will also help in increasing the global RV vaccine coverage. Note that the three NRRV antigens are abbreviated as P[4], P[6] and P[8] in this dissertation.

For the successful development of the trivalent RV vaccine, it will be important to address and conquer the analytical challenges and formulation hurdles to maintain the safety and efficacy of the vaccine throughout its shelf-life. Presence of Alhydrogel as an adjuvant and the need to add a preservative in the final drug product (to make multi-dose presentation) further complicates the analytics and formulation development. This dissertation work accomplished the following major

goals as part of the analytical and formulation development efforts with the NRRV vaccine candidate: (1) robust analytical characterization tools were developed to complement standard quality control (QC) tests and to support formulation development, comparability assessments, storage stability analyses, and process validation studies during technology transfer (chapter 2), (2) physicochemical degradation pathways were elucidated for each NRRV antigen under various environmental stresses which could be detrimental to the development of this vaccine (chapter 2), (3) formulations were developed for long-term storage of the frozen liquid bulks of each NRRV antigen in a common formulation buffer to ensure antigen stability during storage and operational flexibility during fill finish (chapter 3), (4) compatibility of the monovalent NRRV antigens with aluminum-based adjuvant (Alhydrogel) and commonly used preservatives (thimerosal and 2-phenoxyethanol) was assessed to evaluate overall drug product stability (chapter 4).

5.1 Chapter 2

We started with physicochemical comparisons and stability evaluations of the three NRRV protein antigens. A wide variety of analytical techniques (> 25) were employed to characterize and evaluate their physicochemical properties (e.g., primary and higher-order structures, post-translational modifications, conformational stability, and purity including presence of aggregates). Each protein contained an extra Met residue at the N-terminus based on the primary sequences provided by the collaborators at PATH. Higher order structure (HOS) was overall similar for each antigen and P[6] was the most hydrophobic of the three antigens. Physical stability analyses under thermal stress conditions revealed that P[8] antigen is most stable conformationally (and P[4] is slightly more stable than P[6]). A pH dependent destabilization was observed for each antigen at lower pH values (with P[6] being least stable at pH 4.0 and pH 5.0). In addition, forced degradation studies were performed to elucidate degradation pathways of chemically labile amino acid residues

or “weak spots”. Analytical tools were also developed to monitor/quantify degradative changes. Forced chemical degradation studies revealed, for each antigen, (1) Met¹ is most susceptible to oxidation followed by other Met residues, and intact protein mass measurement and peptide mapping by LC-MS methods are assays of choice to detect and monitor this degradation, (2) single Cys residue (at position 173/172) is susceptible to non-native disulfide bond formation leading to dimer formation, P[6] is more susceptible compared to P[4] and P[8] antigens, and non-reducing SDS-PAGE method can be used to assess this reaction, and (3) Asn⁷ residue is most labile to deamidation, and LC-MS peptide mapping method is able to detect and quantify the degradation products. Both chemical and physical degradation pathways elucidated in this work could be detrimental to the development of NRRV vaccine without optimal formulation development. The analytical tools developed were used to develop stable frozen liquid bulk formulations to minimize aggregation and particle formation as described in chapter 3. In addition, these tools were modified and adapted to characterize the interaction of these antigens with aluminum adjuvant and to assess the compatibility with two commonly used preservatives in chapter 4. Also, a down-selected subset of the physicochemical tools developed are currently being used in our laboratories to perform analytical comparability assessments of different lots of each antigen produced by a manufacturing partner.

In the future, it will be important to correlate the physicochemical changes observed in this work under stressed conditions with *in vitro* potency assays such as ELISA, bio-layer interferometry or surface plasmon resonance using antigen-specific neutralizing antibodies. Further, such *in vitro* results could be correlated with *in vivo* studies in animal models to establish a link between physicochemical changes and biological activity of the vaccine. Also, it will be interesting to assess the impact of point mutations on the pharmaceutical stability of the three

different NRRV antigens by replacing the three most degradation prone residues in each antigen (i.e., Met¹, Asn⁷ and Cys^{172/173}). However, these mutations could also impair the structural stability and biological activity of the antigens and thus need to be evaluated using suitable physicochemical and potency assays.

5.2 Chapter 3

Visible particles and precipitation were observed during thawing of frozen NRRV antigen bulk solutions at a large scale in suboptimal formulations (data not shown). This chapter focuses on better understanding the aggregation propensity of the three NRRV antigens when subjected to freeze-thaw and shaking/agitation stresses. The goal was to develop stable candidate formulations for storage of frozen liquid bulks of each antigen in a common formulation buffer. Since the final NRRV drug product will be a trivalent aluminum adjuvanted vaccine in a common formulation buffer, it was important to develop a common formulation buffer for storage of bulk antigens so that a buffer exchange step is not required after the bulk antigens are thawed for fill finish. The P[8] antigen is most prone to shaking/agitation induced aggregation and particle formation, however, it is also most stable against thermal induced structural alteration (see chapter 2). This is presumably due to lower colloidal stability of the P[8] compared with the other two antigens. The nature and composition of the aggregates generated were studied using a combination of physicochemical tools. Aggregates were opaque and fibrillar in morphology, higher inter-molecular β -sheet content was recorded with loss of native secondary structure, and tertiary structure was altered with increased exposure of apolar regions. Also, aggregates were linked with non-native inter-molecular disulfide bonds of reducible nature. The observed physicochemical characteristics of aggregates is similar to that of an IgG mAb previously studied in our laboratories¹⁸⁰. Polysorbate 80 at 0.05% w/v was optimum at preventing NRRV protein loss due to aggregation

during freeze-thaw. Eight candidate frozen liquid bulk formulations were designed to prevent particle formation due to freeze-thaw stress and to minimize shaking induced aggregation.

An interesting avenue to explore in future work will be to better understand the differences in the colloidal stability profiles of the three NRRV antigens. This can be achieved by measuring protein-protein interactions using second virial coefficient (B_{22}) or diffusion interaction parameter (K_d)^{176,177}. It is interesting to see P[8] antigen exhibiting lowest colloidal stability despite being most conformationally stable. Correlations between the protein's isoelectric point, solubility and physical stability under different formulation conditions could help to better understand these observations. It will also be essential to evaluate the longer-term storage stability of the three NRRV antigens stored as bulk in the frozen state at different storage temperatures such as -80°C and -20°C . This will help guide the storage conditions and the time period for which each monovalent bulk antigen can be stored before thawing and fill finish. Due to limited material availability, the excipient screening studies were conducted at dilute protein concentrations with assays optimized for low protein consumption and stability indicating nature, however, in the future, excipient screening can be performed against freeze thaw stress at higher protein concentrations at which the bulk drug substance is stored.

5.3 Chapter 4

Adjuvants are often added to subunit vaccine antigens to enhance immune responses. An aluminum based adjuvant was added to the NRRV vaccine candidate since it enhanced the neutralizing antibody titers against RV in guinea pigs⁴⁵. Adjuvants can also help reduce the overall cost of vaccination by dose sparing and reducing the number of shots required. Another strategy to reduce the cost is to develop a multi-dose presentation. However, such formulations need a preservative to prevent microbial contamination during multiple withdrawals from same vial. The

focus of this last chapter of the dissertation is the NRRV drug product stability including evaluation of the effects of aluminum adjuvant and preservatives on the structural integrity and physicochemical stability of the three antigens. The extent and strength of binding between antigen and aluminum adjuvant is considered important for optimum immune response^{193,194,200-203}. Addition of increasing amounts of phosphate buffer reduced the extent of NRRV antigen binding suggesting that the primary binding force is in the form of non-covalent electrostatic interactions. The antigen-adjuvant binding is also known to affect the structural stability of the antigen. Several groups have reported an enhanced, decreased or no effect of antigen-adjuvant binding on the stability of various recombinant vaccine antigens and model proteins^{205,207,209}. The structural integrity of NRRV antigens is not perturbed in the presence of aluminum adjuvant as measured by immunochemical, biophysical and biochemical assays. Non-native intermolecular disulfide bond formation at the single Cys residue and deamidation of Asn⁷ are the major chemical modifications that can occur in these antigens in the bound state. These modifications were also observed with NRRV antigens in the solution state as described in chapter 2. Addition of thimerosal resulted in an instantaneous destabilizing effect on the thermal stability of each antigen. Over three months of storage, varying levels of incompatibility with thimerosal was observed depending on the antigen, storage temperature, and analytical assay. In general, the P[8] antigen is the most stable followed by P[4] and P[6] in the bound state, similar results to the stability of these antigens in solution. As expected, storage stability was better at lower temperature conditions both in the presence and absence of thimerosal. Conformational stability analysis by DSC and antibody binding using ELISA were the most informative assays. A very good correlation was observed between antibody binding ability and apparent enthalpy of unfolding for P[8] and P[4] antigens. Thimerosal destabilization effect appears to be mediated by the ethyl mercury adduct formation

with the free Cys in each protein, however, another preservative (2-phenoxyethanol) which is devoid of the sulfhydryl chemistry also resulted in similar destabilization. Overall, all three monovalent aluminum bound antigens are stable at 4°C up to three months in the absence of preservative.

An exciting opportunity in the future will be to assess the compatibility of other preservatives used in vaccines and biopharmaceutical products with the NRRV vaccine candidate to develop a multi-dose formulation. Apart from testing the available preservatives alone at their current in-use concentrations, it is also possible to evaluate their combinations at lower than current in-use concentrations to keep the vaccine antigens stable, and at the same time, potentially impart a synergistic anti-microbial effectiveness. This will require significant research efforts since the novel combinations of preservatives will require analyses of their anti-microbial effectiveness as per regulatory guidelines apart from their compatibility with the antigens during long term storage. Since long-term goal of this NRRV subunit vaccine candidate is to combine it with the current childhood combination vaccines in the developing countries, which contain thimerosal, it will be beneficial to deduce the molecular mechanism of thimerosal induced destabilization. This can be achieved by using a combination of intact mass analysis and high-resolution hydrogen deuterium exchange mass spectrometry technique to localize the interaction sites of thimerosal and its effects on the protein dynamics and conformation. Further, protein engineering can be used to generate Cys mutants which could potentially be more compatible with thimerosal, however, this approach would require extensive testing of the mutants to ensure their biological activity. Another avenue worth exploring would be to further correlate the loss in apparent enthalpy of unfolding (DSC) and decreased antibody binding (ELISA) with *in-vivo* potency in animal models. This would help develop a robust, high throughput and inexpensive *in-vitro* potency assays for the routine lot

release testing to assess batch to batch consistency. Finally, the extent and strength of interaction between NRRV antigens and aluminum adjuvant could be optimized in the future to attain optimal immunopotential effect of the adjuvant. This can be accomplished by monitoring the elution profile of the antigen from the aluminum adjuvant upon contact with interstitial fluid and correlating it with the observed immune response in animal models.

Bibliography

1. Troeger C, Khalil IA, Rao PC, Cao S, Blacker BF, Ahmed T, Armah G, Bines JE, Brewer TG, Colombara DV, Kang G, Kirkpatrick BD, Kirkwood CD, Mwenda JM, Parashar UD, Petri WA, Jr., Riddle MS, Steele AD, Thompson RL, Walson JL, Sanders JW, Mokdad AH, Murray CJL, Hay SI, Reiner RC, Jr. 2018. Rotavirus Vaccination and the Global Burden of Rotavirus Diarrhea Among Children Younger Than 5 Years. *JAMA Pediatr* 172(10):958-965.
2. Umesh D, Parashar EGH, Joseph S, Bresee, Mark A. Miller, and Roger I. Glass 2003. Global Illness and Deaths Caused by Rotavirus Disease in Children. *Emerging Infectious Diseases* 9(5):566-572.
3. WHO. 2017. Rotavirus (RotaC) immunization coverage. ed.
4. Deen J, Lopez AL, Kanungo S, Wang XY, Anh DD, Tapia M, Grais RF 2018. Improving rotavirus vaccine coverage: Can newer-generation and locally produced vaccines help? *Hum Vaccin Immunother* 14(2):495-499.
5. Angel J, Franco MA, Greenberg HB 2007. Rotavirus vaccines: recent developments and future considerations. *Nat Rev Microbiol* 5(7):529-539.
6. Crawford SE, Ramani S, Tate JE, Parashar UD, Svensson L, Hagbom M, Franco MA, Greenberg HB, O'Ryan M, Kang G, Desselberger U, Estes MK 2018. Rotavirus infection. *Nat Rev Dis Primers* 3:17083.
7. Matthijnsens J, Ciarlet M, Rahman M, Attoui H, Banyai K, Estes MK, Gentsch JR, Iturriza-Gomara M, Kirkwood CD, Martella V, Mertens PP, Nakagomi O, Patton JT, Ruggeri FM, Saif LJ, Santos N, Steyer A, Taniguchi K, Desselberger U, Van Ranst M 2008. Recommendations for the classification of group A rotaviruses using all 11 genomic RNA segments. *Arch Virol* 153(8):1621-1629.
8. Sadiq A, Bostan N, Yinda KC, Naseem S, Sattar S 2018. Rotavirus: Genetics, pathogenesis and vaccine advances. *Rev Med Virol* 28(6):e2003.
9. Troeger C, Forouzanfar M, Rao PC, Khalil I, Brown A, Reiner RC, Fullman N, Thompson RL, Abajobir A, Ahmed M, Alemayohu MA, Alvis-Guzman N, Amare AT, Antonio CA, Asayesh H, Avokpaho E, Awasthi A, Bacha U, Barac A, Betsue BD, Beyene AS, Boneya DJ, Malta DC, Dandona L, Dandona R, Dubey M, Eshrati B, Fitchett JRA, Gebrehiwot TT, Hailu GB, Horino M, Hotez PJ, Jibat T, Jonas JB, Kasaeian A, Kissoon N, Kotloff K, Koyanagi A, Kumar GA, Rai RK, Lal A, El Rizek HMA, Mengistie MA, Moe C, Patton G, Platts-Mills JA, Qorbani M, Ram U, Roba HS, Sanabria J, Sartorius B, Sawhney M, Shigematsu M, Sreeramareddy C, Swaminathan S, Tedla BA, Jagiellonian RT-M, Ukwaja K, Werdecker A, Widdowson M-A, Yonemoto N, El Sayed Zaki M, Lim SS, Naghavi M, Vos T, Hay SI, Murray CJL, Mokdad AH 2017. Estimates of global, regional, and national morbidity, mortality, and aetiologies of diarrhoeal diseases: a systematic analysis for the Global Burden of Disease Study 2015. *The Lancet Infectious Diseases* 17(9):909-948.
10. Rotavirus Classification Working Group. 2018.
11. Doro R, Laszlo B, Martella V, Leshem E, Gentsch J, Parashar U, Banyai K 2014. Review of global rotavirus strain prevalence data from six years post vaccine licensure surveillance: is there evidence of strain selection from vaccine pressure? *Infect Genet Evol* 28:446-461.
12. Gomez-Rial J, Sanchez-Batan S, Rivero-Calle I, Pardo-Seco J, Martinon-Martinez JM, Salas A, Martinon-Torres F 2019. Rotavirus infection beyond the gut. *Infect Drug Resist* 12:55-64.
13. Keith Grimwood SBLaRJM 2010. Rotavirus infections and vaccines- burden of illness and potential impact of vaccination. *Pediatr Drugs* 12(4):235-256.
14. Jiang B, Patel M, Glass RI 2019. Polio endgame: Lessons for the global rotavirus vaccination program. *Vaccine* 37(23):3040-3049.
15. Tissera MS, Cowley D, Bogdanovic-Sakran N, Hutton ML, Lyras D, Kirkwood CD, Buttery JP 2017. Options for improving effectiveness of rotavirus vaccines in developing countries. *Hum Vaccin Immunother* 13(4):921-927.

16. Baoming Jiang JRG, and Roger I. Glass 2002. The Role of Serum Antibodies in the Protection against rotavirus: An overview. *CID* 34:1351-1361.
17. Angel J, Steele AD, Franco MA 2014. Correlates of protection for rotavirus vaccines: Possible alternative trial endpoints, opportunities, and challenges. *Hum Vaccin Immunother* 10(12):3659-3671.
18. Clarke E, Desselberger U 2015. Correlates of protection against human rotavirus disease and the factors influencing protection in low-income settings. *Mucosal Immunol* 8(1):1-17.
19. Velázquez FR MD, Calva JJ, Guerrero L, Morrow AL, Carter-Campbell S, Glass RI, Estes MK, Pickering LK, Ruiz-Palacios GM. 1996. Rotavirus Infection in Infants as Protection against Subsequent Infections. *N Engl J Med* 335(14):1022-1028.
20. Victoria Jiang BJ, Jacqueline Tate, Umesh D. Parashar and Manish M. Patel 2010. Performance of rotavirus vaccines in developed and developing countries. *Human vaccines* 6(7):532-542.
21. Tate JE, Parashar UD 2019. Approaches to monitoring intussusception following rotavirus vaccination. *Expert Opin Drug Saf* 18(1):21-27.
22. Georges Peter MGM 2002. Intussusception, Rotavirus, and Oral Vaccines: Summary of a Workshop. *Pediatrics* 110(6).
23. Jonesteller CL, Burnett E, Yen C, Tate JE, Parashar UD 2017. Effectiveness of Rotavirus Vaccination: A Systematic Review of the First Decade of Global Postlicensure Data, 2006-2016. *Clin Infect Dis* 65(5):840-850.
24. Rha B TJ, Weintraub E, Haber P, Yen C, Patel M, Cortese MM, DeStefano F, Parashar UD. 2014. Intussusception following rotavirus vaccination: an updated review of the available evidence. *Expert Rev Vaccines* 13(11):1339-1348.
25. Riddle MS, Chen WH, Kirkwood CD, MacLennan CA 2018. Update on vaccines for enteric pathogens. *Clin Microbiol Infect* 24(10):1039-1045.
26. Pollard SL, Malpica-Llanos T, Friberg IK, Fischer-Walker C, Ashraf S, Walker N 2015. Estimating the herd immunity effect of rotavirus vaccine. *Vaccine* 33(32):3795-3800.
27. Edward PK Parker SR, Benjamin A Lopman, James A Church, Miren Iturriza-Gómara, Andrew J Prendergast & Nicholas C Grassly 2017. Causes of impaired oral vaccine efficacy in developing countries. *Future Microbiology* 13(1):97-118.
28. Shumetie G, Gedefaw M, Kebede A, Derso T 2018. Exclusive breastfeeding and rotavirus vaccination are associated with decreased diarrheal morbidity among under-five children in Bahir Dar, northwest Ethiopia. *Public Health Rev* 39:28.
29. Burnett E, Parashar U, Tate J 2018. Rotavirus Vaccines: Effectiveness, Safety, and Future Directions. *Paediatr Drugs* 20(3):223-233.
30. O’Ryan M 2017. Rotavirus Vaccines: a story of success with challenges ahead. *F1000Res* 6:1517.
31. Magwira CA, Taylor MB 2018. Composition of gut microbiota and its influence on the immunogenicity of oral rotavirus vaccines. *Vaccine* 36(24):3427-3433.
32. Mwila K, Chilengi R, Simuyandi M, Permar SR, Becker-Dreps S 2017. Contribution of Maternal Immunity to Decreased Rotavirus Vaccine Performance in Low- and Middle-Income Countries. *Clin Vaccine Immunol* 24(1).
33. Rongsen-Chandola T, Strand TA, Goyal N, Flem E, Rathore SS, Arya A, Winje BA, Lazarus R, Shanmugasundaram E, Babji S, Sommerfelt H, Vainio K, Kang G, Bhandari N 2014. Effect of withholding breastfeeding on the immune response to a live oral rotavirus vaccine in North Indian infants. *Vaccine* 32 Suppl 1:A134-139.
34. Becker-Dreps S, Choi WS, Stamper L, Vilchez S, Velasquez DE, Moon SS, Hudgens MG, Jiang B, Permar SR 2017. Innate Immune Factors in Mothers' Breast Milk and Their Lack of Association With Rotavirus Vaccine Immunogenicity in Nicaraguan Infants. *J Pediatric Infect Dis Soc* 6(1):87-90.
35. Lazarus RP, John J, Shanmugasundaram E, Rajan AK, Thiagarajan S, Giri S, Babji S, Sarkar R, Kaliappan PS, Venugopal S, Praharaj I, Raman U, Paranjpe M, Grassly NC, Parker EPK, Parashar UD, Tate JE, Fleming JA, Steele AD, Muliylil J, Abraham AM, Kang G 2018. The effect of probiotics

- and zinc supplementation on the immune response to oral rotavirus vaccine: A randomized, factorial design, placebo-controlled study among Indian infants. *Vaccine* 36(2):273-279.
36. Krawczyk A, Lewis MG, Venkatesh BT, Nair SN 2016. Effect of Exclusive Breastfeeding on Rotavirus Infection among Children. *Indian J Pediatr* 83(3):220-225.
 37. Niraj C. Patel PMH, Mary K. Estes, Maite de la Morena, Ann M. Petru, Lenora M. Noroski, Paula A. Revell, I. Celine Hanson, Mary E. Paul, Howard M. Rosenblatt, and Stuart L. Abramson 2010. Vaccine-Acquired Rotavirus in Infants with Severe Combined Immunodeficiency. *N Engl J Med* 362(4):314-319.
 38. Bucardo F, Rippinger CM, Svensson L, Patton JT 2012. Vaccine-derived NSP2 segment in rotaviruses from vaccinated children with gastroenteritis in Nicaragua. *Infect Genet Evol* 12(6):1282-1294.
 39. Hemming M, Vesikari T 2014. Detection of rotateq vaccine-derived, double-reassortant rotavirus in a 7-year-old child with acute gastroenteritis. *Pediatr Infect Dis J* 33(6):655-656.
 40. O’Ryan M, Lopman BA 2017. Parenteral protein-based rotavirus vaccine. *The Lancet Infectious Diseases* 17(8):786-787.
 41. Council R. 2016. Rotavirus vaccine pricing. ed.
 42. Rose J, Homa L, Meropol SB, Debanne SM, Bielefeld R, Hoyen C, Singer ME 2017. Health impact and cost-effectiveness of a domestically-produced rotavirus vaccine in India: A model based analysis. *PLoS One* 12(11):e0187446.
 43. Lee AW, Jordanov E, Boissnard F, Marshall GS 2017. DTaP5-IPV-Hib-HepB, a hexavalent vaccine for infants and toddlers. *Expert Rev Vaccines* 16(2):85-92.
 44. Wen X, Cao D, Jones RW, Li J, Szu S, Hoshino Y 2012. Construction and characterization of human rotavirus recombinant VP8* subunit parenteral vaccine candidates. *Vaccine* 30(43):6121-6126.
 45. Wen X, Wen K, Cao D, Li G, Jones RW, Li J, Szu S, Hoshino Y, Yuan L 2014. Inclusion of a universal tetanus toxoid CD4(+) T cell epitope P2 significantly enhanced the immunogenicity of recombinant rotavirus DeltaVP8* subunit parenteral vaccines. *Vaccine* 32(35):4420-4427.
 46. Fix AD, Harro C, McNeal M, Dally L, Flores J, Robertson G, Boslego JW, Cryz S 2015. Safety and immunogenicity of a parenterally administered rotavirus VP8 subunit vaccine in healthy adults. *Vaccine* 33(31):3766-3772.
 47. Groome MJ, Koen A, Fix A, Page N, Jose L, Madhi SA, McNeal M, Dally L, Cho I, Power M, Flores J, Cryz S 2017. Safety and immunogenicity of a parenteral P2-VP8-P[8] subunit rotavirus vaccine in toddlers and infants in South Africa: a randomised, double-blind, placebo-controlled trial. *The Lancet Infectious Diseases* 17(8):843-853.
 48. Lebron JA, Wolf JJ, Kaplanski CV, Ledwith BJ 2005. Ensuring the quality, potency and safety of vaccines during preclinical development. *Expert Rev Vaccines* 4(6):855-866.
 49. Metz B vdDG, van Els C, van der Gun J, Levels L, van der Pol L, Rots N, Kersten G. 2009. Quality-control issues and approaches in vaccine development. *Expert Rev Vaccines* 8(2):227-238.
 50. Volkin DB, Middaugh CR 2010. Vaccines as physically and chemically well-defined pharmaceutical dosage forms. *Expert Rev Vaccines* 9(7):689-691.
 51. Q6B IG 1999. SPECIFICATIONS: TEST PROCEDURES AND ACCEPTANCE CRITERIA FOR BIOTECHNOLOGICAL/BIOLOGICAL PRODUCTS Q6B.
 52. Buckland BC 2005. The process development challenge for a new vaccine. *Nat Med* 11(4 Suppl):S16-19.
 53. Plitnik LM. 2013. Global regulatory guidelines for vaccines. *Nonclinical Development of Novel Biologics, Biosimilars, Vaccines and Specialty Biologics*, ed.
 54. Shin J, Lei D, Conrad C, Knezevic I, Wood D 2011. International regulatory requirements for vaccine safety and potency testing: a WHO perspective. *Procedia in Vaccinology* 5:164-170.
 55. Suresh Kumar MPS, Vijay K. Bharti, Ramendra Pati Pandey 2018. Quality control of vaccines-A journey from classical approach to 3Rs. *Microbiol Curr Res* 2(3):45-61.
 56. McFarland R, Verthelyi D, Casey W, Arciniega J, Isbrucker R, Schmitt M, Finn T, Descamps J, Horiuchi Y, Sesardic D, Stickings P, Johnson NW, Lipscomb E, Allen D 2011. Non-animal

- replacement methods for human vaccine potency testing: state of the science and future directions. *Procedia in Vaccinology* 5:16-32.
57. Thorsten Verch JJTMS-R 2018. Principles of vaccine potency assays. *Bioanalysis* 10(3):163-180.
 58. Robert D. Sitrin QZ, Clinton S. Potter, Bridget Carragher, Michael W. Washabaugh. 2014. Recombinant Virus-like Particle Protein Vaccines. In Nunnally B. TV, Sitrin R. , editor *Vaccine Analysis: Strategies, Principles, and Control*, ed., Berlin, Heidelberg: Springer.
 59. Hendriksen CF 2009. Replacement, reduction and refinement alternatives to animal use in vaccine potency measurement. *Expert Rev Vaccines* 8(3):313-322.
 60. Todd Ranheim NM, William Egan. 2014. Vaccine Potency Assays. In Sitrin BKNETD, editor *Vaccine Analysis: Strategies, Principles, and Control*, ed., Switzerland Springer Nature. p 521-541.
 61. Ellington AA, Kullo IJ, Bailey KR, Klee GG 2009. Measurement and quality control issues in multiplex protein assays: a case study. *Clin Chem* 55(6):1092-1099.
 62. Bolton DL, Roederer M 2009. Flow cytometry and the future of vaccine development. *Expert Review of Vaccines* 8:779+.
 63. Saade F, Gorski SA, Petrovsky N 2014. Pushing the frontiers of T-cell vaccines: accurate measurement of human T-cell responses. *Expert Review of Vaccines* 11(12):1459-1470.
 64. Slota M, Lim JB, Dang Y, Disis ML 2011. ELISpot for measuring human immune responses to vaccines. *Expert Rev Vaccines* 10(3):299-306.
 65. Sims S, Willberg C, Klenerman P 2010. MHC-peptide tetramers for the analysis of antigen-specific T cells. *Expert Rev Vaccines* 9(7):765-774.
 66. Koivunen ME, Krogsrud RL 2006. Principles of Immunochemical Techniques Used in Clinical Laboratories. *Laboratory Medicine* 37(8):490-497.
 67. Engelhardt OG, Edge C, Dunleavy U, Guilfoyle K, Harvey R, Major D, Newman R, Penn R, Skeldon S, Storey C, Wheeler J, Wood J, Minor P 2018. Comparison of single radial immunodiffusion, SDS-PAGE and HPLC potency assays for inactivated influenza vaccines shows differences in ability to predict immunogenicity of haemagglutinin antigen. *Vaccine* 36(29):4339-4345.
 68. Minor PD 2015. Assaying the Potency of Influenza Vaccines. *Vaccines (Basel)* 3(1):90-104.
 69. Dennison SM, Reichartz M, Seaton KE, Dutta S, Wille-Reece U, Hill AVS, Ewer KJ, Rountree W, Sarzotti-Kelsoe M, Ozaki DA, Alam SM, Tomaras GD 2018. Qualified Biolayer Interferometry Avidity Measurements Distinguish the Heterogeneity of Antibody Interactions with Plasmodium falciparum Circumsporozoite Protein Antigens. *J Immunol* 201(4):1315-1326.
 70. Hearty S, Conroy PJ, Ayyar BV, Byrne B, O'Kennedy R 2010. Surface plasmon resonance for vaccine design and efficacy studies: recent applications and future trends. *Expert Rev Vaccines* 9(6):645-664.
 71. Petersen RL 2017. Strategies Using Bio-Layer Interferometry Biosensor Technology for Vaccine Research and Development. *Biosensors (Basel)* 7(4).
 72. Dey AK, Malyala P, Singh M 2014. Physicochemical and functional characterization of vaccine antigens and adjuvants. *Expert Rev Vaccines* 13(5):671-685.
 73. Filipe V, Hawe A, Carpenter JF, Jiskoot W 2013. Analytical approaches to assess the degradation of therapeutic proteins. *TrAC Trends in Analytical Chemistry* 49:118-125.
 74. Hem SL, HogenEsch H, Middaugh CR, Volkin DB 2010. Preformulation studies--The next advance in aluminum adjuvant-containing vaccines. *Vaccine* 28(31):4868-4870.
 75. HogenEsch H, O'Hagan DT, Fox CB 2018. Optimizing the utilization of aluminum adjuvants in vaccines: you might just get what you want. *NPJ Vaccines* 3:51.
 76. L.Hem S 2002. Elimination of aluminum adjuvants. *Vaccine* 20(S3):S40-S43.
 77. Joseph V. Rinella Jr JLWaSLH 1996. Treatment of aluminium hydroxide adjuvant to optimize the adsorption basic proteins. *Vaccine* 14(4):298-300.
 78. Kumru OS, Joshi SB, Smith DE, Middaugh CR, Prusik T, Volkin DB 2014. Vaccine instability in the cold chain: mechanisms, analysis and formulation strategies. *Biologicals* 42(5):237-259.

79. MIDDLEDAUGH TSPACR. 2014. Stabilization and Formulation of Vaccines. In Emily P. Wen RJE, Narahari S. Pujar, editor Vaccine Production and Manufacturing, ed.: John Wiley & Sons, Incorporated.
80. Brito LA, Malyala P, O'Hagan DT 2013. Vaccine adjuvant formulations: a pharmaceutical perspective. *Semin Immunol* 25(2):130-145.
81. Manning MC, Chou DK, Murphy BM, Payne RW, Katayama DS 2010. Stability of protein pharmaceuticals: an update. *Pharm Res* 27(4):544-575.
82. Frokjaer S, Otzen DE 2005. Protein drug stability: a formulation challenge. *Nat Rev Drug Discov* 4(4):298-306.
83. Morefield GL 2011. A rational, systematic approach for the development of vaccine formulations. *AAPS J* 13(2):191-200.
84. Kris Howard MN, Martin Friede 2017. Establishing Manufacturing Capabilities for Human Vaccines. WHITE PAPER, WHO.
85. Kis Z, Shattock R, Shah N, Kontoravdi C 2019. Emerging Technologies for Low-Cost, Rapid Vaccine Manufacture. *Biotechnol J* 14(1):e1800376.
86. Smith J, Lipsitch M, Almond JW 2011. Vaccine production, distribution, access, and uptake. *The Lancet* 378(9789):428-438.
87. PATH 2015. Investing in Vaccines for the Developing World.
88. Fox CB, Kramer RM, Barnes VL, Dowling QM, Vedvick TS 2013. Working together: interactions between vaccine antigens and adjuvants. *Ther Adv Vaccines* 1(1):7-20.
89. Norman W, Baylor WE, Paul Richman 2002. Aluminum salts in vaccines - US perspective. *Vaccine* 20:S18-S23.
90. Kurzatkowski W, Kartoglu U, Gorska P, Glowka M, Woznica K, Zasada AA, Szczepanska G, Trykowski G, Gniadek M, Donten M 2018. Physical and chemical changes in Alhydrogel damaged by freezing. *Vaccine* 36(46):6902-6910.
91. Kurzatkowski W, Kartoglu U, Staniszevska M, Gorska P, Krause A, Wysocki MJ 2013. Structural damages in adsorbed vaccines affected by freezing. *Biologicals* 41(2):71-76.
92. Clapp T, Siebert P, Chen D, Jones Braun L 2011. Vaccines with aluminum-containing adjuvants: optimizing vaccine efficacy and thermal stability. *J Pharm Sci* 100(2):388-401.
93. Paul K, Drain CMN, and John S. Lloyd. 2003. Single-dose versus multi-dose vaccine vials for immunization programmes in developing countries. *Bulletin of the World Health Organization*, ed. p 726-731.
94. Preiss S, Garcon N, Cunningham AL, Strugnell R, Friedland LR 2016. Vaccine provision: Delivering sustained & widespread use. *Vaccine* 34(52):6665-6671.
95. Lee BY, Norman BA, Assi T-M, Chen S-I, Bailey RR, Rajgopal J, Brown ST, Waring AE, Burke DS 2010. Single versus multi-dose vaccine vials: An economic computational model. *Vaccine* 28(32):5292-5300.
96. Meyer BK, Ni A, Hu B, Shi L 2007. Antimicrobial preservative use in parenteral products: past and present. *J Pharm Sci* 96(12):3155-3167.
97. Inglis S, Shaw A, Koenig S 2006. Chapter 11: HPV vaccines: commercial research & development. *Vaccine* 24 Suppl 3:S3/99-105.
98. Sawyer LA MJ, Patel A, Horne AD, Albrecht P. 1994. Deleterious effect of thimerosal on the potency of inactivated poliovirus vaccine. *Vaccine* 12(9):851-856.
99. Harmsen MM, Fijten HP, Westra DF, Coco-Martin JM 2011. Effect of thiomersal on dissociation of intact (146S) foot-and-mouth disease virions into 12S particles as assessed by novel ELISAs specific for either 146S or 12S particles. *Vaccine* 29(15):2682-2690.
100. Arash Mahboubi MRF, Nasrin Samadi, Rasoul Dinarvand and Saeed Azadi 2011. Evaluation of Thimerosal Removal on Immunogenicity of Aluminum Salts Adjuvanted Recombinant Hepatitis B Vaccine. *Iranian Journal of Pharmaceutical Research* 11(1):39-46.
101. Maman K, Zollner Y, Greco D, Duru G, Sendyona S, Remy V 2015. The value of childhood combination vaccines: From beliefs to evidence. *Hum Vaccin Immunother* 11(9):2132-2141.

102. Decker MD, Edwards KM, Howe BJ 2018. Combination Vaccines.198-227.e113.
103. Quadros JLDfCd 2001. Considerations for Combination Vaccine Development and Use in the Developing World. *Clinical Infectious Diseases* 33:S340–345.
104. Appaiahgari MB, Glass R, Singh S, Taneja S, Rongsen-Chandola T, Bhandari N, Mishra S, Vrati S 2014. Transplacental rotavirus IgG interferes with immune response to live oral rotavirus vaccine ORV-116E in Indian infants. *Vaccine* 32(6):651-656.
105. Emperador DM, Velasquez DE, Estivariz CF, Lopman B, Jiang B, Parashar U, Anand A, Zaman K 2016. Interference of Monovalent, Bivalent, and Trivalent Oral Poliovirus Vaccines on Monovalent Rotavirus Vaccine Immunogenicity in Rural Bangladesh. *Clin Infect Dis* 62(2):150-156.
106. Parker EPK, Praharaj I, Zekavati A, Lazarus RP, Giri S, Operario DJ, Liu J, Houpt E, Iturriza-Gomara M, Kampmann B, John J, Kang G, Grassly NC 2018. Influence of the intestinal microbiota on the immunogenicity of oral rotavirus vaccine given to infants in south India. *Vaccine* 36(2):264-272.
107. Serazin AC, Shackelton LA, Wilson C, Bhan MK 2010. Improving the performance of enteric vaccines in the developing world. *Nat Immunol* 11(9):769-773.
108. Qadri F, Bhuiyan TR, Sack DA, Svennerholm AM 2013. Immune responses and protection in children in developing countries induced by oral vaccines. *Vaccine* 31(3):452-460.
109. Desselberger U 2017. Differences of Rotavirus Vaccine Effectiveness by Country: Likely Causes and Contributing Factors. *Pathogens* 6(4).
110. Praharaj I, John SM, Bandyopadhyay R, Kang G 2015. Probiotics, antibiotics and the immune responses to vaccines. *Philos Trans R Soc Lond B Biol Sci* 370(1671).
111. Wang CM, Chen SC, Chen KT 2015. Current status of rotavirus vaccines. *World J Pediatr* 11(4):300-308.
112. Aruna Chandran SF, Anjie Zhen, Mathuram Santosham 2010. Prevention of rotavirus gastroenteritis in infants and children- rotavirus vaccine safety, efficacy, and potential impact of vaccines. *Biologics: Targets & Therapy* 4.
113. Tate JE, Parashar UD 2014. Rotavirus vaccines in routine use. *Clin Infect Dis* 59(9):1291-1301.
114. Pasetti MF, Simon JK, Szein MB, Levine MM 2011. Immunology of gut mucosal vaccines. *Immunol Rev* 239(1):125-148.
115. Jiang B, Gentsch JR, Glass RI 2008. Inactivated rotavirus vaccines: a priority for accelerated vaccine development. *Vaccine* 26(52):6754-6758.
116. Franco MA, Angel J, Greenberg HB 2006. Immunity and correlates of protection for rotavirus vaccines. *Vaccine* 24(15):2718-2731.
117. Hickey JM, Toprani VM, Kaur K, Mishra RPN, Goel A, Oganessian N, Lees A, Sitrin R, Joshi SB, Volkin DB 2018. Analytical Comparability Assessments of 5 Recombinant CRM197 Proteins From Different Manufacturers and Expression Systems. *J Pharm Sci* 107(7):1806-1819.
118. Federici M, Lubiniecki A, Manikwar P, Volkin DB 2013. Analytical lessons learned from selected therapeutic protein drug comparability studies. *Biologicals* 41(3):131-147.
119. Lubiniecki A, Volkin DB, Federici M, Bond MD, Nedved ML, Hendricks L, Mehndiratta P, Bruner M, Burman S, Dalmonte P, Kline J, Ni A, Panek ME, Pikounis B, Powers G, Vafa O, Siegel R 2011. Comparability assessments of process and product changes made during development of two different monoclonal antibodies. *Biologicals* 39(1):9-22.
120. Kim JH, Iyer V, Joshi SB, Volkin DB, Middaugh CR 2012. Improved data visualization techniques for analyzing macromolecule structural changes. *Protein Sci* 21(10):1540-1553.
121. Yang J, Zhang Y 2015. I-TASSER server: new development for protein structure and function predictions. *Nucleic Acids Res* 43(W1):W174-181.
122. Zhang Y 2009. I-TASSER: fully automated protein structure prediction in CASP8. *Proteins* 77 Suppl 9:100-113.
123. Roy A, Yang J, Zhang Y 2012. COFACTOR: an accurate comparative algorithm for structure-based protein function annotation. *Nucleic Acids Res* 40(Web Server issue):W471-477.

124. Blanchard H, Yu X, Coulson BS, von Itzstein M 2007. Insight into host cell carbohydrate-recognition by human and porcine rotavirus from crystal structures of the virion spike associated carbohydrate-binding domain (VP8*). *J Mol Biol* 367(4):1215-1226.
125. Monnier N, Higo-Moriguchi K, Sun ZY, Prasad BV, Taniguchi K, Dormitzer PR 2006. High-resolution molecular and antigen structure of the VP8* core of a sialic acid-independent human rotavirus strain. *J Virol* 80(3):1513-1523.
126. More AS, Toth RT, Okbazghi SZ, Middaugh CR, Joshi SB, Tolbert TJ, Volkin DB, Weis DD 2018. Impact of Glycosylation on the Local Backbone Flexibility of Well-Defined IgG1-Fc Glycoforms Using Hydrogen Exchange-Mass Spectrometry. *J Pharm Sci* 107(9):2315-2324.
127. More AS, Toprani VM, Okbazghi SZ, Kim JH, Joshi SB, Middaugh CR, Tolbert TJ, Volkin DB 2016. Correlating the Impact of Well-Defined Oligosaccharide Structures on Physical Stability Profiles of IgG1-Fc Glycoforms. *J Pharm Sci* 105(2):588-601.
128. Toprani VM, Joshi SB, Kuelzto LA, Schwartz RM, Middaugh CR, Volkin DB 2016. A Micro-Polyethylene Glycol Precipitation Assay as a Relative Solubility Screening Tool for Monoclonal Antibody Design and Formulation Development. *J Pharm Sci* 105(8):2319-2327.
129. Zbacnik TJ, Holcomb RE, Katayama DS, Murphy BM, Payne RW, Coccaro RC, Evans GJ, Matsuura JE, Henry CS, Manning MC 2017. Role of Buffers in Protein Formulations. *J Pharm Sci* 106(3):713-733.
130. Giglione C, Fieulaine S, Meinel T 2015. N-terminal protein modifications: Bringing back into play the ribosome. *Biochimie* 114:134-146.
131. PH.HERVt HIREL J-MS, PHILIPPE DESSEN, GuY FAYAT, AND SYLVAIN BLANQUET 1989. Extent of N-terminal methionine excision from Escherichia coli proteins is governed by the side-chain length of the penultimate amino acid. *Proc Natl Acad Sci U S A* 86:8247-8251.
132. Anelia Vassileva-Atanassova RM, Genoveva Nacheva, Ivan Ivanov 1998. N-terminal methionine in recombinant proteins expressed in two different Escherichia coli strains. *Journal of Biotechnology* 69(1):63-67.
133. Shihong Li CS, and Ronald T. Borchardt 1995. Chemical instability of protein pharmaceuticals-Mechanisms of oxidation and strategies for stabilization. *Biotechnology and Bioengineering* 48:490-500.
134. Torosantucci R, Schoneich C, Jiskoot W 2014. Oxidation of therapeutic proteins and peptides: structural and biological consequences. *Pharm Res* 31(3):541-553.
135. Zika WJCaRG 1983. Photochemical formation of hydrogen peroxide in surface and ground waters exposed to sunlight. *Science* 220(4598):711-712.
136. William J. Cooper RGZ, Robert G. Petasne, and John M. C. Plane 1988. Photochemical formation of hydrogen peroxide in natural waters exposed to sunlight. *Environ Sel Technol* 22(10):1156-1160.
137. EMILY HA WW, Y. JOHN WANG 2002. Peroxide Formation in Polysorbate 80 and Protein Stability. *J Pharm Sci* 2252-2264(10).
138. Wasylaschuk WR, Harmon PA, Wagner G, Harman AB, Templeton AC, Xu H, Reed RA 2007. Evaluation of hydroperoxides in common pharmaceutical excipients. *J Pharm Sci* 96(1):106-116.
139. ANDREW A. KOSKY UOR, MICHAEL J. TREUHEIT, and DAVID N. BREMS 1999. The effects of alpha-helix on the stability of Asn residues: deamidation rates in peptides of varying helicity. *Protein Science* 8:2519-2523.
140. Noah E. Robinson aABR 2001. Molecular clocks. *98 398(3):944-949.*
141. Mason BD, Schoneich C, Kerwin BA 2012. Effect of pH and light on aggregation and conformation of an IgG1 mAb. *Mol Pharm* 9(4):774-790.
142. Li CH, Narhi LO, Wen J, Dimitrova M, Wen ZQ, Li J, Pollastrini J, Nguyen X, Tsuruda T, Jiang Y 2012. Effect of pH, temperature, and salt on the stability of Escherichia coli- and Chinese hamster ovary cell-derived IgG1 Fc. *Biochemistry* 51(50):10056-10065.
143. Qi W, Zeng Y, Orgel S, Francon A, Kim JH, Randolph TW, Carpenter JF, Middaugh CR 2014. Preformulation study of highly purified inactivated polio vaccine, serotype 3. *J Pharm Sci* 103(1):140-151.

144. Kumru OS, Joshi SB, Thapa P, Pheasey N, Bullock PS, Bashiri H, Siska CS, Kerwin BA, He F, Volkin DB, Middaugh CR 2015. Characterization of an oncolytic herpes simplex virus drug candidate. *J Pharm Sci* 104(2):485-494.
145. Kissmann J, Joshi SB, Haynes JR, Dokken L, Richardson C, Middaugh CR 2011. H1N1 influenza virus-like particles: physical degradation pathways and identification of stabilizers. *J Pharm Sci* 100(2):634-645.
146. Liu J, Blasie CA, Shi S, Joshi SB, Middaugh CR, Volkin DB 2013. Characterization and stabilization of recombinant human protein pentraxin (rhPTX-2). *J Pharm Sci* 102(3):827-841.
147. Shi S, Liu J, Joshi SB, Krasnoperov V, Gill P, Middaugh CR, Volkin DB 2012. Biophysical characterization and stabilization of the recombinant albumin fusion protein sEphB4-HSA. *J Pharm Sci* 101(6):1969-1984.
148. Plieskatt JL, Rezende WC, Olsen CM, Trefethen JM, Joshi SB, Middaugh CR, Hotez PJ, Bottazzi ME 2012. Advances in vaccines against neglected tropical diseases: enhancing physical stability of a recombinant hookworm vaccine through biophysical and formulation studies. *Hum Vaccin Immunother* 8(6):765-776.
149. Alsenaidy MA, Wang T, Kim JH, Joshi SB, Lee J, Blaber M, Volkin DB, Middaugh CR 2012. An empirical phase diagram approach to investigate conformational stability of "second-generation" functional mutants of acidic fibroblast growth factor-1. *Protein Sci* 21(3):418-432.
150. Kirkwood CD, Ma LF, Carey ME, Steele AD 2017. The rotavirus vaccine development pipeline. *Vaccine*.
151. Harris VC, Armah G, Fuentes S, Korpela KE, Parashar U, Victor JC, Tate J, de Weerth C, Giaquinto C, Wiersinga WJ, Lewis KD, de Vos WM 2017. Significant Correlation Between the Infant Gut Microbiome and Rotavirus Vaccine Response in Rural Ghana. *J Infect Dis* 215(1):34-41.
152. 2017. Global Health Observatory data ed.: WHO.
153. Kartoglu U, Milstien J 2014. Tools and approaches to ensure quality of vaccines throughout the cold chain. *Expert Rev Vaccines* 13(7):843-854.
154. Kallerup RS, Foged C. 2015. Classification of Vaccines. *Subunit Vaccine Delivery*, ed. p 15-29.
155. Li Y, Xue M, Yu L, Luo G, Yang H, Jia L, Zeng Y, Li T, Ge S, Xia N 2018. Expression and characterization of a novel truncated rotavirus VP4 for the development of a recombinant rotavirus vaccine. *Vaccine* 36(16):2086-2092.
156. Zhao B, Pan X, Teng Y, Xia W, Wang J, Wen Y, Chen Y 2015. Rotavirus VP7 epitope chimeric proteins elicit cross-immunoreactivity in guinea pigs. *Virol Sin* 30(5):363-370.
157. Xue M, Yu L, Che Y, Lin H, Zeng Y, Fang M, Li T, Ge S, Xia N 2015. Characterization and protective efficacy in an animal model of a novel truncated rotavirus VP8 subunit parenteral vaccine candidate. *Vaccine* 33(22):2606-2613.
158. Xie L, Yan M, Wang X, Ye J, Mi K, Yan S, Niu X, Li H, Sun M 2015. Immunogenicity and efficacy in mice of an adenovirus-based bicistronic rotavirus vaccine expressing NSP4 and VP7. *Virus Res* 210:298-307.
159. Lappalainen S, Pastor AR, Malm M, Lopez-Guerrero V, Esquivel-Guadarrama F, Palomares LA, Vesikari T, Blazevic V 2015. Protection against live rotavirus challenge in mice induced by parenteral and mucosal delivery of VP6 subunit rotavirus vaccine. *Arch Virol* 160(8):2075-2078.
160. Agarwal S, Hickey JM, Sahni N, Toth RT, Robertson GA, Sitrin R, Cryz S, Joshi SB, Volkin DB 2019. Recombinant subunit rotavirus trivalent vaccine candidate: physicochemical comparisons and stability evaluations of three protein antigens.
161. Akers MJ. 2006. Special Challenges in Production of Biopharmaceutical Dosage Forms. *BioProcess International*, ed.
162. Yamniuk AP, Ditto N, Patel M, Dai J, Sejwal P, Stetsko P, Doyle ML 2013. Application of a kosmotrope-based solubility assay to multiple protein therapeutic classes indicates broad use as a high-throughput screen for protein therapeutic aggregation propensity. *J Pharm Sci* 102(8):2424-2439.

163. Al-Hussein A, Gieseler H 2012. The effect of mannitol crystallization in mannitol-sucrose systems on LDH stability during freeze-drying. *J Pharm Sci* 101(7):2534-2544.
164. Piedmonte DM, Summers C, McAuley A, Karamujic L, Ratnaswamy G 2007. Sorbitol crystallization can lead to protein aggregation in frozen protein formulations. *Pharm Res* 24(1):136-146.
165. Piedmonte DM, Hair A, Baker P, Brych L, Nagapudi K, Lin H, Cao W, Hershenson S, Ratnaswamy G 2015. Sorbitol crystallization-induced aggregation in frozen mAb formulations. *J Pharm Sci* 104(2):686-697.
166. Hu L, Joshi SB, Liyanage MR, Pansalawatta M, Alderson MR, Tate A, Robertson G, Maisonneuve J, Volkin DB, Middaugh CR 2013. Physical characterization and formulation development of a recombinant pneumolysoid protein-based pneumococcal vaccine. *J Pharm Sci* 102(2):387-400.
167. Kramer RM, Zeng Y, Sahni N, Kuelzo LA, Schwartz RM, Srivastava IK, Crane L, Joshi SB, Volkin DB, Middaugh CR 2013. Development of a stable virus-like particle vaccine formulation against Chikungunya virus and investigation of the effects of polyanions. *J Pharm Sci* 102(12):4305-4314.
168. Kamerzell TJ, Esfandiary R, Joshi SB, Middaugh CR, Volkin DB 2011. Protein-excipient interactions: mechanisms and biophysical characterization applied to protein formulation development. *Adv Drug Deliv Rev* 63(13):1118-1159.
169. Laber JR, Dear BJ, Martins ML, Jackson DE, DiVenere A, Gollihar JD, Ellington AD, Truskett TM, Johnston KP, Maynard JA 2017. Charge Shielding Prevents Aggregation of Supercharged GFP Variants at High Protein Concentration. *Mol Pharm* 14(10):3269-3280.
170. Lehermayr C, Mahler HC, Mader K, Fischer S 2011. Assessment of net charge and protein-protein interactions of different monoclonal antibodies. *J Pharm Sci* 100(7):2551-2562.
171. Ratanji KD, Derrick JP, Dearman RJ, Kimber I 2014. Immunogenicity of therapeutic proteins: influence of aggregation. *J Immunotoxicol* 11(2):99-109.
172. Joubert MK, Hokom M, Eakin C, Zhou L, Deshpande M, Baker MP, Goletz TJ, Kerwin BA, Chirmule N, Narhi LO, Jawa V 2012. Highly aggregated antibody therapeutics can enhance the in vitro innate and late-stage T-cell immune responses. *J Biol Chem* 287(30):25266-25279.
173. Sauna ZE, Lagasse D, Pedras-Vasconcelos J, Golding B, Rosenberg AS 2018. Evaluating and Mitigating the Immunogenicity of Therapeutic Proteins. *Trends Biotechnol*.
174. P.A. Patten aHS. 2003. The immunogenicity of biopharmaceuticals: Lessons learned and consequences for protein drug development. In Brown F. aM-SAR, editor *Immunogenicity of Therapeutic Biological Products*, ed., Basel: Karger. p 81-97.
175. Kamal MZ, Kumar V, Satyamurthi K, Das KK, Rao NM 2016. Mutational probing of protein aggregates to design aggregation-resistant proteins. *FEBS Open Bio* 6(2):126-134.
176. Nicoud L, Owczarz M, Arosio P, Morbidelli M 2015. A multiscale view of therapeutic protein aggregation: a colloid science perspective. *Biotechnol J* 10(3):367-378.
177. Saito S, Hasegawa J, Kobayashi N, Tomitsuka T, Uchiyama S, Fukui K 2013. Effects of ionic strength and sugars on the aggregation propensity of monoclonal antibodies: influence of colloidal and conformational stabilities. *Pharm Res* 30(5):1263-1280.
178. Gibson TJ, McCarty K, McFadyen IJ, Cash E, Dalmonte P, Hinds KD, Dinerman AA, Alvarez JC, Volkin DB 2011. Application of a high-throughput screening procedure with PEG-induced precipitation to compare relative protein solubility during formulation development with IgG1 monoclonal antibodies. *J Pharm Sci* 100(3):1009-1021.
179. Banks DD, Latypov RF, Ketchem RR, Woodard J, Scavezze JL, Siska CC, Razinkov VI 2012. Native-state solubility and transfer free energy as predictive tools for selecting excipients to include in protein formulation development studies. *J Pharm Sci* 101(8):2720-2732.
180. Telikepalli SN, Kumru OS, Kalonia C, Esfandiary R, Joshi SB, Middaugh CR, Volkin DB 2014. Structural characterization of IgG1 mAb aggregates and particles generated under various stress conditions. *J Pharm Sci* 103(3):796-809.
181. Lee HJ, McAuley A, Schilke KF, McGuire J 2011. Molecular origins of surfactant-mediated stabilization of protein drugs. *Adv Drug Deliv Rev* 63(13):1160-1171.
182. James C LaSNT 1981. The stabilization of proteins by sucrose. *J Biol Chem* 256(14):7193-7201.

183. Manasi Puri SM-M, George Crotts, and Douglas Nesta 2015. Evaluating Freeze-Thaw processes in biopharmaceutical development. *BioProcess International* 13(1):34-45.
184. Journal GBSaMG 2007. Protein stability in ice. *Biophysical Journal* 92(6):2131–2138.
185. Liu L, Braun LJ, Wang W, Randolph TW, Carpenter JF 2014. Freezing-induced perturbation of tertiary structure of a monoclonal antibody. *J Pharm Sci* 103(7):1979-1986.
186. Schwegman JJ, Carpenter JF, Nail SL 2009. Evidence of partial unfolding of proteins at the ice/freeze-concentrate interface by infrared microscopy. *J Pharm Sci* 98(9):3239-3246.
187. Miller MA, Rodrigues MA, Glass MA, Singh SK, Johnston KP, Maynard JA 2013. Frozen-state storage stability of a monoclonal antibody: aggregation is impacted by freezing rate and solute distribution. *J Pharm Sci* 102(4):1194-1208.
188. Hawe A, Wiggernhorn M, van de Weert M, Garbe JH, Mahler HC, Jiskoot W 2012. Forced degradation of therapeutic proteins. *J Pharm Sci* 101(3):895-913.
189. Kuelto LA, Wang W, Randolph TW, Carpenter JF 2008. Effects of solution conditions, processing parameters, and container materials on aggregation of a monoclonal antibody during freeze-thawing. *J Pharm Sci* 97(5):1801-1812.
190. WHO 2007. Recommendations for whole-cell pertussis vaccine. WHO Technical Report Series No 941.
191. Wei Y, Larson NR, Angalakurthi SK, Russell Middaugh C 2018. Improved Fluorescence Methods for High-Throughput Protein Formulation Screening. *SLAS Technol* 23(6):516-528.
192. Prevention CfDCA 2018. Vaccine Excipient & Media Summary.
193. Xiao Y, Zeng Y, Alexander E, Mehta S, Joshi SB, Buchman GW, Volkin DB, Middaugh CR, Isaacs SN 2013. Adsorption of recombinant poxvirus L1-protein to aluminum hydroxide/CpG vaccine adjuvants enhances immune responses and protection of mice from vaccinia virus challenge. *Vaccine* 31(2):319-326.
194. Ljusic B, Ochs M, Messham B, Ming M, Dookie A, Harper K, Ausar SF 2012. Formulation, stability and immunogenicity of a trivalent pneumococcal protein vaccine formulated with aluminum salt adjuvants. *Vaccine* 30(19):2981-2988.
195. Seema Iyer HH, Stanley L. Hem 2003. Relationship between the degree of antigen adsorption to aluminum hydroxide adjuvant in interstitial fluid and antibody production. *Vaccine* 21:1219 – 1223.
196. Romero Mendez IZ, Shi Y, HogenEsch H, Hem SL 2007. Potentiation of the immune response to non-adsorbed antigens by aluminum-containing adjuvants. *Vaccine* 25(5):825-833.
197. Berthold I, Pombo ML, Wagner L, Arciniega JL 2005. Immunogenicity in mice of anthrax recombinant protective antigen in the presence of aluminum adjuvants. *Vaccine* 23(16):1993-1999.
198. Jiang D, Morefield GL, HogenEsch H, Hem SL 2006. Relationship of adsorption mechanism of antigens by aluminum-containing adjuvants to in vitro elution in interstitial fluid. *Vaccine* 24(10):1665-1669.
199. Mei-Fang Chang YS, Steven L. Nail, Harm HogenEsch, Stephen B. Adams, Joe L. White, Stanley L. Hem 2001. Degree of antigen adsorption in the vaccine or interstitial fluid and its effect on the antibody response in rabbits. *Vaccine* 19:2884–2889.
200. Hansen B, Belfast M, Soung G, Song L, Egan PM, Capen R, Hogenesch H, Mancinelli R, Hem SL 2009. Effect of the strength of adsorption of hepatitis B surface antigen to aluminum hydroxide adjuvant on the immune response. *Vaccine* 27(6):888-892.
201. Egan PM, Belfast MT, Gimenez JA, Sitrin RD, Mancinelli RJ 2009. Relationship between tightness of binding and immunogenicity in an aluminum-containing adjuvant-adsorbed hepatitis B vaccine. *Vaccine* 27(24):3175-3180.
202. Hansen B, Malyala P, Singh M, Sun Y, Srivastava I, Hogenesch H, Hem SL 2011. Effect of the strength of adsorption of HIV 1 SF162dV2gp140 to aluminum-containing adjuvants on the immune response. *J Pharm Sci* 100(8):3245-3250.
203. Watkinson A, Soliakov A, Ganesan A, Hirst K, Lebutt C, Fleetwood K, Fusco PC, Fuerst TR, Lakey JH 2013. Increasing the potency of an alhydrogel-formulated anthrax vaccine by minimizing antigen-adjuvant interactions. *Clin Vaccine Immunol* 20(11):1659-1668.

204. Hansen B, Sokolovska A, HogenEsch H, Hem SL 2007. Relationship between the strength of antigen adsorption to an aluminum-containing adjuvant and the immune response. *Vaccine* 25(36):6618-6624.
205. Peek LJ, Martin TT, Elk Nation C, Pegram SA, Middaugh CR 2007. Effects of stabilizers on the destabilization of proteins upon adsorption to aluminum salt adjuvants. *J Pharm Sci* 96(3):547-557.
206. Jones LS, Peek LJ, Power J, Markham A, Yazzie B, Middaugh CR 2005. Effects of adsorption to aluminum salt adjuvants on the structure and stability of model protein antigens. *J Biol Chem* 280(14):13406-13414.
207. Dong A, Jones LS, Kerwin BA, Krishnan S, Carpenter JF 2006. Secondary structures of proteins adsorbed onto aluminum hydroxide: infrared spectroscopic analysis of proteins from low solution concentrations. *Anal Biochem* 351(2):282-289.
208. Agopian A, Ronzon F, Sauzeat E, Sodoyer R, El Habib R, Buchet R, Chevalier M 2007. Secondary structure analysis of HIV-1-gp41 in solution and adsorbed to aluminum hydroxide by Fourier transform infrared spectroscopy. *Biochim Biophys Acta* 1774(3):351-358.
209. Dvorah Diminsky NM, Marian Gorecki, Yechezkel Barenho 1999. Physical, chemical and immunological stability of CHO-derived hepatitis B surface antigen (HBsAg) particles. *Vaccine* 18(1-2):3-17.
210. Le Tallec D, Doucet D, Elouahabi A, Harvengt P, Deschuyteneer M, Deschamps M 2009. Cervarix, the GSK HPV-16/HPV-18 AS04-adjuvanted cervical cancer vaccine, demonstrates stability upon long-term storage and under simulated cold chain break conditions. *Hum Vaccin* 5(7):467-474.
211. Agarwal S, Sahni N, Hickey JM, Robertson GA, Sitrin R, Cryz S, Joshi SB, Volkin DB 2019. Developing stable frozen liquid bulk formulations to minimize aggregation and particle formation of three recombinant protein vaccine antigens for use in a trivalent rotavirus vaccine candidate. *Journal of Pharmaceutical Sciences*.
212. Wittayanukulluk A, Jiang D, Regnier FE, Hem SL 2004. Effect of microenvironment pH of aluminum hydroxide adjuvant on the chemical stability of adsorbed antigen. *Vaccine* 22(9-10):1172-1176.
213. D'Souza AJ, Mar KD, Huang J, Majumdar S, Ford BM, Dyas B, Ulrich RG, Sullivan VJ 2013. Rapid deamidation of recombinant protective antigen when adsorbed on aluminum hydroxide gel correlates with reduced potency of vaccine. *J Pharm Sci* 102(2):454-461.
214. Verma A, Burns DL 2018. Improving the stability of recombinant anthrax protective antigen vaccine. *Vaccine* 36(43):6379-6382.
215. Estey T, Vessely C, Randolph TW, Henderson I, Braun LJ, Nayar R, Carpenter JF 2009. Evaluation of chemical degradation of a trivalent recombinant protein vaccine against botulinum neurotoxin by LysC peptide mapping and MALDI-TOF mass spectrometry. *J Pharm Sci* 98(9):2994-3012.
216. Vessely C, Estey T, Randolph TW, Henderson I, Cooper J, Nayar R, Braun LJ, Carpenter JF 2009. Stability of a trivalent recombinant protein vaccine formulation against botulinum neurotoxin during storage in aqueous solution. *J Pharm Sci* 98(9):2970-2993.
217. I. Caraballo AMRaMF-A 1993. Study of thimerosal degradation mechanism. *International Journal of Pharmaceutics* 89:213-221.
218. Trümpler S, Lohmann W, Meermann B, Buscher W, Sperling M, Karst U 2009. Interaction of thimerosal with proteins—ethylmercuryadduct formation of human serum albumin and β -lactoglobulin A. *Metallomics* 1(1):87-91.
219. Santos JCN, da Silva IM, Braga TC, de Fatima A, Figueiredo IM, Santos JCC 2018. Thimerosal changes protein conformation and increase the rate of fibrillation in physiological conditions: Spectroscopic studies using bovine serum albumin (BSA). *Int J Biol Macromol* 113:1032-1040.